MULTISLICE COMPUTED TOMOGRAPHY CORONARY ANGIOGRAPHY

Filippo Cademartiri

ISBN 90-9019136-4

Lay-out: A.W.Zwamborn
Cover: F. Cademartiri and A.W.Zwamborn
Illustrations: F. Cademartiri

Printed by Ridderprint B.V. Ridderkerk

MULTISLICE COMPUTED TOMOGRAPHY CORONARY ANGIOGRAPHY

MULTISLICE COMPUTER TOMOGRAFIE ANGIOGRAFIE VAN DE KRANSARTERIËN

PROEFSCHRIFT

ter verkrijging van de graad van doctor aan de
Erasmus Universiteit Rotterdam
op gezag van de
Rector Magnificus

Prof. dr. S.W.J. Lamberts

en volgens besluit van het College voor Promoties.

De openbare verdediging zal plaatsvinden op
woensdag 16 Maart 2005 om 15:45 Uur

door

Filippo Cademartiri
geboren te Parma - Italië

PROMOTIECOMMISSIE

Promotoren:	Prof. dr. G.P. Krestin Prof. dr. P.J. de Feyter
Overige leden:	Prof. dr. A.J.J.C. Bogers Prof. dr. D. Poldermans Prof. dr. M.L. Simoons

Financial support by the department of Radiology, Erasmus MC, University Medical Center Rotterdam, for the publication of this thesis is gratefully acknowledged.

For my parents

PART II – CLINICAL IMPLEMENTATION

INTRODUCTION

CHAPTER

HISTORY AND BACKGROUND

Computed Tomography (CT) imaging is also known as "CAT scanning" (Computed Axial Tomography). Tomography is from the Greek word "tomos" meaning "slice" or "section" and "graphia" meaning "describing".

CT was invented in 1972 by British engineer Godfrey Hounsfield of EMI Laboratories, England, and independently by South African born physicist Allan Cormack of Tufts University, Massachusetts.[1,2] Hounsfield was later awarded the Nobel Peace Prize and honoured with Knighthood in England for his contributions to medicine and science.

The first clinical CT scanners were installed between 1974 and 1976. The original systems were dedicated to head imaging only, but "whole body" systems with larger patient openings became available in 1976. CT became widely available by about 1980. There are now about 30.000 installed worldwide.

The first CT scanner developed by Hounsfield in his lab at EMI took several hours to acquire the raw data for a single scan or "slice" and took days to reconstruct a single image from this raw data. The latest multislice CT systems can collect up to 64 slices of data in one rotation of about 333ms and reconstruct up to 20 slices/s with a 512x512-matrix.

During its 25-year history, CT has made great improvements in speed, patient comfort, and resolution. As CT scan times have gotten faster, more anatomy can be scanned in less time. Faster scanning helps to eliminate artefacts from patient motion such as breathing or peristalsis.

Computed tomography (CT) has been regarded in the late '80 and '90 as the "workhorse" of radiological routine, the minor sister of the more "fashionable" Magnetic Resonance (MRI). Actually, CT was born and remains a mono-parametric technique when compared with MRI that is multi-parametric.

CT TECHNIQUE

The CT information is basically a density (also defined as attenuation) profile. The measurement unit is defined as Hounsfield Unit (HU) and is based on a linear scale where "0" represents water, -1024 is air, and values in the range of +1000 represent bone. The profile of density is displayed in images.

In the earlier generations of scanners images corresponded to scans. Every scan resulted in one image. Between each scan/image there was a pause that allowed the scanner to change table position and scan the next level in the cranio-caudal direction (also defined as longitudinal axis or z-axis). This is the reason why CT native images are regarded as axial images and why CT was earlier defined as CAT.

After the introduction of spiral/helical/volumetric CT, the limitation of axial scanning has been overcome.[3] The CT scan is performed during the continuous motion of the table. The scan and the slices are two different things and also two different moments in the procedure. The scan corresponds to a volume of data that can be reconstructed in axial slices at any arbitrary table position along the z-axis. In principle, an axial slice is only one of the possible output of spiral CT.[3] A powerful enough hardware and software could perform directly sagittal or coronal images from the acquired volume of data.

The differentiation between tissues in CT is based on the variable attenuation. When attenuation is significantly different between two different tissues the visualisation is easy. For instance, in the case of lung (high contrast between air and lung parenchyma) and bones (high contrast between soft tissue compact bone).

In several cases, though, the difference of attenuation is not sufficient or is just not present (low contrast soft tissues and vessels). In this case the density profile within the images should be modified to improve the lack of natural contrast between soft tissues. This can be achieved using a contrast material.

The contrast material is usually radio-opaque. This means that the presence of contrast material determines a local increase in the attenuation. These contrast materials are usually iodinated.

GENERAL CT

Computed tomography and spiral CT has been regarded for decades as a baseline imaging modality that you can perform in the first instance for neurological and muscle-skeletal applications, or as a second line modality for many other applications.

In the late '90, though, CT has become increasingly recognized as a robust and reliable clinical tool in several fields of diagnostic radiology. In particular, after the introduction of spiral CT, body applications have become a cornerstone of clinical medicine. One of the fields that has significantly improved and become a standard in several diseases is thoracic imaging.[4-6]

This is because of the short scan time that allows to perform a CT of the thorax with in a single breath-hold. In addition, CT angiography of the thorax both for pulmonary arteries and thoracic aorta has become a primary investigation overruling other non-invasive and invasive modalities.

The vessels of the thorax can be seen as the vascular engine of the human body. The thorax is the region of the body where fuel (e.g. the blood) is washed out from "leftovers" (e.g. carbonic dioxide), loaded with energy (e.g. oxygen) and where the "vis a tergo" is created to deliver the energy in the entire body.

In this region stands the engine of the human body, namely the heart. All non-invasive imaging techniques dealing with the heart until now, had to face the challenge of high temporal resolution in order to reduce and eventually eliminate the motion due to the heartbeat and also to comply with the constraint due the breathing motion. Therefore, high temporal resolution should be intended as the one required to generate a single piece of information (e.g. the axial image) but also the one that allows to scan the entire volume of information within a single breath-hold.

CARDIAC CT

The introduction of electrocardiographic (ECG) triggering/gating in CT, coupled with improvement in detector and scanner technology (multiple detector rows) has led to the first multislice CT (MSCT) capable of scanning the heart within one breath-hold.[7]

This first experience was performed on a 4-row MSCT scanner in 1999/2000.[8,9] The minimum collimation/slice thickness was 1/1.25mm, the gantry rotation time was 500ms resulting in a scan time of about 40s. The temporal resolution of about 250ms did not allow to obtain good results unless the heart rate was low (<60bpm).[8,9] Nevertheless, the promise of this technique was evident: become the non-invasive technique for coronary arteries.

Then in 2002 a new generation of MSCT scanners was introduced.[10] The technical features were 16 rows of thinner (0.75mm) detectors and an increased gantry rotation speed (420ms/rotation). The results of this new generation of MSCT scanners were immediately confirming what was the potential of this technique.[11,12]

Compared to previous series with 4-row MSCT scanners, the 16-row MSCT scanners offered a more complete and detailed assessment of the coronary tree.[13] Less or no coronary segments could be excluded from the evaluation when using a threshold of 2mm in vessel diameter. An aggressive approach to heart rate with aggressive beta-blocking treatment coupled with the improved temporal resolution (between 210ms and 187ms) allows to scan patients with higher heart rates. This results in a broadening of the population of potential patients that could benefit from a MSCT coronary angiography performed instead of a conventional catheter coronary angiography.

THIS THESIS

Based on the promising preliminary results, the task for this technique was more in the field of reproducibility of the results, optimisation of the scan technique, and exploration of possible clinical applications.

The optimisation of the entire process is particularly important because cardiac imaging performed with MSCT requires state-of-the-art technology used by optimally trained teams. There are several reasons why an MSCT scan can be not diagnostic.

At each step of the procedure there are several details that have to be optimised. Each one of these steps can be source of artefacts that can reduce image quality and in the end even compromise the success of the procedure.

The two main objectives of this thesis were the technical optimisation of the protocol and the clinical implementation in a few settings. This mixed approach is represented in the cooperation between Radiology and Cardiology. On one side the technical radiological expertise allows to obtain and optimise the results, and on the other side the clinical cardiology knowledge allows to fit a new technique in the medical practice.

Within the technical aspects (**Chapter 2**) this thesis will deal with the problems related to the administration of contrast material (**Chapter 3**) and the anatomical approach to coronary arteries (**Chapter 4**) and the problems associated with pre- and post-processing of the datasets (**Chapter 5**). In the clinical implementation section instead, this thesis will deal with the problems associated the assessment of the coronary vessels at the level of the vessel lumen (stenosis) whether native (**Chapter 6**) or after treatment percutaneous intervention (**Chapter 7**), and at the level of vessel wall (**Chapter 8**).

CONCLUSION

Not all the aspects that can be optimised have been explored in this thesis but mainly the ones that are appearing at first to the scientist. Based on this thesis several other topics have been explored and more procedural optimisation has been and will be performed.

In addition, we already started working with a new generation of MSCT scanner characterized by 64 slices per rotation and isotropic spatial resolution. This implies that a further step of optimisation and implementation have to be made. This thesis allows to perform this operation in an easier way because it provides the direction and clues for the modification of parameters.

The entire thesis was possible because of the integration between Radiology and Cardiology. This is progressively resulting in a new area of knowledge, namely Non-invasive Cardiac Imaging. This area will keep improving its results with a constant effort aimed at the integration of competences from both sides.

REFERENCES

1. Hounsfield GN. Computerized transverse axial scanning (tomography). 1. Description of system. Br J Radiol. 1973;46:1016-22.
2. Cormack AM. Reconstruction of densities from their projections, with applications in radiological physics. Phys Med Biol. 1973;18:195-207.
3. Kalender WA, Seissler W, Klotz E, Vock P. Spiral volumetric CT with single-breath-hold technique, continuous transport, and continuous scanner rotation. Radiology. 1990;176:181-3.
4. Schoepf UJ, Kessler MA, Rieger CT, Herzog P, Klotz E, Wiesgigl S, Becker CR, Exarhos DN, Reiser MF. Multislice CT imaging of pulmonary embolism. Eur Radiol. 2001;11:2278-86.
5. Ghaye B, Szapiro D, Mastora I, Delannoy V, Duhamel A, Remy J, Remy-Jardin M. Peripheral pulmonary arteries: how far in the lung does multi-detector row spiral CT allow analysis? Radiology. 2001;219:629-36.
6. Kopp AF, Kuttner A, Trabold T, Heuschmid M, Schroder S, Claussen CD. Cardiac and vascular MDCT: thoracic imaging. Eur Radiol. 2003;13 Suppl 5:M73-81.
7. Ohnesorge B, Flohr T, Becker C, Kopp AF, Schoepf UJ, Baum U, Knez A, Klingenbeck-Regn K, Reiser MF. Cardiac imaging by means of electrocardiographically gated multisection spiral CT: initial experience. Radiology. 2000;217:564-71.
8. Achenbach S, Ulzheimer S, Baum U, Kachelriess M, Ropers D, Giesler T, Bautz W, Daniel WG, Kalender WA, Moshage W. Noninvasive coronary angiography by retrospectively ECG-gated multislice spiral CT. Circulation. 2000;102:2823-8.
9. Nieman K, Oudkerk M, Rensing BJ, van Ooijen P, Munne A, van Geuns RJ, de Feyter PJ. Coronary angiography with multi-slice computed tomography. Lancet. 2001;357:599-603.
10. Flohr TG, Schoepf UJ, Kuettner A, Halliburton S, Bruder H, Suess C, Schmidt B, Hofmann L, Yucel EK, Schaller S, Ohnesorge BM. Advances in cardiac imaging with 16-section CT systems. Acad Radiol. 2003;10:386-401.
11. Nieman K, Cademartiri F, Lemos PA, Raaijmakers R, Pattynama PM, de Feyter PJ. Reliable noninvasive coronary angiography with fast submillimeter multislice spiral computed tomography. Circulation. 2002;106:2051-4.
12. Ropers D, Baum U, Pohle K, Anders K, Ulzheimer S, Ohnesorge B, Schlundt C, Bautz W, Daniel WG, Achenbach S. Detection of coronary artery stenoses with thin-slice multi-detector row spiral computed tomography and multiplanar reconstruction. Circulation. 2003;107:664-6.
13. Mollet NR, Cademartiri F, Nieman K, Saia F, Lemos PA, McFadden EP, Pattynama PM, Serruys PW, Krestin GP, de Feyter PJ. Multislice spiral computed tomography coronary angiography in patients with stable angina pectoris. J Am Coll Cardiol. 2004;43:2265-70.

PART 1 - TECHNICAL OPTIMISATION

2. TECHNIQUE

CHAPTER 2.1

16-ROW MULTISLICE COMPUTED TOMOGRAPHY: BASIC CONCEPTS, PROTOCOLS AND ENHANCED CLINICAL APPLICATIONS.

F. Cademartiri, MD[1]
G. Luccichenti, MD[3]
A. van der Lugt, MD, PhD[1]
P. Pavone, MD[3]
P.M.T. Pattynama,MD, PhD[1]
P.J. de Feyter, MD, PhD[1,2]
G.P. Krestin, MD, PhD[1]

From the Departments of Radiology[1] and Cardiology[2] Erasmus Medical Center, Rotterdam, the Netherlands, and Department of Radiology[3] University of Parma, Parma, Italy.

Seminars in Ultrasound, CT, and MR,
Feb;25(1):2-16, 2004.

Since its introduction, spiral computed tomography (CT) technology underwent a continuous and fast technical and clinical development. In particular, spatial and temporal resolutions were constantly increased during the last decade. The main breakthrough for clinical application was the introduction of multislice technology, first with 2-row and 4-row equipment and more recently with 16-row scanners. A high-resolution sub-millimeter CT dataset can be acquired easily, although with an increased x-ray exposure for the patient. The high speed of the scan requires up-to-date and careful protocol optimization. Scanner technology and geometry affect image formation procedure and imaging protocols should be adapted accordingly. The technical foundations of spiral CT imaging and the main scan and reconstruction parameters are described in this article. Updated protocols and clinical examples of the latest applications are also discussed.

Cross-sectional imaging has been one of the major break-throughs of diagnostic radiology in recent decades. After the introduction of computed tomography (CT), ultrasound (US), and magnetic resonance imaging (MRI), our approach to diagnosis, treatment, and follow-up of diseases has completely changed. In particular, spiral CT has become the workhorse of cross-sectional imaging, owing to its robustness, moderate invasiveness, and relatively cheap management. Several applications of spiral CT are current standards in clinical practice.

Multislice computed tomography (MSCT, also known as multidetector-row CT, multidetector CT, and multisection CT) has improved the performance of spiral CT with the introduction of 2-row and 4-row MSCT scanners. In particular, CT angiography was significantly enhanced by sub-second rotation speed and thin collimation. This scenario further improved after the recent introduction of 16-row MSCT scanners. Sub-halfsecond rotation speed and sub-millimeter resolution allow wide areas to be scanned with astonishing image detail. Nevertheless, a 16-row MSCT scanner cannot be regarded simply as a 2-or 4-row scanner with more detector rows. In fact, several issues affect image quality with the increased number of thinner detectors, resulting in a more complex geometry of the scanner and of the image reconstruction algorithm. Moreover, the improved performance of 16-row MSCT scanners challenges the optimization of completely new applications such as coronary artery angiography[1-4]. With 16- row MSCT scanners, new fields of application, such as population screening, are under investigation[5-7]. For this reason, and also because CT is increasingly responsible for population radiation exposure, the applied x-ray dose is becoming an important issue[5,8-10].

Several parameters affect image formation and image quality, and after these parameters are set scan and reconstruction parameters should be adapted accordingly. In addition, the increased scan speed requires accurate timing in contrastenhanced examinations[11]. Therefore, technical knowledge and protocol optimization are the key for fully exploiting the potential of 16-row MSCT technology in clinical applications.

Basics of spiral and multislice ct imaging

Spiral CT generates cross-sectional images of a volume by obtaining multiple measurements of the x-rays attenuation from several projections. The requirement for image reconstruction is that all the above-mentioned measurements should lie in the same plane, which is not the case in spiral CT since scanning is performed with simultaneous patient translation. The complete in-plane dataset of measurements is obtained through interpolation from the measurements that precede and follow that plane[12,13]. Given the need for interpolation, we should consider that the more distant the measurements, the less accurate the interpolated values. The distance between the measurements depends on the table feed and on the gantry rotation period. Two additional factors affect CT scan flexibility: maximum x-ray tube load and x-ray beam collimation. These factors limit

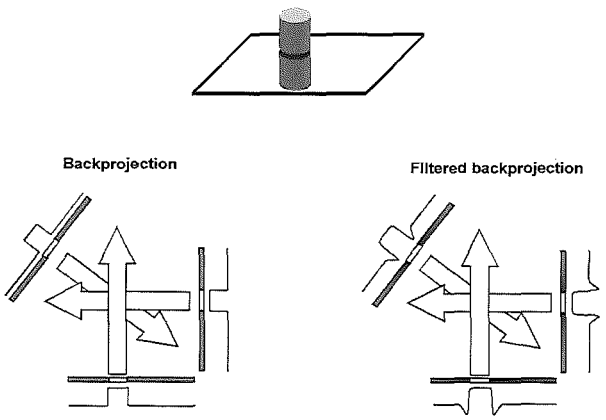

Figure 1. Backprojection and filtered backprojection. The value of the cross-sectional image pixel is obtained by assigning the values of the measurements of the projection lines passing through that pixel. This process is called backprojection (left panel). In simple words, the operation "spats" the projections on the surface of the image. A convolution filtering before the backprojection overcomes the additive nature of the reconstruction technique by enhancing the edges of the structures (right panel).

spatial and contrast resolution, maximum volume coverage, and temporal resolution, in addition to determining image pixel noise and artifacts.

In spiral CT, images can be reconstructed at any *z*-axis position within the scanned volume since missing information is obtained through interpolation. In MSCT, image reconstruction is performed using a filtered backprojection kernel[14]. Backprojection is an approximated algorithm that assigns to a defined pixel the values that are collected along projection lines passing through the same pixel (Fig 1). A convolution filtering before the backprojection is needed to overcome the additive nature of the reconstruction technique. Image filtering is generally used to enhance specific features such as edges (Fig 1). However, image filtering affects image pixel noise and, as a consequence, image contrast.

The limitations of spiral CT have been significantly reduced with MSCT. Increased number of detectors and faster gantry rotation speed permit an increase in the overall scan speed ranging from 4 to more than 25 times, compared with single detector array equipment[15]. To achieve this speed, other software and hardware improvements are needed. From the hardware point of view, the x-ray tube must become more powerful, the whole gantry must become more stable (therefore a lighter x-ray tube would be also needed), and the detector elements must provide a good dynamic range and a fast decay speed. From the software point of view, the data transfer rate must increase, the algorithm for the reconstruction must account for cone beam deformation, and computer speed must increase to be able to process the increasing amount of data with a speed that provides an optimal workflow.

The prominent role of image post-processing techniques should be stressed, such as 3-dimensional reconstructions, which include multiplanar reformation, curved image reformation, maximum intensity projection, and surface and volume rendering. An increasingly important part of the examination is going to be represented by image analysis, which requires highly trained personnel and advanced workstations. Thus, image processing is becoming time and cost expensive.

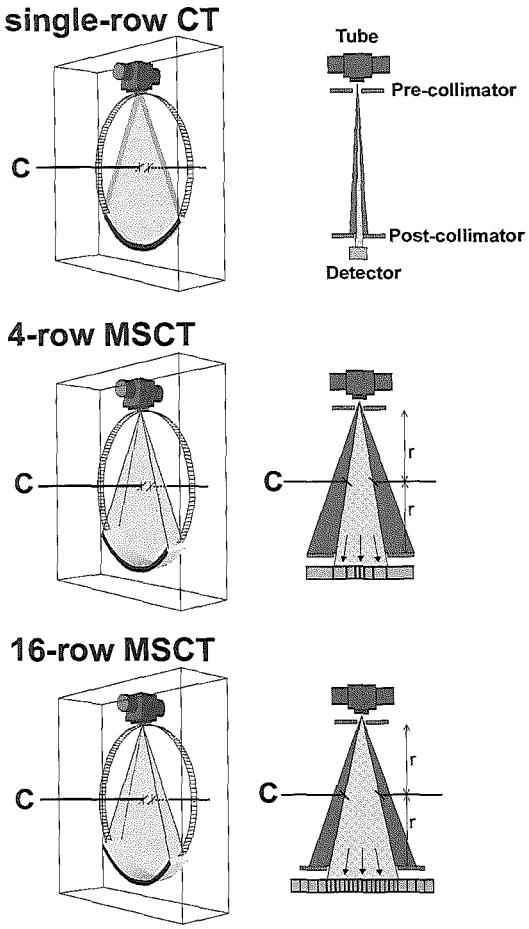

Figure 2. Single-row, 4-row, and 16-row MSCT scanners. The x-ray tube faces the detector system and both are rotating. The collimation (C) is defined as the thickness of the x-ray beam at the scanner isocenter. In single-row scanners (top panel) the x-ray collimation determines the fraction of the detector that is hit by x-rays. In this case x-ray collimation corresponds to slice thickness. In 4-row multidetector (middle panel) scanners the beam collimation determines how many detector rows x-rays will hit. Different slice widths are obtained combining several adjacent detectors. In 16-row multidetector scanners (bottom panel), the x-ray beams that hit the external rows of the detector system cannot be considered parallel to the axial scanning plane.

Finally, data storage represents a further issue the be confronted when dealing with the implementation of MSCT in a clinical routine.

Scan and reconstruction parameters

Since CT technology affects image formation procedure, scanning parameters should be set accordingly.

X-ray beam collimation (eg, collimation) refers to the beam width along the longitudinal axis at the scanner iso-center[16]. As a general rule, increasing the collimation reduces spatial resolution and image pixel noise[17,18]. In MSCT the collimated x-ray beam hits several detectors (Fig 2). The combination of more detectors determines the effective slice width.

The pitch (Fig 3A) reflects how wide the helix is that is created by the rotating gantry and table feed. Scan pitch can be defined as detector pitch (table feed/number of detectors x slice collimation) or beam/volume pitch (table feed/slice collimation)[15,16,19].

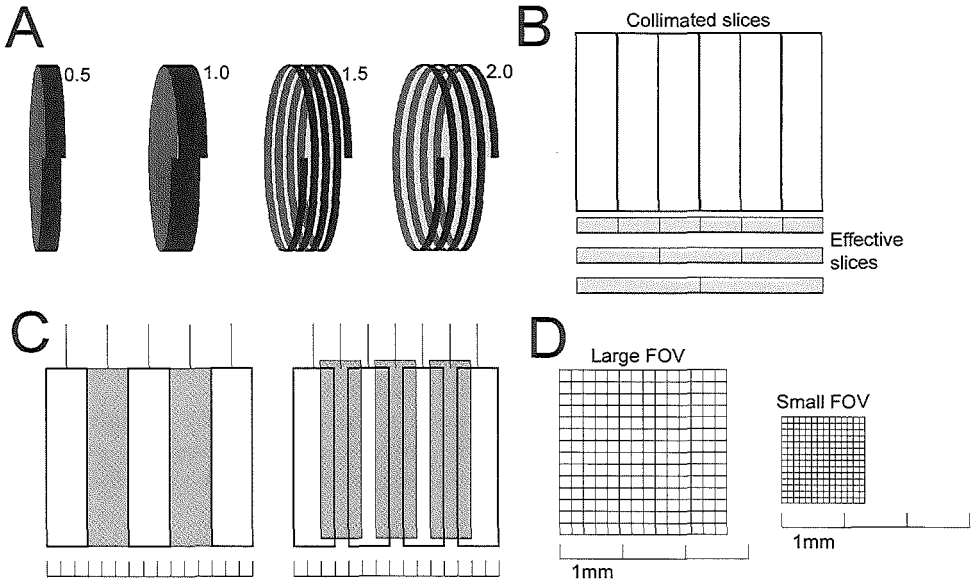

Figure 3. Pitch, effective slice width, increment and FOV. In A, the effect of the pitch on data sampling is displayed. The plot shows the spiral trajectory of the x-ray beam. High pitch increases the distance between the spires. This stretch of the spiral path corresponds to a reduction of data sampling frequency, creating gaps that will be filled by interpolation. The effective slice thickness (B) can be determined by combining the information of thinner contiguous detectors. The reconstruction increment (C) defines the distance between two contiguous reconstructed images. They are contiguous (left) if the effective slice thickness equals the increment, and they are overlapped (right) if the effective slice thickness is larger than the increment. The pixel size on the axial image (D) depends on the matrix and field of view (FOV). The matrix determines how many pixels form the image and it is set at a constant 512 512. The FOV defines image size. By keeping the matrix constant and decreasing the FOV, a smaller pixel size will be obtained.

We prefer to use the detector pitch definition because it is not affected by the number of detectors that characterize the scanner, and because it gives a sharper idea of the data sampling rate for that specific protocol. A high pitch reduces spatial and contrast resolution, although below a detector pitch of 2 image quality is not signifi cantly affected[16]. As a general rule, for the depiction of high-contrast structures, narrow collimation with high pitch is preferable to the contrary[17]. This criterion is particularly useful when performing CT angiography with single-row spiral CT scanners or with large areas of coverage.

Table feed represents the speed of the patient's translation along the *z*-axis. A fast table feed determines a faster scan speed.

The milliampere per second (mA/s) count of the x-ray beam represents the number of photons that are produced and actually pass through the patient. A higher mA/s count improves the contrast-tonoise ratio (eg, image quality), assuming that other parameters remain constant.

The kilovolt (kV) represents the energy of the photons. Most of the applications in routine MSCT are performed with 120 or 140 kV. Recently,

it has been suggested that MSCT could be performed with a lower patient dose, using protocols with 80/100 kV and increasing the mA/s[5].

Effective slice width refers to the slice thickness in the longitudinal axis from which an image is generated (Fig 3B). Effective slice width can be thicker but not thinner than the widest detector that is used. As a general rule, images obtained with detectors that are narrower than the effective slice width are more prone to reconstruction artifacts but provide higher spatial resolution[20].

The reconstruction increment, which is the distance between consecutive slices, affects spatial and contrast resolution (Fig 3C). Reconstruction increment can be set to generate partially overlapping slices. Narrow reconstruction increments minimize aliasing along the longitudinal axis in 3-dimensional reconstructions[20,21].

The field of view (FOV; Fig 3D) represents the size of the image that is going to be reconstructed. Because the matrix of the image is constant (512 x 512), a large FOV corresponds to larger pixels and therefore lower in-plane resolution.

Issues in msct scan geometry and main features

Multislice CT scanners are mainly characterized by multiple detector rows and faster gantry rotation speed. Even though this is a detailed summary of the features of MSCT scanners, the main issues in the development of a good scanner are related to these two parameters.

The geometry of the detectors depends on the manufacturers (Fig 4). In 4- and 8-row MSCT scanners, two main configurations were available: adaptive array detectors and matrix detectors. In 16-row MSCT scanners all manufacturers use an adaptive array configuration in which the inner rows are thin while the outer rows are thick. Generally speaking, the maximum detector width is a multiple of the minimum detector width.

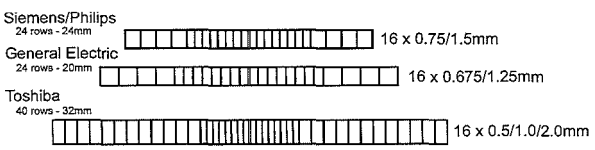

Figure 4. Detector geometry and size for 16-row MSCT scanners. The geometry of the detector is almost the same between manufacturers, while the detector element size is different. A smaller detector element unit will provide higher through-plane spatial resolution, but it will result in a shorter coverage and increased x-ray dose for a comparable contrastto-noise ratio. A larger detector element will provide lower through-plane spatial resolution, and it will result in a larger coverage and in a reduced x-ray dose for a comparable contrast-to-noise ratio.

The main issues for the implementation of 16- row MSCT scanners are 3-fold as follows:

1. The deformation of object geometry due to cone beam artifacts is not negligible anymore.
2. A very large amount of information must be transferred from the rotating system to the fixed part of the gantry.
3. Greater power is needed for the increased gantry rotation speed.

The assumption that x-rays are parallel to the scan plane (which is basically wrong but negligible until a certain point) can be maintained up to the 4- and 8-row MSCT scanners, depending of detector width[16,22-24]. The wider the x-ray beam, the more oblique the external x-ray projects compared to the central axis of the scan (Fig 2). The cone-shaped x-ray beam introduces a more complicated image reconstruction algorithm. In simple words, cone beam spiral CT imaging produces measurements that lie in planes that are not parallel. For this reason, an advanced reconstruction algorithm must be developed, to account for the lack of consistency between neighboring projections.

The reduced rotation period (increased speed) of the gantry determines a concomitant increase in the data acquisition rate and requires an increased data transfer rate between the rotating structures to the not-rotating gantry. Data transfer performance can represent the bottleneck for faster rotation and/or more detector rows. In fact, even though the hardware could rotate faster, if data cannot be transferred from the scanner during the scan, the procedure cannot be successful.

A more powerful x-ray tube is mandatory to produce a faster gantry rotation while maintaining a constant or even increased peak mA/s load (especially required in cardiac retrospectively ECGgated imaging). This x-ray tube can easily become more powerful, but with increased weight. Therefore, the developmental challenge of this is to create a very powerful and very light x-ray tube.

Given the technical limitations discussed above, the improvements evident in the current generation of 16-row MSCT scanners are consistent among the CT manufacturers, and they address the three main MSCT parameters, ie, (1) collimation, (2) number of detector rows, and (3) gantry rotation time.

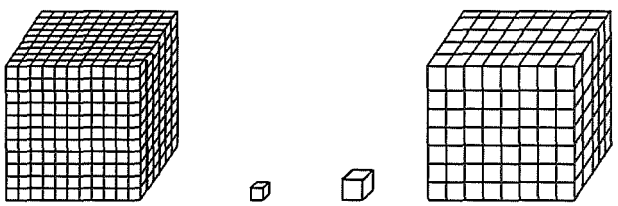

Figure 5. The concept of voxel. Elementary units called pixels (picture element) form 2-dimensional digital images, while elementary units called voxels form a 3-dimensional volume. The matrix of the volume defines the number of voxels forming the volume and the volume size determines the size of its smallest element.

The first parameter (collimation) ranges between 0.5 and 0.75 mm. This improvement affects inplane and longitudinal spatial resolution, and allows the acquisition of almost isotropic voxels (eg, a voxel approximately like a cube, in which the three sides are almost the same in length; Fig 5).

The second parameter (number of detectors), is for all vendors 16 detectors and mainly affects scan speed.

The third parameter (gantry rotation time) ranges around 0.4 second. This mainly affects the scan speed but more importantly affects in-plane temporal resolution. This improvement is particularly important for

applications where moving organs are studied (eg, cardiac and coronary applications).

Pros and cons of 16-row msct scanners

From the clinical standpoint, the introduction of 16-row MSCT has impacted mainly on applications that require high spatial and temporal resolution. The principal applications that were signifi cantly improved by the introduction of 16-MSCT are as follows:

1. All areas of CT angiography, such as the thoracoabdominal aorta and peripheral arteries, the bracheocephalic aortic trunks from the aortic arch to the circle of Willis, and the coronary arteries;
2. Patients with limited ability to cooperate, such as children and mentally disabled individuals; and
3. Applications requiring advanced postprocessing, such as studies with multiplanar and 3-dimensional reconstructions[15,25-28].

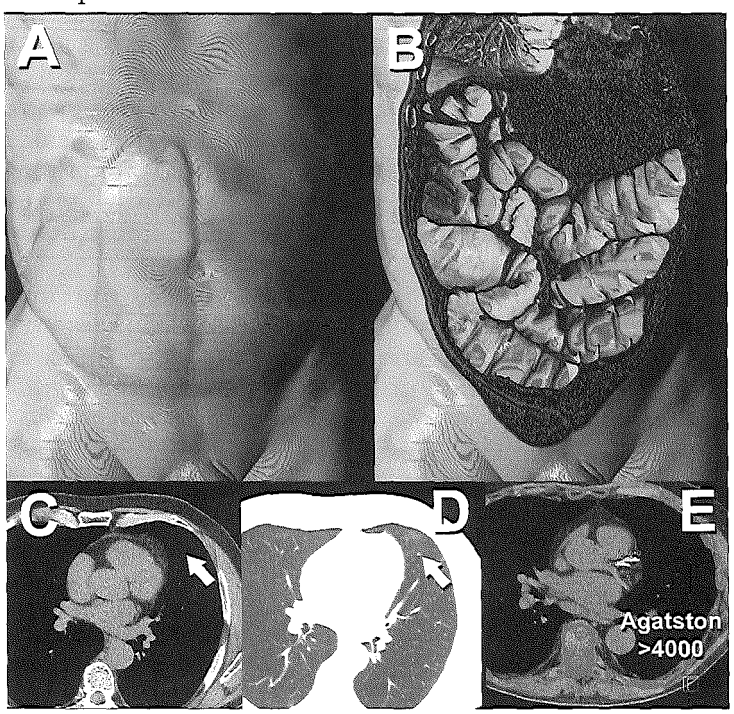

Figure 6. Screening MSCT applications. The main screening applications for MSCT are colon cancer (**A and B**), lung cancer (**C and D**), and coronary artery disease (**E**). Virtual colonography with MSCT shows considerable potential because of its high resolution but mostly because of the demonstrated progression from polyp to colon cancer that takes up to 10 years. The early detection of lung nodules, even though feasible with low-dose MSCT, has not yet provided good evidences of a low cost-to-benefit ratio. The biology of lung cancer and the high rate of false positives and collateral findings raise concerns about the widespread use of this technique. The main problem remains the management of small lung nodules (arrow in **C and D**). Coronary artery calcium score is a well-established technique to assess risk for coronary events (E). The experience was gained with electron-beam tomography (EBT)-based trials and it is expected that the same or similar outcomes will be obtained with MSCT. (A full color version of this illustration can be found in the color section (chapter 12)).

The counterpart for these improved performance levels is the increased amount of data generated, image noise, and patient radiation dose[15]. For all three parameters cited above, the solution carries a cost in terms of increased demands on visualization systems, workstations, and PACS (data), increased mA/s (image noise), and therefore increased patient dose. Radiation dose is increasingly emerging as an issue not only because of the widespread use of MSCT for routine clinical work, but also due to the increasing use of MSCT for population screening. The lack of epidemiological evidence regarding the effectiveness of MSCT-based population screening for colon polyps (Fig 6A and B) and lung nodules (Fig 6C) will persist for many years, since large clinical trials were started only recently. For coronary artery calcium assessment (Fig 6D), evidence was provided by the extensive experience gained with electron-beam tomography (EBT), which addressed the presence and amount of coronary calcium as a predictive factor for future coronary events[29]. Nevertheless, the question about the cost of the screening itself, and of the additional studies needed to assess the clinical relevance of collateral findings, is still unanswered[30,31].

Scan protocols

Protocols for scanning with 16-row MSCT are provided in Tables 1, 2, and 3. The optimization of protocols for 16-row MSCT scan can be outlined as follows:

1. the choice of scan parameters and intravenous contrast material administration (if needed),
2. the choice of the reconstruction parameters based on purpose and indication, and
3. the choice of the postprocessing techniques and methodology.

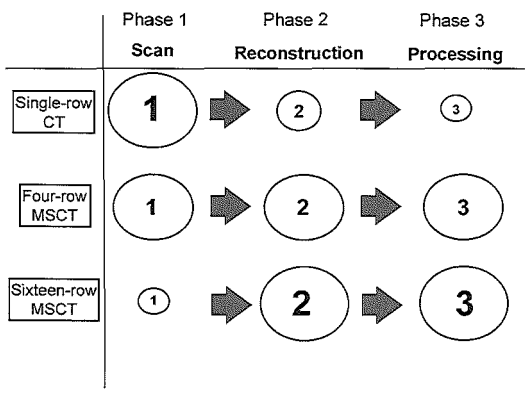

Figure 7. Relative importance of scan, reconstruction, and processing with single-row, 4-row, and 16-row MSCT. With the development of faster spiral CT scanners, an increasingly important part of the overall examination is represented by reconstruction and processing.

The relative importance of each of these phases was different with scanners from previous generations. The importance of the first phase was predominant in the past, with single-row scanners, and affected all the further steps; whereas with 16-row MSCT scanners, the second and third phases play the predominant role (Fig 7). As an example, we will discuss

Table 1. Protocols for 16-Row MSCT: Scan and IV Contrast Material Parameters*

	Angiography						
Region	Circle of Willis	Supra-aortic Trunks Run-Off	Ascending Aorta/ Aortic Arch	Thoracic Aorta	Pulmonary Arteries	Pulmonary Veins	Coronary Arteries
Scan							
Rows	16	16	16	16	16	16	16
Collimation (mm)	0.75	0.75	0.75	0.75	0.75	1.5	0.75
Rot. time (s)	0.5	0.4	0.4	0.5	0.5	0.5	0.4
Feed (mm)/rot.	12.0	12.0	3.0	12.0	12.0	36.0	3.0
Pitch	1	1	0.25	1	1	1.5	0.25
Eff. mAs	100	160/200	400	140/160	130	140	500
kV	120	120	120	120	120	120	120
ECG gating	—	—	Retro	—	—	—	Retro
Direction	Ca-Cr	Ca-Cr	Ca-Cr	Ca-Cr	Ca-Cr	Ca-Cr	Ca-Cr
IV contrast material							
CM volume (ml)	60	80	80/100	100	80	60	100
CM rate (ml/s)	4	4	4	4	4	2.5	4
CM iodine (mgI/ml)	>300	>300	>300	>300	>300	>300	>350
Chaser volume (ml)	40	40	40	40	40	—	40
Chaser rate (ml/s)	4	4	4	4	4	—	4
Synchronization	Visual	Auto	Auto	Auto	Auto	Auto	Auto
ROI position	—	AsA	AsA	AsA	AsA	AsA	AsA
ROI threshold (HU)	1st CES	75	100	100	75	75	100
Prescan delay (s)	4	4	4	4	4	4	4

The table shows a quick overview of the scan and IV contrast material administration parameters for 16-row MSCT scanners.
Abbreviations: 1st CES ? 1st contrast-enhanced slice; AsA ? ascending aorta; AbA ? abdominal aorta; Ca-Cr ? caudo-cranial; Cr-Ca ? cranio-caudal; IV ? intravenous.
*Parameters based on Sensation 16®, Siemens Medical Solutions, Forchheim, Germany.

			General			Screening			ER
Abdominal Arteries	Renal Arteries	Peripheral Run-Off	3-Phase Upper Abdomen	Renal Calculi	Staging & FU of Lymphoma	Coronary Calcium Score	CT Lung Screening	CT-Colonography	Emergency
16	16	16	16	16	16	16	16	16	16
0.75	0.75	0.75/1.5	0.75	0.75	1.5	1.5	0.75	0.75/1.5	1.5
0.5	0.5	0.5	0.5	0.5	0.5	0.4	0.5	0.5	0.5
12.0	12.0	12.0/24.0	12.0	18.0	38.0	6.0	12.0	12.0	36.0
1	1	1	1	1.5	1.5	0.25	1	1	1.5
200	140	200	160	160	160	150	60/80	100	130
120	120	120	120	120	120	120	120	120	120
—	—	—	—	—	—	Retro	—	—	—
Ca-Cr	Ca-Cr	Ca-Cr	Ca-Cr	Ca-Cr	Ca-Cr	Ca-Cr	Ca-Cr	Ca-Cr	Ca-Cr
100	60	125	125	—	125	—	—	—	125
4	4	4	4	—	2.5	—	—	—	3
>300	>350	>350	>300	—	>300	—	—	—	>300
40	40	40	—	—	—	—	—	—	40
4	4	4	—	—	—	—	—	—	4
Auto	Auto	Auto	Auto	—	Fixed	—	—	—	Visual
AbA	AbA	AbA	AbA	—	—	—	—	—	AsA
150	150	175-200	150	—	—	—	—	—	Optimal
4	4	4	4	4	50	4	4	4	25

Table 2. Protocols for 16-Row MSCT: Reconstruction Parameters*

	Angiography						
	Circle of Willis	Supra-aortic Trunks Run-Off	Ascending Aorta/ Aortic Arch	Thoracic Aorta	Pulmonary Arteries	Pulmonary Veins	Coronary Arteries
Reconstruction							
Processing dataset							
Eff. slice width (mm)	1	1	1	1	1	2	1
Increment (mm)	0.6	0.6	0.6	0.6	0.6	1	0.6
FOV (mm)‡	<140	<140	180	200	250	160	<160
Kernel	med	med	med	med	med	med	med
Number of images	200	450	350	450	350	180	250
Review dataset							
Eff. slice width (mm)	2	3	3	3	5	5	3
Increment (mm)	2	3	3	3	5	5	3
FOV (mm)	160	160	250	250	280	180	160
Kernel	med	med	med	med	med	med	med
Number of images	60	90	70	90	70	36	50

The table-shows an overview of the reconstruction parameters for 16-row MSCT scanners.
Abbreviations:
*Parameters based on Sensation 16®. Siemens Medical Solutions, Forchheim, Germany.
†The parameters are provided per phase.
‡Variable depending on the size of the patient

the protocol for coronary imaging owing to its peculiar scan geometry and reconstruction architecture.

Phase 1: Choice of Scan and IV Contrast Material Parameters (Table 1)

For all 16-row MSCT scanners, the choice of scan parameters is reduced to two or at most three collimations: a high-resolution, thin collimation (0.5-0.75 mm) protocol, or a high-speed, thick collimation (1.0-2.0 mm) protocol. Table/feed, and therefore pitch, rarely need to be adjusted because of the extremely high scan speed. Except for special applications, the kV is set at 120-140, while the mA/s should be adapted to the patient's weight or body mass index (especially in body applications)[32].

			General			Screening			ER
Abdominal Arteries	Renal Arteries	Peripheral Run-Off	3-Phase Upper Abdomen †	Renal Calculi	Staging & FU of Lymphoma	Coronary Calcium Score	CT Lung Screening	CT-Colonography	Emergency
1	1	1 / 2	1	1	2	3	1	1	2
0.6	0.6	0.6 / 1	0.6	0.6	1	1.5	0.6	0.6	1
300	200	300/200	300	250	300	<180	250	300	250/300
med	med	med	med	med	med	—	high	med	med / high
450	250	2500/1500	400	450	600	100	350	450	400-900
3	3	5	5	5	5	—	5	5	8
3	3	5	5	5	5	—	5	5	8
300	300	300	300	300	300	—	250	300	300
med	med	med	med	med	med	—	high	med	med / high
90	90	300	85	90	120	—	70	90	50/115

The main issue in the choice of mA/s is that a better contrast-to-noise ratio (better images) can be obtained by using a high mA/s, but at the expense of a concomitant increase in patient x-ray dose. Therefore, the increased mA/s should be restricted to the application where a superior contrast- to-noise ratio is required in an environment of low-contrast structures. For instance, abdominal scanning and plaque imaging require high image contrast in areas of low x-ray attenuation, while lung parenchyma imaging or virtual colonoscopy can rely on a very high natural contrast level generated by the presence of air.

When intravenous (IV) contrast material is required, the injection parameters and method for synchronization must be adapted to the specific indication.

There are two main rationales for using IV contrast material: nonangiographic studies, and angiographic studies. For nonangiographic studies the problem is the amount of contrast required in relation to the duration of the scan. For instance, in the staging and follow-up of lymphomas, delayed enhancement is required; in this case, accurate synchronization and a high injection rate are not needed. For angiographic studies, however, accurate timing and optimized rapid injection protocols are required to ensure that the scan is performed during the peak of arterial attenuation (first pass of contrast material) and prior to venous enhancement. Normally, attenuation higher than 200 HU in the arteries is considered acceptable for MSCT angiography purposes, even though in our experience a better diagnostic confidence level is achieved with attenuation higher than 300 HU.

In angiography with 16-row MSCT, the short scan duration requires high accuracy in timing the scan with the passage of the bolus of contrast material. Three techniques are primarily used. A fixed scanning delay, following a standardized contrast bolus injection, is accurate enough to ensure selective arterial enhancement in high flow vascular segments, such as the circle of Willis, carotid and renal arteries, or when an angiographic study is performed in patients with variable left ventricular function. The test bolus method consists of the dynamic monitoring of a small bolus of contrast material. The delay between the administration of contrast and the start of the scan is obtained by calculating the peak attenuation in the test bolus in an artery of interest. The bolus tracking technique utilizes real-time monitoring of the arrival of the contrast material in a defined vessel by means of a region of interest determined by the technologist. A threshold of attenuation is selected, and the scan is automatically triggered when the attenuation value reaches the threshold.

Phase 2: Choice of Reconstruction Parameters (Table 2)

The reconstruction phase is becoming increasingly important along with the increased potential of MSCT scanners. This is the phase when the diagnostic datasets are generated. The proper generation of these data allows proper processing and ultimately correct diagnostic evaluation. In general, there are two main types of reconstructed datasets: the processing dataset (high-resolution, thin slices, high number of images; useful for postprocessing and storage), and the review dataset (low-resolution, thick slices, low number of images; useful for print-out and/or network sharing and storage). The processing dataset is characterized by an effective slice width comparable to the slice collimation (eg, for a collimation of 0.75 mm, an effective slice width of 0.75-1.00 mm) and by a 30% to 50% overlap increment (eg, for an effective slice width of 1.00 mm, a reconstruction increment of 0.5-0.6 mm). These features of the processing dataset permit multiplanar reconstructions with isotropic resolution. The review dataset is characterized by an effective slice width of >3-5 mm and contiguous nonoverlapping slices.

The size of the field of view (FOV) must be tailored to each specific application. A smaller FOV increases the in-plane spatial resolution to a certain point. A FOV smaller than 100-120 mm does not provide higher resolution, but normally only increases the pixel size.

The usual x-ray filtering level is medium; but for specific applications, such as lung parenchyma and bone visualization, hard filters are required. The same concept can be applied to calcified arteries, atherosclerotic plaques, and stents, especially when located in small vessels, such as the coronary arteries. In these cases, better assessment of the vessel lumen can be achieved by increasing the edge filtering.

Phase 3: Choice of Processing Technique and Methodology (Table 3)

Image processing is becoming increasingly important, given the high resolution of the dataset created by MSCT. A larger amount of information is contained within the dataset, and therefore, to fully exploit this plethora of information, conventional processing techniques, used with single-detector CT, must be upgraded with new tools, and eventually with new techniques.

Table 3. Protocols for 16-Row MSCT: Processing Technique and Methodology

	Angiography										General			Screening			ER
Region	Circle of Willis	Supra-AorticTrunks Run-Off	Ascending Aorta/ Aortic Arch	Thoracic Aorta	Pulmonary Arteries	Pulmonary Veins	Coronary Arteries	Abdominal Arteries	Renal Arteries	Peripheral Run-Off	3-Phase Upper Abdomen	Renal Calculi	Staging & FU of	Coronary Calcium	CT Lung Screening	CT Colonography	Emergency
Processing																	
Axial	yes	yes	yes	yes	yes	yes	yes	yes	yes	yes	yes	yes	yes	yes	yes	yes	yes
MPR	yes	yes	yes	yes	yes	yes	yes	yes	yes	yes	yes	yes	yes	yes	yes	yes	yes
Axial MIP	yes	yes	yes	yes	yes	no	yes	yes	yes	yes	yes	yes	no	no	yes	yes	yes
Multiplana	yes	yes	yes	yes	yes	no	yes	yes	yes	yes	yes	yes	no	no	yes	yes	yes
Curved	no	yes	no	no	no	no	yes	yes	yes	yes	no	no	no	no	no	no	yes
MinIP	no	no	no	no	no	no	no	no	no	no	no	no	no	no	yes	no	no
3D VR	yes	no	yes	yes	no	no	yes	yes	yes	no	no	no	no	no	no	yes	no
3D	no	yes	no	no	no	no	yes	yes	yes	no	no	no	no	no	no	no	no
Dedicated	no	no	no	no	no	no	no	no	no	no	no	no	no	yes	yes	yes	no

The table shows an overview of the reconstruction parameters for 16-row MSCT scanners.
Abbreviations:
MPR = multiplanar reconstruction; MIP = maximum intensity projections;
MinIP = minimum intensity projections; 3D VR = three-dimensional volume rendering.

An MSCT dataset cannot be reviewed solely using film, unless the examination deals with previously known problems (eg, follow-up studies). When initial diagnosis is required, the full spectrum of possibilities can be explored by using only a workstation that is capable, at a minimum, of performing multiplanar reconstructions. Unfortunately, this is not possible at every institution, due to restrictions in computer power, number of workstations, and so forth. In principle, any MSCT scan could be reviewed for parenchymal diseases, vascular diseases (if the scan is performed in the first pass of contrast material), and for bone anomalies. The frequency with which collateral findings can be detected on nonenhanced CT studies performed for other purposes is well known[30,31,33,34].

For proper image processing, a dedicated dataset must be prepared (as described previously). Based on this dataset, the starting point for interpretation remains axial imaging, which is completed by multiplanar (MPR)/oblique reformats. During the reformation phase, windowing and magnification permit attention to be focused on specific areas. After this phase, and especially for angiographic studies, maximum intensity projections (MIP) can be created using thick slabs. The thickness of the slabs is variable and cannot be standardized. In fact, slab thickness depends on the size of the vessel (smaller vessels require thin slabs), on the amount of calcium present in the wall of the vessel (calcified vessels require thin slabs), and on the regional anatomy (tortuous vascular anatomy is hard to depict with MIP reformats). To improve the visualization of vessels of small diameter and/or tortuous anatomy, curved MPR reformats are extremely useful. They can be obtained manually by drawing a line on MPR planes or they can be semi-automatically/automatically created by dedicated software. This software tends to perform better on large vessels and works best in a semiautomatic fashion (eg, the operator drops several reference points along the vessel and the software connects them following a central lumen line). Minimum intensity projections, as opposed to maximum intensity projections, have limited use in clinical practice.

Three-dimensional volume rendering (3D-VR), though available for many years, has been increasingly applied in clinical practice for three main reasons: datasets are becoming too large for conventional CT interpretation, workstations are more widely available, and computer power allows one to interact in real-time with the volume of data. Vascular anatomy is easily depicted with 3D-VR, but the assessment of wall abnormalities and the evaluation of stenosis should not be done on these images. 3D-VR is useful for presentation, however, as a roadmap for surgery and as summary pictures for the referring physician.

Cardiac MSCT Scanning

Multislice CT for the evaluation of the heart and coronary arteries (Fig 8) was introduced with the 4-row generation of instruments in 1999. Cardiac scanning is characterized by spiral geometry with a very low pitch, generally 0.25-0.37, which allows for oversampling the information throughout the cardiac cycle while the electrocardiogram (ECG) is recorded[35].

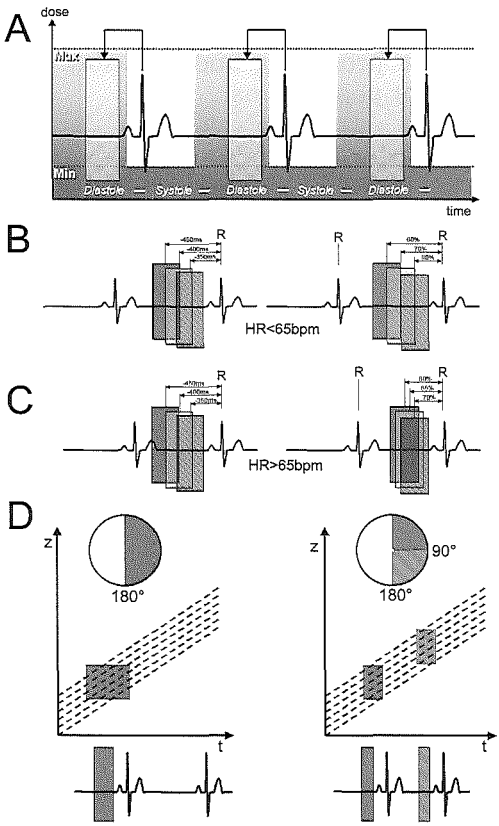

Figure 8. Retrospectively ECG-gated MSCT reconstruction. (A) The prospective tube-modulation algorithm is displayed. The maximum x-ray dose is delivered during the diastolic phase while during the systolic phase the mA/s drops. Depending on the heart rate, the x-ray exposure can be reduced by 50% with this technique. To locate the proper reconstruction window in the diastolic phase, two main techniques can be used: absolute reverse delay (-400 ms), and percentage delay (65%). The reference point for the gating it is always the R wave. (B and C) The difference between the two techniques is evident if we show how they perform at low (<65 bpm; B), and high heart rates (>65 bpm; C). The absolute reverse delay keeps a constant distance between the R wave and the start of the reconstruction window, regardless the heart rate, while the percentage delay keeps the start of the reconstruction window more in the center of diastole, regardless of the heart rate. Both techniques are routinely used in cardiac MSCT imaging. (D) The concept of multisegmental reconstruction is displayed. For heart rates above 70 bpm it can be worthwhile to split the information needed to reconstruct one image between two neighboring heart cycles, producing a virtual temporal resolution of ~100 ms. This method is based on the assumption that two consecutive heart beats are equal in terms of kinetics and position of anatomic structures, and therefore it works properly with extremely stable heart rates.

In some cases the pitch can be even lower, as in respiratory gated sequences, or very low/very high heart rate protocols. After the scan is performed, the raw data are retrospectively reconstructed in the diastolic phase of the heart cycle using the ECG as the reference point. Within the ECG the R wave is widely used as a triggering pint, because it is an easy wave for the software to recognize. One image can be reconstructed using the information derived from 180° of gantry rotation [35]. Therefore, if the gantry rotation time is 500 ms, the temporal resolution for a single image will be 250 ms. Sixteen-row MSCT scanners have a gantry rotation time in the range of ~0.4 s, with a resulting effective temporal resolution of ~0.2 s. Still this level of resolution is far from the range of ~50 ms that characterizes EBT and magnetic resonance imaging. Nevertheless, 16-row MSCT can provide high spatial resolution (<1 mm) and retrospective reconstruction algorithms. The optimal motion-free cardiac phase can always be found in patients with heart rates below 65 bpm[27,28]. Beside the technical issues inherent to coronary MSCT scanning, the future role of this technique remains unclear. On one hand, the possibility of assessing the coronary arteries with a noninvasive technique is extremely appealing, both from the medical and commercial point of view; but on the other

hand, the radiation exposure (7.1 to 10.9 mSv) and the lacking evidence for effective clinical benefit are still major concerns[5,36-38]. Nevertheless, coronary imaging with MSCT appears to be promising and probably will soon enter the clinical field in selected patient populations.

Enhanced applications

Briefly, we will mention the applications that in our institution gained clinical acceptance after the introduction of 16-row MSCT scanners. Cardiovascular applications are significantly improved by using 16-row MSCT, and in three fields 16-row MSCT angiography is becoming the standard imaging modality.

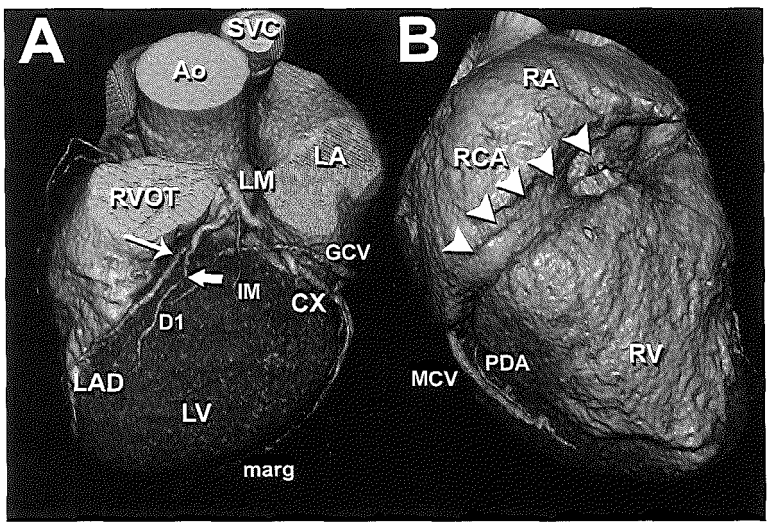

Figure 9. Coronary angiography with 16-row MSCT. Three-dimensional volume rendering images. (**A**) In an oblique right anterolateral view, a diseased left anterior descending (LAD; thin arrow) and a stenosis of the first diagonal branch (D1; thick arrow) are shown. (**B**) In the oblique left lateral view an occluded right coronary artery (RCA) is displayed (arrowheads).
Abbreviations: Ao = ascending aorta; CX = circumflex; D1 = first diagonal branch; GCV = great cardiac vein; IM = intermediate branch; LAD = left anterior descending; LM = left main; LV = left ventricle; marg marginal branch; MCV = median cardiac vein; PDA = posterior descending artery; RA = right atrium; RCA = right coronary artery; RV = right ventricle; RVOT = right ventricle outflow tract; VSC = superior vena cava. (A full color version of this illustration can be found in the color section (chapter 12)).

The first is noninvasive coronary artery imaging. Although only certain patients are candidates for CT cardiac studies, this population still represents a large number of people[27,28]. In particular, this group includes young asymptomatic patients with a high risk for cardiovascular disease, symptomatic patients with nonconclusive conventional tests (eg, ECG, US, stress-Echo), and patients being followed for coronary graft patency (Fig 9).

The second cardiovascular application is the noninvasive evaluation of the supra-aortic trunks for suspected cerebrovascular diseases (Fig 10).

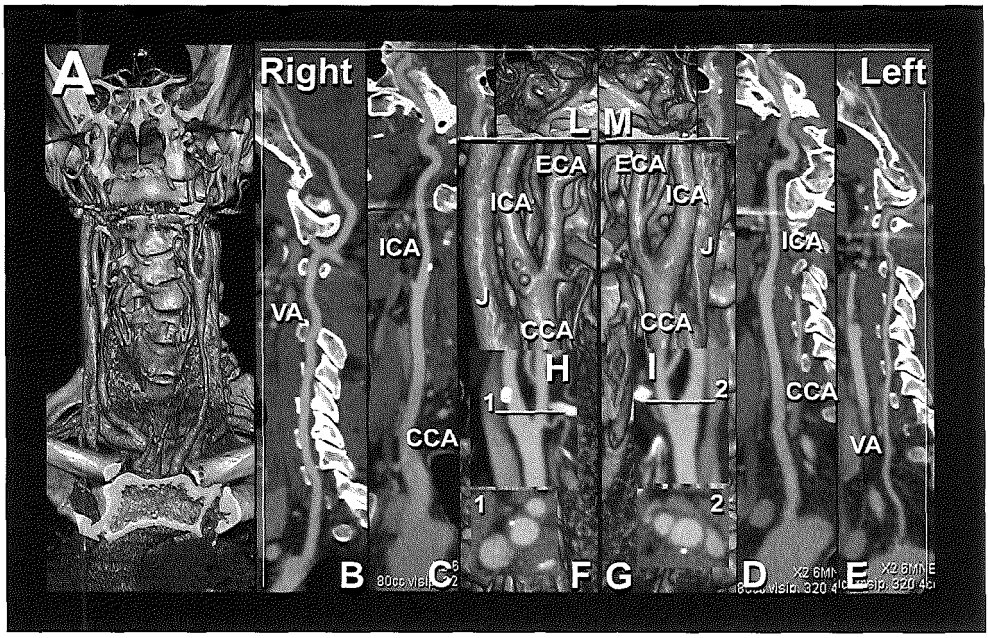

Figure 10. Carotid-vertebral circulation examined with 16-row MSCT angiography. (**A**) The panoramic view, with 3-dimensional volume rendering, demonstrates the whole scan range from the aortic arch to the circle of Willis. (**B-E**) To study both the carotid and vertebral arteries, curved MPR can be performed throughout the dataset. (**F and G**) To study the carotid bifurcation, 3-dimensional volume rendering can be used; but to evaluate patency and plaque morphology, MIPs (**H and I**) are required, and targeted axial cuts (**1 and 2**) are especially useful. (**L and M**) The intracranial portion of the internal carotid artery can be easily studied with 3-dimensional volume rendering (**L and M**; inner images) and curved MPR (**L and M**; lateral images). Abbreviations: CCA = common carotid artery; ECA = external carotid artery; ICA = internal carotid artery; J = jugular vein. (A full color version of this illustration can be found in the color section (chapter 12)).

Multislice CT for this application is robust, easy to perform, patient friendly, and non-operator-dependent. Furthermore, with the implementation of brain perfusion assessment, it could be applied in the acute settings[39].

The third application is noninvasive peripheral artery evaluation (Fig 11). In this field, MSCT can rely again on its robustness and its ease of application[40].

CONCLUSIONS

Multidetector CT is a rapidly evolving field of research. Scanning and reconstruction parameters should be optimized according to the scanner technology. Further improvements will lead to lighter and more powerful x-ray tubes and to an increase in the number of detector rows. These changes will result in faster rotation and scan speed with a concomitant increase in spatial resolution. Concerns persist because of the significant x-ray exposure with MSCT, especially in screening applications. Effective methods for reduction and optimization of the x-ray dose will allow the widespread use of MSCT technology.

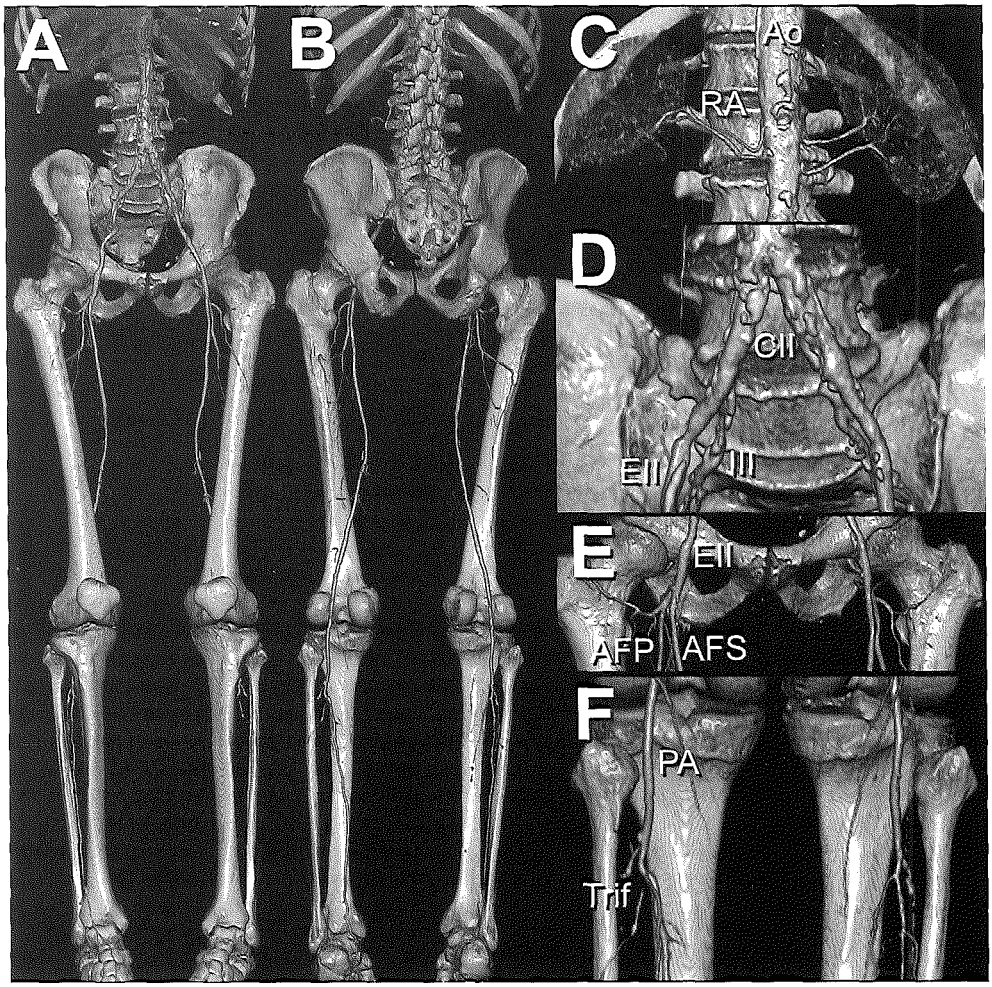

Figure 11. Peripheral run-off with 16-row MSCT angiography. The anterior (**A**) and posterior (**B**) views of the entire scan range for a peripheral run-off study are displayed with 3-dimensional volume rendering in a diffusely diseased patient. Magnified images show the level of the renal artery (**C**), where accessory vessels are present on both sides, the level of aortic bifurcation (**D**), the level of femoral bifurcation (**E**), and the level of popliteal trifurcation (**F**). Abbreviations: Ao = aorta; CII = common iliac arteries; EII = external iliac arteries; IIA = internal iliac arteries; AFP = arteria femoralis profunda; AFS = arteria femoralis superficialis; PA = popliteal artery; trif trifurcation. (A full color version of this illustration can be found in the color section (chapter 12)).

References

1. Flohr TG, Schoepf UJ, Kuettner A, et al: Advances in cardiac imaging with 16-section CT systems. Acad Radiol 10:386-401, 2003
2. Flohr T, Stierstorfer K, Bruder H, et al: Image reconstruction and image quality evaluation for a 16-slice CT scanner. Med Phys 30:832-845, 2003
3. Flohr T, Bruder H, Stierstorfer K, et al: New technical developments in multislice CT—part 2: Sub-millimeter 16-slice scanning and increased gantry rotation speed for cardiac imaging. Rofo Fortschr Geb Rontgenstr Neuen Bildgeb Verfahr 174:1022-1027, 2002

4. Flohr T, Stierstorfer K, Bruder H, et al: New technical developments in multislice CT—Part 1: Approaching isotropic resolution with sub-millimeter 16-slice scanning. Rofo Fortschr Geb Rontgenstr Neuen Bildgeb Verfahr 174:839-845, 2002
5. Jakobs TF, Wintersperger BJ, Herzog P, et al: Ultra-lowdose coronary artery calcium screening using multislice CT with retrospective ECG gating. Eur Radiol 13(8):1323-1330, 2003
6. Ji H, Rolnick JA, Haker S, et al: Multislice CT colonography: Current status and limitations. Eur J Radiol 47:123-134, 2003
7. Ko JP, Naidich DP: Lung nodule detection and characterization with multislice CT. Radiol Clin North Am 41:575-597, 2003
8. Jakobs TF, Becker CR, Ohnesorge B, et al: Multislice helical CT of the heart with retrospective ECG gating: Reduction of radiation exposure by ECG-controlled tube current modulation. Eur Radiol 12:1081-1086, 2002
9. Cohnen M, Poll L, Puttmann C, et al: Radiation exposure in multi-slice CT of the heart. Rofo Fortschr Geb Rontgenstr Neuen Bildgeb Verfahr 173:295-299, 2001
10. Poll LW, Cohnen M, Brachten S, et al: Dose reduction in multi-slice CT of the heart by use of ECG-controlled tube current modulation ("ECG pulsing"): Phantom measurements. Rofo Fortschr Geb Rontgenstr Neuen Bildgeb Verfahr 174: 1500-1505, 2002
11. Cademartiri F, van der Lugt A, Luccichenti G, et al: Parameters affecting bolus geometry in CTA: A review. J Comput Assist Tomogr 26:598-607, 2002
12. Kalender WA, Seissler W, Klotz E, et al: Spiral volumetric CT with single-breath-hold technique, continuous transport, and continuous scanner rotation. Radiology 176:181-183, 1990
13. Crawford CR, King KF: Computed tomography scanning with simultaneous patient translation. Med Phys 17:967-982, 1990
14. Brooks RA, Di Chiro G: Theory of image reconstruction in computed tomography. Radiology 117:561-72, 1975
15. Prokop M: General principles of MDCT. Eur J Radiol 45(Suppl 1):S4-S10, 2003
16. Hu H: Multi-slice helical CT: Scan and reconstruction. Med Phys 26:5-18, 1999
17. Hu H, Fox SH: The effect of helical pitch and beam collimation on the lesion contrast and slice profile in helical CT imaging. Med Phys 23:1943-1954, 1996
18. Diederichs CG, Keating DP, Glatting G, et al: Blurring of vessels in spiral CT angiography: Effects of collimation width, pitch, viewing plane, and windowing in maximum intensity projection. J Comput Assist Tomogr 20:965-974, 1996
19. Brink JA, Heiken JP, Forman HP, et al: Hepatic spiral CT: Reduction of dose of intravenous contrast material. Radiology 197:83-88, 1995
20. Fleischmann D, Rubin GD, Paik DS, et al: Stair-step artifacts with single versus multiple detector-row helical CT. Radiology 216:185-196, 2000
21. Yen SY, Rubin GD, Napel S: Spatially varying longitudinal aliasing and resolution in spiral computed tomography. Med Phys 26:2617-2625, 1999
22. Schaller S, Flohr T, Klingenbeck K, et al: Spiral interpolation algorithm for multislice spiral CT—part I: Theory. IEEE Trans Med Imaging 19:822-834, 2000
23. Fuchs T, Krause J, Schaller S, et al: Spiral interpolation algorithms for multislice spiral CT—part II: Measurement and evaluation of slice sensitivity profiles and noise at a clinical multislice system. IEEE Trans Med Imaging 19:835-847, 2000

24. Kachelriess M, Fuchs T, Schaller S, et al: Advanced single-slice rebinning for tilted spiral cone-beam CT. Med Phys 28:1033-1041, 2001
25. Cademartiri F, Nieman K, Mollet NR: The dynamics of an ascending aorta dissection by 16 row multislice computed tomography. Heart 89:970, 2003
26. Cademartiri F, Nieman K, Mollet N: An unusual case of chest murmur demonstrated with three dimensional volume rendering with 16 row multislice spiral computed tomography. Heart 89:586, 2003
27. Nieman K, Cademartiri F, Lemos PA, et al: Reliable noninvasive coronary angiography with fast submillimeter multislice spiral computed tomography. Circulation 106:2051-2054, 2002
28. Ropers D, Baum U, Pohle K, et al: Detection of coronary artery stenoses with thin-slice multi-detector row spiral computed tomography and multiplanar reconstruction. Circulation 107:664-666, 2003
29. Rumberger JA, Kaufman L: A rosetta stone for coronary calcium risk stratification: Agatston, volume, and mass scores in 11, 490 individuals. AJR Am J Roentgenol 181:743-748, 2003
30. Hunold P, Schmermund A, Seibel RM, et al: Prevalence and clinical significance of accidental findings in electron-beam tomographic scans for coronary artery calcification. Eur Heart J 22:1748-1758, 2001
31. Horton KM, Post WS, Blumenthal RS, et al: Prevalence of significant noncardiac findings on electron-beam computed tomography coronary artery calcium screening examinations. Circulation 106:532-534, 2002
32. Wildberger JE, Mahnken AH, Schmitz-Rode T, et al: Individually adapted examination protocols for reduction of radiation exposure in chest CT. Invest Radiol 36:604-611, 2001
33. Hara AK, Johnson CD, MacCarty RL, et al: Incidental extracolonic findings at CT colonography. Radiology 215:353-357, 2000
34. Gluecker TM, Johnson CD, Wilson LA, et al: Extracolonic findings at CT colonography: Evaluation of prevalence and cost in a screening population. Gastroenterology 124:911-916, 2003
35. Ohnesorge B, Flohr T, Becker C, et al: Cardiac imaging by means of electrocardiographically gated multisection spiral CT: Initial experience. Radiology 217:564-571, 2000
36. Trabold T, Buchgeister M, Kuttner A, et al: Estimation of radiation exposure in 16-detector row computed tomography of the heart with retrospective ECG-gating. Rofo Fortschr Geb Rontgenstr Neuen Bildgeb Verfahr 175:1051-1055, 2003
37. Hunold P, Vogt FM, Schmermund A, et al: Radiation exposure during cardiac CT: Effective doses at multi-detector row CT and electron-beam CT. Radiology 226:145-152, 2003
38. Morin RL, Gerber TC, McCollough CH: Radiation dose in computed tomography of the heart. Circulation 107:917-922, 2003
39. Wintermark M, Reichhart M, Cuisenaire O, et al: Comparison of admission perfusion computed tomography and qualitative diffusion and perfusion-weighted magnetic resonance imaging in acute stroke patients. Stroke 33:2025-2031, 2002
40. Rubin GD: MDCT imaging of the aorta and peripheral vessels. Eur J Radiol 45(Suppl 1):S42-S49, 2003

3. CONTRAST MATERIAL

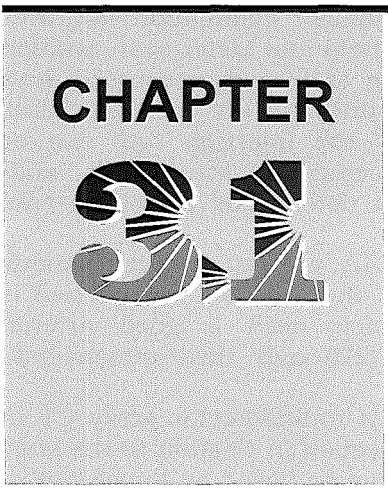

Parameters Affecting Bolus Geometry in CTA: A Review

Filippo Cademartiri[1,2]
Aad van der Lugt[1]
Giacomo Luccichenti[2]
Paolo Pavone[2]
Gabriel P. Krestin[1]

From the Department of Radiology, Erasmus MC, University Medical Center Rotterdam[1], The Netherlands, and the Department of Radiology, University of Parma[2], Italy

Journal of Computer Assisted Tomography, 106:2051-2054 26(4):598-607, 2002.

ABSTRACT:

CT angiography (CTA) is based on acquisition of data during the arterial phase of contrast material passage. CTA needs timing of the contrast bolus, which should be based on accurate knowledge of bolus geometry. Experimental and human studies on bolus geometry and bolus timing in CTA were reviewed. Important parameters of bolus geometry and methods of bolus timing (test bolus and bolus tracking) are described. Recommendations are given for an optimal CTA protocol.

Compared with CT, in which parenchymal enhancement is needed for an optimal examination, prominent vascular enhancement is necessary for CT angiography (CTA). CTA is based on fast acquisition of data during the arterial phase of contrast passage. This procedure allows the display of maximum contrast enhancement between the arterial vasculature and surrounding structures. In addition, CTA is performed before diffuse and microvascular enhancement and reflow of contrast material in venous structures.

CT angiography has been advocated as an alternative to digital subtraction angiography (DSA) in several body regions.

In the study of thoracic-abdominal aorta, CTA is already an established standard.[1-3] In other applications, such as the study of brain circulation,[4-9] carotid arteries,[5,6,10] renal arteries[11,12], and peripheral run-offs,[13] CTA has demonstrated accuracy comparable with the actual gold standards.

Recently, a new advanced application of CTA in the visualization of coronary arteries provided interesting results.[14,15] It is expected that CTA with multidetector CT scanners will result in better image quality than with single detector CT scanners because smaller collimation improves resolution (especially in the longitudinal direction) and faster scan rotation and multiple detectors increase the coverage and/or decrease the scan duration. The advantages of a shorter scan duration are threefold:[1] less contrast material (30%-50%) can be used;[2] the injection rate can be increased with a concomitant better enhancement of the vessels, and[3] most of the data can be acquired during a determined phase (arterial phase in CTA).

Scanning during the arterial phase in CTA without a clear venous enhancement may enable optimal analysis of the acquired images and is critical for postprocessing techniques, which need a good arterial enhancement to generate two-dimensional (2D) and three-dimensional (3D) angiographic images.

Therefore, to fully exploit the advantages of multidetector array CT in CTA, accurate timing of the contrast bolus injection in relation to the start of data acquisition is important. This timing can be based on knowledge of the bolus geometry.

This review describes the optimal bolus geometry and compares this with the actual bolus geometry experienced in animal experiments and human studies. The main advantage of animal studies is that they allow the repeat of contrast material injections with just one parameter changed and the others kept constant, whereas in human studies, the influence of parameters is normally studied by comparison of two or more groups of patients who may differ with regard to baseline parameters. Some human studies have used a dynamic single level CT scan to investigate the geometry of the test bolus[16] or main bolus.[17-19] However, most human studies have investigated the main bolus geometry by measuring the attenuation in vessels in consecutive slices, which correspond with a certain time increment. As a result, the measurements varied in spatial location.

Literature on bolus timing and bolus geometry in CT and CTA has been reviewed, and data on parameters that influence the bolus geometry have been extracted (Tables 1, 2). Some of these studies have focused on CTA,[16,20-33] whereas others have focused on liver enhancement patterns to improve detection of focal lesions. However, most of these studies also included data on aortic enhancement.[17-19,34-38]

In addition, different methods to predict bolus geometry are reviewed. Finally, recommendations are given for an optimal and robust scan protocol for single and multidetector CTA.

Bolus geometry

Bolus geometry is defined as the pattern of enhancement, measured in a region of interest (ROI), plotted on a time(s)/attenuation (Hounsfield units [HU]) diagram, after intravascular injection of contrast material.

Enhancement is calculated by subtracting the attenuation value of an unenhanced baseline scan, from the attenuation values in the enhanced scans.

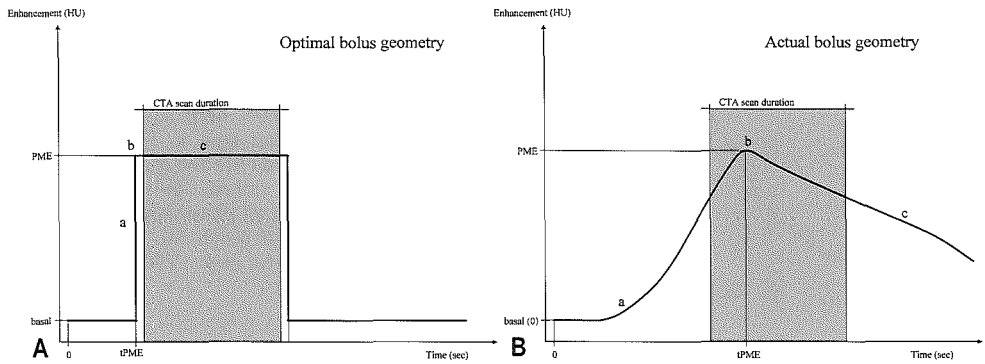

Figure 1. Bolus geometry. **A:** Optimal bolus geometry: immediate increase (a) in the enhancement of the studied artery to a peak (b) just before the start of the acquisition of CT data and a steady state (c) in which the enhancement does not alter during the data acquisition. **B:** Actual bolus geometry: steady increase in the arterial enhancement (a) until the peak of maximum enhancement (b) and then a steady decline (c). Normally CT angiography will be performed during the upslope and downslope of the enhancement curve.

The optimal bolus geometry for CTA is an immediate increase in the enhancement of the studied artery to a high maximum value of enhancement (high HU) just before the start of the acquisition of CT data and a steady state in which the enhancement does not alter during data acquisition (Fig. 1A).

However, the actual bolus geometry is different from the optimal one. After intravascular injection of contrast material with a fixed injection rate, there is a steady increase in enhancement, and the top of the curve will be reached after the end of contrast material injection, followed by a steady decrease in enhancement. Normally CTA will be performed during the upslope and downslope of the enhancement curve (Fig. 1B).

The actual bolus geometry can be characterized by several parameters: peak of maximum enhancement (PME) in HU, and time to PME in seconds (tPME). The time(s)/attenuation (HU) curve generates other parameters, but these are less important (Fig. 2).

PARAMETERS INFLUENCING BOLUS GEOMETRY

Demographics

Several studies reported that tPME is not affected by age,[21,25,39] weight,[21,25,26,39] height,[25,39] body surface,[25,39] blood pressure,[25] heart rate,[25,26] or gender,[21,25] whereas PME is not affected by age and gender[21] (Table 1).

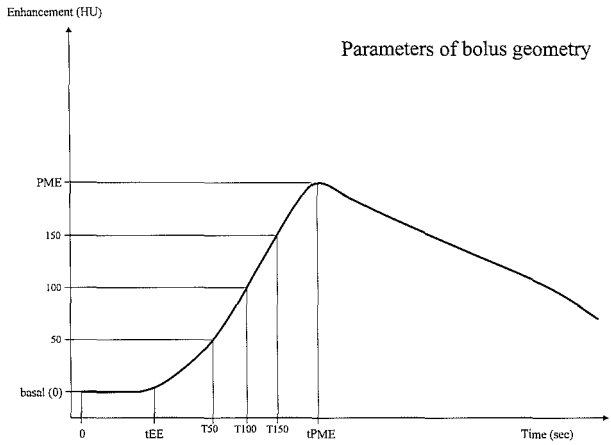

Figure 2. Parameters of time(s)/attenuation (Hounsfield unit [HU]) curve. Peak of maximum enhancement (PME) in HU and time to PME (tPME) in seconds are the main parameters. The curve generates other important parameters, such as the time to reach 50, 100, 150, and 200 HU (e.g., T50, T100, T150, T200).

TABLE 1. Parameters affecting bolus geometry

		Effect			
Parameters		PME	References	tPME	References
Demographics	Age	Unaffected	(21)	Later	(20)
				Unaffected,	(21, 25)
				Unaffected****	(39)
				Correlation***	(26)
	Weight	Lower	(21)	Unaffected	(21, 25)
		Lower*	(23)	Unaffected****	(39)
				Unaffected***	(26)
	Height			Unaffected	(25)
				Unaffected****	(39)
	Body surface			Unaffected	(25)
				Unaffected****	(39)
	Blood pressure			Unaffected	(25)
	Heart rate				
				Unaffected	(25)
	Men			Unaffected	(26)
		Unaffected	(21)	Unaffected	(21, 25)
				Slower****	(39)
Diseases	Heart disease	Higher	(27)	Slower	(20, 27)
	Severe SAH			Slower	(20)
Injection volume	Higher	Higher	(34, 35, 37)	Slower	(34, 35)
Injection rate	Higher	Higher	(17, 21, 24, 32, 34, 35)	Faster	(17, 21, 32, 34, 35)
Iodine concentration	Higher	Higher	(35)	Unaffected	(35)
Bolus chaser	With	Higher**	(44, 45)	Slower**	(44, 45)
Postprandial delivery	With	Unaffected	(18)	Unaffected	(18)
Hand exercise	With	Unaffected**	(49)		

SAH, subarachnoid hemorrhage; PME, peak of maximum enhancement; tPME, time to peak of maximum enhancement; * mean enhancement; ** attenuation (not PME) in a defined vessel segment; *** time to enhancement with 50 Hounsfield units; **** time to enhancement with 100 Hounsfield units.

However, other studies reported an inverse correlation between body weight and aortic PME[21] or mean enhancement,[23] but no explanation for this correlation is given. A higher body weight is generally associated with a higher intravascular fluid volume, which results in a lower iodine concentration (see Iodine Concentration) in blood and, consequently, in a decrease in PME.

Two studies reported a faster tPME in younger patients compared with older patients,[20,26] which may be related to better cardiac function (see Diseases) in younger patients.

Diseases

A porcine study on the effect of reduced cardiac output on aortic and liver enhancement showed that a progressive decrease in cardiac output produces a proportionally higher PME and longer tPME in the aortic bolus geometry.[27]

This was explained by the increase in circulation time and the lack of contrast material dilution, which occur during decreased cardiac output.[27] This result was confirmed in one clinical study that reported a slower tPME in patients with a history of cardiopulmonary arrest.[20] No other clinical studies have reported that cardiac function may influence bolus geometry. However, several authors may have suspected that this relationship exists because they excluded patients with cardiovascular disease from their studies on bolus geometry.[17,37,39]

In a CTA study for the detection of cerebral aneurysms, a severe grade of subarachnoid hemorrhage (SAH) was related to a slower tPME (in a test bolus).[20] This observation could be explained by neurogenic myocardial stunning after SAH, causing ventricular dysfunction.[40,41]

Injection Volume

Animal studies with different volumes of injection normalized for body weight (mL/kg) demonstrated that a higher volume of contrast material shifts the time/attenuation curve upward and rightward (Fig. 3A). This results in a higher PME and a longer tPME. The relation is independent from injection rate and iodine concentration.[34,35]

These observations are confirmed by a clinical study in which increasing contrast material volumes (1.5 mL/kg, 2.0 mL/kg, and 2.5 mL/kg) determined a proportional increase in PME (238 HU, 253 HU, and 270 HU);[37] in this study, tPME was not analyzed.

Although the normalized contrast volume seems to be a fundamental parameter for bolus geometry because it will give a predictable PME, most studies have been performed with fixed doses of contrast material.

Injection Rate

Animal studies clearly demonstrated that increasing the injection rate produces a proportionally higher PME and faster tPME with a shift of the time/attenuation curve upward and leftward (Fig. 3B). This relation is independent from iodine concentration and volume of injection.[32,34,35]

TABLE 2. Synopsis of literature on bolus geometry

Authors (reference number)	Patient variables	Volume	Iodine concentration (mI/sec)	Rate (mg/ml)	Delay	ROI	Main bolus & Test bolus: PME (HU) Mean ± SD (range)	Main bolus & Test bolus: tPME (sec) Mean ± SD (range)	Main bolus & Test bolus: T50/100/150(sec) Mean ± SD
Yamashita et al. (37)		1.5 ml/kg 2.0 mg/kg 2.5 ml/kg 100 ml	300	3.0		AA E	238 253 270 247		
Kim et al. (17)		90 ml	300	2.0 3.0 4.0 5.0		AA E	210 ± 43 288 ± 49 319 ± 59 364 ± 70	52 ± 4 37 ± 4 31 ± 3 27 ± 3	T100=26±5 T100=19±3 T100=18±4 T100=18±4
Luboldt et al. (24)		120 ml 100 ml 100 ml	300 300 400	3.0 4.5 4.0		AA A	243 ± 46 337 ± 52 434 ± 86		
Platt et al. (21)		150 ml 150 ml 15 ml (TB)	300	3.0 4.0 3.0/4.0		AA E	281 ± 49 320 ± 58	51 ± 5 45 ± 5 19 ± 4	T200=30 T200=23
Haage et al. (44)		75 ml 60 ml + 30 ml saline	370	3.0	20 sec	AsA A	240.8 ± 69.1$_1$ 238.3 ± 63.9$_1$		
Hopper et al. (45)		75 ml + 50 ml saline 125 ml	60% nonionic	2.5	20 sec	AsA A	254.8 ± 83.7$_1$ 225.2 ± 100.7$_1$		
Bader et al. (19)		40 ml + 40 ml saline	300	10		AA E	358.4 ± 79.6	15.5	
Sheafor et al. (18)	Preprandial Postprandial	150 ml 150 ml	300	4.0		AA A	389.3 367.3	39.0 39.2	
Puskas et al. (25)		20 ml (TB)	300	5.0		ICA E	66 (23–145)	16.4	
Kirchner et al. (39)	 Men Women	75 ml 75 ml	300	2.0	BTt=100	PT E AA AA AA	120 ± 21.5 112 ± 13.97	22.3 ± 7.8 28.9 ± 7.4 30.8 ± 7.4 26.6 ± 6.7	T100=22.3 ± 7.8 T100=27.4 ± 7.5
Shimizu et al. (51)		100 ml	350	2.0 2.5 3.0	BTt=100	AA E	248.3 ± 42.2$_2$ 295.2 ± 56.9$_2$ 333.5 ± 53.2$_2$		T100=30.9 ± 4.2$_3$ T100=28.7 ± 2.9$_3$ T100=28.0 ± 3.7$_3$
Van Hoe et al. (26		12 ml (TB) 90 ml	380	3.0	 TB	AA E	69 ± 18 222 ± 36	20 ± 6.15	 T50=16.7 ± 5.1 T100=18.8 ± 4.8 T150=21.3 ± 4.8
Kaatee et al. (22)		140 ml 15 ml (TB)	300	3.0	27 sec or TB	AA E	236 ± 50	51 ± 5.1 22 ± 4.5	
Bae et al. (31)		50 ml/75 ml 125 ml 125 ml	320	2.5/1.0 2.5 5		AA E	163.4 205.8 313.7		
Fleishman et al. (23)		16 ml + 20 ml saline (TB)	300	4.0		AA E		22(16–29) 19(16–24)	
Sheiman et al.(16)		10 ml (TB)	320	3.5		AA E		21.3 ± 3.2	
Nakajima et al. (20)	Age <69 yrs Age >70 yrs CPA: yes CPA: no	15 ml (TB)	300	4.0		ICA E		10.7 ± 2.3 19.7 ± 7.1 20.3 ± 8.3 11.3 ± 3.4	

Btt = Bolus tracking threshold; CPA, cardiopulmonary arrest; TB, test bolus; PME, peak of maximum enhancement; tPME, time to peak of maximum enhancement; T50, time to enhancement with 50 Hounsfield units; ROI, region of interest; AA, abdominal aorta; AsA, ascending aorta; ICA, internal carotid artery; PT, pulmonary trunk; E, enhancement; A, attentuation; 1, these values are the attenution in the ascending aorta (no PME); 2, enhancement values in the first slice of the arterial phase; 3, values extracted from the last monitoring scan (>100 HU) during bolus tracking technique.

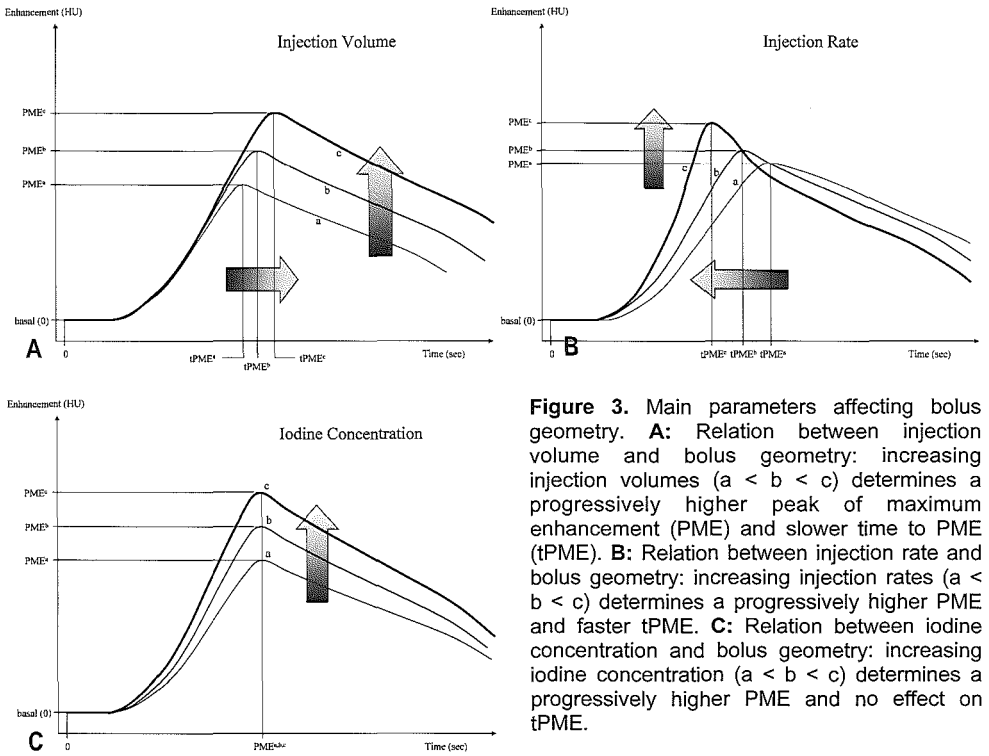

Figure 3. Main parameters affecting bolus geometry. **A:** Relation between injection volume and bolus geometry: increasing injection volumes (a < b < c) determines a progressively higher peak of maximum enhancement (PME) and slower time to PME (tPME). **B:** Relation between injection rate and bolus geometry: increasing injection rates (a < b < c) determines a progressively higher PME and faster tPME. **C:** Relation between iodine concentration and bolus geometry: increasing iodine concentration (a < b < c) determines a progressively higher PME and no effect on tPME.

Clinical studies have confirmed these experimental observations. Kim et al.[17] found that 90 mL contrast material volume with an injection rate of 2 mL/s, 3 mL/s, 4 mL/s, and 5 mL/s resulted in a mean PME of 210 HU, 288 HU, 319 HU, and 364 HU and a mean tPME of 52 seconds, 37 seconds, 31 seconds, and 27 seconds, respectively. Other studies reported similar findings.[21,24]

One study found that higher injection rates resulted in a lower PME and a slower tPME.[42] This apparently contradictory observation is easily explained: the CT scan was started with a fixed delay of 50 seconds; with a higher injection rate, the tPME is less than 50 seconds, and the dynamic scan is performed after the PME during the downslope of the curve, whereas with a lower injection rate, the PME is still to come.

Some groups have studied multiphasic protocols in which the injection rate is decreased during the contrast injection.[23,29-31,33] A bolus with constant volume, rate, and iodine concentration normally results in an enhancement curve that increases the end of the contrast material administration, after which a decrease of enhancement led to the equilibrium phase. The aim of multiphasic techniques is to get a plateau of enhancement during the scan.

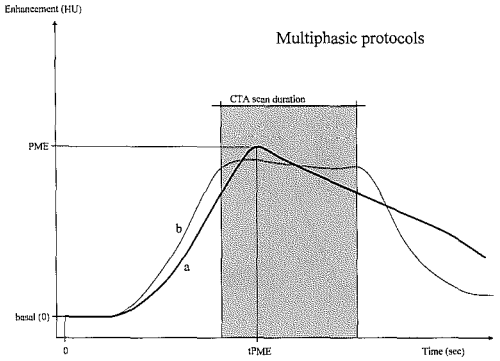

Figure 4. Effect of multiphasic injection protocols. Normal uniphasic bolus geometry with a consistant injection rate, volume, and iodine concentration (a) and biphasic bolus geometry (b) are shown. The enhancement of the biphasic protocol is more homogeneous and more prolonged than the uniphasic one.

A higher injection rate at the beginning of the injection and a lower rate in the second part of the injection produce a curve more similar to the "optimal" bolus geometry with a plateau of enhancement (Fig. 4). Because of their complex approach, multiphasic protocols are not performed in routine clinical practice.

Iodine Concentration

Animal studies demonstrated that higher iodine concentrations produce a proportionally higher PME (Fig. 3C). As expected, tPME was unaffected.[35,43] With different iodine concentrations and with constant rate and volume, the injection duration remains unchanged, meaning that the tPME remains the same.

Bolus Chaser

A bolus chaser is a saline solution pushed through the injection line immediately after the injection of the main bolus (Fig. 5). This technique is mostly used for MRI gadolinium injection or intravenous DSA. Several authors found advantages from this technique in CT.[19,44,45]

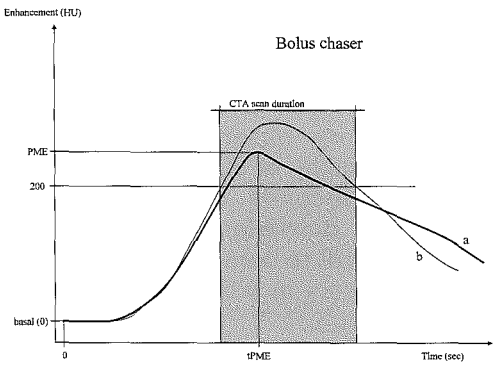

Figure 5. Effect of bolus chaser on main bolus geometry. Normal bolus geometry (a) and the effect of a bolus chaser (b) are displayed. The upslope of the curves is almost the same, but the chaser increases the enhancement even after the end of contrast injection, resulting in an increased peak to maximum enhancement (PME) and a slower time to PME (tPME; injection rate is the same). The advantage of this technique is that arterial enhancement remains above a certain level for a longer period than without using a bolus chaser.

Bolus chaser could be administered by a parallel power-injectors technique[44] or by layering the saline solution above the contrast material within the same syringe.[19,45] Two clinical studies compared contrast bolus administration with and without a bolus chaser while the contrast volume had been lowered in the injection regimen, which included a bolus chaser. With less contrast and a bolus chaser, the same PME was observed as with more contrast material but without bolus chaser: in one study, the

same attenuation (not PME) in the ascending aorta was experienced comparing a 60 mL contrast material and 30 mL saline chaser versus a 75 mL contrast material (240 HU for both);[44] in another study, almost the same attenuation (not PME) in the ascending aorta was observed using 75 mL contrast material with 50 mL bolus chaser and 125 mL contrast material alone (254 HU vs. 225 HU, respectively).[45] No information about tPME is provided in these studies.

The advantage of bolus chaser seems to be twofold.

1) Less contrast material volume (20% - 40% less) is needed for a CTA scan, while a significant arterial enhancement can still be obtained. For example, a mean aortic PME of 358 HU can be reached with a 40 mL bolus of contrast material (iodine concentration = 300 mg/mL) followed immediately by a 40 mL saline chaser through an antecubital vein at a 10 mL/s rate.[19]
2) A reduction of superior vena cava artefacts with the same arterial enhancement.

The explanation of these findings is also twofold.

1) The saline chaser pushes the injected contrast material through the veins of the forearm, which will give the same result as the injection of a larger contrast volume. An increase in PME and tPME is therefore expected if a bolus chaser is added to the contrast injection,[36] whereas no increase in PME and tPME is expected if a bolus chaser is added to the injected volume with a concomitant decrease in the contrast volume, resulting in an unchanged total injection volume.
2) Saline chaser prevents the decrease of the contrast material flow in the arm veins, which may normally cause an increase in the contrast material concentration after the end of the contrast injection. However, the ability to decrease the total amount of contrast is the main cause of the reduction of perivenous artefacts.[44,45]

Pre- and Postprandial Delivery

Sheafor et al.[18] studied differences in aortic and liver contrast enhancement before and after a liquid meal. They presupposed that the increase of superior mesenteric artery blood flow and volume after a meal could affect liver enhancement.[46-48] This might have resulted in a lower PME and a faster tPME in aortic enhancement caused by increased cardiac output. However, they found no significant differences in liver and aortic contrast enhancement pre- and postprandial.[18]

Hand Exercise During Bolus Delivery

One study reported that an intermittent squeezing of a hand-sized ball during delivery of contrast material produces a reduction of perivenous artefacts in the apex of thorax, while the same image quality was provided with the same arterial attenuation and less venous attenuation.[49] However, the injection rates in that study were different in each patient (to allow the overall injection time to be constant), and it is not possible to assess the exact influence of injection protocol on arterial enhancement. The reduction in perivenous artefacts suggests that the effect of hand exercise is comparable with the use of a bolus chaser because the increase in

muscular tone will prevent the stasis of contrast material in the arm veins after the end of contrast injection.

Injection Site

Two typical sites of injection of contrast material for CTA have been used:

1) an antecubital vein, which is generally easy to find in the anterior region of elbow joint; these veins drain directly into the deep venous circulation of the arm (basilic vein); and
2) a forearm vein, which is part of the superficial venous plexus of the forearm and drains directly into the deep venous circulation of the forearm and subsequently into the deep venous circulation at the elbow joint or into the subclavian vein through the cephalic vein.

In many studies, contrast material has been administered through an antecubital vein in all the patients[19,22-25,39,44] or in most of them.[21] In other studies, it was not clear which venous access was used[18] or if the investigators included all venous accesses.[50] No study demonstrated whether an antecubital access is better than a forearm access in terms of bolus geometry. In one recent study, a peripheral cubital access was compared with a central (superior vena cava) one. The biphasic injection protocol was based on a predicted time-attenuation response of a test bolus. As expected, the deviation of the observed from the predicted enhancement was larger, and the calculated delay of the main bolus was longer in the patients with peripheral injection. This might have been because of small amounts of contrast material remaining in the peripheral venous system, which does not contribute to the test bolus geometry. The calculated injection rates were systematically higher than actually needed.[29] It is therefore expected that forearm injection is inferior to antecubital injection for test bolus and main bolus.

PREDICTION OF BOLUS GEOMETRY

Patient Demographics

Puskas et al.[25] proposed an algorithm ($t = N \times 60 \times f^{-1}$; N = duration of 12 heart actions; t = tPME; f = heart rate) to predict venoarterial circulation time (tPME) for intracranial vasculature. They compared the results with the actual tPME assessed with a test bolus (20 mL; 5 mL/s). However, no correlation was found between the calculated tPME and actual tPME. Another clinical study demonstrated poor results (poor image quality in 31% of the cases) when using this algorithm for calculation of the delay time.[20].

Bolus Tracking

In bolus tracking technique, an ROI is plotted inside the lumen of an artery close to the region that is to be studied, and a trigger attenuation value (threshold) is arbitrarily chosen before starting the CTA data acquisition. A single level low-dose dynamic scan is performed at determined intervals of time during the injection of contrast material. When the contrast material arrives at the level of the ROI, the change in attenuation is detected, and a CT scan is started after reaching the triggering threshold.

Parameters of great importance during bolus tracking technique are transition delay (TD) and interscan delay (ID).

Transition delay is the delay between the time at which the threshold is reached, and the start of the actual CTA scan. Different values of TD ranging from 5 to 15 seconds have been reported.[36,38,50,51] In some cases, this long time depends partly on repositioning of the table, especially when the dynamic scan is done at a different level than the main scan.[38,50]

Interscan delay is the time between the consecutive dynamic scans. Reported ID ranged from 0.33 seconds to 6.0 seconds.[36,38,50,51]

These two parameters (TD and ID) modify the starting time of the CTA scan. With an ID of 6 seconds, the CTA scan would probably start later than with an ID of 1 second. With a long ID, it would not be possible to avoid prominent venous enhancement. With a short ID, the same problem is encountered if the TD is too long.

Newer scanners have a TD of 4 seconds, even if the monitoring scans are not performed at the same level of the scan start. These 4 seconds are useful to give the patient breathing instructions when the region being scanned is the chest or the abdomen. The threshold should be 100-150 HU above the baseline level of the ROI. With these settings, the first monitoring slice with a value equal or above 100-150 HU starts the procedure. After 4 seconds, the scan starts, and generally the enhancement of the arterial vessel is more than 250 HU (absolute value).

The advantages of bolus tracking are twofold. Bolus tracking resulted in a better timing of the CT scan in relation to the time/attenuation curve and allows the use of less contrast material at a higher injection rate.

In one study, bolus tracking was compared with fixed delay (20 seconds). In the group with fixed delay, the CT scan started before the beginning of the arterial phase of enhancement (not PME) in aorta (defined as a splenic parenchymal enhancement of 10 HU) in 17% of the patients, whereas bolus tracking resulted in the scanning after the onset of the arterial phase in all patients.[38]

In another study, 548 patients underwent thoracic and abdominal CT scan with bolus tracking technique. The scan was started when the threshold was reached in the abdominal aorta or in the main trunk of the pulmonary artery (mean bolus of 75 mL). Failure was encountered in 48 CT studies because of nonachievement of the 100 HU threshold (n = 25), no significant enhancement after 80 seconds (n = 8), or computer problems leading to interruption of data acquisition (n 15).[39]

When the threshold is not reached, it is still possible to start the scan manually. In this case, it is difficult to obtain a high quality CTA because of the later start of the scan and the decreased amount of contrast material inside the vessels.

Test Bolus

In test bolus technique, an ROI is plotted inside the lumen of an artery close to the region that is to be studied. A small amount of contrast material (10-15 mL) at the same rate of the main bolus is injected while a single level low-dose dynamic scan is performed at determined intervals of

time. When the contrast material arrives inside the lumen of the artery at the level of the ROI, the test bolus geometry is assessed, and the time between the start of the test bolus injection and a determined point of the time/attenuation curve of the test bolus is used as delay time for the injection of the main bolus.

The use of a test bolus to assess the venoarterial circulation time (tPME) for intracranial vasculature resulted in correct timing of CTA in all patients.[25] The use of a test bolus presupposes a relationship between the bolus geometry of the test bolus and main bolus. Two studies did not find a correlation between test bolus tPME and moderate correlation.[22] However, a strong correlation was found between test bolus tPME and time to reach determined attenuation thresholds like T50,[26] T100,[26] T150,[21,26] and T200[21] (i.e., the time from the beginning of the injection to reach 50, 100, 150, and 200 HU in the ROI) in main bolus (Fig. 6). These observations support the hypothesis that test bolus has a different geometry than the main bolus, which is related to the lack of injection power after the injection of the test bolus that results in a pooling of the test bolus in the venous system. In other words, the test bolus is left alone in the venous system after the injection, without the help of saline solution (bolus chaser) or adjunctive contrast material (main bolus) pushing it forward. This phenomenon results in dilution and slowing of the test bolus.

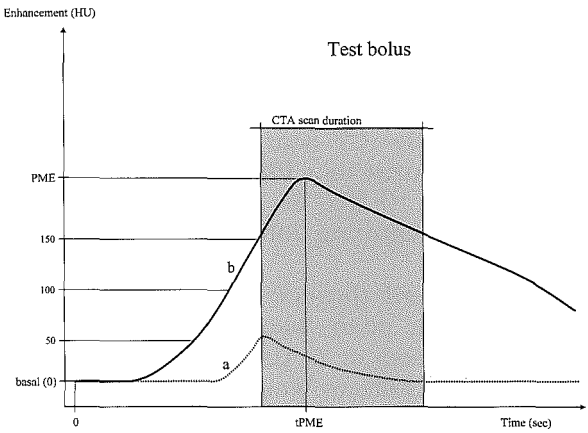

Figure 6. Expected correlation between test bolus and main bolus. Test bolus peak to maximum enhancement (PME) is known to lack correlation with main bolus PME, but a good correlation has been demonstrated between test bolus PME and the time to reach 150 HU and 200 HU in main bolus.

The use of a test bolus to assess the delay time for CTA has been compared with fixed delays. One study reported better results (image quality)[20] with the use of a test bolus, whereas another study did not demonstrate a better enhancement.[21]

Mathematical Modeling

Two mathematical models have recently been developed to predict main bolus geometry.[23,28-33] Fleishmann et al.[30] considered the patient as a complex system that can be described as a black box and can be analyzed by the input and output of the system. The transfer function of the system can be calculated from the arterial time-attenuation response (output) to the test bolus (input). With this function, it is possible to calculate the

bolus protocol that is supposed to achieve a defined "ideal" arterial enhancement. The "ideal" bolus protocol is approximated into a practically applicable optimized biphasic injection protocol.

The input is

1) parameters of test bolus injection (volume and injection rate),
2) respective time-attenuation response,
3) anticipated duration of CTA, and
4) level of desired enhancement. The output is a biphasic, customized protocol (injection rates, volumes, and delay) for bolus administration.

Comparison of uniphasic contrast material injection (4 mL/s) with a delay based on the tPME of a test bolus versus a computed biphasic injection protocol (based on the time-attenuation response of a test bolus) resulted in a significantly less plateau deviation with a more uniform enhancement in the patients with a calculated biphasic protocol.[23]

Bae et al. developed a compartmental pharmacokinetic model.[31-33] Based on body habitus data (weight, gender, height), parameters that influenced the bolus geometry (cardiac output and blood volume) were calculated, and the expected distribution of contrast material inside the system was assessed. The time-enhancement curve for a given contrast material protocol could be calculated. They found good agreement between the simulated and the empiric curve of enhancement in a human study (mean percent difference in aortic enhancement = 7.4%).

RECOMMENDATIONS

Single detector ct angiography

Single detector CTA is limited by several factors. A high resolution in the z axis combined with a long coverage is not possible because of limited tube load, relative long rotation times, and constraints on data transfer and storage. An increase in coverage is possible by an increase in table feed per rotation (pitch), which subsequently leads to broadening of the slice sensitivity profile and a decrease in resolution. To extend the coverage, an increased pitch is preferable above a larger collimation because the image degradation resulting from the increased pitch is far outweighed by the ability to use thinner collimations.[52] The long scan time is problematic for CTA acquistion in the thorax and abdomen, where breath-hold scans are necessary to obtain optimal images. In addition, long scan times result in prominent venous enhancement, which may hamper interpretation or postprocessing. Finally, long scan duration needs a long contrast material injection with lower injection rates than preferable.

The protocol design will be governed by the following steps:

1. Assess the length of the scan volume (coverage).
2. Assess the maximum length of scan time possible, given the required kVp and mA or given the maximum length of breath-hold capability.
3. Calculate the table speed (table movement/s) and the table feed per gantry rotation (speed/rotation time) for the fastest rotation time.
4. Set the smallest collimation allowed with a pitch (feed/collimation) 2.

5. The scan time and the use of bolus timing techniques determine the injection rate and the amount of contrast material.

Multidetector CT Angiography

Multidetector CTA has fewer limitations. Even without an increase in tube load and an increase in maximum scan time, there is a substantial increase in performance because of the increase in rotation time and the number of detectors. Besides that, an increase in pitch does not lead to a broadening of the slice sensitivity profile (until pitch of 8) because of the application of dedicated reconstruction algorithms. This increased performance can be used to reduce the scan time and the amount of contrast material or to increase the resolution in the z axis. The protocol design will be governed by the following steps:

1. Assess the length of the scan volume (coverage).
2. Determine the necessary spatial resolution in the z axis (detector collimation of 0.5, 1.0, or 2.5 mm). Small arteries, like cerebral, renal, and coronary arteries, need a collimation of 0.5-1.0 mm. Larger arteries, like the aorta and carotid, pulmonary, iliac, and femoral arteries, need a 1.0-2.5 mm collimation.
3. Assess the maximum scan time in case of thoracic or abdominal CTA based on the breath-hold capabilities.
4. Based on the scan volume, collimation, and scan time, the pitch can be calculated (pitch scan volume/(scan time x rotation time x number of detectors x collimation).
5. The scan time and the use of bolus timing techniques determine the injection rate and the amount of contrast material.

Contrast Material (Volume, Injection Rate, and Delay)

The ideal situation is a contrast volume normalized for body weight because this will give a predictable enhancement of the arteries. In daily practice, a fixed amount of contrast material is generally applied (100 - 125 mL). The injection rate will depend on the ability to use bolus-timing techniques, such as bolus tracking or test bolus technique. Without such techniques, scan delay is fixed and based on experience with regard to the mean arteriovenous transit time. For neck, brain, and thoracic CTA, delay times of 15-20 seconds, and for abdominal and peripheral arteries, delay times of 25-30 seconds have been proposed. In this case, injection rate is normally not more than 2-3 mL/s because this will result in a long injection duration (longer than the scan time). This increases the probability that the CTA is performed during the arterial passage of contrast material. In case of bolus timing techniques, the injection duration can be the same as the scan time, and the injection rate is determined by the formula: contrast material volume/injection duration in case of a fixed amount of contrast, or the amount of contrast material is determined by the formula: injection rate x injection duration in the case of a fixed injection rate (4-5 mL/s). Increasing the injection rate above 5 mL/s will not provide significant improvement in the enhancement of the arterial structures.

REFERENCES

1. Prokop M. Multislice CT angiography. Eur J Radiol 2000;36: 86-96.
2. Wu CM, Urban BA, Fishman EK. Spiral CT of the thoracic aorta with 3-D volume rendering: a pictorial review of current applications. Cardiovasc Intervent Radiol 1999;22:159-67.
3. Jeffrey RB Jr. CT angiography of the abdominal and thoracic aorta. Semin Ultrasound CT MR 1998;19:405-12.
4. Anderson GB, Steinke DE, Petruk KC, et al. Computed tomographic angiography versus digital subtraction angiography for the diagnosis and early treatment of ruptured intracranial aneurysms. Neurosurgery 1999;45:1315-20.
5. Seemann MD, Englmeier K, Schuhmann DR, et al. Evaluation of the carotid and vertebral arteries: comparison of 3D SCTA and IA-DSA-work in progress. Eur Radiol 1999;9:105-12.
6. Verhoek G, Costello P, Khoo EW, et al. Carotid bifurcation CT angiography: assessment of interactive volume rendering. J Comput Assist Tomogr 1999;23:590-6.
7. Aoki S, Sasaki Y, Machida T, et al. 3D-CT angiography of cerebral arteriovenous malformations. Radiat Med 1998;16:263-71.
8. Velthuis BK, Rinkel GJ, Ramos LM, et al. Subarachnoid hemorrhage: aneurysm detection and preoperative evaluation with CT angiography. Radiology 1998;208:423-30.
9. White PM, Wardlaw JM, Easton V. Can noninvasive imaging accurately depict intracranial aneurysms? A systematic review. Radiology 2000;217:361-70.
10. Belsky M, Gaitini D, Goldsher D, et al. Color-coded duplex ultrasound compared to CT angiography for detection and quantification of carotid artery stenosis. Eur J Ultrasound 2000;12:49-60.
11. Prokop M. Protocols and future directions in imaging of renal artery stenosis: CT angiography. J Comput Assist Tomogr 1999; 23:S101-10.
12. Smith PA, Fishman EK. Three-dimensional CT angiography: renal applications. Semin Ultrasound CT MR 1998;19:413-24.
13. Rieker O, Duber C, Schmiedt W, et al. Prospective comparison of CT angiography of the legs with intraarterial digital subtraction angiography. AJR Am J Roentgenol 1996;166:269-76.
14. Nieman K, Oudkerk M, Rensing B, et al. Coronary angiography with multislice helical computed tomography. Lancet 2001;357: 599-603.
15. Achenbach S, Ulzheimer S, Baum U, et al. Noninvasive coronary angiography by retrospectively ECG-gated multislice spiral CT. Circulation 2000;102:2823-8.
16. Sheiman RG, Prassopoulos P, Raptopoulos V. CT detection of layering of i.v. contrast material in the abdominal aorta. AJR Am J Roentgenol 1998;171:1291-5.
17. Kim T, Murakami T, Takahashi S, et al. Effects of injection rates of contrast material on arterial phase hepatic CT. AJR Am J Roentgenol 1998;171:429-32.
18. Sheafor DH, Keogan MT, DeLong DM, et al. Dynamic helical CT of the abdomen: prospective comparison of pre- and postprandial contrast enhancement. Radiology 1998;206:359-63.
19. Bader TR, Prokesch RW, Grabenwoger F. Timing of the hepatic arterial phase during contrast-enhanced computed tomography of the liver: assessment of normal values in 25 volunteers. Invest Radiol 2000;35:486-92.

20. Nakajima Y, Yoshimine T, Yoshida H, et al. Computerized tomography angiography of ruptured cerebral aneurysms: factors affecting time to maximum contrast concentration. J Neurosurg 1998;88:663-9.
21. Platt JF, Reige KA, Ellis JH. Aortic enhancement during abdominal CT angiography: correlation with test injections, flow rates, and patient demographics. AJR Am J Roentgenol 1999;172:53-6.
22. Kaatee R, Van Leeuwen MS, De Lange EE, et al. Spiral CT angiography of the renal arteries: should a scan delay based on a test bolus injection or a fixed scan delay be used to obtain maximum enhancement of the vessels? J Comput Assist Tomogr 1998;22: 541-7.
23. Fleischmann D, Rubin GD, Bankier AA, et al. Improved uniformity of aortic enhancement with customized contrast medium injection protocols at CT angiography. Radiology 2000;214:363-71.
24. Luboldt W, Straub J, Seemann M, et al. Effective contrast use in CT angiography and dual-phase hepatic CT performed with a subsecond scanner. Invest Radiol 1999;34:751-60.
25. Puskas Z, Schuierer G. Kreislaufzeitbestimmung zur Optimierung der Kontrastmittelapplikation bei der CT-Angiographie. Radiologe 1996;36:750-7.
26. van Hoe L, Marchal G, Baert AL, et al. Determination of scan delay time in spiral CT-angiography: utility of a test bolus injection. J Comput Assist Tomogr 1995;19:216-20.
27. Bae KT, Heiken JP, Brink JA. Aortic and hepatic contrast medium enhancement at CT. Part II. Effect of reduced cardiac output in a porcine model. Radiology 1998;207:657-62.
28. Hittmair K, Wunderbaldinger P, Fleischmann D. Bolusoptimierte CT-Angiographie. Radiologe 1999;39:93-9.
29. Hittmair K, Fleischmann D. Accuracy of predicting and controlling time-dependent aortic enhancement from a test bolus injection. J Comput Assist Tomogr 2001;25:287-94.
30. Fleischmann D, Hittmair K. Mathematical analysis of arterial enhancement and optimization of bolus geometry for CT angiography using the discrete fourier transform. J Comput Assist Tomogr 1999;23:474-84.
31. Bae KT, Heiken JP, Brink JA. Aortic and hepatic contrast medium enhancement at CT. Part I. Prediction with a computer model. Radiology 1998;207:647-55.
32. Bae KT, Heiken JP, Brink JA. Aortic and hepatic peak enhancement at CT: effect of contrast medium injection rate-pharmacokinetic analysis and experimental porcine model. Radiology 1998; 206:455-64.
33. Bae KT, Tran HQ, Heiken JP. Multiphasic injection method for uniform prolonged vascular enhancement at CT angiography: pharmacokinetic analysis and experimental porcine model. Radiology 2000;216:872-80.
34. Garcia P, Genin G, Bret PM, et al. Hepatic CT enhancement: effect of the rate and volume of contrast medium injection in an animal model. Abdom Imaging 1999;24:597-603.
35. Han JK, Kim AY, Lee KY, et al. Factors influencing vascular and hepatic enhancement at CT: experimental study on injection protocol using a canine model. J Comput Assist Tomogr 2000;24: 400-6.
36. Sadick M, Lehmann KJ, Diehl SJ, et al. Bolustriggerung und NaCl- Bolus bei der biphasischen Spiral-CT des Abdomens. Rofo Fortschr Geb Rontgenstr Neuen Bildgeb Verfahr 1997;167:371-6.

37. Yamashita Y, Komohara Y, Takahashi M, et al. Abdominal helical CT: evaluation of optimal doses of intravenous contrast material— a prospective randomized study. Radiology 2000;216: 718-23.
38. Kopka L, Rodenwaldt J, Fischer U, et al. Dual-phase helical CT of the liver: effects of bolus tracking and different volumes of contrast material. Radiology 1996;201:321-6.
39. Kirchner J, Kickuth R, Laufer U, et al. Optimized enhancement in helical CT: experiences with a real-time bolus tracking system in 628 patients. Clin Radiol 2000;55:368-73.
40. Handlin LR, Kindred LH, Beauchamp GD, et al. Reversible left ventricular dysfunction after subarachnoid hemorrhage. Am Heart J 1993;126:235-40.
41. Kono T, Morita H, Kuroiwa T, et al. Left ventricular wall motion abnormalities in patients with subarachnoid hemorrhage: neurogenic stunned myocardium. J Am Coll Cardiol 1994;24:636-40.
42. Gocke P, Gocke C, Neumann K, et al. Prospective randomized study for an injection protocol for intravenous contrast media in abdominal and pelvic helical CT. Acta Radiol 1999;40:515-20.
43. Bluemke DA, Fishman EK, Anderson JH. Effect of contrast concentration on abdominal enhancement in the rabbit: spiral computed tomography evaluation. Acad Radiol 1995;2:226-31.
44. Haage P, Schmitz-Rode T, Hubner D, et al. Reduction of contrast material dose and artifacts by a saline flush using a double power injector in helical CT of the thorax. AJR Am J Roentgenol 2000; 174:1049-53.
45. Hopper KD, Mosher TJ, Kasales CJ, et al. Thoracic spiral CT: delivery of contrast material pushed with injectable saline solution in a power injector. Radiology 1997;205:269-71.
46. Burkart DJ, Johnson CD, Reading CC, et al. MR measurements of mesenteric venous flow: prospective evaluation in healthy volunteers and patients with suspected chronic mesenteric ischemia. Radiology 1995;194:801-6.
47. Sidery MB, Cowley AJ, MacDonald IA. Cardiovascular responses to a high-fat and a high-carbohydrate meal in healthy elderly subjects. Clin Sci 1993;84:263-70.
48. Pugliese D, Ohnishi K, Tsunoda T, et al. Portal hemodynamics after meal in normal subjects and in patients with chronic liver disease studied by echo-Doppler flowmeter. Am J Gastroenterol 1987;82:1052-6.
49. Nakayama M, Yamashita Y, Oyama Y, et al. Hand exercise during contrast medium delivery at thoracic helical CT: a simple method to minimize perivenous artifact. J Comput Assist Tomogr 2000;24: 432-6.
50. Paulson EK, Fisher AJ, DeLong DM, et al. Helical liver CT with computer-assisted bolus-tracking technology: is it possible to predict which patients will not achieve a threshold of enhancement? Radiology 1998;209:787-92.
51. Shimizu T, Misaki T, Yamamoto K, et al. Helical CT of the liver with computer-assisted bolus-tracking technology: scan delay of arterial phase scanning and effect of flow rates. J Comput Assist Tomogr 2000;24:219-23.
52. Hu H, He HD, Foley WD, et al. Four multidetector-row helical CT: image quality and volume coverage speed. Radiology 2000;215: 55-62.

3. CONTRAST MATERIAL

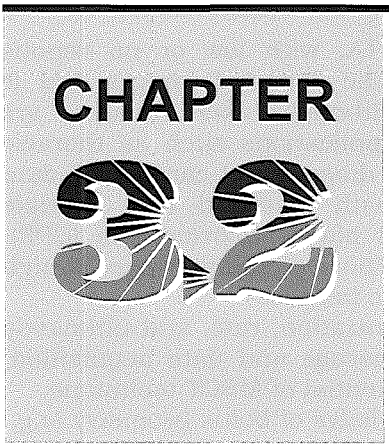

CONTRAST MATERIAL INJECTION TECHNIQUES FOR CT ANGIOGRAPHY OF THE CORONARY ARTERIES

Filippo Cademartiri, MD
Koen Nieman, MD

From the Department of Radiology,
Erasmus MC, University Medical Center Rotterdam,
The Netherlands.

CT of the Heart: Principles and Applications;
Edited by: U. Joseph Schoepf – pp. 237-245;

INTRODUCTION

Conventional catheter angiography is based on capturing X-ray images of the iodinated contrast material (CM) while it flows into the vessels. Computed tomography angiography (CTA) is based on the same concept, scanning the patient and his/her heart while a high concentration of iodinated CM flows through the coronary arteries.[1] The CM inside the vessels increases the density of the vessel lumen compared to the surrounding tissues, and allows us to distinguish between lumen and soft tissues.

Because the CM is administered intravenously in CTA, the optimal phase to scan coronary arteries will be the arterial one. In fact, during the delayed phase, several tissues enhance due to the CM perfusion, and the CM itself dilutes into the extracellular fluid, reducing the intravascular attenuation. Then vessels are no longer easily visualized as in the arterial phase.[1]

Helical/spiral computed tomography technology was limited by low speed and spatial resolution. Multislice computed tomography (MSCT) technology provides better image quality because of thinner slice thickness, and faster acquisition time because of reduced scan rotation time and multiple detector rows. The advantages of MSCT technology related to CM use are:

1) use of less CM (30-50%)
2) the injection rate can be increased with a concomitant better enhancement of the vessels and
3) most of the data can be acquired during a defined phase (e.g., arterial phase for CTA).[1]

The latest generation of helical/spiral computed tomography (CT) scanner, featuring up to 16-row MSCT technology, provides fast data acquisition, increasing the need for an accurate optimization of CM administration and synchronization techniques.

Scanning during the arterial phase in CTA, with low or no venous enhancement, enables optimal analysis of the acquired images and is critical for postprocessing techniques. Although axial images are commonly used for other conventional CT applications such as thoracic and abdominal imaging, for visualization and diagnosis of cardiac CT data sets, 2D multiplanar reformations (MPR) with standard and multiple intensity projection (MIP) algorithms, curved planar reformations (CPR), and 3D reconstructions are more important. Those techniques need a high vascular contrast in order to provide diagnostic images.

For all of these reasons, CM volume, concentration, rate, and ultimately the synchronization between CM material passage and data acquisition, need to be optimized in order to exploit the potential of MSCT technique.

The bolus timing can be based on the knowledge of bolus geometry (e.g., demographics-based delay or fixed delay), but can better rely on synchronization techniques. An optimal timing is achieved by predicting the veno-arterial transit time (e.g., test bolus), or synchronizing data acquisition with CM passage (e.g., bolus tracking).

BASICS OF BOLUS GEOMETRY

Bolus geometry is the pattern of enhancement plotted on a time(s)/attenuation (Hounsfield units-HU) curve, after intravascular injection of contrast material, and measured in a region of interest (ROI).[1] The value of enhancement is extracted by subtracting the attenuation value in an unenhanced baseline scan from the attenuation values in the enhanced scans.[1]

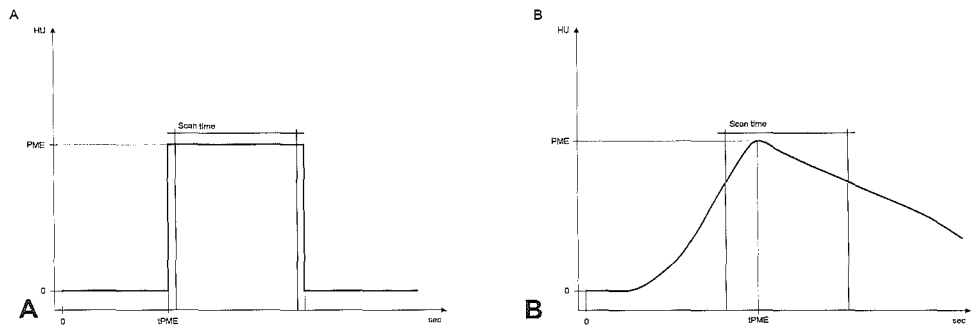

Figure 1. Optimal and actual bolus geometry in CT angiography (CTA). (**A**) Optimal bolus geometry. The abrupt rise and the steady plateau of attenuation characterize the optimal pattern of bolus geometry. Ideally, the scan time tightly overlaps with the length of the plateau of enhancement in order to use the entire volume of contrast material (CM) administered for the acquisition. (**B**) Actual bolus geometry. The pattern of actual bolus geometry is quite different from the ideal one. Before and after the peak of maximum enhancement there are slopes of enhancement. Generally the up-slope is steeper than the down-slope, especially with CM administration protocols for CTA characterized by a high injection rate.

Optimal bolus geometry, for the purpose of CTA, corresponds to an immediate rise to the maximum value of enhancement (high attenuation-HU) just before the start of the acquisition of CT data, and a steady state in which the enhancement does not alter during data acquisition (Fig. 1A). Actual bolus geometry is different. After intravascular injection of CM, there is a steady increase in enhancement; the peak of the curve will be reached after the end of contrast injection, followed by a steady decline in the enhancement. Normally, CTA will be performed during the upslope and downslope of the enhancement curve, and the peak of maximum enhancement (PME) will be inside the scan period (Fig. 1B).

The actual bolus geometry can be defined by the peak of maximum enhancement in HU (PME) and the time to reach that peak in seconds (tPME).[1]

PARAMETERS INFLUENCING BOLUS GEOMETRY

1. Demographics.

The time to peak (tPME) is not affected by age,[2-4] weight,[2-5] height,[3,4] body surface,[3,4] blood pressure,[3] heart rate,[3,5] and gender,[2,3] and PME is not affected by age or gender.[2] A heavier body weight is associated with a higher extracellular intravascular fluid volume. This results in a dilution of CM with a lower iodine concentration in blood, and therefore a reduced PME.

2. Diseases

A reduced cardiac output produces a proportionally higher PME and longer tPME in the aortic bolus geometry.[6] This is a result of the increase in circulation time and CM "pooling," which occur during reduced cardiac output conditions.[6]

3. Injection Volume

A higher volume of CM shifts the time/attenuation curve upwards and rightwards (Fig. 2A).[1] This determines a higher PME and a longer tPME. The relation is independent of injection rate and iodine concentration.[7-9]

4. Injection Rate

Increasing the injection rate produces a proportionally higher PME and earlier tPME with a shift of the time/attenuation curve upwards and leftwards (Fig. 2B).[1] The relationship is independent of iodine concentration and CM injection volume.[2,6-8,10,11]

5. Iodine Concentration

Higher iodine concentration produces a higher PME (Fig. 2C).[18,12] Different iodine concentrations with constant rate and volume, do not affect the injection duration, and this means that the tPME remains unchanged.

6. Bolus chaser

A bolus chaser is a saline solution pushed through the injection line immediately after the injection of the main bolus.[1] Advantages are reported from this technique applied in CT.[13-15] Bolus chaser is generally administered by a doublehead power injector system.[13] With bolus chaser, less contrast medium volume (up to 40% less) can be used for a CTA scan,

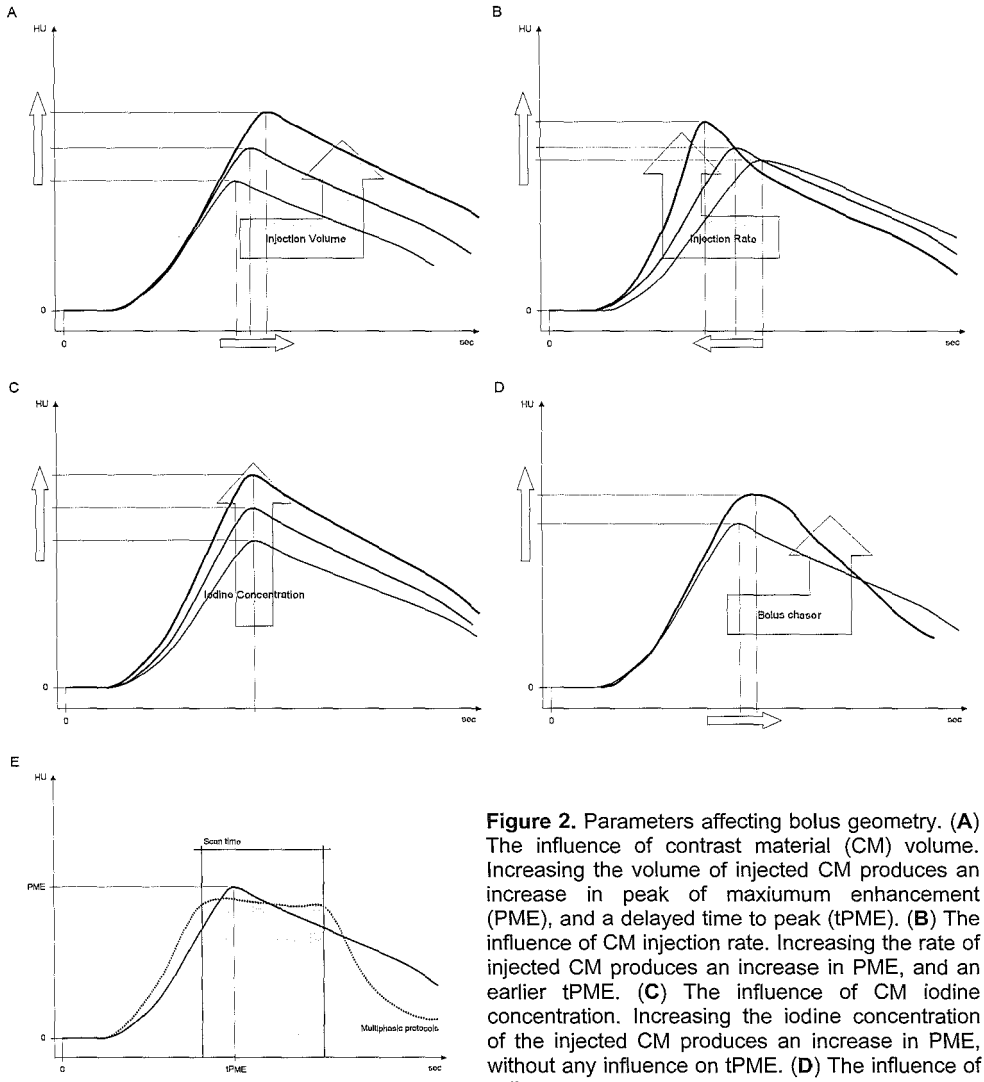

Figure 2. Parameters affecting bolus geometry. (**A**) The influence of contrast material (CM) volume. Increasing the volume of injected CM produces an increase in peak of maxiumum enhancement (PME), and a delayed time to peak (tPME). (**B**) The influence of CM injection rate. Increasing the rate of injected CM produces an increase in PME, and an earlier tPME. (**C**) The influence of CM iodine concentration. Increasing the iodine concentration of the injected CM produces an increase in PME, without any influence on tPME. (**D**) The influence of saline chaser.
The saline chaser pushes the injected contrast medium through the veins of the forearm, providing a result similar to the injection of a larger contrast volume. The example shows the effect of a 50-mL saline chaser (thicker curve), using a bolus with the same volume, rate, and iodine concentration. Moreover, the saline chaser prevents the decrease of the CM in the arm veins, which may normally cause an increase in the CM concentration after the end of the contrast injection. (**E**) The influence of multiphasic protocols. Multiphasic protocols allow producing a longer plateau of enhancement. If the scan time is long (approx 30 - 35 s), then advantages are consistent, but with a shorter scan time, as with 16-row multislice CT, the importance of a long plateau of enhancement is reduced if compared to the impact of a very high PME.

without affecting arterial enhancement and diagnostic accuracy.[15] The PME is higher and the tPME is longer when a bolus chaser is added to the CM injection,[16] while no increase in PME and tPME are expected if a bolus

chaser is added to the injected volume with a concomitant decrease in the contrast volume, resulting in an unchanged total injection volume (Fig. 2D).

7. Multiphasic protocols

Multiphasic protocols are characterized by a decreasing of the injection rate during CM administration.[6,17-20] The aim of multiphasic protocols is to create a steady plateau of enhancement during the scan by means of a higher injection rate at the beginning of the injection and a lower rate in the second part (Fig. 2E).[17] The introduction of the last generation of MSCT scanners with shorter scan times reduced the importance of multiphasic protocols. A higher PME can be far more important for the qualitative outcome of the CTA scan.

8. Injection site

Contrast material can be administered through an antecubital vein that drains directly into the deep venous circulation of the arm (basilic vein), or a forearm vein that drains into the deep venous circulation of the forearm and subsequently in the deep venous circulation at the elbow joint or into the subclavian vein through the cephalic vein. Larger veins allow higher rates and more safety.

PREDICTION AND SYNCHRONISATION OF BOLUS GEOMETRY

1. Patients demographics

No or poor correlation was reported between a calculated tPME and the actual tPME.[3,21] Nevertheless, it is not possible to exclude that in the future a relationship between demographics and bolus timing parameters will be found.

2. Fixed delay

Fixed delay is a routinely applied technique for CTA. The increased scan speed of MSCT scanners needs a more careful CM administration. The risks of a fixed-delay technique are related to the fact that, in a percentage of patients, circulation time is quite different from the protocol applied. In those cases the scan could be successful if the circulation time is shorter than that fixed delay, even if a prominent venous enhancement can be observed; but when the circulation time is longer than fixed delay, the scan fails because of the lack of proper attenuation inside the coronary arteries (Fig. 3A).

3. Test Bolus

Test bolus technique entails that a ROI is plotted inside the lumen of an artery close to the region that needs to be studied. A small amount of CM (10-15 mL, or around 10% of the main bolus) is injected at the same rate as the main bolus while a single level dynamic scan (e.g., monitoring scan) is performed at short intervals (approx 1-2 s). When CM arrives in the lumen of the artery at the level of the ROI, test bolus geometry is assessed and the time between the start of the test bolus injection and a determined point of the time/attenuation curve of the test bolus is used as delay time for the injection of the main bolus (Fig. 3B).[1]

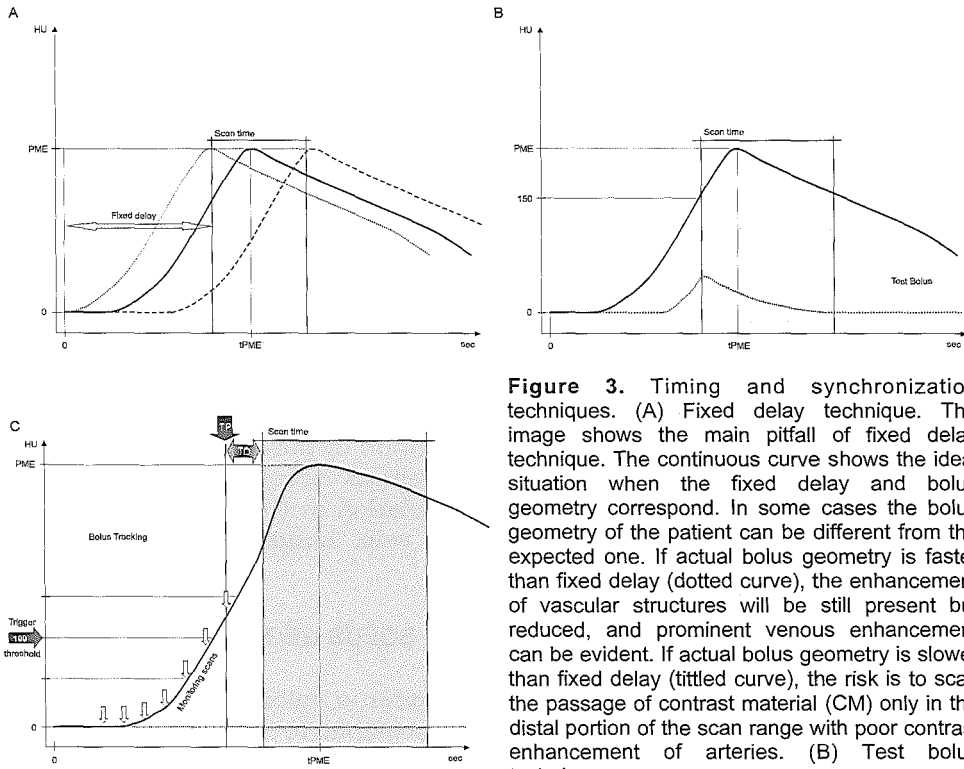

Figure 3. Timing and synchronization techniques. (A) Fixed delay technique. The image shows the main pitfall of fixed delay technique. The continuous curve shows the ideal situation when the fixed delay and bolus geometry correspond. In some cases the bolus geometry of the patient can be different from the expected one. If actual bolus geometry is faster than fixed delay (dotted curve), the enhancement of vascular structures will be still present but reduced, and prominent venous enhancement can be evident. If actual bolus geometry is slower than fixed delay (tittled curve), the risk is to scan the passage of contrast material (CM) only in the distal portion of the scan range with poor contrast enhancement of arteries. (B) Test bolus technique. The correlation between test bolus time to peak of maximum enhancement (tPME) and main bolus tPME is displayed. In this case, the test bolus tPME correlates with the time to reach 150 HU in main bolus. A main scan based on this information will be successful, even though not optimal as a CT angiography (CTA). In fact the vascular attenuation of 150 HU at the beginning of the scan is too low for optimal CTA. Worse results are obtained when the correlation is with the time to reach 50 HU or 100 HU. Test bolus actually has a different geometry than main bolus. The lack of injection power after the end of the injection of test bolus determines a pooling of the test bolus in the venous system without any vis a tergo. In other words, test bolus is left alone in the venous system of the arm, without the help of saline solution (bolus chaser) or adjunctive contrast media (main bolus) that pushes it forward. (C) Bolus tracking technique. The sequence for real-time bolus tracking is displayed. After the topogram is acquired, the monitoring scan is set at the level of aortic root and the region of interest (ROI) inside the lumen of ascending aorta. The trigger threshold is set at 100 HU. Then, CM administration and monitoring sequence are started at the same time, and when the attenuation in the ROI reaches a value greater than 100 HU at the triggering point (TP), a transition delay (TD - generally 4 s are enough for this procedure) starts while the table reaches its starting position and the patient receives breath-holding instructions.

The use of test bolus is based on a relationship between the geometry of the test bolus and that of the main bolus. There is no or poor correlation between test bolus tPME and main bolus tPME,[2,5,22] while there is a strong correlation between test bolus tPME and time to reach determined attenuation thresholds like T50, T100, T150, and T200[2,5] (i.e., the time from the beginning of the injection to reach 50/100/150/200 HU in the ROI) in main bolus (Fig. 3B). The result of this is that with conventional

test bolus technique the scan is safe but can be too early, especially if the vessels of interest are located at the beginning of the scan range.

4. Bolus Tracking

Bolus tracking technique is real-time bolus triggering technique. It is based on an ROI that is plotted inside the lumen of an artery close to the region which has to be studied, and a trigger attenuation value (threshold) that is arbitrarily chosen before starting the CTA data acquisition.[1] A single level dynamic scan (e.g., monitoring scan) is performed at short intervals (1-2 s) during the injection of CM. When the CM arrives at the level of the ROI, the change in attenuation is detected and a CT scan is started after reaching the triggering threshold (Fig. 3C).[1]

Bolus tracking provides a better timing and allows the use of less CM with a higher injection rate. A pitfall of this technique occurs when the threshold is not reached. Even though it is a very rare event when the protocol is optimized, it is always possible to start the scan manually. In this case it is difficult to obtain a high-quality CTA because of the later start of the scan, the decreased amount of contrast medium inside the vessels, and the prominent venous enhancement.

PATTERNS OF ENHANCEMENT OF CORONARY ARTERIES

Coronary arteries originate at the root of the ascending aorta, and the intravenous CM arrives at that level already diluted, after pulmonary circulation and left-ventricle contraction. Therefore, it can be assumed that the characteristics and the dynamics of bolus geometry inside coronary arteries are the same as in the ascending aorta. Differences in attenuation between ascending aorta and coronary arteries can be determined by stenosis or occlusions. In this case, in fact, there can be various degrees of attenuation inside coronary arteries and their branches depending on the flow through the stenotic vessel or on the backflow provided by collateral circulation. In a patent coronary artery, the flow speed guarantees an optimal enhancement in a few seconds. With stenosis and occlusions, the flow speed can be reduced. The MSCT scanners with 16 slices and approx 0.4-s rotation time provide a scan time of less than 20 s. With a good synchronization technique, the heart has at least 4-6 s before the smaller branches (diagonal and marginal) of the coronary arteries are acquired with a scan performed in the cranio-caudal direction. This time span is generally enough to allow an arterial perfusion and even the collateral circulation to fill in the case of stenosis or occlusion of one or more vessels.

BOLUS TIMING TECHNIQUES WITH 16-ROW MULTISLICE CT

For cardiac and coronary MSCT imaging, fixed delay, test bolus, and bolus tracking techniques have been applied.[23-28] There are no published data comparing bolus timing techniques applied to coronary imaging in the 4-slice era. In fact, the modalities applied for bolus timing have been severely influenced by the speed of acquisition and by the hyperventilation

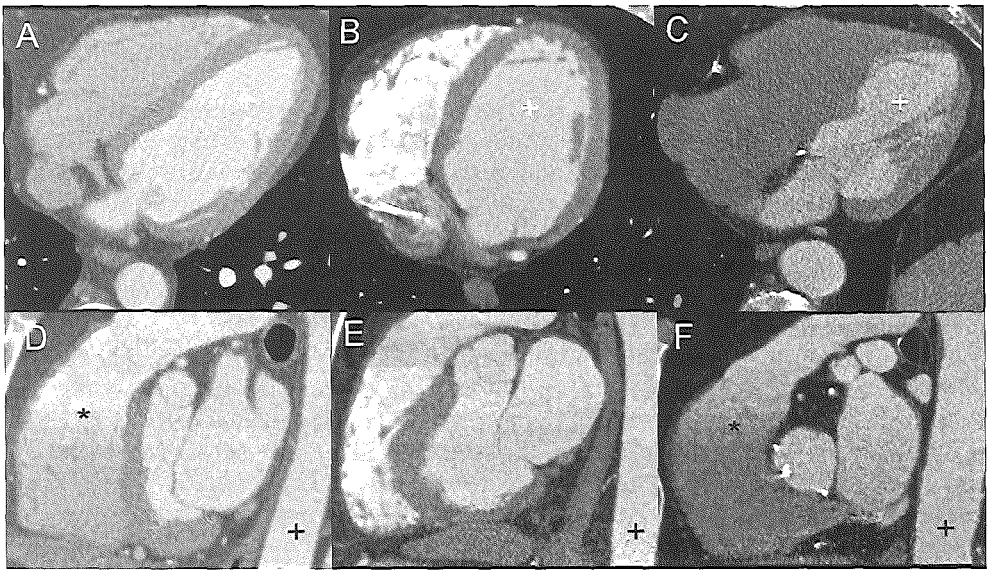

Figure 4. Examples of different contrast material administration protocols in 16-row multislice coronary CT angiography. Axial (A, B, and C) and sagittal (D, E, and F) multiplanar reformations of three different protocols of CM administration are displayed: 100 mL of 320 mgI/mL CM at 4 mL/s (A and D); 140 mL of 320 mgI/mL CM at 4 mL/s (B and E); 100 mL of 320 mgI/mL CM + 40 mL of saline chase at 4 mL/s (C and F). The images from the protocol with 100 mL and the images with 100 mL + 40 mL are similar, as expected, and show a decreasing craniocaudal gradient of attenuation inside the pulmonary artery (D and F; black asterisks), that is not present in the protocol with 140 mL (E). The enhancement in the descending aorta is preserved in every protocol (D, E, and F; black +), as well as the enhancement in the left ventricle (A, B, and C; white +).

performed just before the scan to allow a longer apnea. In some cases, the use of oxygen to increase the apnea has been reported. For these reasons, bolus tracking was not possible with 4-row MSCT scanners.

With scanners that have 6 or more rows, the scan time can be reduced significantly, especially if there is a parallel reduction in gantry rotation time (<500 ms). With those features, scan time can be reduced below 30 s. Apnea becomes more "affordable" for a larger number of patients without prescan hyperventilation or oxygen administration.

Bolus tracking is an optimal method for CM synchronization in noninvasive CTA (Fig. 4). Bolus tracking, in fact, is less time consuming than test bolus techniques (because of the calculation needed with test bolus), allows the use of less CM (the larger bolus needed to have a wider enhancement plateau with fixed delay, or the 20 mL needed for test bolus), and prevents suboptimal synchronization (determined by inter-individual veno-arterial circulation time with fixed delay, and by the lack of reliable relationship between the tPME of test bolus and main bolus). No significant differences are observed regarding the attenuation reached at the level of aortic root, whether an injection volume of 100 mL or 140 mL is used. Therefore, a volume of 100 mL, especially if followed by a saline chaser, provides optimal enhancement with reduced volume and renal

toxicity for the patient. A rate of injection of 4 mL/s is optimal because it is feasible in almost every patient through a 18-gauge venflon (green), with a very low risk of CM extravasation. Iodine concentration is proportional to the attenuation value obtained, and concentrations of 320-350 mgI/mL are optimal for coronary angiography purposes. Bolus chaser is always recommended because it allows using a reduced volume of CM more effectively.

GUIDELINES FOR CONTRAST MATERIAL ADMINISTRATION

CM administration technique for the purpose of noninvasive CTA with multislice scanners can be summarized as follows:

1. Choice of CM

use nonionic iodinated CM. Higher iodine concentrations will provide higher attenuation, and different molecules will not affect the final result significantly. The iodine concentration ranges between 300 mgI/mL and 400 mgI/mL.

2. Site of administration

start with the right antecubital access and then use the left one if there are difficulties. Use forearm or hand only if the antecubital accesses are not available. When using central IV lines, reduce the rate of infusion slightly to 2.5-3.0 mL/s.

3. Administration device

an 18-gage venflon (green) is suitable in all patients. In women or younger patients, the access could be easier with a 20-gage venflon (pink), even though a reduced rate is recommended in this case (3.0 mL/s).

4. Volume

with the 16-row generation scanners, 100 mL of CM provides optimal enhancement if a bolus tracking technique is properly applied. With a lower number of detector rows, an increased volume is needed, down to 150 mL of CM with 4-row generation scanners.

5. Rate

a 4 mL/s rate provides optimal results. Reduced injection rates (3.0 mL/s) are needed with smaller venflons and/or in patients with small or fragile veins.

6. Bolus chaser

the use of bolus chaser, when possible, is strongly recommended to increase the amount of CM used during the scan and/or to reduce the overall amount of CM administered.

TIMING AND SYNCHRONISATION TECHNIQUES

Fixed delay technique: a delay of 18 s allows a good scan in most of the patients. In patients with mildly or severely impaired cardiac function, a delay of 25 s is recommended.

Test bolus technique: calculate the tPME of the test bolus and then add 4 s for an optimal scan delay.

Bolus tracking technique: is safe and allows a tailored scan synchronization. The trigger threshold is set at 100 HU with a transition

delay of 4 s needed to give breath-hold instructions to the patient. It requires proper training of the patient, and of the technician.

REFERENCES

1. Cademartiri F, van der Lugt A, Luccichenti G, Pavone P, Krestin GP. Parameters affecting bolus geometry in CTA: a review. J Comput Assist Tomogr 2002;26:596-607.
2. Platt JF, Reige KA, Ellis JH. Aortic enhancement during abdominal CT angiography: correlation with test injections, flow rates, and patient demographics. AJR Am J Roentgenol 1999;172:53-56.
3. Puskas Z, Schuierer G. [Determination of blood circulation time for optimizing contrast medium administration in CT angiography] Kreislaufzeitbestimmung zur Optimierung der Kontrastmittelapplikation bei der CT-Angiographie. Radiologe 1996;36:750-757.
4. Kirchner J, Kickuth R, Laufer U, Noack M, Liermann D. Optimized enhancement in helical CT: experiences with a real-time bolus tracking system in 628 patients. Clin Radiol 2000;55:368-373.
5. van Hoe L, Marchal G, Baert AL, Gryspeerdt S, Mertens L. Determination of scan delay time in spiral CT-angiography: utility of a test bolus injection. J Comput Assist Tomogr 1995;19:216-220.
6. Bae KT, Heiken JP, Brink JA. Aortic and hepatic contrast medium enhancement at CT. Part II. Effect of reduced cardiac output in a porcine model. Radiology 1998;207:657-662.
7. Garcia P, Genin G, Bret PM, Bonaldi VM, Reinhold C, Atri M. Hepatic CT enhancement: effect of the rate and volume of contrast medium injection in an animal model. Abdom Imaging 1999;24:597-603.
8. Han JK, Kim AY, Lee KY, et al. Factors influencing vascular and hepatic enhancement at CT: experimental study on injection protocol using a canine model. J Comput Assist Tomogr 2000;24:400-406.
9. Nakayama M, Yamashita Y, Oyama Y, Ando M, Kadota M, Takahashi M. Hand exercise during contrast medium delivery at thoracic helical CT: a simple method to minimize perivenous artifact. J Comput Assist Tomogr 2000;24:432-436.
10. Coche EE, Muller NL, Kim KI, Wiggs BR, Mayo JR. Acute pulmonary embolism: ancillary findings at spiral CT. Radiology 1998;207:753-758.
11. Luboldt W, Straub J, Seemann M, Helmberger T, Reiser M. Effective contrast use in CT angiography and dual-phase hepatic CT performed with a subsecond scanner. Invest Radiol 1999;34:751-760.
12. Bluemke DA, Fishman EK, Anderson JH. Effect of contrast concentration on abdominal enhancement in the rabbit: spiral computed tomography evaluation. Acad Radiol 1995;2:226-231.
13. Haage P, Schmitz-Rode T, Hubner D, Piroth W, Gunther RW. Reduction of contrast material dose and artifacts by a saline flush using a double power injector in helical CT of the thorax. AJR Am J Roentgenol 2000;174:1049-1053.
14. Hopper KD, Mosher TJ, Kasales CJ, TenHave TR, Tully DA, Weaver JS. Thoracic spiral CT: delivery of contrast material pushed with injectable saline solution in a power injector. Radiology 1997;205:269-271.
15. Bader TR, Prokesch RW, Grabenwoger F. Timing of the hepatic arterial phase during contrast-enhanced computed tomography of the liver: assessment of normal values in 25 volunteers. Invest Radiol 2000;35:486-492.

16. Sadick M, Lehmann KJ, Diehl SJ, Wild J, Georgi M. [Bolus tracking and NaCl bolus in biphasic spiral CT of the abdomen] Bolustriggerung und NaCl-Bolus bei der biphasischen Spiral-CT des Abdomens. Rofo Fortschr Geb Rontgenstr Neuen Bildgeb Verfahr 1997;167:371-376.
17. Fleischmann D, Rubin GD, Bankier AA, Hittmair K. Improved uniformity of aortic enhancement with customized contrast medium injection protocols at CT angiography. Radiology 2000;214:363-371.
18. Hittmair K, Fleischmann D. Accuracy of predicting and controlling time-dependent aortic enhancement from a test bolus injection. J Comput Assist Tomogr 2001;25:287-294.
19. Fleischmann D, Hittmair K. Mathematical analysis of arterial enhancement and optimization of bolus geometry for CT angiography using the discrete Fourier transform. J Comput Assist Tomogr 1999;23:474-484.
20. Bae KT, Tran HQ, Heiken JP. Multiphasic injection method for uniform prolonged vascular enhancement at CT angiography: pharmacokinetic analysis and experimental porcine model. Radiology 2000;216:872-880.
21. Nakajima Y, Yoshimine T, Yoshida H, et al. Computerized tomography angiography of ruptured cerebral aneurysms: factors affecting time to maximum contrast concentration. J Neurosurg 1998;88:663-669.
22. Kaatee R, Van Leeuwen MS, De Lange EE, et al. Spiral CT angiography of the renal arteries: should a scan delay based on a test bolus injection or a fixed scan delay be used to obtain maximum enhancement of the vessels? J Comput Assist Tomogr 1998;22:541-547.
23. Nieman K, Oudkerk M, Rensig BJ, et al. Coronary angiography with multislice computed tomography. Lancet 2001;357:599-603.
24. Achenbach S, Ulzheimer S, Baum U, et al. Noninvasive coronary angiography by retrospectively ECG-gated multislice spiral CT. Circulation 2000;102:2823-2828.
25. Knez A, Becker CR, Leber A, et al. Usefulness of multislice spiral computed tomography angiography for determination of coronary artery stenoses. Am J Cardiol 2001;88:1191-1194.
26. Nieman K, Rensing BJ, van Geuns RJ, et al. Usefulness of multislice computed tomography for detecting obstructive coronary artery disease. Am J Cardiol 2002;89:913-918.
27. Vogl TJ, Abolmaali ND, Diebold T, et al. Techniques for the detection of coronary atherosclerosis: multi-detector row CT coronary angiography. Radiology 2002;223:212-220.
28. Nieman K, Cademartiri F, Lemos PA, Raaijmakers R, Pattynama PM, de Feyter PJ. Reliable noninvasive coronary angiography with fast submillimeter multislice spiral computed tomography. Circulation 2002;106:2051-2054.

3. CONTRAST MATERIAL

CHAPTER 3

IV CONTRAST ADMINISTRATION FOR CT CORONARY ANGIOGRAPHY ON A 16-MULTIDETECTOR-ROW HELICAL CT SCANNER: TEST BOLUS VS. BOLUS TRACKING

Filippo Cademartiri[1], MD
Koen Nieman[1,2], MD
Aad van der Lugt[1], MD, PhD
Rolf H Raaijmakers[1], RT
Nico Mollet[1,2], MD
Peter MT Pattynama[1], MD, PhD
Pim J de Feyter[1,2], MD, PhD
Gabriel P Krestin[1], MD, PhD

From the Departments of Radiology[1] and Cardiology[2], Thoraxcentrum, Erasmus M C, University Medical Center Rotterdam , The Netherlands.

Radiology, 233: 817-823, 2004

ABSTRACT

Purpose:
To compare test bolus and bolus tracking technique for iv contrast administration in coronary angiography with a 16-multidetector-row ct (16-mdct) scanner.

Methods and material:
38 patients (3 female; mean age 60 years) were randomised into two groups with respect to the bolus timing technique: group 1 (20ml test bolus + 100ml main bolus), and group 2 (bolus tracking with 100ml main bolus). All patients underwent ecg-gated 16-mdct coronary angiography with the following parameters: number of detectors/collimation 12/0.75mm, rotation time 420ms. In group 1, the test bolus peak of attenuation was used as delay, while in group 2 a threshold of +100hu in the ascending aorta triggered the angiographic acquisition with an additional delay of 4s for patient instructions. The attenuation was measured in three main vessels in the longitudinal direction throughout the scan: 1) ascending aorta (roi1); 2) descending aorta (roi2); 3) main pulmonary artery (roi3). The mean attenuation and the slope of the bolus geometry curve were calculated in each patient and in each roi. The attenuation at the origin of coronary arteries was measured. A student's t test was used to compare results.

Results:
the mean scan delay was 6 seconds longer in group 2 ($p<0.05$). The average attenuation values in roi1 were 307±44hu and 328±59hu ($p<0.05$), in roi2 were 292±45hu and 326±63hu ($p<0.05$), in roi3 were 355±78hu and 305±71u ($p>0.05$), for group 1 and 2, respectively. The average slope values in roi1 were 5.8 and -0.8 ($p<0.05$), in roi2 were 7.7 and 0.7 ($p<0.05$), in roi3 were -1.0 and -13.3 ($p<0.05$), for group 1 and 2, respectively. The average attenuation values in left main, left anterior descending, and circumflex were significantly higher in group 2, while there were no significant difference between the two groups in the right coronary artery.

Conclusion:
Bolus tracking technique provides more homogenous enhancement compared with test bolus technique.

INTRODUCTION

Retrospective ECG-gated four-multidetector-row CT (4-MDCT), has been investigated for the detection of coronary artery disease (CAD).[1-3] Even though the results are promising, routine use of 4-MDCT has been limited due to restrictions in temporal and spatial resolution, and a considerable long scan time of approximately 40s.[1-3]

Several manufacturers have recently introduced a new generation of MSCT scanner with 16 rows of detectors (16-MDCT) and increased spatial and temporal resolution.[4-6] Due to the increased number of detector rows and faster gantry rotation, the time needed to cover the entire heart has been reduced to ~20s.[6] Early experiences show improved results in the detection of significant stenosis in coronary arteries (6-8).

A pre-requisite for successful CT angiography is optimal synchronisation between the arterial passage of contrast material and CT data acquisition.[9] However, the reduction of scan time raises questions concerning contrast bolus optimisation.[10, 11]

In general, for helical CT or multidetector-row helical CT, bolus timing techniques most frequently used are:

1) fixed delay,
2) determination of the transit time by test bolus injection, and
3) bolus tracking.

Although bolus tracking technique has previously been proposed as an effective tool to better synchronise the scan with contrast enhancement,[12-16] controversies are still present on whether bolus timing techniques result in actual advantages or not in terms of optimal vascular attenuation.[17]

Nevertheless, for cardiac and coronary MDCT imaging only fixed delay and test bolus technique have been used up to now.[1-3, 18, 19] The relatively long scan time in 4-MDCT may require hyperventilation or oxygen before the start of data acquisition. The large respiratory movements in hyperventilation do not allow a reliable monitoring sequence for bolus tracking at the level of the ascending aorta. The shorter scan time in 16-MDCT allows the use of bolus tracking technique in coronary CT angiography.

Thus, the purpose of our study was to compare test bolus and bolus tracking technique for IV contrast administration in coronary angiography with a 16-MDCT scanner.

MATERIALS AND METHODS

Patients

Between July and August 2002, 38 patients, 35 male and 3 female (mean age: 60; range 42-81), undergoing coronary angiography with 16-MDCT, were prospectively enrolled in the study. All patients meeting the inclusion criteria referred from the outpatient clinic of our and neighbouring hospitals were enrolled. The referring diagnosis was known or suspected coronary artery disease (e.g. clinical symptoms referred to stable angina, non-conclusive stress ECG test). Exclusion criteria were: irregular heart

rates, previous allergic reaction to iodinated contrast material, renal insufficiency (serum creatinine >120mmol/L), pregnancy, respiratory impairment, unstable clinical status, or marked heart failure. The Institutional Review Board approved the study and patients gave informed consent.

After enrolment, patients were randomised into two groups using a table of random numbers. In one group test bolus technique was used (Group 1; n=19) while in the other group bolus tracking technique was applied (Group 2; n=19). In each patient age, sex, body weight and heart rate during the scan were recorded.

Scan protocol

Studies were performed on a 16-MDCT scanner (Sensation 16-Siemens Medical Solutions, Forchheim, Germany). Prior to the examination the heart rate (HR) was measured. Patients with a pre-scan HR equal or above 65 bpm, were given 100 mg of metoprolol per os one hour before the scan. Patients were thoroughly instructed with respect to the examination and the breath-hold procedure. They were required to perform a deep inspiration and to continue to hold the breath without pushing (Valsalva maneuver). During this tryout the operator was observing the patient for compliance and the ECG track for significant anomalies.

The contrast material (Iodixanol 320 mgI/ml-Visipaque-Amersham Health, Little Chalfont, UK) was injected using a power injector (EnVision-MedRAD, Pittsburgh, PN, USA) through a 18G needle, in the antecubital vein. Contrast material volume and injection rate for test bolus were 20 ml and 4 ml/s respectively, and for main angiographic bolus 100 ml and 4 ml/s (total injection time of 25 s). For the retrospective ECG-gated scan of coronary arteries the 12 central detector rows were used.

The main scan parameters were: number of detectors 12 (because the retrospectively ECG-gated protocol did not allow the use of all 16 rows), individual detector width 0.75 mm, gantry rotation time 420 ms, kV 120, mAs 400, feed/rotation 2.8 mm, feed/second 6.7, scan direction cranio-caudal. For the purpose of the present study, two datasets have been reconstructed, both with retrospective ECG gating with time window starting at 400 ms before the next R wave on the ECG, FOV 200 mm, and a medium smooth convolution filter (B30f). Two datasets were reconstructed with an effective slice width and a reconstruction interval of 1 mm and 3 mm, 0.6 mm and 3 mm, respectively. The images were transferred to a stand-alone workstation and evaluated using dedicated analysis software (Leonardo-Siemens Medical Solutions, Forchheim, Germany). Bolus timing procedures and main scans were successfully completed in all patients. No significant adverse reactions to contrast material were observed. All patients were able to hold their breath during the scan.

Test Bolus technique

This technique is based on a small amount of contrast material (20mL - generally 15-20% of the main bolus) injected intravenously during a series of dynamic low dose monitoring scans (120 kV, 20mAs) at the level of the vessel of interest.

In the present study the dynamic monitoring scan was set at the level of the ascending aorta. The delay between each monitoring scan was 1.25s. The dynamic monitoring scans started 10s after the beginning of injection of intravenous contrast material (20ml of contrast material injected at 4ml/s). A region of interest (ROI), as large as the aortic root, was plotted inside the lumen by one operator (R.H.R.), to generate an enhancement curve, which shows the time needed to reach the peak of maximum enhancement for the test bolus (DynEVA - Siemens Medical Solutions, Forchheim, Germany). The time of the peak of maximum enhancement in the ascending aorta for the test bolus was the delay that was applied for the angiographic scan as previously described.[1, 3, 19, 20]

Bolus Tracking technique

This technique is based on real time monitoring of the main bolus during injection with a series of dynamic low dose monitoring scans (120 kV, 20mAs) at the level of the vessel of interest (CARE bolus - Siemens Medical Solutions). It is possible to start the main scan manually or automatically with a trigger threshold. In the present study the monitoring scan was performed at the level of the ascending aorta. A ROI as large as the aortic root was plotted by one operator (R.H.R.). The dynamic monitoring scans started 10s after the beginning of injection of intravenous contrast material. The trigger threshold inside the ROI was set at +100HU above the baseline (±140-160HU in absolute value). The delay between each monitoring scan was 1.25s. As soon as the threshold was reached the table moved to the cranial start position while the patient was instructed to take a deep breath and hold it. During this interval (4s which were necessary to give to patient breath-hold instruction safely), the contrast material concentration increased up to the desired level of enhancement. The rationale for the choice of a rather low threshold is based on those extra 4s needed to start the scan.

Data collection

One radiologist (F.C.), with 3 years of experience in cardiac CT, performed and collected all the measurements at the workstation.

Two main sets of measurements have been performed:

1) bolus geometry in the great vessels (e.g. the variation in the attenuation inside a vessel during time, after the administration of intravenous contrast material), and

2) the attenuation in the coronary arteries.

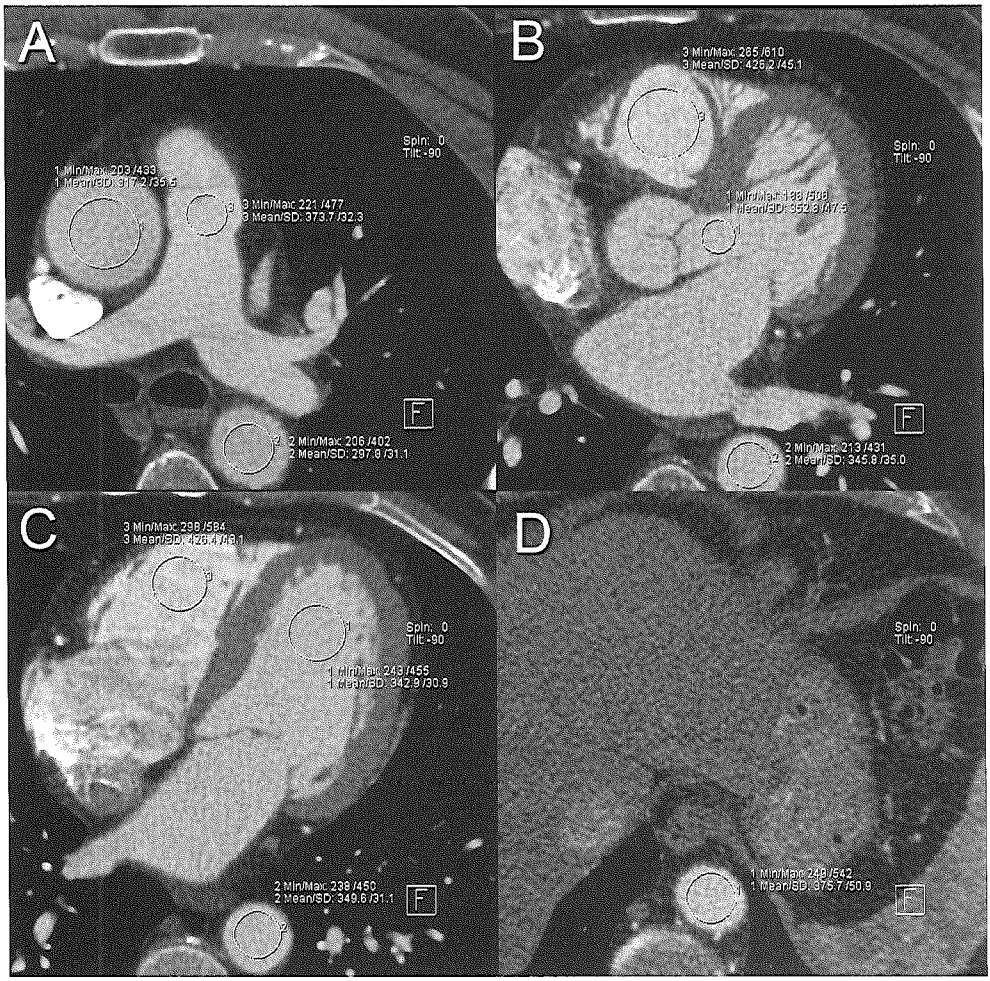

Figure 1. Axial slices at different levels during the main angiographic spiral CT scan. In the first image of the dataset (**A**), the three region of interest (ROI) are easily drawn in ascending aorta, descending aorta, and main pulmonary artery. At this level the high attenuation in the superior vena cava (arrow) is displayed, due to the remnant contrast material. At the level of aortic valve (**B**), the ROIs are drawn in the left ventricle outflow tract, descending aorta, and right ventricle. At the level of the tricuspid valve (**C**), the ROIs are drawn in the left ventricle, descending aorta, and right ventricle. In the last part of the scan (**D**), only the descending aorta is assessable for an ROI.

Bolus geometry in the great vessels

In order to generate a plot of bolus geometry during the main angiographic scan, the attenuation values have been extracted from the datasets as follows. The DICOM layout of the images allows reading the exact time (down to hundreds of sec^{-1}) of the data acquisition in each reconstructed slice. The attenuation value in HU have been assessed on axial images on the dataset with effective slice width of 3mm and reconstruction interval of 3mm. At intervals of 1 second, in each slice, a ROI was drawn, throughout the entire data-set into three main regions (Figure 1 and 2): 1) the

ascending aorta (ROI1); 2) the descending aorta (ROI2); and 3) the main pulmonary artery (ROI3). The ROIs were drawn as large as the anatomic configuration of the area allowed in the axial slice.

The varying size and morphology of the heart and great vessels in the individual subjects, resulted in different scan time as well as in different length of the ROIs along the *z*-axis. Only time-related contrast measurements for each respective vessel that were available in all patients were included in the study to achieve consistent results.

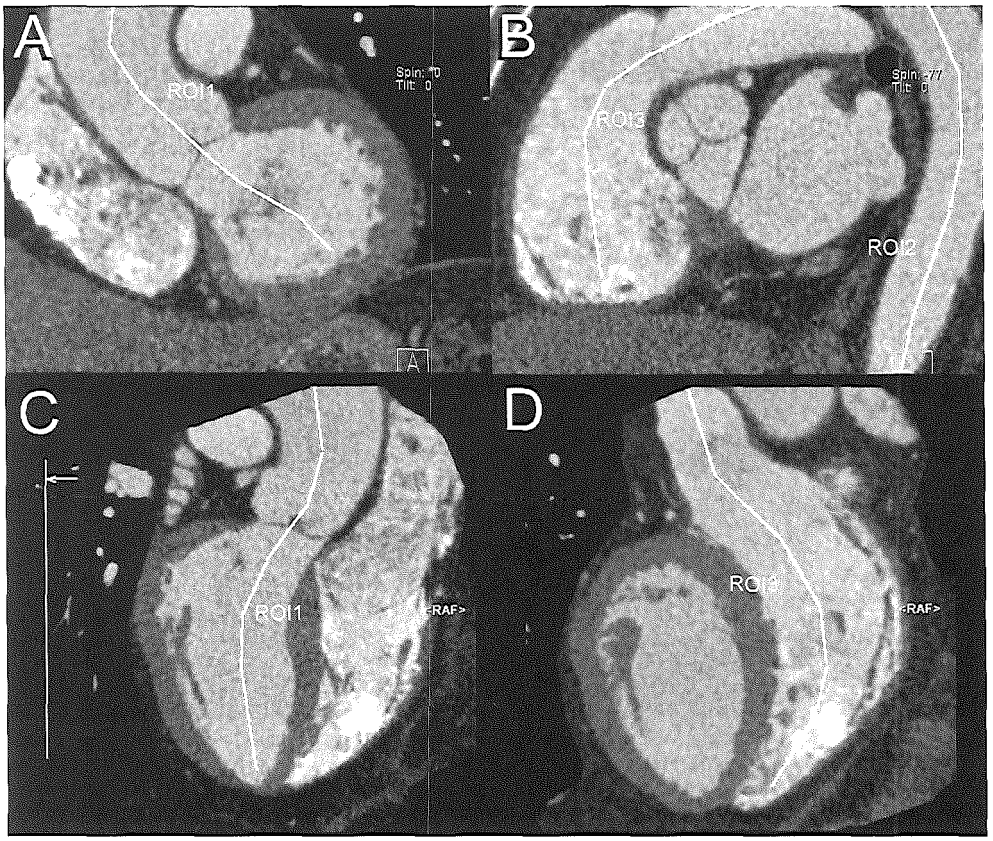

Figure 2. Multiplanar reconstruction (MPR) and curved reconstruction (CMPR) of the main angiographic dataset throughout the path of the ROIs in the z-axis. A coronal MPR (**A**) and the corresponding CMPR (**B**), show the path of ROI 1 in the ascending aorta and left ventricle. A sagittal MPR (**C**), shows the path of ROI 2. A sagittal MPR (**C**) and the corresponding CMPR (**D**), show the path of ROI 3.

Attenuation in the coronary arteries

In order to provide information regarding the efficacy of contrast material protocol on coronary artery enhancement, the attenuation was measured at the origin of four coronary artery branches. The dataset with effective slice width of 1 mm and reconstruction interval of 0.6 mm was used. This dataset has, in fact, a higher spatial resolution in the *z*-axis allowing to measure more accurately structures with a diameter of 3-5mm. A ROI was plotted on the axial image as large as the vessel lumen, choosing a slice where the lumen was easily identified. Calcification of the coronary wall and soft plaques have been carefully avoided. Four vessels (and four ROIs) have been considered: left main coronary artery (LM), left anterior descending coronary artery (LAD), left circumflex (CX), and right coronary artery (RCA).

Data and statistical analysis

To rule out significant differences between the two sample populations, an ANOVA test was applied to the following parameters: age, weight, mean HR during the scan.

The scan delays have been extracted from the test bolus dynamic series in group 1 and from the bolus tracking dynamic series in group 2.

Bolus geometry in the great vessels

To analyse the geometry of the bolus, time/attenuation curves have been generated. In each of the three main ROIs and in each patient, the start of the main scan was synchronised as time 0 for both groups. Average time/attenuation curve for each ROI in each group were generated (mean ± standard deviation).

The evaluation of the efficacy of synchronisation protocol (test bolus vs. bolus tracking) was performed on several parameters: 1) the average attenuation (the mean attenuation calculated in each sample during the scan); 2) the slope of the time/attenuation curve; both were calculated in each ROI of each patient. The average attenuation represents an assessment of the amount of contrast material that was present inside the vessel during the scan, while the slope represents an assessment of the position of the scan in relation to bolus geometry. For instance, a positive slope (>0) means that the scan was performed during an increasing attenuation (e.g. early in bolus geometry), a negative slope (<0) means that the scan was performed during a decreasing attenuation (e.g. late in bolus geometry), while a slope around 0 means that the scan was performed during the plateau or the peak of attenuation (e.g. central in bolus geometry); 3) the attenuation value at time 0; 4) the maximum enhancement value (MEV) was evaluated in each ROI; the time to the MEV. Differences between groups were assessed with a Student's T test, and a $p<0.05$ was considered significant.

Attenuation in the coronary arteries

For coronary arteries, the attenuation recorded at the origin of LM, LAD, CX, and RCA were measured (mean±SD). Differences between groups were assessed with a Student's T test, and a $p<0.05$ was considered significant.

Interdependency between measurements

In order to address to problem of inter-dependency of the measurements between different vessels the following analysis was performed. The paired parameters used for the description of the curves (Average attenuation, Slope, Time 0, MEV and tMEV) were subtracted in the two groups and the differences obtained were compared using a paired T-test. The analysis was performed for each great vessel and for each coronary vessel. A $p<0.05$ indicated low interdependency, while a $p<0.01$ indicated no interdependency.

RESULTS

Patients demographics were not significantly different in the two groups for age, weight, and mean heart rate. Additional beta-blockers were administered in 16 patients. In group 1 there were 17 males while in group 2 there were 18 males. The scan delay calculated in Group 1, based on the test bolus procedure, was 14.6±1.3s, while the mean scan delay resulting from bolus tracking procedure in Group 2 was 20.6±2.7s ($p<0.05$). Thus, on average, the scan delay was 6s longer in Group 2 (Table I).

Table I. Patient Data.

	Group 1 - TB	Group 2 - BT
Number of patients	19	19
Male/Female	17/2	18/1
Mean age (range) yrs	59 (42-78)	61 (45-81)
Weight (range) kg	73.6 (68-89)	74.7 (65-110)
Mean heart rate (range) bpm	56.6 (45-66)	57.1 (48-68)
Scan delay*	14.6±1.3s	20.6±2.7s

*$p<0.05$

Abbreviations: TB = test bolus; BT = bolus tracking; yrs = years; kg = kilogram; bpm = beats per minute.

Ascending aorta (Table II and Figure 3)

The average attenuation was higher in group 2 but not significantly different ($p>0.05$). The slope, instead, was significantly higher for group 1 ($p<0.05$). Attenuation values at time 0 were 255.1±43.1 HU and 316.5±66.4 HU in group 1 and 2, respectively ($p<0.05$). The average MEV was 356.7±57.0 HU in group 1 and 369.9±59.9 HU in group 2 ($p>0.05$). The average tMEV was 9.1 s in group 1 and 6.2 s in group 2 ($p<0.05$).

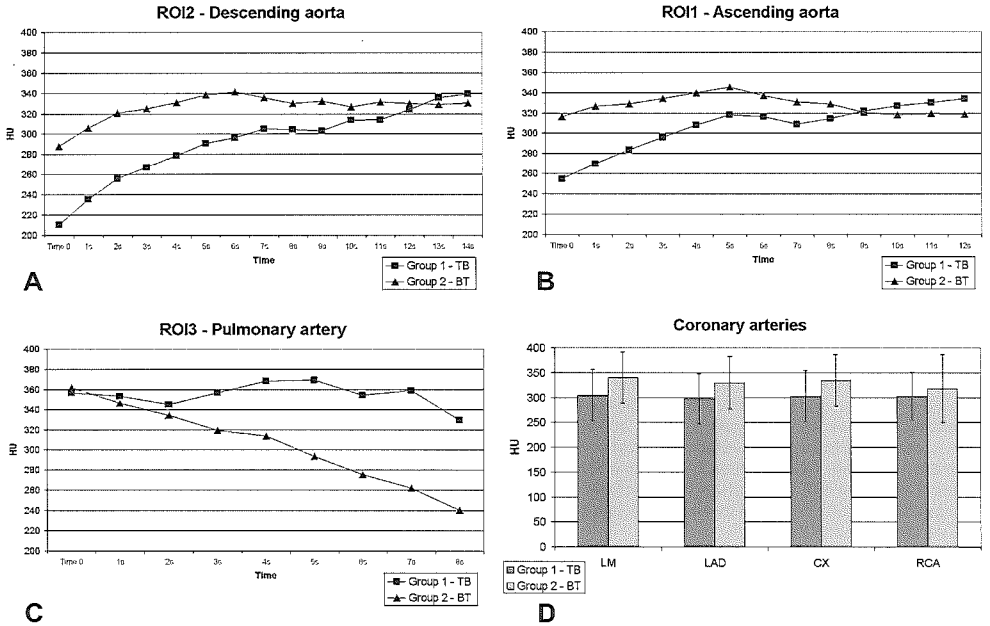

Figure 3. Average time-attenuation curves of the ascending aorta obtained in group 1 – Test Bolus (TB), and group 2 – Bolus Tracking (BT). The time-attenuation curve in the ascending aorta (**A**), suggests that group 2 start with a higher enhancement compared to group 1, and tends to remain above 300HU for the entire range of measurements. Time/attenuation curve in descending aorta (**B**), shows a similar behaviour as in A. Group 2 starts with a higher enhancement and remains above the curve of group 1 for almost the entire range of measurements. Time/attenuation curve in pulmonary artery (**C**), shows that the curve of group 1 remains higher for the entire range. This means more pooling of contrast material in the right heart during the scan.
The attenuation at the level of the origin of coronary arteries (D), shows significant differences in left main (LM), left anterior descending (LAD) and circumflex (CX). In the right coronary artery (RCA) the BT group shows higher attenuation but not significant.

Descending aorta (Table II and Figure 3)

The average attenuation was higher in group 2 but, as for the ascending aorta, not significantly different ($p>0.05$). The slope was significantly higher for group 1 ($p<0.05$). Attenuation values at time 0 were 210.5±55.3 HU and 288.3±73.4 HU in group 1 and 2, respectively ($p<0.05$). The average MEV was 353.6±60.1 HU in group 1 and 376.1±69.9 HU in group 2 ($p>0.05$). The average tMEV was 11.9 s in group 1 and 9.2 s in group 2 ($p<0.05$).

Main pulmonary artery (Table II and Figure 3)

The average attenuation was lower in group 2 and significantly different ($p<0.05$). The slope was significantly higher for group 1 ($p<0.05$). Attenuation values at time 0 were 356.8±79.8 HU and 361.9±90.6 HU in group 1 and 2, respectively ($p>0.05$). The average MEV was 426.9±80.5 HU in group 1 and 394.5±85.6 HU in group 2 ($p>0.05$). The average tMEV was 4.1 s in group 1 and 2.1 s in group 2 ($p<0.05$).

Table II. Results: average time-attenuation curves.

	Ascending Aorta			Descending Aorta			Main pulmonary Artery		
	TB	BT	p	TB	BT	p	TB	BT	p
Average attenuation (HU)	306.6±44.0	328.2±58.6	>.05	291.6±45.1	326.4±62.6	>.05	354.7±78.0	305,3±71.4	<.05
Slope	5.8±6.4	-0.8±8.9	<.05	7.7±5.5	0,7±8.2	<.05	-1.0±15.6	-13.3±15.8	<.05
Time 0 value (HU)	255.1±43.1	316.5±66.4	<.05	210.5±55.3	288.3±73.4	<.05	356.8±79.8	361.9±90.6	>.05
MEV (HU)	356.7±57.0	369.9±59.9	>.05	353.6±60.1	376.1±69.9	>.05	426.9±80.5	394.5±85.6	>.05
tMEV (s)	9.1s	6.2s	<.05	11.9s	9.2s	<.05	4.1s	2.1s	<.05

The table shows the results of the average time-attenuation curves in the three ROIs plot in the ascending aorta, descending aorta, and pulmonary artery. Group 1 with test bolus and group 2 with bolus tracking are compared, regarding their average attenuation, slope, attenuation value at time 0, average maximum enhancement value, and time to reach the MEV. The average attenuation is significantly different in ROI3, while the slope resulted significantly different in all three ROIs. At time 0 ROI1 and ROI2 showed significant differences. The MEV was not significantly different while the tMEV was always significantly different.
Abbreviations: ROI= region of interest; TB= test bolus; BT= bolus tracking; MEV= maximum enhancement value; tMEV= time to reach the MEV.

Coronary arteries (Table III and Figure 3)

The average attenuation was higher in group 2 and significantly different ($p<0.05$) for LM, LAD, and CX, while for RCA, even though attenuation was higher for group 2, the difference was not significant ($p>0.05$).

Table III. Results: coronary arteries.

	Group 1 - TB	Group 2 - BT	p
LM (HU)	304.7±52.1	339.7±51.8	<.05
LAD (HU)	297.2±50.8	329.3±53.2	<.05
CX (HU)	302.3±51.9	334.4±52.3	<.05
RCA (HU)	302.3±48.1	317.9±68.2	>.05

The attenuation at the origin of the four main branches of the coronary arteries in group 1 and group 2, showed significant differences for left main, left anterior descending, and circumflex, but not for the right coronary artery.
Abbreviations: TB= test bolus; BT= bolus tracking; LM= left main; LAD= left anterior descending; CX= circumflex; RCA= right coronary artery; HU= Hounsfield units.

Interdependency between measurements

The results of the analysis for interdependency showed dis-homogeneous results for the great vessels of the thorax. In fact, between ascending and descending aorta there was a variable degree of interdependency (except for time 0). In the comparison between ascending aorta and pulmonary artery and in the one between descending aorta and pulmonary artery, average and MEV were not interdependent, while Time 0 showed low interdependency. Coronary arteries were also dis-homogeneous. Very high interdependency was found between LAD and CX, while lower degrees of interdependency were found between all the other combination of vessels.

DISCUSSION

The introduction of MDCT technology with shorter acquisition time requires further optimisation and synchronisation between the passage of contrast material and data acquisition, in order to obtain consistent computed tomography angiography (CTA) images.[21]

A few techniques allow to synchronise contrast material administration and the start of data acquisition in clinical practice, namely: fixed delay (based on experience and related to angiographic data), test bolus and bolus tracking.[9] Even though the synchronisation between contrast material administration is becoming increasingly important, due to the introduction of faster spiral CT scanners, still controversies remains on the opportunity of using these techniques. In a study from Macari et al. a fixed delay of 25s has been used to image the abdominal aorta with the intravenous administration of 150ml of contrast material. The attenuation, measured throughout the dataset into the aorta and iliac arteries, have been above the value of 200HU, considered adequate by the Authors for angiographic evaluation, in 98% of the measurements.[17]

In the present study, test bolus (TB) and bolus tracking (BT) techniques in CT angiography of the coronary arteries have been compared. The enhancement in these vessels has been measured in the 1) ascending aorta, the 2) descending aorta, and the 3) pulmonary artery. The ascending aorta represents the contrast material that drains into the coronary arteries, therefore the attenuation achieved at this level plays a major role in the optimal enhancement of the coronary arteries. The descending aorta represents a monitoring vessel for arterial bolus geometry because it runs parallel to the *z*-axis (e.g. longitudinal or temporal axis). The pulmonary artery evaluation can be useful to monitor the pooling of contrast material in the right heart.

In addition, to measure the effect of the two synchronisation protocols on the attenuation in the coronary arteries, the attenuation at the origin of LM, LAD, CX, and RCA were assessed.

The BT group showed better synchronisation between the scan and contrast material administration. In fact the BT group had a more homogeneous and steady enhancement compared to the TB, with less pooling of contrast material in the pulmonary vessel and right heart. The amount of contrast material used was also reduced by 20%. This resulted in a higher attenuation at the level of the coronary arteries. In particular, the left coronary artery (LM) and its main branches (LAD and CX) showed a significantly higher attenuation in BT group. Also in RCA the attenuation was higher in BT group but not significantly different. The calculated scan delay was 6s later in the BT group in comparison with TB group. It is reasonable to state that only because of this difference the geometry of contrast material attenuation would be different in the two groups.

In fact, even though the average attenuation was not different in ascending and descending aorta, the slopes were significantly different: in the BT group the slope was approximately 0, meaning that the scan was

performed during the plateau of enhancement of bolus geometry at the level of the thoracic aorta. Conversely, the slope in the TB group was >0, meaning that the scan was performed during the upslope of attenuation when the contrast is still increasing. The mirror image of this behaviour is displayed in the pulmonary artery, where in the TB group the average attenuation was significantly higher (more contrast material was still present in the right side of the pulmonary circulation), and the slope was significantly lower and negative (the trend was a decreasing attenuation in the right side of the pulmonary circulation) in comparison to the BT group. In simple words, using the bolus tracking protocol, the scan is performed during the plateau of attenuation and there is less "pooling" of contrast material in the right side of the heart.

To confirm this observation the attenuation value at time 0 (the start of the scan) were significantly lower for TB group in ascending and descending aorta, because the geometry was still in the upslope. The MEV was not significantly different in all three locations, meaning that the peak of attenuation fell within the scan duration in both groups, but at different moments: the tMEV was significantly different in all three locations. The MEV in the TB group was three seconds later than in the BT group, in ascending and descending aorta. This discrepancy between the difference in the start delay (6s) and the difference in tMEV can be explained with the increased intra-thoracic pressure caused by the apnoea that occurs 6 seconds earlier in the TB group. In fact, the Valsalva manoeuvre reduces the incoming flow of contrast material through the innominate veins. This phenomenon could also explain the slightly lower MEV, even though not significant, in the TB group.

The mean scan delay was 6s longer in Group 2, meaning that the protocol for test bolus needed a "t" factor to be added to the delay calculated from the peak of maximum enhancement in the test bolus sequence. Probably the "t" factor could be approximately 6s but more accurate studies are needed to optimise this approach.

A limitation of the study is that, for practical reasons, bolus geometry during the main scan was assessed during table movement. This means that the scan was not performed at the same level during the passage of contrast material.

Another limitation is related to the evaluation of coronary arteries. Ideally the best way to assess the efficacy of a contrast material protocol would be to measure the length of coronary arteries, and the number of side branches that can be visualised. We preferred to assess quantitatively the origin of the main coronary arteries because the group of patients was too small to account for the many variables that can affect coronary artery visualisation: the high heart rate, the small vessel size, the variable anatomy, the heavily calcified vessel wall, the presence of stenosis or occluded vessels can heavily affect the capability of visualisation of coronary arteries regardless the attenuation of the vessel.

CONCLUSION

Fixed delay and test bolus techniques have been used successfully until now in MDCT coronary angiography. More optimal synchronisation of the contrast material passage and data acquisition is available using bolus tracking technique and a 16-row MDCT scanner, resulting in consistently high and homogeneous contrast enhancement in coronary angiography. Also 20% less contrast material volume is administered using bolus tracking technique. We believe that bolus tracking technique should be integrated in the routine protocol for 16-row MDCT coronary angiography.

REFERENCES

1. Achenbach S, Ulzheimer S, Baum U, Kachelriess M, Ropers D, Giesler T, Bautz W, Daniel WG, Kalender WA, Moshage W: Noninvasive coronary angiography by retrospectively ECG-gated multislice spiral CT. Circulation 2000; 102:2823-8.
2. Nieman K, Oudkerk M, Rensig BJ, van Ooijen P, Munne A, van Geuns RJ, de Feyter PJ: Coronary angiography with multislice computed tomography. Lancet 2001; 357:599-603.
3. Knez A, Becker CR, Leber A, Ohnesorge B, Becker A, White C, Haberl R, Reiser MF, Steinbeck G: Usefulness of multislice spiral computed tomography angiography for determination of coronary artery stenoses. Am J Cardiol 2001; 88:1191-4.
4. Flohr T, Stierstorfer K, Bruder H, Simon J, Schaller S: New technical developments in multislice CT - Part 1: Approaching isotropic resolution withsub-millimeter 16-slice scanning. Rofo 2002; 174:839-45.
5. Flohr T, Bruder H, Stierstorfer K, Simon J, Schaller S, Ohnesorge B: New Technical Developments in Multislice CT, Part 2: Sub-Millimeter 16-Slice Scanning and Increased Gantry Rotation Speed for Cardiac Imaging. Rofo 2002; 174:1022-7.
6. Heuschmid M, Kuttner A, Flohr T, Wildberger JE, Lell M, Kopp AF, Schroder S, Baum U, Schaller S, Hartung A, Ohnesorge B, Claussen CD: [Visualization of coronary arteries in CT as assessed by a new 16 slice technology and reduced gantry rotation time: first experiences]. Rofo 2002; 174:721-4.
7. Nieman K, Cademartiri F, Lemos PA, Raaijmakers R, Pattynama PM, de Feyter PJ: Reliable noninvasive coronary angiography with fast submillimeter multislice spiral computed tomography. Circulation 2002; 106:2051-4.
8. Ropers D, Baum U, Pohle K, Anders K, Ulzheimer S, Ohnesorge B, Schlundt C, Bautz W, Daniel WG, Achenbach S: Detection of coronary artery stenoses with thin-slice multi-detector row spiral computed tomography and multiplanar reconstruction. Circulation 2003; 107:664-6.
9. Cademartiri F, van der Lugt A, Luccichenti G, Pavone P, Krestin GP: Parameters affecting bolus geometry in CTA: a review. J Comput Assist Tomogr 2002; 26:596-607.
10. Bae KT, Heiken JP, Brink JA: Aortic and hepatic peak enhancement at CT: effect of contrast medium injection rate--pharmacokinetic analysis and experimental porcine model. Radiology 1998; 206:455-64.
11. Fleischmann D, Rubin GD, Bankier AA, Hittmair K: Improved uniformity of aortic enhancement with customized contrast medium injection protocols at CT angiography. Radiology 2000; 214:363-71.

12. Kopka L, Rodenwaldt J, Fischer U, Mueller DW, Oestmann JW, Grabbe E: Dual-phase helical CT of the liver: effects of bolus tracking and different volumes of contrast material. Radiology 1996; 201:321-6.
13. Kirchner J, Kickuth R, Laufer U, Noack M, Liermann D: Optimized enhancement in helical CT: experiences with a real-time bolus tracking system in 628 patients. Clin Radiol 2000; 55:368-73.
14. Mehnert F, Pereira PL, Trubenbach J, Kopp AF, Claussen CD: Automatic bolus tracking in monophasic spiral CT of the liver: liver-to-lesion conspicuity. Eur Radiol 2001; 11:580-4.
15. Mehnert F, Pereira PL, Trubenbach J, Kopp AF, Claussen CD: Biphasic spiral CT of the liver: automatic bolus tracking or time delay? Eur Radiol 2001; 11:427-31.
16. Sandstede JJ, Tschammler A, Beer M, Vogelsang C, Wittenberg G, Hahn D: Optimization of automatic bolus tracking for timing of the arterial phase of helical liver CT. Eur Radiol 2001; 11:1396-400.
17. Macari M, Israel GM, Berman P, Lisi M, Tolia AJ, Adelman M, Megibow AJ: Infrarenal abdominal aortic aneurysms at multi-detector row CT angiography: intravascular enhancement without a timing acquisition. Radiology 2001; 220:519-23.
18. Nieman K, Rensing BJ, van Geuns RJ, Munne A, Ligthart JM, Pattynama PM, Krestin GP, Serruys PW, de Feyter PJ: Usefulness of multislice computed tomography for detecting obstructive coronary artery disease. Am J Cardiol 2002; 89:913-8.
19. Vogl TJ, Abolmaali ND, Diebold T, Engelmann K, Ay M, Dogan S, Wimmer-Greinecker G, Moritz A, Herzog C: Techniques for the detection of coronary atherosclerosis: multi-detector row CT coronary angiography. Radiology 2002; 223:212-20.
20. Achenbach S, Giesler T, Ropers D, Ulzheimer S, Derlien H, Schulte C, Wenkel E, Moshage W, Bautz W, Daniel WG, Kalender WA, Baum U: Detection of coronary artery stenoses by contrast-enhanced, retrospectively electrocardiographically-gated, multislice spiral computed tomography. Circulation 2001; 103:2535-8.
21. Prokop M: Multislice CT angiography. Eur J Radiol 2000; 36:86-96.

3. CONTRAST MATERIAL

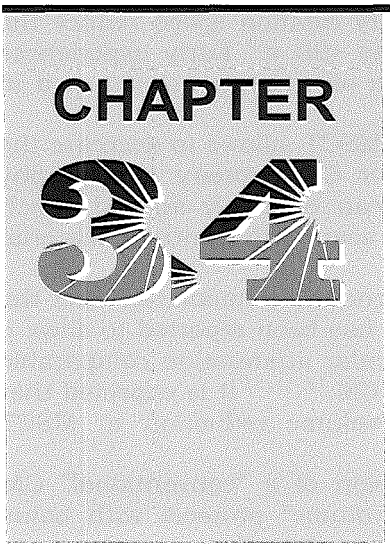

Non-invasive 16-row multislice CT coronary angiography: usefulness of saline chaser

Filippo Cademartiri, MD[1]
Nico Mollet, MD[1,2]
Aad van der Lugt, MD, PhD[1]
Koen Nieman, MD[1,2]
Peter MT Pattynama, MD, PhD[1]
Pim J de Feyter, MD, PhD[1,2]
Gabriel P Krestin, MD, PhD[1]

From the Departments of Radiology[1] and Cardiology[2], Thoraxcentrum, Erasmus M C, University Medical Center Rotterdam , The Netherlands.

Eur Radiol, 14:178–183, 2004.

ABSTRACT

The aim of this study was to investigate the usefulness of saline chaser in 16-row multislice CT (16- MSCT) coronary angiography. Fortytwo patients were divided into two groups for contrast material (CM) administration: group 1 (140 ml at 4 ml/s) and group 2 (100 ml at 4 ml/s followed by 40 ml of saline chaser at 4 ml/s). All patients underwent retrospectively ECG-gated 16-MSCT coronary angiography. The attenuation at the origin coronary vessels was assessed. Three regions of interest (ROIs) were drawn throughout the data set: (a) ascending aorta (ROI 1); (b) descending aorta (ROI 2); and (c) pulmonary artery (ROI 3). The attenuation in the superior vena cava was recorded (ROI 4). The average attenuation and the slope were calculated in each ROI and differences were assessed with a Student's *t* test. The average attenuation in the coronary vessels was not significantly different in the two groups. The average attenuations in ROI 1 were 325 and 327 HU, in ROI 2 were 328 and 329 HU and in ROI 3 were 357 and 320 HU, for groups 1 and 2, respectively ($p>0.05$). The slopes in ROI 1 were -0.2 and 1.1, in ROI 2 were 2.8 and 2.1 ($p>0.05$) and in ROI3 were 3.9 and -9.0 ($p<0.05$), for groups 1 and 2, respectively. The average attenuations in ROI 4 were 927 and 643 HU ($p<0.05$), for groups 1 and 2, respectively. One hundred milliliters of CM with 40 ml of saline chaser provides the same attenuation as 140 ml of CM (35% less) with decreased hyper-attenuation in the superior vena cava.

INTRODUCTION

Multislice-CT scanners with 16 rows of detectors (16-row MSCT) and increased spatial and temporal resolution have been introduced.[1, 2, 3] The increased number of detector rows and gantry rotation speed reduce the time needed to scan the coronary arteries to <20 s.[3] Early experiences reported improved results in the visualisation of coronary arteries and in the detection of coronary artery disease.[3, 4, 5, 6]

The shorter scan time, provided by 16-row MSCT, allows to decrease the volume of contrast material (CM) needed for CT coronary angiography (CTA).[7] Moreover, bolus-tracking technique can be easily applied which allows a better synchronisation of the CTA scan with contrast material passage.[4, 7, 8, 9, 10, 11, 12]

The use of a saline solution injected intravenously immediately after the CM main bolus, also known as bolus chaser, has been reported to allow a significant reduction of CM volume with vascular attenuation comparable with the one obtained with larger volumes of CM.[13, 14, 15] It is expected that the use of bolus chaser also allows CM volume reduction in MSCT coronary angiography.[16, 17, 18]

The aim of this study was the comparison of a "conventional" CM protocol without bolus chaser with a "low-volume" protocol with bolus chaser in non-invasive 16-row MSCT coronary angiography.

MATERIALS AND METHODS

Patient population

In November and December 2002, 42 patients (30 men and 12 women; mean age 59 years, age range 34–79 years), undergoing non-invasive MSCT coronary angiography for suspected coronary artery disease were prospectively enrolled in the study. Exclusion criteria for coronary CTA were irregular heart rates, previous allergic reaction to iodine contrast media, renal insufficiency (serum creatinine >120 mmol/l), pregnancy, respiratory impairment, unstable clinical status, or marked heart failure. The Institutional Review Board approved the study and patients gave informed consent.

After enrollment, patients were randomly divided into two groups with different protocols for intravenous contrast material (Visipaque 320 mg I/ml, Amersham Health, Little Chalfont, UK) administration: group 1 (conventional) 140 ml administered at 4 ml/s and group 2 (low-volume) 100 ml at 4 ml/s followed by 40 ml of saline at 4 ml/s. In each patient, age, body weight and heart rate were recorded.

Multislice-CT scan

Prior to the examination, the patients' heart rate (HR) was measured. Patients with a pre-scan HR ≥65 bpm were given 100 mg of metoprolol per os 1 h before the scan.

The scan parameters for MSCT coronary angiography (Sensation 16, Siemens, Forchheim, Germany) were: number of detectors 12; individual detector width 0.75 mm; gantry rotation time 420 ms; 120 kV; 400–500 mAs; feed/rotation 2.8 mm; and scan direction cranio-caudal.

The heart rate during the scan was also recorded. Contrast material administration and synchronisation protocols The iodinated CM was administered intravenously using a prototype of double-head power injector (Stellant, MedRAD, Pittsburgh, Pa.) through an 18-G venflon in the antecubital vein. Two different injection protocols were applied.

Synchronisation between the passage of CM and data acquisition was achieved with real-time bolus tracking (CARE bolus, Siemens, Forchheim, Germany) using an ROI in the ascending aorta for monitoring a threshold of +100 HU above the baseline attenuation to trigger the scan.

Data collection

Two data sets were reconstructed using retrospective ECG gating with time window starting 400 ms before the next R wave. The first data set was reconstructed for the purpose of coronary artery attenuation assessment with effective slice width 1 mm, reconstruction interval 0.5 mm, field of view (FOV) 160 mm and convolution filter medium smooth. The second data set was reconstructed for the purpose of great thoracic vessel assessment with effective slice width 3 mm, reconstruction interval 3 mm, FOV 200 mm and convolution filter medium smooth.

Coronary artery attenuation

Axial slices in the data set were scrolled to find the best location to measure the attenuation at the origin of the main coronary arteries (Fig. 1): left main coronary artery; left anterior descending; circumflex artery; and right coronary artery (RCA).

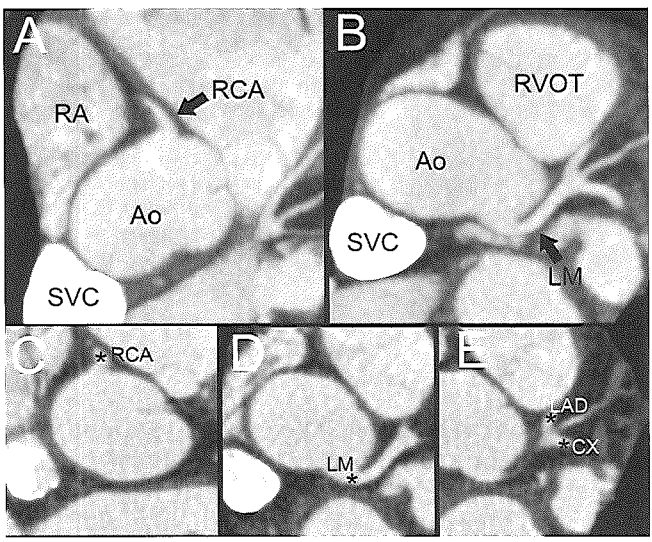

Figure 1A–E. Assessment of attenuation at the origin of coronary vessels. In **A and B** two oblique para-axial maximum intensity projection reconstructions show the ascending aorta (Ao), the origin of the right coronary artery (RCA; arrow) and left main coronary artery (LM; arrow). The superior vena cava (SVC) is also shown with very high attenuation.
The assessments of attenuation at the origin of the main coronary arteries are performed for RCA (asterisk), for LM (asterisk), for the left anterior descending (LAD; asterisk) and for the circumflex (CX; asterisk) as shown in **C, D and E**, respectively. RA right atrium, RVOT right ventricle outflow tract

The ROI was Fig. 1A–E Assessment of attenuation at the origin of coronary vessels. In A and B two oblique para-axial maximum intensity projection reconstructions show the ascending aorta (Ao), the origin of the right coronary artery (RCA; arrow) and left main coronary artery (LM; arrow). The superior vena cava (SVC) is also shown with very high attenuation.

The assessments of attenuation at the origin of the main coronary arteries are performed for RCA (asterisk), for LM (asterisk), for the left anterior descending (LAD; asterisk) and for the circumflex (CX; asterisk) as shown in C, D and E, respectively. RA right atrium, RVOT right ventricle outflow tract drawn as large as possible and calcifications, plaques and stenosis were carefully avoided.

Bolus geometry of great vessels

The attenuation in Hounsfield units was measured in three arteries drawing a ROI in consecutive slices (at intervals of ~1 s.) through the data set (Fig. 2): (a) the ascending aorta–left ventricle (ROI 1); (b) the descending aorta (ROI 2); and (c) the pulmonary artery– right ventricle (ROI 3). In addition, the attenuation inside the superior vena cava (ROI 4) at the beginning of the scan (e.g. first slice of the data set) was recorded. Time-related contrast measurements for each vessel, which were available in all patients, were included in the study to maintain homogeneous results.

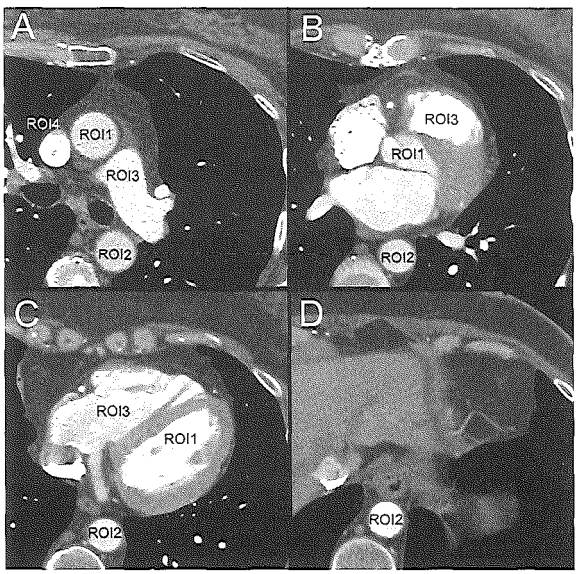

Figure 2A–D. Assessment of bolus geometry through the data set. The assessment of bolus geometry in the great vessels of the thorax have been performed using four regions of interest (ROIs). **A, B** The first (ROI1) is located in the ascending aorta at the beginning of the scan, whereas **C** the second part follows the path of the contrast material into the left ventricle. **A–D** The second ROI (ROI2) is located in the descending aorta all through the data set. **A** The third ROI (ROI3) is located in the pulmonary artery at the beginning of the scan, and then **B** follows into the right ventricle outflow tract and C into the right ventricle. The fourth ROI (ROI4) is plotted into the superior vena cava at the beginning of the scan

Data analysis

The attenuation values obtained from the three ROIs in each patient were averaged at each time point to generate the average time/density curves. Bolus geometry was described by two parameters, which represented quantitatively, the amount of CM present in the vessel during the scan (average attenuation) and the pattern of enhancement in the vessel (slope of attenuation). Three additional parameters were considered descriptive of bolus geometry: the attenuation value at the beginning of the scan (time 0), the Fig. 2A–D Assessment of bolus geometry through the data set. The assessment of bolus geometry in the great vessels of the thorax have been performed using four regions of interest (ROIs). A, B The first (ROI1) is

located in the ascending aorta at the beginning of the scan, whereas C the second part follows the path of the contrast material into the left ventricle. A–D The second ROI (ROI2) is located in the descending aorta all through the data set. A The third ROI (ROI3) is located in the pulmonary artery at the beginning of the scan, and then B follows into the right ventricle outflow tract and C into the right ventricle. The fourth ROI (ROI4) is plotted into the superior vena cava at the beginning of the scan maximum enhancement value (MEV; the peak of attenuation) and the time to reach the MEV (tMEV). Significant differences between the two groups were assessed using Student's *t* test. A p value <0.05 was considered significant.

RESULTS

Scans and bolus timing procedures were successfully completed in all patients. No significant adverse reactions to CM were observed. Age, weight, mean heart rate during the scan, mean scan delay and mean scan time were not significantly different in the two groups (Table 1).

Table 1. Patient data

	Group 1	Group 2
No. of patients	21	21
Male/female	16/5	14/7
Mean age (years)*	59 (34–74)	59 (39–79)
Mean weight (kg)*	72 (53–90)	74 (60–95)
Mean heart rate (bpm)*	60 (48–72)	60 (49–80)
Mean scan delay (s)	21.5±1.7	20.9±2.3
Mean scan time (s)	17.9±0.9	18.2±1.6

No significant differences were detected between the two groups (p>0.05)
*Range in parentheses

Coronary artery attenuation

The attenuation at the origin of the four main coronary vessels was higher in group 1, but there was not a significant difference between the two groups (Fig. 3A; Table 2). Ascending aorta-left ventricle The average attenuation and the slope were slightly higher in group 2 but not significantly different (p>0.05; Fig. 3B; Table 3). The attenuation values at time 0, the MEV and the tMEV were slightly higher in group 2 but not significantly different (p>0.05).

Descending aorta

The average attenuation and the slope were slightly higher in group 2 but not significantly different (p>0.05; Fig. 3C; Table 3). The attenuation values at time 0 and the MEV were slightly higher in group 2 but not

significantly different (p>0.05). The tMEV was significantly higher in group 1 (p<0.05).

Table 2. Coronary vessel attenuation. LM left main, LAD left anterior descending, CX circumflex, RCA right coronary artery

	Group 1	Group 2
LM	324±45	319±46
LAD	318±46	312±42
CX	313±41	304±37
RCA	321±42	319±46

Measurements are in Hounsfield units
The mean density (±SD) at the origin of coronary vessels for group 1 (conventional 140-ml protocol) and group 2 (low-volume protocol with bolus chaser) shows no significant differences (p>0.05)

Table 3. Bolus geometry in the great vessels of the thorax. MEV maximum enhancement value, tMEV time to reach the MEV

	Ascending aorta			Descending aorta			Pulmonary artery			Superior vena cava		
	Group 1	Group 2	p value	Group 1	Group 2	p value	Group 1	Group 2	p value	Group 1	Group 2	p value
Average (HU)	325±39	327±48	>0.05	328±49	329±55	>0.05	357±73	320±81	>0.05	927±89	643±170	<0.05
Slope	-0.2	1.1	>0.05	2.8	2.1	>0.05	3.9	-9.0	<0.05	-	-	-
Time 0 (HU)	314±36	318±48	>0.05	295±32	298±44	>0.05	341±62	359±67	>0.05	-	-	-
MEV (HU)	350±40	356±56	>0.05	373±64	374±79	>0.05	422±74	409±88	>0.05	-	-	-
tMEV (s)	4.2±1.7	5.4±3.1	>0.05	14.0±3.0	10.7±4.4	<0.05	6.4±3.5	2.8±3.0	<0.05	-	-	-

The quantitative parameters of bolus geometry for the main vessels of the thorax are displayed for group 1 (conventional 140-ml protocol) and group 2 (low-volume protocol with bolus chaser)

Pulmonary artery–right ventricle

The average attenuation was higher in group 1 but not significantly different (p>0.05; Fig. 3D; Table 3). The slope, instead, was significantly higher in group 1 (p<0.05). The attenuation values at time 0 and the MEV were not significantly different between the two groups (p>0.05). The tMEV was significantly higher in group 1 (p<0.05).

Superior vena cava

The average attenuation was significantly higher in group 1 (p>0.001; Table 3).

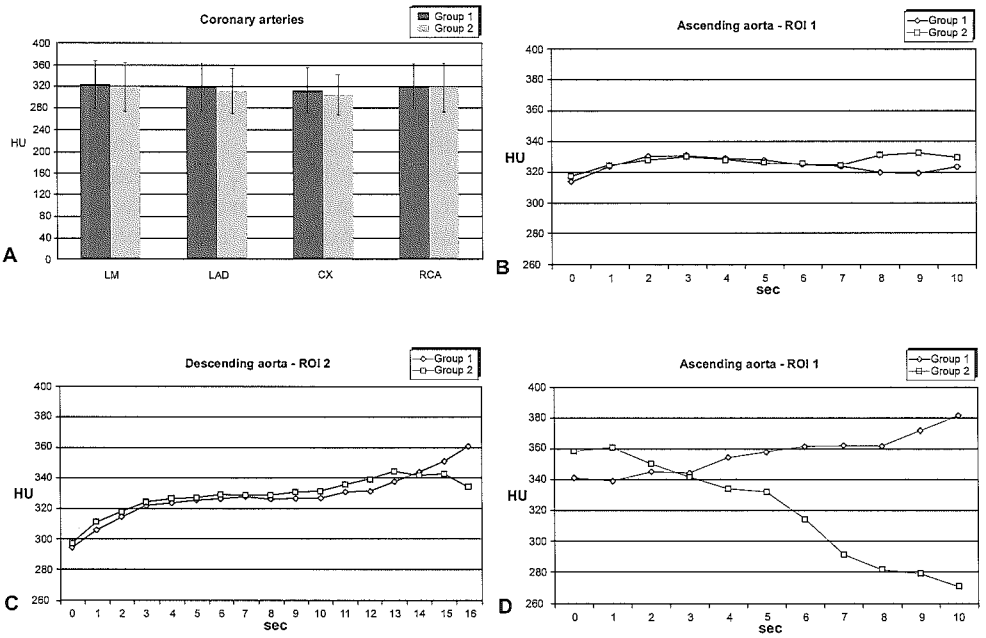

Figure 3A–D. Results of attenuation assessment of coronary arteries and great thoracic vessels. **A** The results of the attenuation assessment at the level of coronary arteries show slightly lower values for group 2 but not significantly different in all four sample regions. **B, C** The average time/density curves in the ascending aorta and descending aorta are almost identical for groups 1 and 2. **D** For the pulmonary artery, instead, group 1 shows more "pooling" of contrast material in the right chambers of the heart

Discussion

With the new generation of MSCT scanners featuring 16 rows of detectors, the time needed to scan the heart for the purpose of coronary CTA has been reduced to ~20 s;[1, 2, 3, 4, 5] yet, no studies have been performed on the optimisation of CM administration in non-invasive coronary imaging with MSCT.

We compared a conventional CM protocol for non-invasive MSCT with a low-volume protocol adding the pushing and washout effects of a bolus chaser. The two protocols showed comparable attenuation values at the level of coronary arteries and similar bolus geometry in the ascending and descending aorta. A significant difference was observed at the level of pulmonary artery where more "pooling" of CM was present for the conventional protocol. This observation is confirmed by the significantly lower attenuation observed in the superior vena cava for the low-volume protocol and supports the conclusion that 100 ml of CM pushed by 40 ml of saline provide optimal coronary artery enhancement with less attenuation in the right cavities of the heart. This result can be beneficial for a better visualisation of the mid-tract (segment 2) of RCA that may suffer from beamhardening artefacts when highly concentrated CM is present in the right atrium and right ventricle. This effect can be a

drawback when cardiac masses need to be studied. In this case a conventional CM protocol must be used.

The attenuation at time 0 and the MEV were not significantly different between the two protocols. The tMEV, instead, was significantly longer in the descending aorta (~3.2 s) and significantly shorter in the pulmonary artery (~3.6 s), for the conventional protocol. We have no clear explanation for the differences detected at this level. Previous experiences with bolus chaser support the evidence that the same results, in terms of vascular and parenchymal attenuation, can be achieved using less CM volume (up to 20–40% less) and with a concomitant reduction of the artefacts at the level of superior vena cava.[13, 14, 15, 19]

The explanation may be that a saline chaser pushes the injected CM through the veins of the forearm which will give the same result as the injection of a larger contrast volume, and that the saline chaser prevents the decrease of the contrast material flow in the arm veins which may normally cause an increase in the CM concentration after the end of the contrast injection.[7]

A limitation of this study is that the evaluation of coronary vessels could have been completed by the assessment of the length of coronary artery visualisation and/or the number of side branches visualised. We did not perform this evaluation because of the variable diameter of coronary arteries, heart rate and the degree of vessels with atherosclerotic disease (soft and calcified lesions, vessel stenosis and vessel occlusions). These parameters severely affect the capability of visualisation of the vessel regardless of the performance of the protocol for CM administration (e.g. the attenuation inside the vessel), and the number of patients enrolled in our study was not large enough to account for these variables.

Conclusion

In conclusion, the integration of bolus chaser in the CM administration protocol for non-invasive coronary artery angiography with 16-row MSCT allows to preserve the optimal intra-vascular attenuation, decreasing the volume of CM (35%) and the hyper-attenuating superior vena cava and right heart, with resulting cost savings and decreased risk of CM nephropathy.

References

1. Flohr T, Stierstorfer K, Bruder H, Simon J, Schaller S (2002) New technical developments in multislice CT. Part 1: approaching isotropic resolution with sub-millimeter 16-slice scanning. Rofo Fortschr Geb Rontgenstr Neuen Bildgeb Verfahr 174:839–845
2. Flohr T, Bruder H, Stierstorfer K, Simon J, Schaller S, Ohnesorge B (2002) New technical developments in multislice CT. Part 2: sub-millimeter 16-slice scanning and increased gantry rotation speed for cardiac imaging. Rofo Fortschr Geb Rontgenstr Neuen Bildgeb Verfahr 174:1022–1027

3. Heuschmid M, Kuttner A, Flohr T, Wildberger JE, Lell M, Kopp AF, Schroder S, Baum U, Schaller S, Hartung A, Ohnesorge B, Claussen CD (2002) Visualization of coronary arteries in CT as assessed by a new 16- slice technology and reduced gantry rotation time: first experiences. Rofo Fortschr Geb Rontgenstr Neuen Bildgeb Verfahr 174:721–724 [in German]
4. Nieman K, Cademartiri F, Lemos PA, Raaijmakers R, Pattynama PM, de Feyter PJ (2002) Reliable noninvasive coronary angiography with fast submillimeter multislice spiral computed tomography. Circulation 106:2051–2054
5. Ropers D, Baum U, Pohle K, Anders K, Ulzheimer S, Ohnesorge B, Schlundt C, Bautz W, Daniel WG, Achenbach S (2003) Detection of coronary artery stenoses with thin-slice multi-detector row spiral computed tomography and multiplanar reconstruction. Circulation 107:664–666
6. Cademartiri F, Nieman K, Raaymakers RH, de Feyter PJ, Flohr T, Alfieri O, Krestin GP (2003) Non-invasive demonstration of coronary artery anomaly performed using 16-slice multidetector spiral computed tomography. Ital Heart J 4:56–59
7. Cademartiri F, van der Lugt A, Luccichenti G, Pavone P, Krestin GP (2002) Parameters affecting bolus geometry in CTA: a review. J Comput Assist Tomogr 26:598–607
8. Kopka L, Rodenwaldt J, Fischer U, Mueller DW, Oestmann JW, Grabbe E (1996) Dual-phase helical CT of the liver: effects of bolus tracking and different volumes of contrast material. Radiology 201:321–326
9. Kirchner J, Kickuth R, Laufer U, Noack M, Liermann D (2000) Optimized enhancement in helical CT: experiences with a real-time bolus tracking system in 628 patients. Clin Radiol 55:368–373
10. Mehnert F, Pereira PL, Trubenbach J, Kopp AF, Claussen CD (2001) Automatic bolus tracking in monophasic spiral CT of the liver: liver-tolesion conspicuity. Eur Radiol 11:580–584
11. Mehnert F, Pereira PL, Trubenbach J, Kopp AF, Claussen CD (2001) Biphasic spiral CT of the liver: Automatic bolus tracking or time delay? Eur Radiol 11:427–431
12. Sandstede JJ, Tschammler A, Beer M, Vogelsang C, Wittenberg G, Hahn D (2001) Optimization of automatic bolus tracking for timing of the arterial phase of helical liver CT. Eur Radiol 11:1396–1400
13. Haage P, Schmitz-Rode T, Hubner D, Piroth W, Gunther RW (2000) Reduction of contrast material dose and artifacts by a saline flush using a double-power injector in helical CT of the thorax. Am J Roentgenol 174:1049–1053
14. Hopper KD, Mosher TJ, Kasales CJ, TenHave TR, Tully DA, Weaver JS (1997) Thoracic spiral CT: delivery of contrast material pushed with injectable saline solution in a power injector. Radiology 205:269–271
15. Bader TR, Prokesch RW, Grabenwoger F (2000) Timing of the hepatic arterial phase during contrast-enhanced computed tomography of the liver: assessment of normal values in 25 volunteers. Invest Radiol 35:486–492
16. Garcia P, Genin G, Bret PM, Bonaldi VM, Reinhold C, Atri M (1999) Hepatic CT enhancement: effect of the rate and volume of contrast medium injection in an animal model. Abdom Imaging 24:597–603
17. Han JK, Kim AY, Lee KY, Seo JB, Kim TK, Choi BI, Lhee CS, Han MC (2000) Factors influencing vascular and hepatic enhancement at CT: experimental study on injection protocol using a canine model. J Comput Assist Tomogr 24:400–406

18. Yamashita Y, Komohara Y, Takahashi M, Uchida M, Hayabuchi N, Shimizu T, Narabayashi I (2000) Abdominal helical CT: evaluation of optimal doses of intravenous contrast material—a prospective randomized study. Radiology 216:718–723
19. Dorio PJ, Lee FT Jr, Henseler KP, Pilot M, Pozniak MA, Winter TC III, Shock SA (2003) Using a saline chaser to decrease contrast media in abdominal CT. Am J Roentgenol 180:929–934

3. CONTRAST MATERIAL

CHAPTER 3.5

IV CONTRAST ADMINISTRATION FOR CT CORONARY ANGIOGRAPHY ON MULTIDETECTOR-ROW HELICAL CT: IMPACT OF IODINE CONCENTRATION ON VASCULAR ATTENUATION

Filippo Cademartiri[1], MD
Nico Mollet[1,2], MD
Aad van der Lugt[1], MD, PhD
Eugene McFadden[2], MB, FRCPI
Theo Stijnen[3], PhD
Pim J de Feyter[1,2], MD, PhD
Gabriel P Krestin[1], MD, PhD

From the Departments of Radiology[1], Cardiology[2], Thoraxcentrum and Epidemiology and Biostatistics[3]
Erasmus M C, University Medical Center Rotterdam, The Netherlands.

Radiology; 2005 (in press)

ABSTRACT

125 patients undergoing retrospectively ECG-gated 16-MDCT coronary angiography were randomized into five groups with respect to the IV administration of a 140ml bolus of contrast material (CM) at 4ml/s: group 1 (Iohexol 300mgI/ml), group 2 (Iodixanol 320mgI/ml), group 3 (Iohexol 350mgI/ml), group 4 (Iomeprol 350mgI/ml), group 5 (Iomeprol 400mgI/ml). The attenuation was measured in the descending aorta and in the coronary arteries. A one-way ANOVA test was used to compare groups.

The mean attenuation values in descending aorta were significantly ($p<0.05$) lower in group 1 and higher in group 5 compared to the other 3 groups. The same pattern was observed in the coronary arteries.

CM with higher iodine concentration provides significantly higher attenuation in the descending aorta and in the coronary arteries.

INTRODUCTION

Significant coronary artery stenosis can be reliably detected with with 16-multidetector-row computed tomography (16-MDCT) angiography.[1-5] The increased number of detector rows and faster gantry rotation with 16-MDCT compared to the previous 4-MDCT generation have improved the diagnostic performance of the technique and reduced the time needed to cover the entire heart to ~20s.[3] The type and iodine concentration of

contrast material (CM) has assumed increasing importance in CT angiography (CTA) to optimize the diagnostic yield[6] as the attenuation that can be achieved in the vessels greatly affects image quality, particularly for small coronary arteries.[7,8]

Two main modulable factors affect the attenuation: techniques that optimize synchronization between the arterial passage of CM and CT data acquisition, and the injection parameters for intravenous (IV) administration of CM.[6]

For optimal synchronization bolus tracking technique can be effectively applied.[9] For injection parameters, there are several variables that can be manipulated to increase vascular attenuation: the rate of injection, the volume injected and the iodine concentration of CM.[6]

The purpose of our study was to compare the impact on vascular attenuation of a scan protocol with different concentrations of three different CM, at the level of the descending aorta and the coronary arteries.

MATERIALS AND METHODS

Patients

Between March and September 2003, 125 patients (104 male and 21 female; mean age: 59±12 years) scheduled for 16-MDCT coronary angiography were prospectively studied. All patients meeting the inclusion criteria (stable angina pectoris, a stable heart rhythm, and able to hold their breath for 20s) referred from our institution or our referring hospitals, were enrolled. Exclusion criteria were: previous allergic reaction to iodinated CM, renal impairment (serum creatinine >120mmol/L); women of child bearing age who were not taking adequate contraception were also excluded. Our Institutional Review Board approved the study and all patients gave written informed consent.

After enrollment, patients were randomized into five groups (n=25 each): group 1 (Iohexol 300mgI/ml), group 2 (Iodixanol 320mgI/ml), group 3 (Iohexol 350mgI/ml), group 4 (Iomeprol 350mgI/ml), group 5 (Iomeprol 400mgI/ml). The molecule of CM was Iohexol (Omnipaque®, Amersham Health, Little Chalfont, UK) for Group 1 and Group 3, Iodixanol (Visipaque®, Amersham Health, Little Chalfont, UK) for Group 2, and Iomeprol (Iomeron® Bracco, Milan, Italy) for Group 4 and 5 (Table I). The injection volume (140ml) and rate (4ml/s) were constant in all groups. In each patient age, gender, body weight and heart rate during the scan were recorded.

Scan protocol

Studies were performed on a 16-MDCT scanner (Sensation 16, Siemens Medical Solutions, Forchheim, Germany). Prior to the examination the heart rate (HR) was measured. Patients with a pre-scan HR equal or above 65 bpm, were administered 100 mg of metoprolol per os one hour before the scan.

The CM was injected using a power injector (EnVision, MedRAD, Pittsburgh, PN, USA) through a 18G cannula in an antecubital vein.

Table 1. Physical properties of the different contrast materials.

	Group 1	Group 2	Group 3	Group 4	Group 5
Contrast material	Iohexol	Iodixanol	Iohexol	Iomeprol	Iomeprol
Commercial name	Omnipaque®	Visipaque®	Omnipaque®	Iomeron®	Iomeron®
Vendor	Amersham	Amersham	Amersham	Bracco	Bracco
Type	Monomeric	Dimeric	Monomeric	Monomeric	Monomeric
Iodine concentration (mgI/ml)	300	320	350	350	400
Osmolality (mOsm/kg water)	672	290	844	618	726
Absolute viscosity 20° C (cP)	11.8	26.6	20.4	14.5	27.5
Absolute viscosity 37° C (cP)	6.3	11.8	10.4	7.5	12.6
Iodine load (g)*	42	44.8	49	49	56
Iodine rate (g/s)*	1.2	1.28	1.4	1.4	1.6

*Using a protocol with a volume of 140ml administered at 4ml/s.
Abbreviations: cP = centiPascal; g = gram; kg = kilogram; mgI = milligrams of iodine; ml = millilitres; mOsm = milliOsmole;
s = seconds.

Contrast material volume and injection rate for main angiographic bolus were respectively 140 ml and 4 ml/s (total injection time of 35s) in all patients. In all groups except group 1 (Iohexol 300mgI/ml), the CM was administered after heating at 37° C. This procedure kept the viscosity of the 5 CM within 7.5 and 11.8 cP.

To synchronize the start of the scan with the arrival of CM a real-time bolus tracking technique was applied.[9]

The main scan parameters were: number of detectors 16, individual detector width 0.75 mm, gantry rotation time 420 ms, kV 120, mAs 400, feed/rotation 3.0 mm, feed/second 8.0, scan direction cranio-caudal. For the purpose of the present study, two datasets were reconstructed, both with retrospective ECG gating with time window starting at 400 ms before the next R wave on the ECG, FOV 200 mm, and a medium smooth convolution filter (B30f). The first dataset (dataset A) was reconstructed with an effective slice width and a reconstruction interval of 3mm and 3mm, respectively; the second dataset (dataset B) was reconstructed with an effective slice width and a reconstruction interval of 1mm and 0.6mm, respectively. The images were transferred to a stand-alone workstation and evaluated using dedicated analysis software (Leonardo, Siemens Medical Solutions, Forchheim, Germany).

Data collection and analysis

One experienced radiologist (F.C.) collected all the measurements at the workstation.

Two sets of measurements were performed:

1) the attenuation in the descending aorta, and
2) in the coronary arteries.

In order to generate a time-attenuation curve of the descending aorta during the angiographic scan, the attenuation values in HU were extracted from the dataset A as follows. The DICOM layout of the images allowed reading the exact time (down to hundreds of sec^{-1}) of the data acquisition in each reconstructed slice. At intervals of 1 second, in each slice, a ROI was drawn, throughout the entire data-set in the descending aorta. The variable individual morphology resulted in different scan times as well as in different length of the ROIs along the *z*-axis. Time-related contrast measurements available in all patients were included in the study.

The mean value (±SD) at each time point in the descending aorta was calculated by averaging the attenuation values. To display the attenuation during time, time/attenuation curve was generated. The start of the main scan was designated as time 0. The mean (±SD) attenuation for all the time points of the time-attenuation curve was calculated.

Dataset B was used to measure the attenuation at the origin of the main coronary artery branches. This dataset has, in fact, a higher spatial resolution in the *z*-axis allowing to measure structures with a diameter of 3-5mm. A ROI was plotted on the axial image as large as the vessel lumen on a slice where the lumen was easily identified. Regions where there were calcifications in the coronary wall and non-calcified plaques were carefully avoided. Four vessels were studied: left main coronary artery (LM), left anterior descending coronary artery (LAD), left circumflex (CX), and right coronary artery (RCA). The attenuation value in HU was measured on axial images on the dataset B. The mean (±SD) value per patient was calculated by averaging the attenuation values obtained in the four coronary vessels.

Statistical analysis

Differences between groups were assessed with a one-way ANOVA test followed by Fischer's LSD procedure to compare all pairs of groups. A $p<0.05$ was considered significant.

RESULTS

Baseline characteristics such as age, gender, weight, and heart rate did not differ among the five groups. Additional beta-blockers were administered in 71 (57%) patients. No relevant differences were observed in the scan delay and scan duration between the five groups (Table II). A single immediate adverse reaction to CM that required treatment was recorded in a patient who received Iomeprol 350mgI/ml. The patient was discharged after 2 hours on oral treatment (anti-histaminic and corticosteroid) and his subsequent course was uneventful.

Table 2. Baseline demographic data and protocol information in the study population.

	Group 1	Group 2	Group 3	Group 4	Group 5
Number of patients		25	25	25	25
Male/Female	22/3	20/5	21/4	21/4	20/5
Mean age (yrs)	63±12	57±11	58±13	60±11	58±11
Weight (kg)	71±8	74± 9	72±7	72±7	74±7
Mean heart rate (bpm)	57±8	60±9	61±9	59±7	59±8
Scan delay (seconds)	21.9±3.7	20.7±2.7	21.4±2.8	22.1±2.2	20.6±3.0
Scan duration (seconds)	16.8±2.1	17.2±1.7	17.6±1.3	17.7±2.0	17.6±2.1

No relevant differences between the groups were found.
Abbreviations: yrs= years; kg= kilogram; bpm= beats per minute.

In the descending aorta (Table III and Figure 1), the mean attenuation in group 1 (277±41HU) and group 5 (386±78HU) was significantly lower and higher, respectively, compared to all the remaining groups ($p<0.05$).
In the coronary arteries (Table IV), the mean coronary artery attenuation was significantly lower in group 1 (273±45HU) and significantly higher in group 5 (397±72HU), respectively, compared to the remaining groups ($p<0.05$).

Table 3. Parameters of the attenuation curve in the study population.

	Descending Aorta				
	Group 1	Group 2	Group 3	Group 4	Group 5
Average (HU)	277±41*	333±50	315±54	318±42	386±78*

Values significantly different ($p<0.05$) from the other groups are highlighted with *.
Abbreviations: HU= Hounsfield Units.

Table 4. Attenuation values in the coronary arteries in the study population.

	Group 1	Group 2	Group 3	Group 4	Group 5
Mean (HU)	273±45*	333±51	320±55	322±43	397±72*

Values significantly different ($p<0.05$) from the other groups are highlighted with *.
Abbreviations: HU= Hounsfield units.

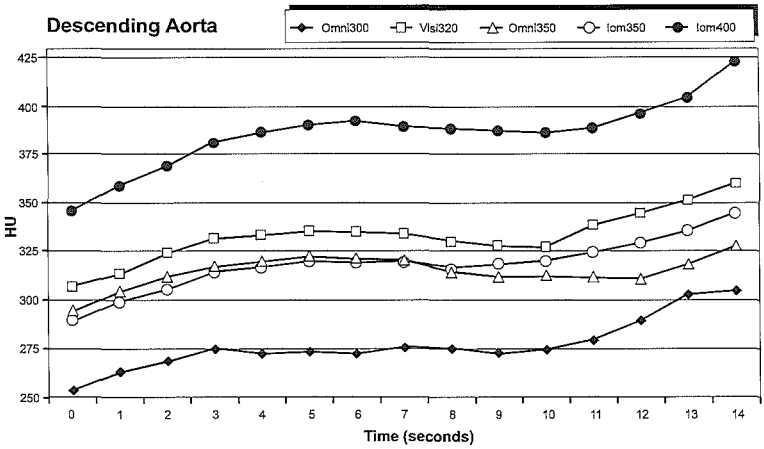

Figure 1. Average time-attenuation curves in the descending aorta. The time-attenuation curve in the descending aorta, shows that group 1 (Omni300) remains constantly below all the other groups while group 5 (Iom400) remains constantly above the all the others. The other groups (Vis320, Omni350, and Iom350) show a comparable attenuation.

DISCUSSION

Imaging of coronary artery suffers from their small size and from stenosis and/or obstruction that reduce the blood flow. A higher iodine concentration in this case allows to depict a vessel which contains a smaller volume of blood.[7, 8] Becker et al. considered an attenuation of 250-300HU as optimal for coronary CT angiography.[10] On one hand it is reasonable to expect that a higher attenuation would progressively obscure coronary calcifications, on the other hand there is no available validation data supporting the statement. In fact, we agree with Becker et al.[10] and we believe that the imaging of coronary calcium and plaques need a rather different approach with CT, than the one required for the assessment of significant stenosis. In the first instance the lumen is less important and therefore a too high attenuation (>300HU) may compromise the assessment of coronary wall. In the second instance, instead, the visualization of the lumen is more important a higher attenuation may improve the visualization of small coronary vessels.

Only a few studies in animals have examined the impact of different types of CM at different concentrations on image quality during CTA and only one such study was performed in the human coronary circulation. These studies demonstrated that, for a given volume of CM administered at the same rate, higher iodine concentration results in a proportionally higher peak of maximum enhancement without significant affecting the time to peak of enhancement.[11, 12]

Recent papers discuss the role of higher iodine concentration for CTA.[13-16] Increasing iodine concentration provide a proportionally higher vascular attenuation.[13] Similarly, an increasing injection rate provides a progressively higher vascular attenuation.[13] The impact of injection rate is more pronounced than the impact of iodine concentration, and, in

principle, one would like to use the injection rate to regulate the amount of vascular attenuation. Unfortunately, the injection rates that are feasible in routine clinical practice are up to 4-5 ml/s. Higher injection rates would require larger needles and larger veins, requiring more time to set the IV and with an increased risk of CM extra-vasation.

Although iodine concentration is not as effective as injection rate in increasing intra-vascular attenuation, it is always feasible in any condition.

A study from Becker et al. compared different iodine concentration (Iomeprol 300 and 400 mgI/ml) and injection rates (2.5 and 3.5 ml/s) while performing 4-MDCT angiography of coronary arteries.[10] The conclusion was that vascular attenuation achieved with 400mgI/ml and 3.5ml/s was significantly higher than the other protocols and that 300mgI/ml and 2.5ml/s provide significantly lower attenuation compared to the other protocols and also insufficient for optimal coronary angiography (range: 148-194HU in the coronary arteries). Based on the results, the authors also conclude that an injection rate of 1gI/s provide the desired iodine load to achieve and maintain the target enhancement.

Our study shows the progressively higher vascular attenuation obtained with higher iodine concentrations.[6] A significant difference was observed between the groups using the two CMs at the extremes of the spectrum of iodine concentration and the remaining groups.

Vascular attenuation was not significantly different between monomeric compounds with an iodine concentration of 350mg/ml (iohexol and iomeprol) and the dimeric compound with an iodine concentration of 320 mg/ml (iodixanol). Following the target attenuation applied by Becker et al. for optimal coronary angiography all of these three compounds with the protocol applied ranged in the optimal value.[10] This result favors the dimeric compound that can also rely on its iso-osmolality, reported less nephro-toxic in high risk patients.[17] The advantage of the 300mgI/ml compound is that its viscosity does not require heating prior to use.

A limitation of the study is related to the evaluation of coronary arteries. Ideally the best way to assess the efficacy of a CM protocol would be to measure the length of coronary arteries, and the number of side branches that can be visualized. We preferred to assess quantitatively the origin of the main coronary arteries because the number of patients was too small to account for the many variables that can affect coronary artery visualization regardless of the attenuation of the vessel: the high heart rate, the small vessel size, the variable anatomy, the heavily calcified vessel wall, the presence of stenosis or occluded vessels.

Moreover, the aim of the study was to show the performance of different CM in terms of vascular attenuation and not the impact of vascular attenuation on diagnostic accuracy.

REFERENCES

1. Nieman K, Cademartiri F, Lemos PA, Raaijmakers R, Pattynama PM, de Feyter PJ: Reliable noninvasive coronary angiography with fast submillimeter multislice spiral computed tomography. Circulation 2002; 106:2051-4.
2. Ropers D, Baum U, Pohle K, Anders K, Ulzheimer S, Ohnesorge B, Schlundt C, Bautz W, Daniel WG, Achenbach S: Detection of coronary artery stenoses with thin-slice multi-detector row spiral computed tomography and multiplanar reconstruction. Circulation 2003; 107:664-6.
3. Heuschmid M, Kuttner A, Flohr T, Wildberger JE, Lell M, Kopp AF, Schroder S, Baum U, Schaller S, Hartung A, Ohnesorge B, Claussen CD: [Visualization of coronary arteries in CT as assessed by a new 16 slice technology and reduced gantry rotation time: first experiences]. Rofo 2002; 174:721-4.
4. Flohr T, Stierstorfer K, Bruder H, Simon J, Schaller S: New technical developments in multislice CT - Part 1: Approaching isotropic resolution withsub-millimeter 16-slice scanning. Rofo 2002; 174:839-45.
5. Flohr T, Bruder H, Stierstorfer K, Simon J, Schaller S, Ohnesorge B: New Technical Developments in Multislice CT, Part 2: Sub-Millimeter 16-Slice Scanning and Increased Gantry Rotation Speed for Cardiac Imaging. Rofo 2002; 174:1022-7.
6. Cademartiri F, van der Lugt A, Luccichenti G, Pavone P, Krestin GP: Parameters affecting bolus geometry in CTA: a review. J Comput Assist Tomogr 2002; 26:596-607.
7. Bae KT, Heiken JP, Brink JA: Aortic and hepatic peak enhancement at CT: effect of contrast medium injection rate--pharmacokinetic analysis and experimental porcine model. Radiology 1998; 206:455-64.
8. Fleischmann D, Rubin GD, Bankier AA, Hittmair K: Improved uniformity of aortic enhancement with customized contrast medium injection protocols at CT angiography. Radiology 2000; 214:363-71.
9. Cademartiri F, Nieman K, van der Lugt A, Raaijmakers RH, Mollet N, Pattynama PM, de Feyter PJ, Krestin GP: IV contrast administration for CT coronary angiography on a 16-multidetector-row helical CT scanner: test bolus vs. bolus tracking. Radiology 2004; (in press):XXX-XXX.
10. Becker CR, Hong C, Knez A, Leber A, Bruening R, Schoepf UJ, Reiser MF: Optimal Contrast Application for Cardiac 4-Detector-Row Computed Tomography. Invest Radiol 2003; 38:690-694.
11. Han JK, Kim AY, Lee KY, Seo JB, Kim TK, Choi BI, Lhee CS, Han MC: Factors influencing vascular and hepatic enhancement at CT: experimental study on injection protocol using a canine model. J Comput Assist Tomogr 2000; 24:400-6.
12. Bluemke DA, Fishman EK, Anderson JH: Effect of contrast concentration on abdominal enhancement in the rabbit: spiral computed tomography evaluation. Acad Radiol 1995; 2:226-31.
13. Fleischmann D: Use of high concentration contrast media: principles and rationale-vascular district. Eur J Radiol 2003; 45 Suppl 1:S88-93.
14. Brink JA: Use of high concentration contrast media (HCCM): principles and rationale--body CT. Eur J Radiol 2003; 45 Suppl 1:S53-8.
15. Brink JA: Contrast optimization and scan timing for single and multidetector-row computed tomography. J Comput Assist Tomogr 2003; 27 Suppl 1:S3-8.
16. Merkle EM, Boll DT, Fenchel S: Helical computed tomography of the pancreas: potential impact of higher concentrated contrast agents and multidetector technology. J Comput Assist Tomogr 2003; 27 Suppl 1:S17-22.

17. Aspelin P, Aubry P, Fransson SG, Strasser R, Willenbrock R, Berg KJ: Nephrotoxic effects in high-risk patients undergoing angiography. N Engl J Med 2003; 348:491-9.

4. CORONARY ANATOMY

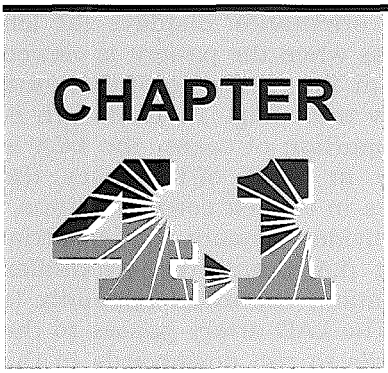

ANATOMY OF THE CORONARY ARTERIES AND VEINS IN CT IMAGING

Robert J. M. van Geuns
Filippo Cademartiri

From the Department of Radiology,
Erasmus MC, University Medical Center Rotterdam,
The Netherlands.

CT of the Heart: Principles and Applications
Edited by: U. Joseph Schoepf – pp. 218-228;

INTRODUCTION

The cardiologist and radiologist interpreting coronary computed tomographyangiography (CTA) should be familiar with coronary artery anatomy. It has a standard logical structure with some common variations and only a few rare abnormalities. In a conventional selective coronary angiography, blood in the chambers and coronary veins does not interfere with the visualization of the coronary arteries. In addition, myocardium and other soft tissues are hardly seen because of their low absorption of X-rays. Invasive selective coronary angiograms use projections performed in various orientations so that the cardiologist can perceive the 3D anatomy of the coronary arteries. This is quite different for imaging techniques such as CTA. In CTA the contrast agent is intravenously injected, which results in enhancement of the myocardium and blood in the cavities, and projection techniques such as maximum intensity projection (MIP) are therefore of limited use. Overlap of structures that obscure coronary imaging can be avoided by multiplanar reformation (MPR) using thin slices in any desired orientation. However, in that case much of the 3D information is not used. With modern postprocessing tools, such as maximum intensity projection (MIP) or the volume rendering technique (VRT), 3D impressions on a 2D surface can be created. These images look much like the gross anatomy of the heart, but they do not resemble the images known from invasive selective coronary angiography. In this chapter we will therefore review the normal coronary artery and venous anatomy as it may be seen on MPR and VRT images of CTA. We will also review the anomalies that may be encountered during investigations for coronary artery disease.

CORONARY ARTERY ANATOMY

Left coronary artery

The left main coronary artery (LCA) arises from the left posterior aortic sinus. In tomographic imaging, the preferred orientation displays the left of the patient in the right side of the images, as when the patient is viewed from the feet. In such images the LCA starts at the right side of the aorta just posterior to the right ventricular outflow tract (Fig. 1). Its length is variable, but usually 1-2 cm.[1] In a small proportion of cases, the LCA is very short and bifurcates almost immediately. In 0.41% of the cases, the LCA is not developed and there are two orifices in the left coronary sinus.[2] In two-thirds of the subjects, the main LCA divides beneath the left atrial appendix, into the left anterior descending (LAD) and the circumflex arteries. When using VRTs for off-line evaluation, the atrial appendix is usually excluded from the data set (Fig. 2).[3] The LAD artery passes to the left of the pulmonary trunk and turns forwards to run downwards in the anterior interventricular groove towards the apex. When MPR is used for evaluation of CTA, data sets and series of parallel slices or curved MPR along the intraventricular groove have to be created for optimal visualization of the vessel (Fig. 3). The LAD artery provides two main groups of branches. First, the septal branches, which supply the anterior two-thirds of the septum, and second, the diagonal branches, which lie on the lateral aspect of the left ventricle. The septal branches arise form the LAD at approximately 90-degree angles. They vary in size, number, and distribution. The first large septal branch may divide into a fork where both branches run parallel into the septum. In other cases, a septal branch may run parallel to the LAD through the myocardium of the septum. By convention, the first septal branch separates the proximal LAD from the middle part of the LAD. The diagonals also vary in number and course (Fig. 4). Usually at least one diagonal is present, and if none is visualized, a total occlusion may be expected. A normal variation of the large diagonal is a parallel course to the LAD. In the majority of the patients, the LAD itself courses around the apex to reach the inferior wall and septum. In the other cases, the distal right coronary artery (RCA) is larger and supplies the blood flow for the apex. This is one of the potential collateral routes if either the RCA or LAD is occluded. The left circumflex artery (LCx) turns backwards shortly beyond its origin to run downwards in the left arterioventricular groove. It too gives rise to a variable number of branches, which lie on the lateral aspect of the left ventricle (the marginal branches, Fig. 4). In one-third of the subjects, the left main coronary artery trifurcates into the aforementioned branches and an intermediate artery, which follows a course between the circumflex and LAD arteries over the anterolateral wall of the left ventricle (Fig. 5).[3] Additional branches of the LCx are small atrial branches that supply the lateral and posterior regions of the left atrium.

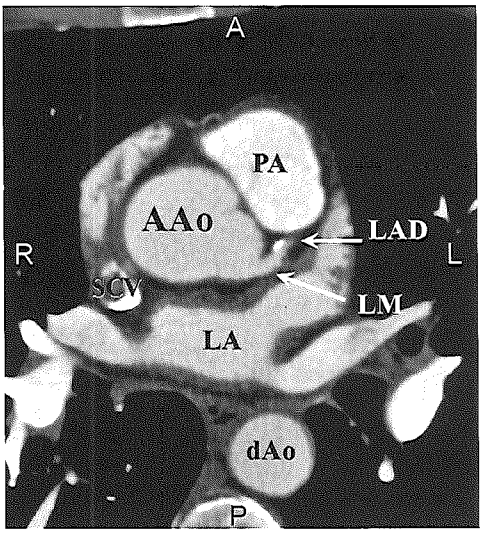

Figure 1. Transverse slice through the aortic root. The left main coronary artery (LM) can clearly be seen, the proximal left anterior descending artery (LAD) turns around the pulmonary artery (PA) anteriorly. AAo, ascending aorta; SCV, superior caval vein; LA, left atrium; dAo, descending aorta; A, anterior thoracic wall; P, posterior (spine); L, left; R, right.

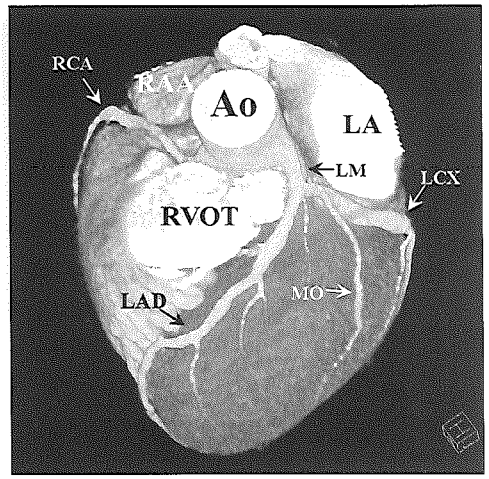

Figure 2. Volume rendering of the left coronary artery after removal of the left atrial appendage and cranial part of the left atrium (LA) in the original topographic slices over 15 levels. Without this processing tool, the left atrial appendage normally overlaps the left main (LM) and proximal circumflex coronary artery (LCx). The right atrial appendage (RAA) may sometimes override the right coronary artery (RCA), but in this case manual removal was not necessary. LAD, left anterior descending coronary artery; RVOT, right ventricular outflow tract; MO, margo obtusus of the circumflex coronary artery.

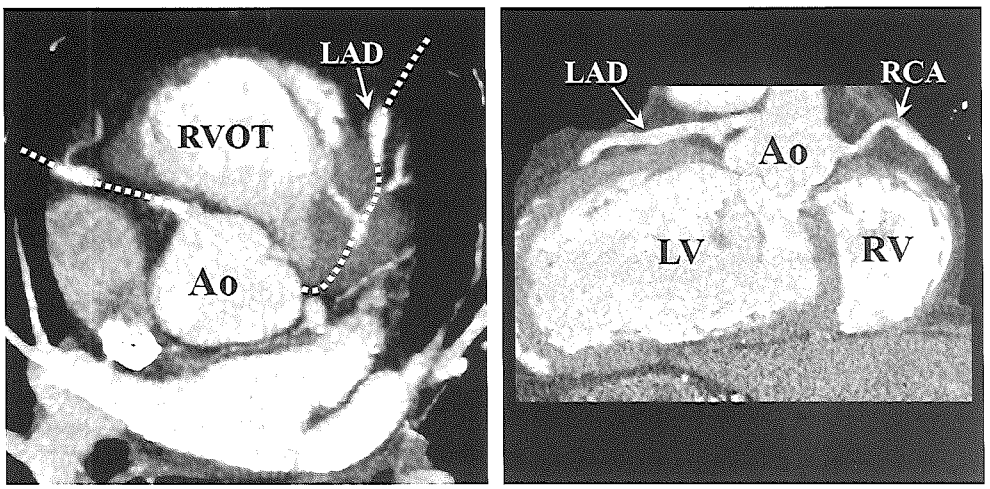

Figure 3. Left anterior descending artery (LAD) and proximal right coronary artery (RCA) in a single plane. (**A**) Starting from a transverse plane through the middle of LAD, a curved reconstruction plane is selected through the proximal RCA, ascending aorta, left main and proximal LAD (dashed line). (**B**) Curved multiplanar reformation (MPR) along LAD and RCA. The LAD follows a course over the anterior wall of the left ventricle to the apex of the heart. RVOT, right ventricular outflow track; Ao, aorta; LV, left ventricle; RV, right ventricle.

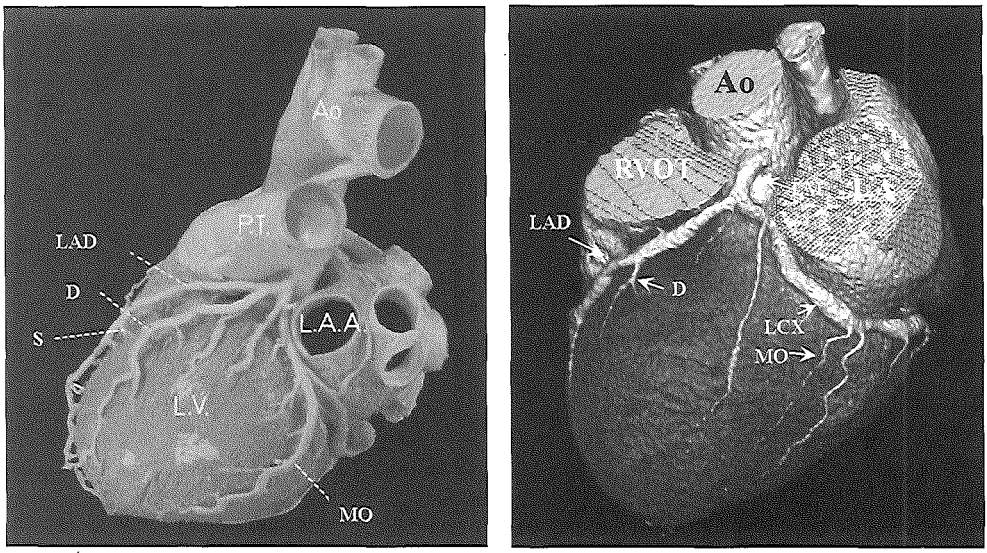

Figure 4. (**A**) Anatomical view of the left coronary artery (reproduced with permission from [13]). The auricle of the left atrium (L.A.A.) overlapping the circumflex coronary artery is removed. The left main (LM) artery divides beneath the L.A.A. in the left anterior descending (LAD) and circumflex (LCx) coronary arteries. From the LAD artery diagonal branches (**D**) arise. The margo obtusus (MO) arises from the LCx artery. (**B**) A comparable noninvasive coronary angiogram with computed tomography. Ao, aorta; PT, pulmonary trunk; LA, left atrium, after removal of the auricle; LV, left ventricle; RVOT, right ventricular outflow track. (A full color version of this illustration can be found in the color section (chapter 12)).

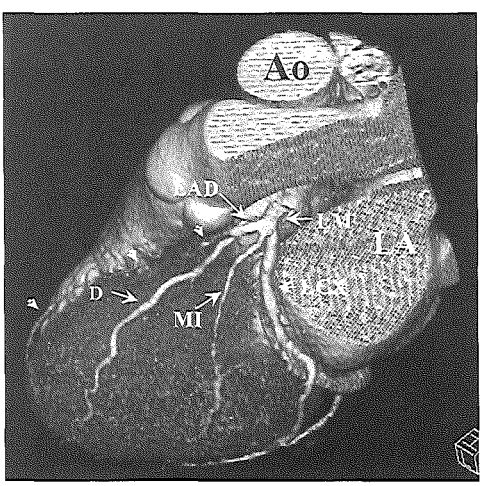

Figure 5. Coronary CT angiography, trifurcation of the left main artery into left anterior descending (LAD), circumflex (LCx), and intermediate (MI) arteries. The LAD is occluded after the first diagonal branch (D) but shows some contrast filling through collateral vessels (arrowheads). (A full color version of this illustration can be found in the color section (chapter 12)).

RIGHT CORONARY ARTERY

The RCA arises from the anterior aortic sinus, somewhat inferior to the origin of the LAD. It passes forwards and then downwards in the right atrioventricular groove (Fig. 6) and continues around the margin of the heart towards the crux, a point below where the atrioventricular groove and the posterior interventricular groove meet. Sometimes a single MPR image displays a long segment of the RCA if an imaging plane through the right atrioventricular groove is selected (Fig. 6). A longer part may be visible if this plane istilted with the caudal side to theback of the patient. The first branch of the RCA is generally the conus artery that runs over the anterior surface of the right ventricular outflow tract (Fig. 7).

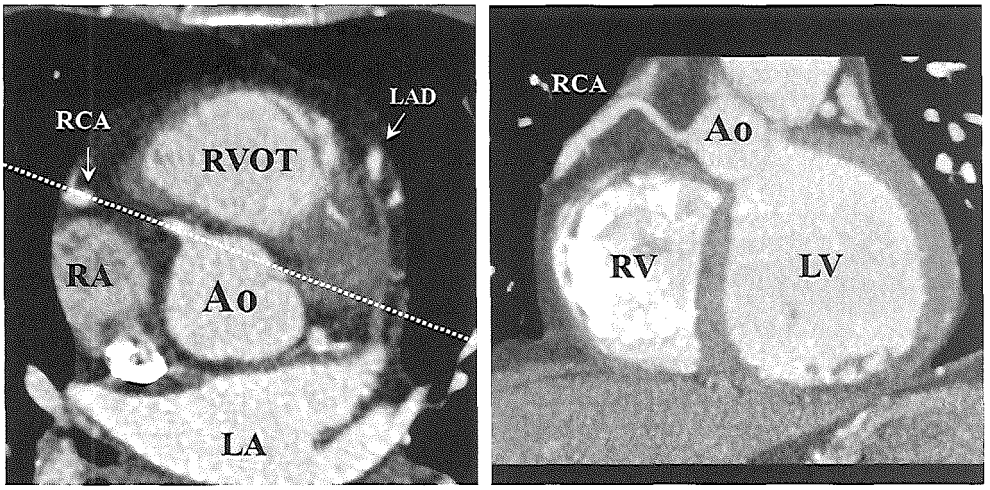

Figure 6. Localization of the right coronary artery (RCA). (A) A transverse plane between the right ventricle outflow track (RVOT) and right atrium (RA) through the proximal RCA is selected (dashed line). (B) Image along the proximal and middle segment of the RCA. RV, right ventricle; LV, left ventricle.

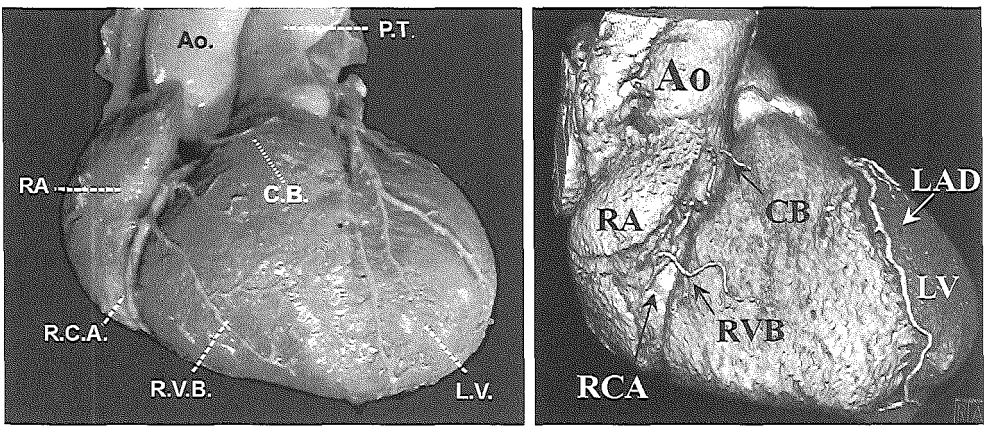

Figure 7. (**A**) A pressure-fixed anatomical specimen showing the proximal and middle right coronary artery (RCA) with its side branches (conus branch [CB] and right ventricular branch [RVB]). Reproduced from McAlpine (13) with permission of Springer-Verlag. (**B**) A 3-D rendering of the right coronary artery. Because of the small size, only the proximal part of the conus branch can be seen. The RCA shows atherosclerotic disease over its full length. At the right side of the picture, the left anterior descending (LAD) coronary artery can be clearly seen. Ao, ascending aorta; PT, pulmonary trunk; LV, left ventricle; RV, right ventricle; RA, right atrium. (A full color version of this illustration can be found in the color section (chapter 12)).

The second branch is usually the sinoatrial node artery; alternatively, the sinus node is supply by a proximal branch of the LCx, and in some cases both routes are available. In the majority (80%) of individuals, the RCA continues forwards from the crux along the posterior interventricular groove to become the posterior descending artery (PDA), running to the apex of the heart (Fig. 8). This is by convention called RCA dominance.[4] Septal branches supplying the posterior third of the septum arise from the

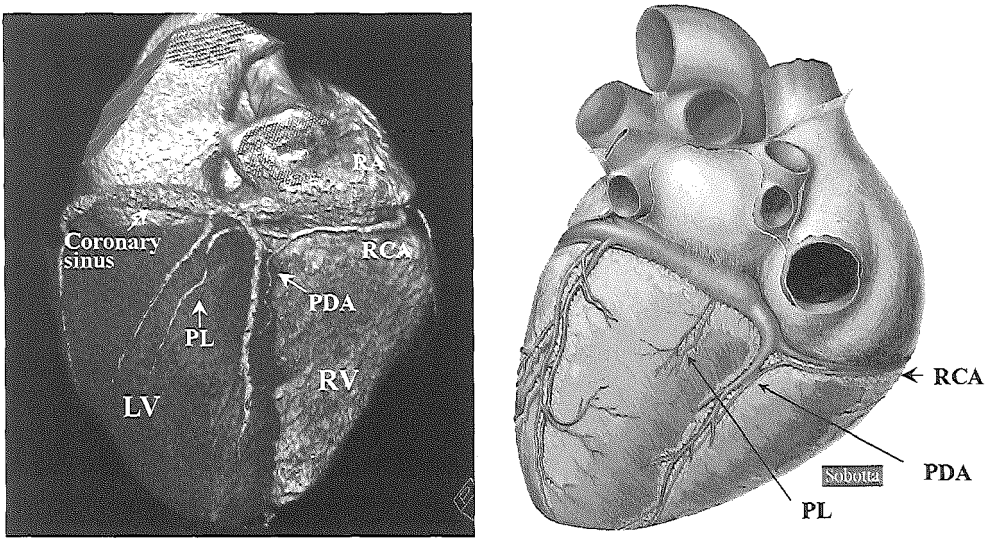

Figure 8. Distal right coronary artery (RCA), diaphragmatic view. (**A**) Coronary CT angiography. At the crux the RCA divides into the posterodescending artery (PDA) and postero-lateral (PL) branch over the inferior wall of the left ventricle (LV). RV, right ventricle; RA, right atrium. (**B**) Anatomical view. (Reproduced with permission from the Medical Illustration Library, Williams & Wilkins, Baltimore.) (A full color version of this illustration can be found in the color section (chapter 12)).

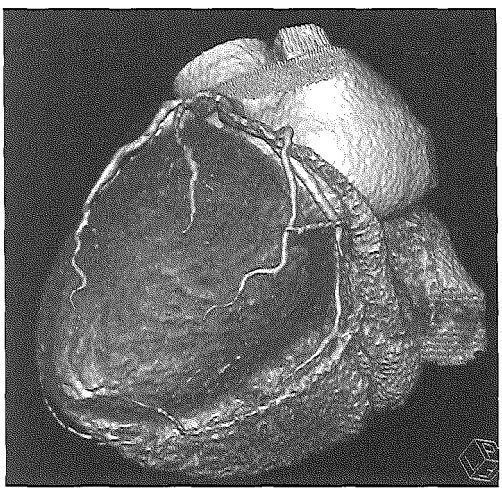

Figure 9. Left coronary artery dominance. Posterior descending artery (PDA) and postero-lateral (PL) branch originate from the circumflex (LCx) coronary artery. LV, left ventricle; RV, right ventricle. (A full color version of this illustration can be found in the color section (chapter 12)).

PDA and can connect with the septal branches from the LAD and form a collateral circulation. The postero-lateral (PL) branch supplying the postero-inferior aspect of the left ventricle also arises from the RCA close to the crux. Shortly the PL is a continuation of the RCA in the left atrioventricular grove but within 1 or 2 cm the crux follows an epical course of the myocardium of the left ventricle parallel to the PDA. Here the RCA can serve as a collateral for an occluded LCx. Also close to the crux a small artery arises that passes upwards to the atrio-ventricular node of the conduction system. Left coronary dominance exists when the PDA arises from the circumflex artery (Fig. 9).

CORONARY VENOUS ANATOMY

With the growing possibilities in electrophysiology where ablation catheters or pacemaker leads are positioned in the coronary veins, there has been a renewed interest in the venous anatomy. There are two major systems of epicardial cardiac veins: tributaries of the coronary sinus and anterior cardiac veins (Fig. 10). In principle, the veins run parallel to the arter- ies. The great cardiac vein (GCV), receiving blood from the anterior two-thirds of the septum, runs parallel to the LAD in the anterior interventricular groove. At the origin of the LAD artery, the GCV turns into the left atrioventricular groove, running parallel to the circumflex artery, where it drains into the coronary sinus. The anatomical transition of the GCV into the coronary sinus is at the site of entrance of the oblique vein of the left atrium.[5] The coronary sinus continues parallel to the circumflex artery and drains into the right atrium. The ostium of the coronary sinus in the right atrium is most frequently covered by a thick valve (the valve of the coronary sinus or Thebesian valve).[5]

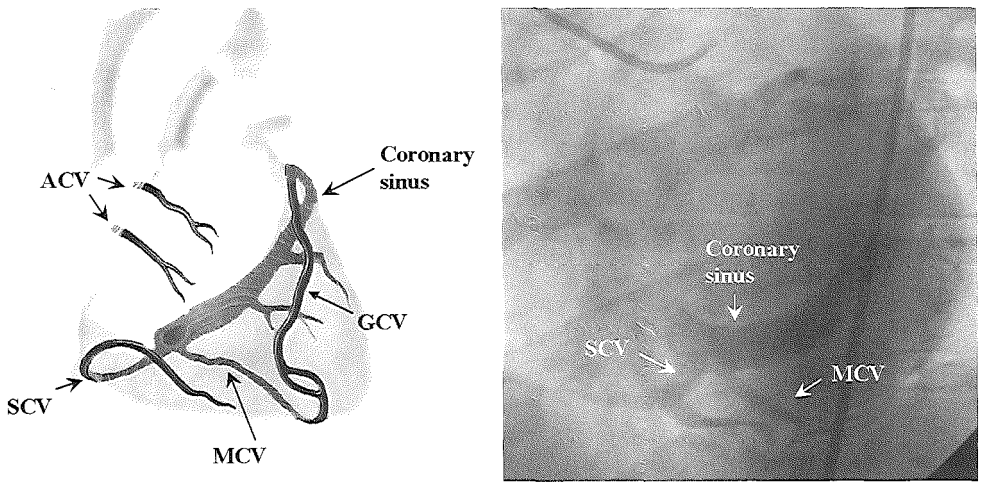

Figure 10. Coronary veins. (**A**) Anatomical view. Two cardiac venous systems: anterior veins (ACV) and tributaries of the coronary sinus (great cardiac vein [GCV], middle cardiac vein [MCV], and small cardiac vein [SCV]). (**B**) Conventional coronary angiography, venous phase.

The GCV and coronary sinus encircle most of the left atrioventricular connection and therefore are frequently used for ablation of assessorial electrical pathways that are present in the Wolff-Parkinson-White syndrome.

The middle cardiac vein (MCV), receiving blood from the posterior third of the septum, runs parallel to the PDA and enters the coronary sinus in 87% of the cases.[6] In only 36% of the cases is there a small cardiac vein, draining the blood of the right ventricle into the coronary sinus.[6] Additional coronary veins drain the lateral wall of the left ventricle and enter the coronary sinus between the GCV and MCV. The largest of these are used for implantation of the second lead of biventricular pacemakers. These lateral veins cover the area of the heart that is depolarized the latest

in the presence of a leftventricular bundle branch block, which makes it the most effective side for additional left-ventricular pacing.

The other epicardial venous system, that of the anterior veins, drains the blood from the right ventricular wall into the right atrium via atrial sinuses.[7] Sometimes this so-called sinus coronarius atrii dextri is quite large[6] and can be confused with the RCA.

RELATION BETWEEN ARTERIES AND VEINS

lca and gcv

The GCV is the longest venous vessel of the heart. The vein originates at the anterior interventricular groove, near the apex of the heart, and it empties into the coronary sinus. In the lower and the middle parts of the interventricular groove, the GCV runs most often to the right of its related artery.[8] The GCV crosses over the LAD artery and all of it branches in 49% of the cases (Fig. 11). On reaching the atrioventricular groove, the GCV crosses the LAD and circumflex arteries, forming the base of the triangle of Brocq and Mouchet.[8] The distance from the GCV of the left main coronary artery is variable (0-7 mm)[8], and sometimes the GCV touches the left main coronary artery and turns with a very sharp angle to the left atrioventricular groove, crossing under the branches of the left main coronary artery (Fig. 12). The circumflex artery is covered by the GCV in 60% of the cases so that the underlying anatomy of circumflex artery is obscured or inadequately visualized.

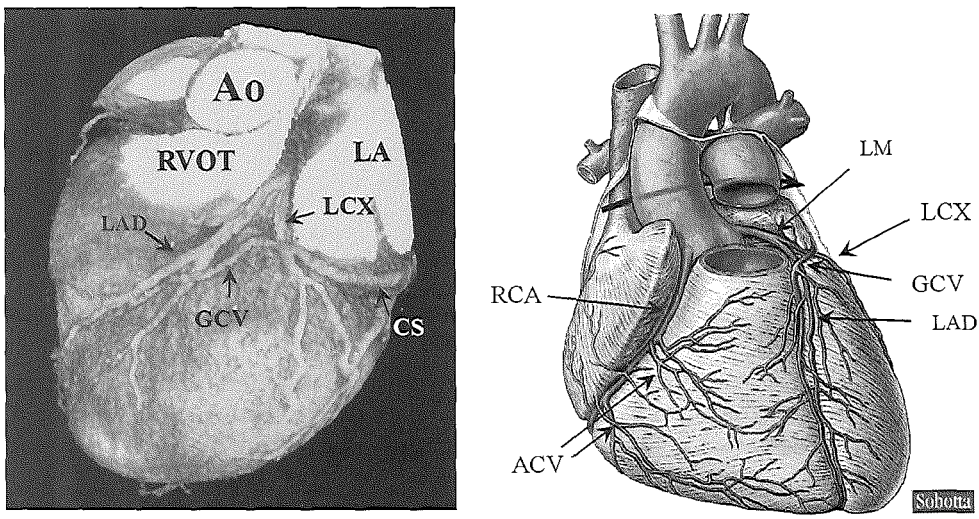

Figure 11. The great cardiac vein (GCV) turns from the anterior interventricular groove into the atrioventricular groove, crossing all the branches of the left coronary artery and forming the triangle of Brocq and Mouchet together with the left anterior descending (LAD) and circumflex (LCx) coronary arteries. (**A**) CTA: the view at the LCx artery is obstructed by the GCV. (**B**) Comparative anatomical view (reproduced with permission from the Medical Illustration Library, Williams & Wilkins, Baltimore). LM, left main artery; RCA, right coronary artery; ACV, anterior cardiac veins. (A full color version of this illustration can be found in the color section (chapter 12)).

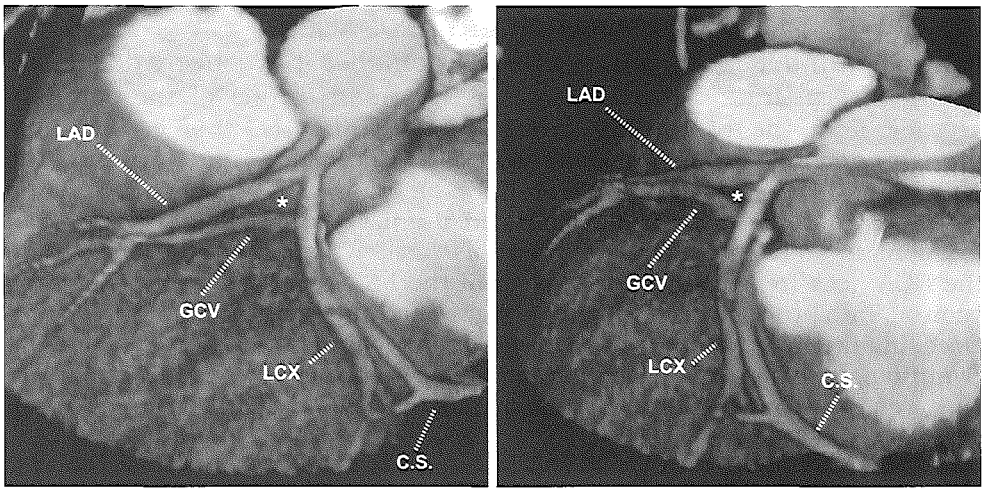

Figure 12. Renderings of the left coronary arterial and venous systems. (**A**) Great cardiac vein (GVC) running parallel to the left anterior descending coronary artery (LAD), crossing under the circumflex artery (LCx) and entering the coronary sinus (CS). Triangle of Brocq and Mouchet formed by the proximal left anterior descending coronary artery, the proximal circumflex coronary artery, and the great cardiac vein crossing from the anterior interventricular groove to the atrioventricular groove. (**B**) 3-D rendering of the same dataset, offering a more lateral and posterior view of the heart, arteries, and veins. This clearly shows the possibility of the 3-D rendering technique to view the object from any angle. Reproduced with permission from (14).

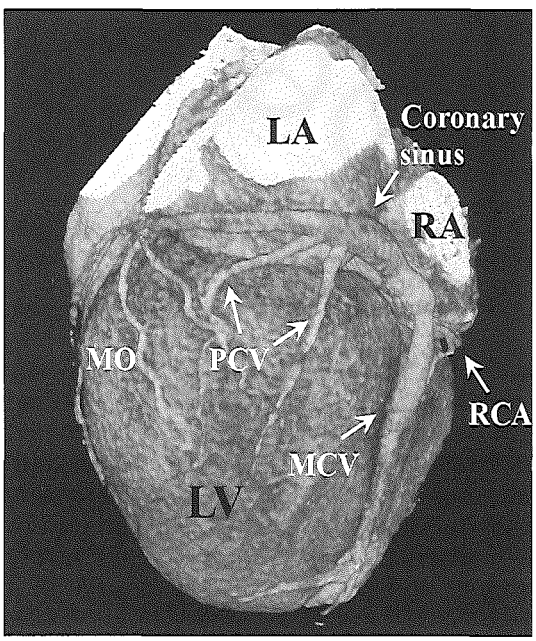

Figure 13. Right coronary artery (RCA) in the inferior atrioventricular groove partly covered by the middle cardiac vein (MCV) and the coronary sinus. PCV, posterior cardiac vein; RA, right atrium; LV, left ventricle.

Rca and coronary sinus

At the crux of the heart the RCA is, with very rare exceptions, inferior to the coronary sinus. The middle cardiac vein crosses over the postero-lateral branch of the RCA and stays left of the PDA when running in the posterior interventricular groove (Fig. 13). In cases of left circumflex artery dominance, veins draining blood from the inferior wall of the left ventricle cross over the artery before entering the coronary sinus.

CORONARY ARTERY ANOMALIES

A large number of coronary artery anomalies have been described in the literature.[2,9] Most extreme is the origin of one of the coronary arteries from the pulmonary artery; most frequently, this is the LAD, probably owing to its normal course underneath and around the pulmonary artery (Fig. 1). Because of the large amount of ischemia in such a case, symptoms are normally noticed the first 4 mo of life.[9,10] The most frequent anomalies are the different fistulae, which normally arise from the RCA; less frequently they arise from the LAD or LCx. Drainage usually occurs into the right ventricle, right atrium, or pulmonary artery. Occasionally, they drain in the left ventricle or superior caval vein. Symptoms of coronary artery fistulae are related to congestive heart failure as a result of left-to-right shunting, infective endocarditis, or myocardial ischemia.

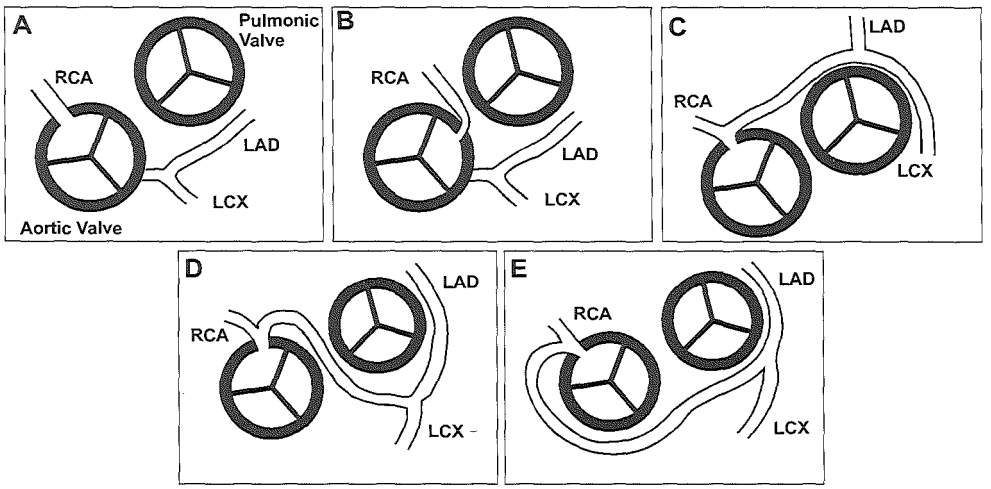

Figure 14. Different pathway of aberrant origin of the coronary artery arteries. (**A**) Normal anatomy. Caudal view. (**B**) RCA from left coronary cusp, inter-arterial course. (**C**) LM from right coronary cusp, anterior course. (**D**) LM from right coronary cusp, inter-arterial course. (**E**) LM from right coronary cusp, posterior course.

Origin of a coronary artery from the contralateral sinus is normally detected only during selective coronary angiography for suspected coronary artery disease.[11,12] They are categorized into anomalies expected to cause myocardial ischemia or those unlikely to cause myocardial ischemia. The latter have been associated with sudden death of young athletes during exercise. This category includes the interarterial course or septal course of the left main or left anterior descending coronary artery originating from the right coronary cusp and the interarterial course of a right coronary artery originating from the left coronary artery (Fig.14B,D). The danger is explained by the slit-like ostium with a sharp angle between the coronary artery and aorta (Fig.15). Another explanation is a possible compression of the vessel between the aorta and pulmonary artery or

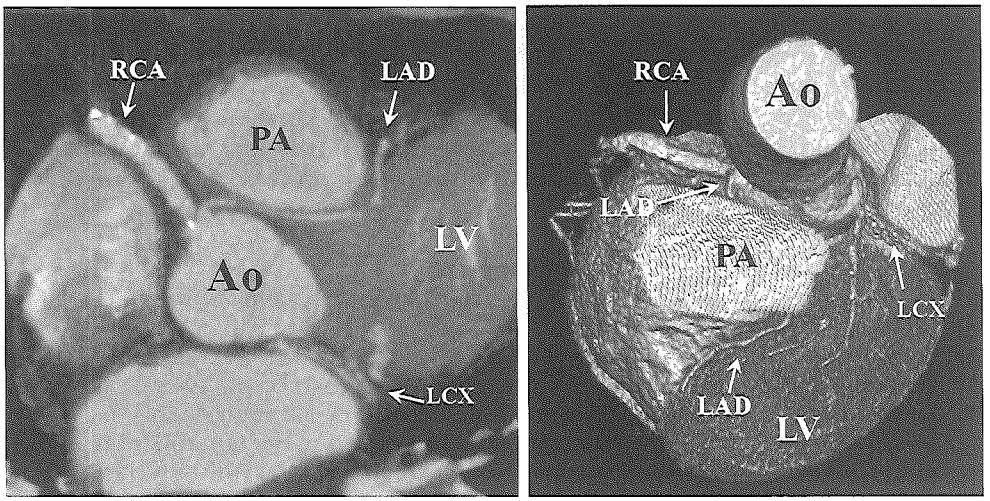

Figure 15. Left anterior descending (LAD) coronary artery from right coronary cusp. (A) Curved axial MIP demonstrating the inter-arterial course of the LAD between the pulmonary artery (PA) and the aorta (Ao). (B) VRT image. The proximal and distal LAD are clearly visible; the interarterial course is covered by the PA. LCx, left circumflex coronary artery; RCA, right coronary artery; LV, left ventricle. (A full color version of this illustration can be found in the color section (chapter 12)).

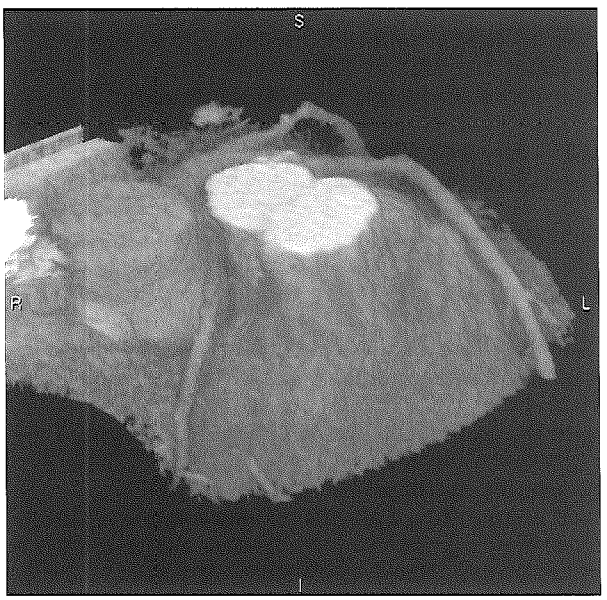

Figure 16. Right coronary artery (RCA) from left coronary cusp with in inter-arterial course. Ao, aorta; PA, pulmonary artery; RV, right ventricle; LAD, left anterior descending artery; LCx, left circumflex coronary artery.

compression within the myocardium of the interventricular septum in such a course (Fig. 16). These abnormal vessels may be prone to earlier atherosclerosis and successive myocardial ischemia.

Coronary artery anomalies not related to ischemia follow a course anterior (Fig. 14C) to the pulmonary artery or a long trajectory posterior around the aorta (retroaortic course) (Fig. 14E).

CONCLUSION

Three-dimensional data sets from noninvasive 3D coronary imaging techniques such as CTA are displayed with MPR or VRT. This provides images of the coronary arteries and veins much like their real anatomy,[13] which are not always familiar to the practicing cardiologist. Knowledge of the course of the epicardial coronary arteries and veins is required for accurate analysis.

REFERENCES

1. James T. Anatomy of the coronary arteries in health and disease. Circulation 1965;32:1020-1033.
2. Yamanaka O, Hobbs R. Coronary artery anomalies in 126,595 patients undergoing coronary arteriography. Cathet Cardiovasc Diagn 1990;21:28-40.
3. Levin DC, Harrington DP, Bettmann MA, Garnic JD, Davidoff A, Lois J. Anatomic variations of the coronary arteries supplying the anterolateral aspect of the left ventricle: possible explanation for the "Unexplained" anterior aneurysm. Invest Radiol 1982;17:458-462.
4. Braunwald E. Heart Disease. A Textbook of Cardiovascular Medicine. 4th ed. W.D. Saunders Company, Philadelphia: 1992.
5. Maric I, Bobinac D, Ostojic L, Petkovic M, Dujmovic M. Tributaries of the human and canine coronary sinus. Acta Anat (Basel) 1996;156:61-69. 6. von Ludinghausen M. Clinical anatomy of cardiac veins, Vv. cardiacae. Surg Radiol Anat 1987;9:159-168.
7. Pina JA. Morphological study on the human anterior cardiac veins, venae cordis anteriores. Acta Anat (Basel) 1975;92:145-159.
8. Pejkovic B, Bogdanovic D. The great cardiac vein. Surg Radiol Anat 1992;14:23-28.
9. Levin DC, Fellows KE, Abrams HL. Hemodynamically significant primary anomalies of the coronary arteries. Angiographic aspects. Circulation 1978;58:25-34.
10. Wilson CL, Dlabal PW, Holeyfield RW, Akins CW, Knauf DG. Anomalous origin of left coronary artery from pulmonary artery. Case report and review of literature concerning teen-agers and adults. J Thorac Cardiovasc Surg 1977;73:887-893.
11. Chaitman BR, Lesperance J, Saltiel J, Bourassa MG. Clinical, angiographic, and hemodynamic findings in patients with anomalous origin of the coronary arteries. Circulation 1976;53:122-131.
12. Kimbiris D, Iskandrian AS, Segal BL, Bemis CE. Anomalous aortic origin of coronary arteries. Circulation 1978;58:606-615.
13. McAlpine. Heart and Coronary Arteries. Springer-Verlag, Berlin: 1975.
14. Rensing BJ, Bongaerts AHH, van Geuns RJ, et al. In vivo assessment of three dimensional coronary anatomy using electron beam computed tomography after intravenous contrast administration. Heart 1999;82(4):523-525.

4. CORONARY ANATOMY

CHAPTER 4.2

NON-INVASIVE DEMONSTRATION OF CORONARY ARTERY ANOMALY PERFORMED USING 16-SLICE MULTIDETECTOR SPIRAL COMPUTED TOMOGRAPHY

Filippo Cademartiri[1]
Koen Nieman[1,2]
Rolf H.J.M. Raaymakers[1]
Pim J. de Feyter[1,2]
Thomas Flohr[3]
Ottavio Alfieri[4]
Gabriel P. Krestin[1]

Departments of Radiology[1] and Cardiology; Thoraxcentrum[2], Erasmus MC University Medical Center Rotterdam, The Netherlands, Siemens AG, Medical Engineering, Computed Tomography, Forchheim, Germany[3], Division of Cardiac Surgery[4], San Raffaele Hospital, Milan, Italy

Ital Heart J, 4 (1): 56-59, 2003.

Coronary artery anomalies are some of the most confusing, neglected topics in cardiology. Presently, no techniques are able to routinely screen those morphological alterations which can create potentially life-threatening complications, especially in young healthy subjects. Many efforts have been made to non-invasively image the coronary arteries using magnetic resonance, electron beam computed tomography, and recently multidetector computed tomography (MDCT). Even though interesting results have been reported, these techniques have hardly become an adequate substitute for conventional catheter coronary angiography. A new generation of MDCT scanners with 16 arrays of detectors and a higher temporal and spatial resolution have recently been introduced. We report a case of an anomalous coronary artery origin documented using a 16-slice MDCT scanner.

INTRODUCTION

Coronary artery anomalies are some of the most confusing, neglected topics in cardiology1. According to the literature, coronary anomalies affect ~1% of the general population; this percentage has been calculated on the basis of the results of cineangiograms performed for suspected obstructive disease.[1-4] One of the main issues in diagnostic cardiology is the assessment of the coronary artery anatomy and patency. Many efforts have been made in the last decade to reach a reasonable accuracy in the non-invasive assessment of the coronary artery anatomy using several techniques, such as magnetic resonance imaging (MRI), electron beam computed tomography (EBCT) and, in the last 4 years, multidetector computed tomography (MDCT).[5-8] Even though interesting results have been reported, these techniques have hardly become an adequate substitute for conventional catheter coronary angiography.

When scanning the heart for the purpose of retrospective coronary imaging, single-detector spiral computed tomography does not allow enough continuous volume coverage in a reasonable scan time.[9,10] Coronary imaging has become feasible following the introduction of MDCT scanners that provide a half-second gantry rotation time, a 4-detector-array and almost submillimeter in-plane spatial resolution. In fact, it is possible to cover the entire cardiac volume within one breath-hold.[10] Despite its high spatial resolution per z-axis coverage, MDCT at higher heart rates has been limited by the relatively low effective temporal resolution (250 ms with the half-rotation algorithm) compared to other non-invasive modalities such as EBCT and MRI.[7,11,12] Several limits mainly concerning the spatial resolution hinder both EBCT and MRI.[5,7,13-15] MDCT can rely on a higher in-plane and longitudinal resolution.

A new generation of MDCT scanners (16-MDCT) with more detector arrays, a faster gantry rotation time, a higher scan speed (temporal resolution) and a thinner slice thickness (spatial resolution) has been recently introduced.[16] Early clinical reports refer a good performance of these systems.[16,17] This generation of MDCT scanners is soon expected to play a major role in the management of the patient with suspected coronary artery disease. It is reasonable to expect that the same technique should be employed for the detection of coronary artery anomalies.

In this paper we report a case of an anomalous coronary artery origin docu- mented using a 16-MDCT scanner. A few technical issues will also be concisely discussed.

CASE REPORT

The patient (F.T.) was a 54-year-old man with mild non-specific complaints and a long lasting antihypercholesterolemic drug therapy. The patient underwent 16-MDCT (Sensation 16, Siemens Medical Solutions, Forchheim, Germany) for the assessment of the coronary artery patency. The patient gave informed consent for the procedure. Two scans were performed: the first non-enhanced scan was performed for calcium scoring purposes, while the second contrast medium enhanced scan was

performed for coronary artery evaluation. The overall examination time was 15 min.

Multidetector computed tomography scan parameters.

The initial heart rate of the patient was 60 b/min with sinus rhythm; therefore it was not necessary to reduce it by oral administration of fast-acting -blockers (100 mg metoprolol as a protocol).

Calcium scoring multidetector computed tomography scan.

The calcium scoring scan was performed with a spiral continuous acquisition and a retrospectively gated reconstruction. The good correlation between the calcium scoring performed using both EBCT and MDCT has already been reported18. With this protocol the scan is synchronized afterwards and the ECG signal recorded during the scan. The acquisition was performed with an ECG-pulsed protocol in order to reduce radiation exposure. Reconstruction was retrospectively gated at -400 ms before the next R wave. The effective slice width was 3.0 mm while the image reconstruction index was 3.0 mm (contiguous slices).

Coronary angiography multidetector computed tomography scan.

For vessel enhancement a volume of 140 ml, at a rate of 4 ml/s of iodinated non-ionic contrast medium (iomeprol 350 mgI/ml, Iomeron, Bracco Imaging, Milan, Italy) was injected through an antecubital vein with automatic power injector (EnVision, MedRad, Pittsburgh, PA, USA). The acquisition was performed according to an ECG pulsing protocol19. The main scan parameters were: number of detectors/collimation 12/0.75 mm, feed/rotation 2.78 mm, rotation time 420 ms, tube voltage 120 kV, tube current 450 effective mAs, and cranio-caudal direction.

Images were reconstructed using retrospective ECG gating. Three conventional reconstruction windows were positioned during the diastolic cardiac phase starting at -350, -400 and -450 ms before the next R wave. The effective slice width was set at 1.0 mm while the image reconstruction index was 0.6 mm. The total longitudinal range of 120 mm was scanned in 20 s.

Reconstructed images were sent to a dedicated postprocessing workstation (Leonardo, Siemens Medical Solutions, Forchheim, Germany) where calcium scoring assessment, multiplanar reconstructions, multiple intensity projections and three-dimensional volume rendering were performed.

RESULTS

The scan was successful. During both calcium scoring and angiographic scans the heart rate was 45 b/min. This allowed optimal scan conditions for the sampling of relevant data during the heart cycle. The calcium scoring scan revealed two spots along the left anterior descending coronary artery where further angiographic study revealed the presence of non-stenotic remodeled atherosclerotic plaques. The calcium score was 37.3 (equivalent Agatston score) in both lesions along the left anterior descending coronary artery.

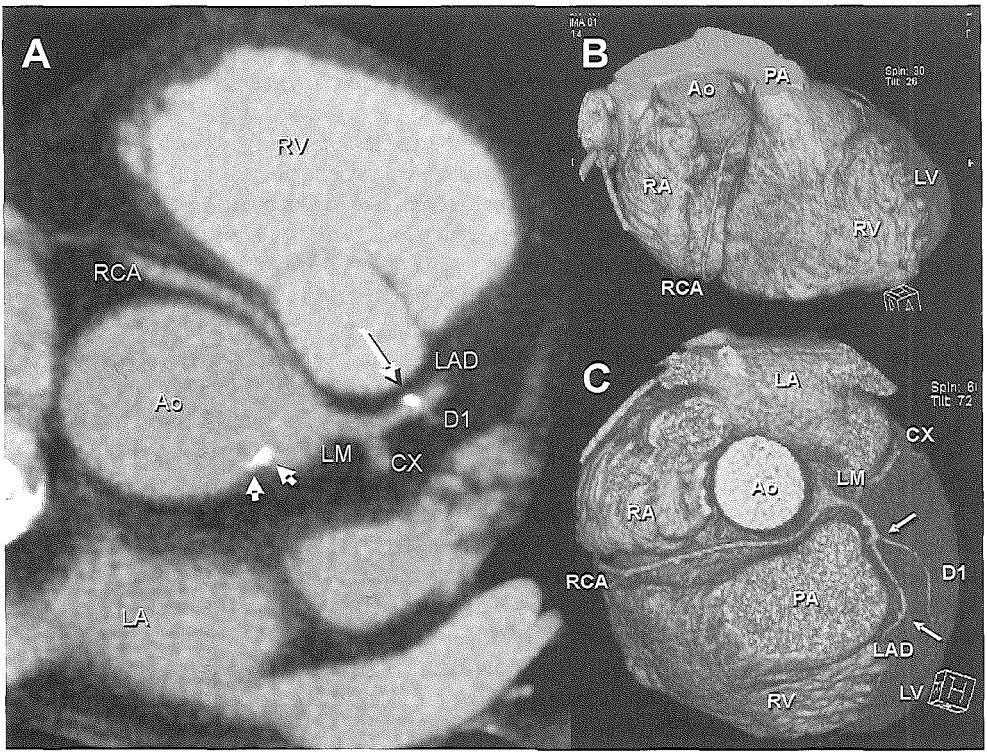

Figure 1. In **A** an axial image with a multiple intensity projection algorithm is displayed. The origin of the right coronary artery (RCA) is located between the anterior wall of the ascending aorta (Ao) and the posterior wall of the pulmonary artery (PA). In **B and C** the data-set is displayed with a three-dimensional volume rendered algorithm. The proximal and mid configurations of the RCA are displayed. A few atherosclerotic lesions with calcification may be seen on the left anterior descending coronary artery (LAD) (arrows) and at the level of the aortic wall (arrowheads). CX = circumflex coronary artery; D1 = diagonal 1; LA = left atrium; LM = left main coronary artery; LV = left ventricle; RA = right atrium; RV = right ventricle.(A full color version of this illustration can be found in the color section (chapter 12)).

A score between 10 and 400 indicates a moderate plaque burden and is associated with an intermediate, although significant risk of future cardiac events, especially for scores > 100.

The angiographic scan was successful and the gating window at -400 ms was chosen for further post-processing. The relatively low calcium along the coronary arteries allowed us to use the multiple intensity projection technique in order to better visualize the path of the main vessels (Fig. 1A). The left main, left anterior descending, circumflex and right coronary arteries were all adequately visualized (Figs. 1B and 1C). The configuration of the right coronary artery appeared anomalous. In fact, the origin of the right coronary artery was located at the sinus of the left main coronary artery (Fig. 1). Then the artery ran horizontally between the ascending aorta and the pulmonary artery to find its normal course.

DISCUSSION

Non-invasive imaging techniques such as MRI, EBCT, and transesophageal ultrasound have already been applied for the detection of coronary artery anomalies.[20-24] In the present case a new generation MDCT scanner with 16 detector arrays was used.[17]

The entire coronary artery system may originate from a single ostium (solitary coronary ostium) in the aorta. This solitary ostium is either located in the left or right coronary sinus of the aorta. When the left main coronary artery originates from the proximal right coronary artery, or vice versa, the anomalous artery takes one of four aberrant pathways to reach its proper vascular territory. These pathways are type A (i.e. anterior to the right ventricular outflow tract), type B (i.e. between the aorta and pulmonary trunk), type C (i.e. through the crista supraventricularis portion of the septum), and type D (i.e. dorsal to the aorta).[20] The anomaly described is a type B variant. Anomalous coronary arteries (origin, course and structure) have a higher incidence in the population of patients with sudden death.[25] The incidence in routine necropsy is 1% while in the population of patients with the sudden death syndrome it is 4-15% in the United States.[2-4,26] The specific importance of single types of coronary artery anomalies is not known.[3] The incidence does not seem to be related to gender.

The age of the patient and his clinical complaints allowed us to exclude any involvement of this arterial anatomical anomaly in possible ischemic acute processes. Moreover, the only possibility for correction of these anomalies is surgical. In the presented case there was no indication for this kind of procedure.

To better understand the improvements provided by this new generation of MDCT scanners, the main differences in the angiographic scan between the latest (16-MDCT) and previous generations (4-MDCT) will be described. There are four main improvements entailed in this new generation of 16-MDCT scanners:

1) the increase in the number of detector arrays from 4 to 16;
2) the decrease in the scan time from 40 to 21 s, with an increase in the scan range from 120 to 140 mm;
3) the collimation (minimum thickness of the axial slice) has been reduced from 1 to 0.75 mm;
4) the gantry rotation time has been reduced from 500 to 420 ms, improving the temporal resolution for a single heart cycle from 250-125 to 210-105 ms depending on the heart rate.[17]

From the clinical point of view, these improvements result in a more "affordable" breath-hold and in a higher capability of resolving small structures such as the coronary arteries and their branches with less sensitivity to motion artifacts. The limit heart rate is also higher and patients with up to 75-80 b/min could be scanned with acceptable results.

In conclusion, this preliminary report shows the good potential of a new generation of 16-slice MDCT scanners in the non-invasive assessment of coronary artery malformations.

REFERENCES

1. Angelini P, Velasco JA, Flamm S. Coronary anomalies: incidence, pathophysiology, and clinical relevance. Circulation 2002; 105: 2449-54.
2. Baltaxe HA, Wixson D. The incidence of congenital anomalies of the coronary arteries in the adult population. Radiology 1977; 122: 47-52.
3. Click RL, Holmes DR Jr, Vlietstra RE, Kosinski AS, Kronmal RA. Anomalous coronary arteries: location, degree of atherosclerosis and effect on survival - a report from the Coronary Artery Surgery Study. J Am Coll Cardiol 1989; 13: 531-7.
4. Yamanaka O, Hobbs RE. Coronary artery anomalies in 126 595 patients undergoing coronary arteriography. Cathet Cardiovasc Diagn 1990; 21: 28-40.
5. Wielopolski PA, van Geuns RJ, de Feyter PJ, Oudkerk M. Coronary arteries. Eur Radiol 2000; 10: 12-35.
6. Nieman K, Oudkerk M, Rensing BJ, et al. Coronary angiography with multi-slice computed tomography. Lancet 2001; 357: 599-603.
7. Rensing BJ, Bongaerts AH, van Geuns RJ, et al. In vivo assessment of three-dimensional coronary anatomy using electron beam computed tomography after intravenous contrast administration. Heart 1999; 82: 523-5.
8. Achenbach S, Ulzheimer S, Baum U, et al. Noninvasive coronary angiography by retrospectively ECG-gated multislice spiral CT. Circulation 2000; 102: 2823-8.
9. Kachelriess M, Kalender WA. Electrocardiogram-correlated image reconstruction from subsecond spiral computed tomography scans of the heart. Med Phys 1998; 25: 2417-31.
10. Ohnesorge B, Flohr T, Becker C, et al. Cardiac imaging by means of electrocardiographically gated multisection spiral CT: initial experience. Radiology 2000; 217: 564-71.
11. Achenbach S, Moshage W, Bachmann K. Noninvasive coronary angiography by contrast-enhanced electron beam computed tomography. Clin Cardiol 1998; 21: 323-30.
12. van Geuns RJ, Wielopolski PA, de Bruin HG, et al. Magnetic resonance imaging of the coronary arteries: techniques and results. Prog Cardiovasc Dis 1999; 42: 157-66.
13. Achenbach S, Moshage W, Ropers D, Nossen J, Bachmann K. Noninvasive, three-dimensional visualization of coronary artery bypass grafts by electron beam tomography. Am J Cardiol 1997; 79: 856-61.
14. Achenbach S, Moshage W, Ropers D, Nossen J, Daniel WG. Value of electron-beam computed tomography for the noninvasive detection of high-grade coronary-artery stenoses and occlusions. N Engl J Med 1998; 339: 1964-71.
15. Achenbach S, Ropers D, Regenfus M, et al. Contrast enhanced electron beam computed tomography to analyse the coronary arteries in patients after acute myocardial infarction. Heart 2000; 84: 489-93.
16. Heuschmid M, Kuttner A, Flohr T, et al. Visualization of coronary arteries in CT as assessed by a new 16 slice technology and reduced gantry rotation time: first experiences. Rofo Fortschr Geb Rontgenstr Neuen Bildgeb Verfahr 2002; 174: 721-4. 58 Ital Heart J Vol 4 January 2003
17. Nieman K, Cademartiri F, Lemos PA, et al. Reliable noninvasive coronary angiography with fast submillimeter multislice spiral computed tomography. Circulation 2002; 106: 2051-4.

18. Becker CR, Kleffel T, Crispin A, et al. Coronary artery calcium measurement: agreement of multirow detector and electron beam CT. AJR Am J Roentgenol 2001; 176: 1295- 8.
19. Jakobs TF, Becker CR, Ohnesorge B, et al. Multislice helical CT of the heart with retrospective ECG gating: reduction of radiation exposure by ECG-controlled tube current modulation. Eur Radiol 2002; 12: 1081-6.
20. Roberts WC, Shirani J. The four subtypes of anomalous origin of the left main coronary artery from the right aortic sinus (or from the right coronary artery). Am J Cardiol 1992; 70: 119-21.
21. Pucillo AL, Schechter AG, Moggio RA, et al. MR imaging in the definition of coronary artery anomalies. J Comput Assist Tomogr 1990; 14: 171-4.
22. McConnell MV, Ganz P, Selwyn AP, et al. Identification of anomalous coronary arteries and their anatomic course by magnetic resonance coronary angiography. Circulation 1995; 92: 3158-62.
23. Giannoccaro PJ, Sochowski RA, Morton BC, Chan KL. Complementary role of transoesophageal echocardiography to coronary angiography in the assessment of coronary artery anomalies. Br Heart J 1993; 70: 70-4.
24. Zeppilli P, dello Russo A, Santini C, et al. In vivo detection of coronary artery anomalies in asymptomatic athletes by echocardiographic screening. Chest 1998; 114: 89-93.
25. Basso C, Maron BJ, Corrado D, Thiene G. Clinical profile of congenital coronary artery anomalies with origin from the wrong aortic sinus leading to sudden death in young competitive athletes. J Am Coll Cardiol 2000; 35: 1493-501.
26. Kragel AH, Roberts WC. Anomalous origin of either the right or left main coronary artery from the aorta with subsequent coursing between aorta and pulmonary trunk: analysis of 32 necropsy cases. Am J Cardiol 1988; 62 (Part 1): 771-7. F Cademartiri et al - Coronary artery anomaly using 16-slice MDCT 59

4. CORONARY ANATOMY

CHAPTER 4.3

RIGHT CORONARY ARTERY ARISING FROM THE LEFT CIRCUMFLEX DEMONSTRATED WITH MULTISLICE COMPUTED TOMOGRAPHY

Filippo Cademartiri, MD[1]
Nico Mollet, MD[1,2]
Koen Nieman, MD[1,2]
Tamas Szili-Torok, MD[2]
Pim J. de Feyter, MD,PhD[1,2]

From the Departments of Radiology[1] and Cardiology[2]
Erasmus MC, University Medical Center Rotterdam, The Netherlands.

Circulation, 109:e185-e186, 2004.

Movies I, II, and III are available in the Data Supplement at http://www.circulationaha.org.

A38-year-old man was referred to our institution for suspected coronary artery disease. Because of his young age and rather atypical symptoms, we decided to perform multislice computed tomography coronary angiography before other invasive studies. The scan was performed with a 16-row multislice computed tomography scanner (Sensation 16; Siemens) after intravenous administration of iodinated contrast material. It revealed absence of the right coronary artery and a split origin of the left coronary artery (Figure 1, Movie I). The left circumflex artery lay in the posterior atrioventricular groove ending near the ascending aorta on the opposite side of its own origin (Figure 1, Movie I). The findings have been confirmed by coronary angiography (Figure 2, Movies II and III).

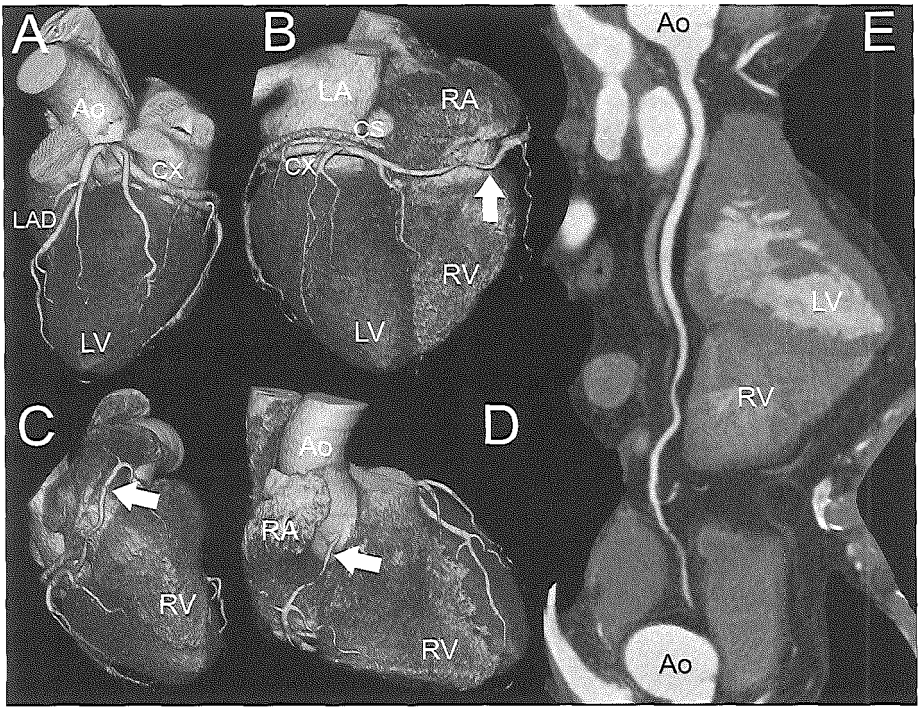

Figure 1. Multislice computed tomography coronary angiography. A 3D volume rendering is applied to the dataset in **A through D**, whereas a curved planar reconstruction is performed along the lumen of the left circumflex in E. The multislice computed tomography scan shows a split origin of the left coronary artery (**A**; Movie I). Therefore, this anomaly cannot be identified as a "single" coronary artery. The left circumflex runs first in the left atrioventricular groove (**A**), crosses the crux (**B**, arrow), and then goes further in the right atrioventricular groove (**C**, arrow), ending 1 cm before the wall of the ascending aorta (**D**, arrow) on the opposite side of its own origin (**E**; Movie I). No ostium of the right coronary artery in the region of the right Valsalva sinus was detected (**D and E**; Movie I). Ao indicates ascending aorta; CS, coronary sinus; CX, circumflex; LAD, left anterior descending; LA, left atrium; LV, left ventricle; RA, right atrium; and RV, right ventricle. (A full color version of this illustration can be found in the color section (chapter 12)).

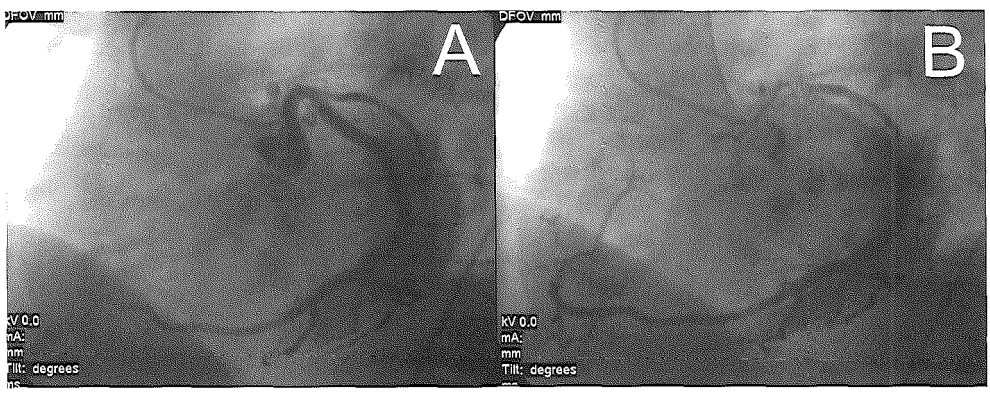

Figure 2. Selective conventional x-ray angiography of the left circumflex coronary artery.

5. PROCESSING

CHAPTER 5.1

REDUCTION OF MOTION ARTEFACTS FROM MILD HEART RHYTHM IRREGULARITIES WITH ECG-EDITING USING MULTIDETECTOR-ROW COMPUTED TOMOGRAPHY CORONARY ANGIOGRAPHY

Filippo Cademartiri[1],MD
Nico R Mollet [1,2],MD
Eugene P McFadden[2],MB,FCRPI
Thomas G Flohr[3],PhD
Bernd Ohnesorge[3],PhD
Pim J de Feyter[1,2],MD,PhD
Gabriel P Krestin[1],MD,PhD

Departments of Radiology[1] and Cardiology[2], Erasmus MC, University Medical Center Rotterdam, The Netherlands
Department of Computed Tomography[3], Siemens Medical Solutions, Forchheim, Germany

American Journal of Roentgenology (in press).

ABSTRACT

Objective: to reduce the artefacts determined by mild heart rhythm irregularities with ECG-editing using multidetector-row CT coronary angiography (MDCT-CA).

Material and Methods: 38 patients (33 male; mean age 59±11 yrs) who underwent MDCT-CA and conventional coronary angiography (CA) were enrolled in the study. The inclusion criterion was the presence of mild heart rhythm irregularities (premature beats, atrial fibrillation, mis-triggering, low heart rate <40bpm) during the scan. All patients underwent MDCT-CA protocol with the following parameters: collimation 16x0.75mm, rotation time 375ms, feed/rotation 3.0mm, kV 120, eff. mAs 500-600. Images were reconstructed in two settings: 1) before ECG-editing; 2) after ECG-editing. The two series of datasets were scored for image quality (Poor; Sufficient; Good) and for the presence of significant stenoses (≥50% lumen reduction) in coronary segments ≥2mm diameter.

Results: Image quality was poor in 22% (91) and 4% (15), sufficient in 21% (88) and 26 (107), and good in 57% (237) and 71% (295) before and after ECG-editing, respectively. Ninety-one (22%) and 14 (3%) segments were excluded from the analysis before and after ECG-editing. After inclusion of all diseased segments the sensitivity, specificity, negative and positive predictive value for the detection of significant stenoses before and after ECG-editing were 72% (41/65) and 91% (78/85), 97% (251/260) and 96% (305/317), 87% (62/71) and 87% (81/93), 91% (251/275) and 98% (305/313), respectively.

Conclusion: ECG-editing reduces the artefacts due to mild heart rate irregularities, thus increasing the number of assessable segments and diagnostic accuracy in a selected population of patients.

INTRODUCTION

Multidetector-row computed tomography (MDCT) scanners with sixteen rows of detectors, and increased spatial and temporal resolution have been recently introduced.[1] The increased number of detector rows and gantry rotation speed reduce the time needed to scan the coronary arteries to less than 20s.[1] Early experiences reported improved results in the visualisation of coronary arteries and in the detection of significant coronary artery disease (≥50% lumen reduction) in selected population of patients.[2, 3]

One limitation of MDCT coronary angiography (MDCT-CA) is that high and/or irregular heart rates prevent an adequate visualisation and assessment of coronary vessels, and for this reason are usually excluded from analysis or from scanning.[4] This is because at high heart rates the motion speed of coronary vessels is increased and the temporal window suited for imaging (e.g. mid- and late-diastole) is shortened. In case of irregular heart rates, such as premature beats and atrial fibrillation, the temporal variability of the diastolic phase is increased between contiguous heart cycles. This creates motion artefacts due to the inaccurate location of temporal windows and/or to the lack of data. This prevents the application of homogenous settings for image reconstructions.

In our experience, it is possible to correct and compensate for part or all of the artefacts produced by mild heart rhythm irregularities by means of ECG editing.

The aim of this study was to compare image quality and diagnostic accuracy in a population of patients with mild heart rhythm irregularities, using two different image reconstruction protocols for MDCT-CA.

MATERIAL AND METHODS

Patient population

Between April 2003 and February 2004, 42 patients (34 male; mean age: 59±11yrs) with stable angina and scheduled for coronary angiography (CA) were prospectively enrolled in the study.

Inclusion criteria for the scan were: heart rate (spontaneous or β-blocker induced) <70bpm, the ability to hold the breath for 20s. Inclusion criteria for the study were (see Appendix I): presence of premature beats (PB), atrial fibrillation (AF) with low ventricular response, mis-triggering (MT) of the R wave (e.g. widening of QRS complex, bundle branch block), and low heart rate (LHR; e.g. below 40bpm). This group of criteria is defined as mild heart rhythm irregularities (MHRI).

Exclusion criteria were: high heart rate (>70bpm) previous allergic reaction to iodine contrast media, renal insufficiency (serum creatinine >120mmol/L), pregnancy, respiratory impairment, unstable clinical status, marked heart failure, previous bypass surgery or percutaneous coronary interventions.

Patients meeting the inclusion criteria underwent also non-invasive MDCT-CA.

The Institutional Review Board approved the study and patients gave informed consent.

Multidetector-row ct scan

On arrival, the heart rate (HR) of the patients was measured. Patients with a pre-scan HR ≥ 65bpm, were given 100mg of metoprolol orally and the scan was performed one hour later. Patients meeting the inclusion criteria were positioned on the CT table and connected to the ECG trace. The variation of HR were observed for 5 minutes and then tested during apnoea (20s). If at rest and during apnoea the variation of HR were compatible with the definition of MHRI the patient underwent the scanning procedure (Figure 1).

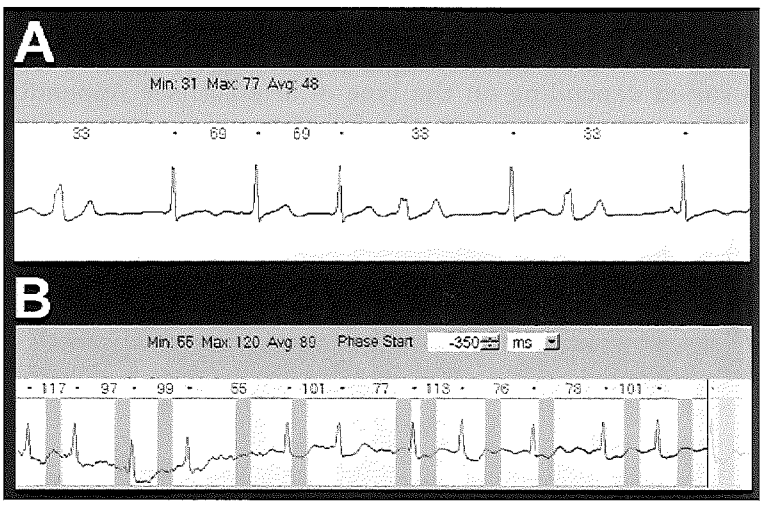

Figure 1. Example of ECG of excluded patients.
Two examples of patients excluded from the study while they were on the scanner table just before starting the procedure. In **A** an example of premature beat originating from the conduction system in a background heart rate too high to rely on the post extra-systolic pause. In **B** an example of a high and irregular heart rate due to atrial flutter. The ventricular response to the flutter wave is irregular.

In all patients, a bolus (100ml at 4ml/s) of iodinated contrast material (Iomeprol 400 mgI/ml, Iomeron®, Bracco) followed by a saline chaser (40ml at 4ml/s) was administered using a double-head power injector (Stellant®, MedRAD) through an 18G cannula, in an antecubital vein.

The scan parameters for MDCT coronary angiography (Sensation 16®, Siemens) were: number of detectors 16, individual detector width 0.75mm, gantry rotation time 375ms, effective temporal resolution 188ms, kV 120, eff. mAs 500-600, feed/rotation 3.0mm, scan direction cranio-caudal. Synchronisation between the passage of contrast material and data acquisition was achieved with real time bolus tracking (CARE bolus®, Siemens) using a region of interest in the ascending aorta for monitoring a threshold of +100HU above the baseline attenuation to trigger the scan. The heart rate and ECG track were recorded during the scan.

Image reconstruction

Two datasets were reconstructed using retrospective ECG gating technique. The first dataset (standard reconstruction protocol - STD) was reconstructed without any ECG editing using temporal windows starting at -350ms, -400ms, and -450ms, prior to the next R wave. Two experienced operators in consensus (F.C. and N.R.M.) selected the dataset with least motion artefacts. The second dataset (ECG-editing reconstruction protocol - EDIT) was reconstructed in consensus by two experienced operators using ECG editing available at the MDCT scanner evaluated in correspondence of anomalies of the ECG signal due to: premature beats (PB - Figure 2), atrial fibrillation (AF), mis-triggering (MT - Figure 3), and heart rate below 40bpm (LHR - Figure 4). The ECG-editing procedure varied depending on the type of artefact (see Appendix I). Both datasets were reconstructed with the following parameters: effective slice width 1mm, reconstruction interval 0.5mm, FOV 160mm, convolution filter medium smooth (B30f).

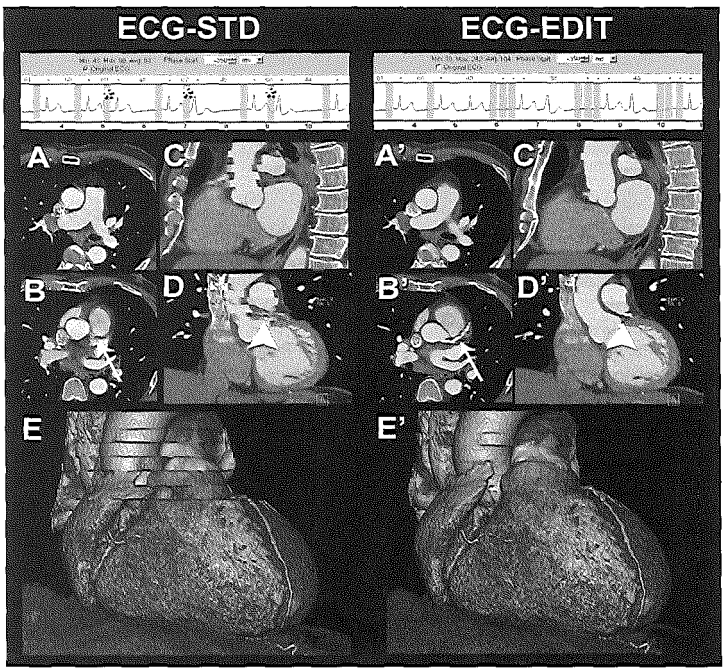

Figure 2. Correction of artefacts from premature beats.
Example of dataset with premature beats before (left panel) and after (right panel) ECG editing. The ECG of the left panel shows three premature beats (asterisks) in a background heart rate of ~45bpm. The dataset resulting from a reconstruction performed without any editing shows motion artefacts at the level of the pulmonary artery (**A**) and at the origin of the left coronary artery (**B** - arrow). Sagittal and coronal reconstructions (**C and D**) show the impact of these three premature beats on the ascending aorta and on the origin of the left coronary artery (**D** - arrowhead). In E a frontal view of the dataset with three-dimensional volume rendering shows the misalignment of the stacks of images in the cranial part of the dataset. After ECG-editing, the artefacts are ruled out and coronary vessels are assessable (**A'-E'**). A significant stenosis of proximal left anterior descending was missed because of the artefacts (**B'** - arrow; **D'** - arrowhead). (A full color version of this illustration can be found in the color section (chapter 12)).

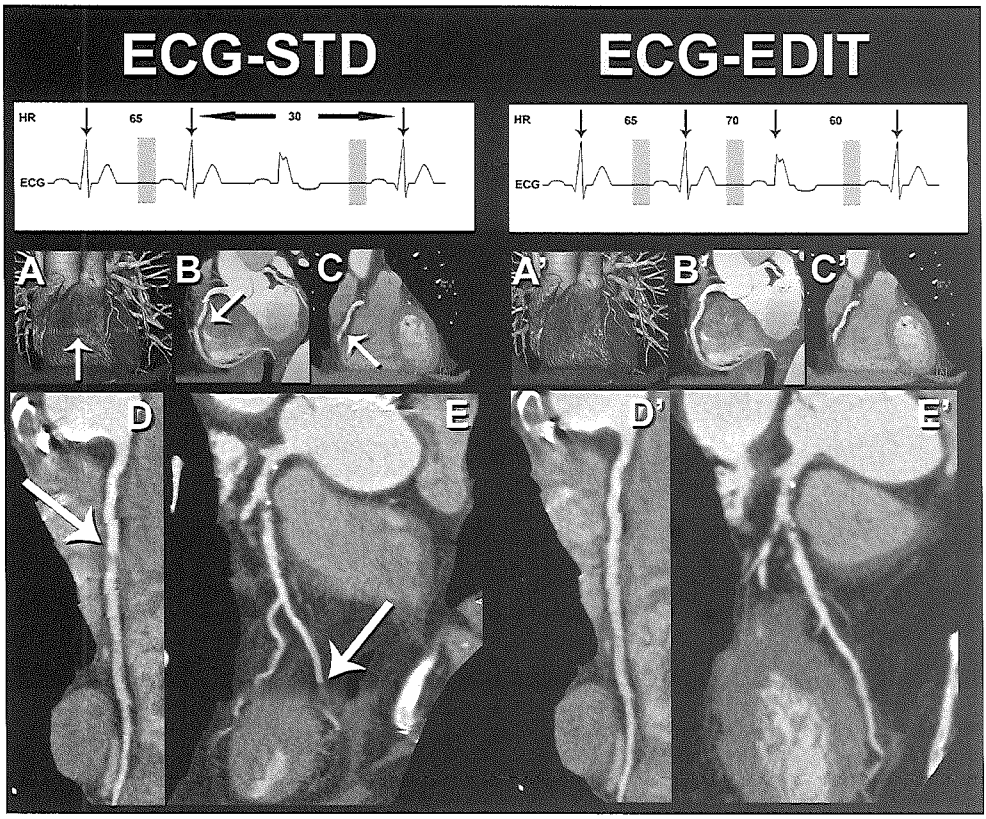

Figure 3. Correction of artefacts from mis-triggering.
Example of dataset with mis-triggering before (left panel) and after (right panel) ECG editing. The ECG on the left panel shows an anomaly of the conduction for one heart beat that result in a missing synchronisation point and very long RR interval. The appearance of this event is showed by the arrow in three-dimensional volume rendering (**A**), a dedicated double oblique MIP for the right coronary artery (**B**), a coronal MIP (**C**), and two curved reconstructions: one for the right coronary artery (**D**), and one for the left main-left anterior descending (**E**). The data are missing because the RR interval is too large, and two coronary segments have to be considered not assessable. After ECG editing by means of inserting the synchronisation point in the correct position (ECG in the right panel), all the images are recovered (**A'-E'**). (A full color version of this illustration can be found in the color section (chapter 12)).

Image analysis

Two experienced observers, blinded to the results of the conventional coronary angiography, assessed in consensus the dataset for image quality (concerning artefacts due to MHRI) and presence of significant stenoses (≥50% lumen reduction). The evaluation of the data was performed 3 months after the reconstruction and selection of the datasets. The evaluation was performed following the classification for coronary segments from the American Heart Association.[5] Image quality was graded as: Poor (artefact present; vessel not visualized); Sufficient (artefact present; vessel visualized); Good (artefact absent; vessel well visualized). Significant stenoses were scored as: absent (<50%) or present (≥50%).

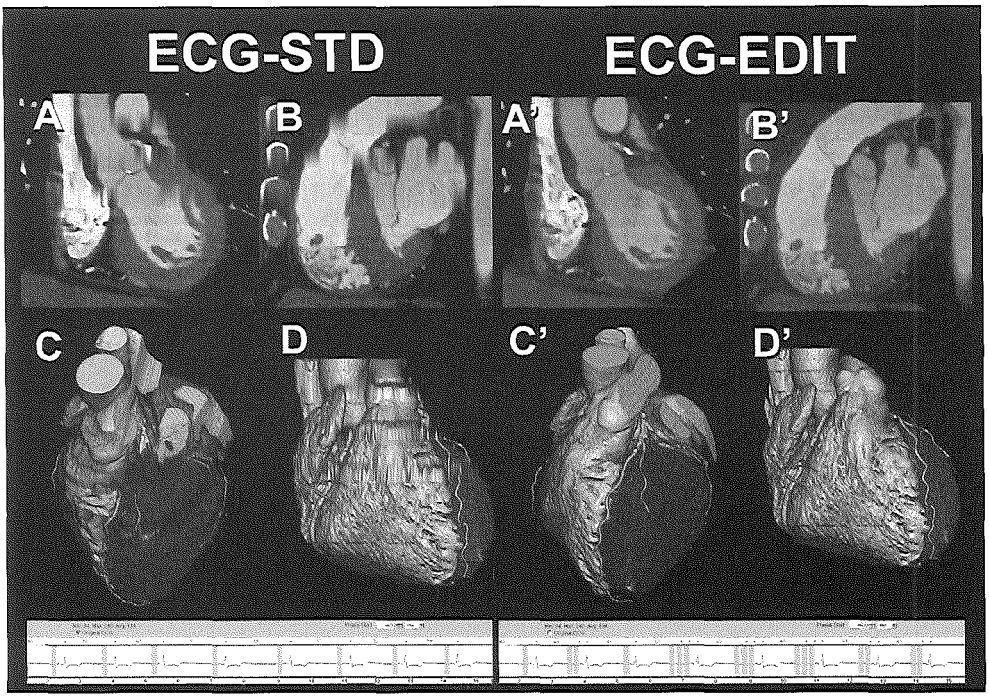

Figure 4. Correction of artefacts from low heart rate.
Example of dataset with low heart rate before (left panel) and after (right panel) ECG editing. The ECG on the left panel shows a very low heart rate almost always below 40bpm. This determines data gaps that appear in coronal (**A**), sagittal (**B**), and three-dimensional reconstructions (**C and D**), as blurring of stacks of images. After ECG editing by means of inserting additional synchronisation points (ECG in the right panel), all the images are recovered (**A'-D'**). (A full color version of this illustration can be found in the color section (chapter 12)).

Conventional coronary angiography

Conventional coronary angiography (CA) was performed within 2 weeks of MDCT-CA using a standard technique. One experienced observer (P.A.L.), unaware of the results of MDCT-CA, determined the diameter of all coronary branches and evaluated the presence of significant stenoses using quantitative coronary angiography (QCA - CAAS®, Pie Medical Imaging). Lesions with an average diameter stenosis of ≥50% in two orthogonal views were considered as significant obstructions.

Data analysis

The result of QCA performed in two orthogonal projections was used as the reference standard to classify stenoses as significant. The reading of the MDCT-CA was used to calculate sensitivity, specificity, positive, and negative predictive value with 95% confidence intervals.

RESULTS

Table 1. Patients data.

	Population
Number of patients	38
Male/Female	33/5
Mean age (yrs)	59±11
Mean heart rate (bpm)	54±9

Abbreviations: yrs = years; bpm = beat per minute; sec= seconds.

No significant adverse reactions to contrast material were recorded. Of the 42 patients enrolled in the study, 4 (10%) did not undergo MDCT-CA because the HR variations observed while the patient was on the CT table were not compatible with inclusion criteria regarding MHRI.

Therefore, 38 patients (33 male; mean age 59±11 yrs; Table I) were suitable for MDCT-CA scan, image reconstruction and data analysis. After exclusion of segments with a diameter <2mm, 416 segments remained available for analysis, 88 (21%) of which with a significant stenosis. Of the 38 patients with MHRI, 21 were classified as PB, 4 as AF, 6 as MT, and 7 as LHR.

Image quality (Table II)

Table 2. Image quality of ECG-STD protocol vs. ECG-EDIT protocol.

			Image quality (%)					
			Poor		Sufficient		Good	
AHA	Segment	n.	ECG-STD	ECG-EDIT	ECG-STD	ECG-EDIT	ECG-STD	ECG-EDIT
1	RCA prox.	38	15 (40)	5 (13)	4 (11)	7 (18)	19 (50)	26 (68)
2	RCA mid.	32	7 (22)	1 (3)	4 (13)	4 (13)	21 (66)	27 (84)
3	RCA distal	23	3 (13)	0 (0)	4 (17)	6 (26)	16 (70)	17 (74)
4	PDA	14	2 (14)	0 (0)	10 (71)	10 (71)	2 (14)	4 (29)
5	LM	38	10 (26)	1 (3)	4 (11)	4 (11)	24 (63)	33 (87)
6	LAD prox.	38	15 (40)	3 (8)	4 (11)	9 (24)	19 (50)	26 (68)
7	LAD mid.	35	12 (34)	2 (6)	7 (20)	8 (23)	16 (46)	25 (71)
8	LAD distal	32	5 (16)	0 (0)	9 (28)	10 (31)	18 (56)	22 (69)
9	1st diag.	28	4 (14)	0 (0)	8 (29)	10 (36)	16 (57)	18 (64)
10	2nd diag.	16	1 (6)	1 (6)	8 (50)	8 (50)	7 (44)	7 (44)
11	CX prox.	37	6 (16)	1 (3)	6 (16)	7 (19)	25 (68)	29 (78)
12	1st marg.	33	7 (21)	0 (0)	4 (12)	6 (18)	22 (67)	27 (82)
13	CX mid.	30	3 (10)	0 (0)	6 (20)	8 (27)	21 (70)	22 (73)
14	2nd marg.	15	1 (7)	0 (0)	3 (20)	3 (20)	11 (73)	12 (80)
15	PL	7	0 (0)	0 (0)	7 (100)	7 (100)	0 (0)	0 (0)
All		416	91 (22)	14 (3)	88 (21)	107 (26)	237 (57)	295 (71)

Abbreviations: ECG-STD= standard ECG protocol; ECG-EDIT= ECG-editing protocol; n.= number; AHA= American Heart Association segmental classification; RCA= right coronary artery; LAD= left anterior descending; LM= left main; CX= circumflex; PL= postero-lateral branch.

Table 3. Diagnostic accuracy of ECG-STD protocol vs. ECG-EDIT protocol

AHA	Segment	n.	SDS (%)	Protocol	NA (%)	SDS in NA (%)	Sensitivity (95% CI)
1	RCA prox.	38	7 (18)	ECG-STD	15 (40)	2 (28)	100 (54-100)
				ECG-EDIT	5 (13)	1 (14)	100 (59-100)
2	RCA mid.	32	17 (53)	ECG-STD	7 (22)	4 (24)	100 (75-100)
				ECG-EDIT	1 (3)	0 (0)	100 (80-100)
3	RCA distal	23	6 (26)	ECG-STD	3 (13)	2 (33)	100 (39-100)
				ECG-EDIT	0 (0)	0 (0)	100 (54-100)
4	PDA	14	2 (14)	ECG-STD	2 (14)	0 (0)	50 (1-87)
				ECG-EDIT	0 (0)	0 (0)	50 (1-87)
5	LM	38	0 (0)	ECG-STD	10 (26)	0 (0)	NA
				ECG-EDIT	1 (3)	0 (0)	NA
6	LAD prox.	38	15 (40)	ECG-STD	15 (40)	6 (40)	77.77 (39-98)
				ECG-EDIT	3 (8)	1 (7)	85.71 (57-98)
7	LAD mid.	35	14 (40)	ECG-STD	12 (34)	5 (36)	100 (63-100)
				ECG-EDIT	2 (6)	2 (14)	100 (73-100)
8	LAD distal	32	3 (9)	ECG-STD	5 (16)	0 (0)	100 (29-100)
				ECG-EDIT	0 (0)	0 (0)	100 (29-100)
9	1st diag.	28	1 (4)	ECG-STD	4 (14)	0 (0)	100 (2-100)
				ECG-EDIT	0 (0)	0 (0)	100 (2-100)
10	2nd diag.	16	0 (0)	ECG-STD	1 (6)	0 (0)	NA
				ECG-EDIT	1 (6)	0 (0)	NA
11	CX prox.	37	7 (19)	ECG-STD	6 (16)	0 (0)	100 (47-100)
				ECG-EDIT	1 (3)	0 (0)	85.71 (42-96)
12	1st marg.	33	10 (30)	ECG-STD	7 (21)	2 (20)	100 (63-100)
				ECG-EDIT	0 (0)	0 (0)	100 (69-100)
13	CX mid.	30	5 (17)	ECG-STD	3 (10)	0 (0)	100 (47-100)
				ECG-EDIT	0 (0)	0 (0)	100 (47-100)
14	2nd marg.	15	0 (0)	ECG-STD	1 (20)	0 (0)	NA
				ECG-EDIT	0 (0)	0 (0)	NA
15	PL	7	1 (14)	ECG-STD	0 (0)	0 (0)	100 (2-100)
				ECG-EDIT	0 (0)	0 (0)	100 (2-100)
All	Assessable	416	88 (21)	ECG-STD	91 (22)	21 (24)	95.38 (87-98)
				ECG-EDIT	14 (3)	4 (5)	95.29 (88-98)
	Assessable[1]			ECG-STD	70 (17)	0 (0)	72.09 (61-88)
				ECG-EDIT	10 (2)	0 (0)	91.01 (83-97)

Abbreviations: ECG-STD= standard ECG protocol; ECG-EDIT= ECG editing protocol; n.= number; AHA= American Heart Association segmental classification; SDS = significantly diseased segments (>50% lumen reduction at Quantitative Coronary Angiography); RCA= right coronary artery; LAD= left anterior descending; LM= left main; CX= circumflex; PL= postero-lateral branch; NA= not assessable; CI= confidence intervals.
1Calculation performed including the significantly diseased segments as false negatives.

Specificity (95% CI)	PPV (95% CI)	NPV (95% CI)	Accuracy (95% CI)
88.23 (63-98)	75 (34-97)	100 (78-100)	91.3 (80-100)
92.3 (74-99)	77.77 (39-98)	100 (85-100)	93.9 (86-100)
83.33 (51-97)	86.66 (59-98)	100 (69-100)	92 (81-100)
85.71 (57-98)	89.47 (66-98)	100 (73-100)	93.55 (85-100)
93.75 (69-99)	80 (28-99)	100 (78-100)	95 (85-100)
94.11 (71-99)	85.71 (42-99)	100 (79-100)	95.65 (87-100)
100 (69-100)	100 (2-100)	90.9 (58-99)	91.67(76-100)
100 (73-100)	100 (2-100)	92.3 (63-99)	92.86 (79-100)
100 (87-100)	NA	100 (87-100)	100 (100-100)
100 (90-100)	NA	100 (90-100)	100 (100-100)
92.85 (66-99)	87.5 (47-99)	86.66 (59-98)	86.96 (73-100)
90.47 (69-98)	85.71 (57-98)	90.47 (69-98)	88.57 (78-99)
100 (78-100)	100 (63-100)	100 (78-100)	100 (100-100)
100 (83-100)	100 (73-100)	100 (83-100)	100 (100-100)
95.83 (78-99)	75 (19-99)	100 (85-100)	96.3 (89-100)
96.55 (82-99)	75 (19-99)	100 (87-100)	96.88 (91-100)
95.65 (78-99)	50 (1-99)	100 (84-100)	95.83 (88-100)
92.59 (75-99)	33.33 (0-95)	100 (86-100)	92.86 (83-100)
100 (78-100)	NA	100 (78-100)	100 (100-100)
100 (78-100)	NA	100 (78-100)	100 (100-100)
100 (86-100)	100 (47-100)	100 (86-100)	100 (100-100)
100 (88-100)	100 (54-100)	96.66 (82-99)	97.22 (92-100)
100 (81-100)	100 (63-100)	100 (81-100)	100 (100-100)
95.65 (78-99)	90.9 (58-99)	100 (84-100)	96.97 (91-100)
95.45 (77-99)	83.33 (35-99)	100 (83-100)	96.3 (89-100)
96 (79-99)	83.33 (35-99)	100 (85-100)	96.67 (90-100)
100 (76-100)	NA	100 (76-100)	100 (100-100)
100 (78-100)	NA	100 (78-100)	100 (100-100)
100 (54-100)	100 (2-100)	100 (54-100)	100 (100-100)
100 (54-100)	100 (2-100)	100 (54-100)	100 (100-100)
96.53 (93-98)	87.32 (77-97)	98.81 (96-99)	96.31 (94-98)
96.21 (93-98)	87.09 (78-94)	98.7 (96-99)	96.02 (94-98)
96.53 (93-98)	87.32 (77-97)	91.27 (87-94)	90.46 (87-94)
96.21 (93-98)	87.09 (78-94)	97.44 (95-98)	95.07 (93-97)

Image quality was poor in 22% (91) and 4% (15), sufficient in 21% (88) and 26 (107), and good in 57% (237) and 71% (295) of the segments before and after editing, respectively . Fourteen (3%) segments that were scored as poor were re-scored as sufficient after ECG-editing. Within this fraction of segments there were 3 significant stenoses. Fifty-eight (14%) segments that were scored as poor were re-scored as good after ECG-editing. Within this fraction of segments there were 12 significant stenoses.

Diagnostic accuracy (Table III)

The segments available for comparison were 325 (78%) and 402 (97%) for STD and EDIT protocol, respectively. The rate of excluded segments was 22% (91) for STD protocol and 3% (14) for EDIT protocol. Twenty-one (24%) significant lesions were excluded from analysis with STD protocol and 4 (5%) with EDIT protocol because located in not assessable segments.

Sensitivity, specificity, negative predictive value and positive predictive value for the detection of significant stenoses for STD and EDIT protocols were 95% (62/65) and 95% (81/85), 97% (251/260) and 96% (305/317), 87% (62/71) and 87% (81/93), 99% (251/254) and 98% (305/309), respectively. Considering significant stenoses in excluded segments as false negatives the value of sensitivity, specificity, negative and positive predictive were 72% (41/65) and 91% (78/85), 97% (251/260) and 96% (305/317), 87% (62/71) and 87% (81/93), 91% (251/275) and 98% (305/313), respectively.

Discussion

With the new generation of MDCT scanners featuring 16 rows of detectors the time needed to scan the heart for the purpose of coronary CTA has been reduced to ~20s.[1-3] Preliminary encouraging results have been published regarding the detection of significant stenoses with 16-row MDCT-CA in selected population of patients.[2, 3] High and irregular hear rates are known as limitations of this technique.[1] To date, they are used as exclusion criteria for the studies and aggressively treated with oral beta-blockers.[2, 3] Yet, for milder hear rate irregularities there remains room for interaction with the raw data and the ECG trace.

The main drawback of high heart rates is the increased speed of coronary arteries and the reduced duration of the diastole.[6] With a temporal resolution of ~200ms this results in a limited possibility to adapt the position of the temporal window within the cardiac cycle.

This limitation is less compromising at lower heart rates and, due to the longer diastolic phase, ECG editing is more flexible. In fact, mild heart rhythm irregularities, as described above and in Appendix I, can be ruled out after careful ECG editing, providing both an increased image quality and diagnostic accuracy.

In our study we compared the reconstruction capabilities of a 16- row MDCT scanner in the presence of mild heart rhythm irregularities before and after ECG editing.

The improvement in image quality is demonstrated by the steep reduction of segments scored as poor (-77 segments; from 22% to 3%) and by concomitant increased number of segments scored as good (+58 segments; from 57% to 71%) after ECG editing. This improvement in image quality has also an impact on diagnostic accuracy in the selected population of patients with stable angina enrolled in this study. In fact, the sensitivity and the negative predictive value for the detection of significant stenoses after inclusion of all diseased segments in the analysis were 72% vs. 91%,

and 91% vs. 97% before and after ECG-editing, respectively. Specificity and positive predictive value did not differ. The difference has to be attributed to the number of significantly diseased segments that were excluded from the analysis.

The effect of mild heart rhythm irregularities on image quality can be quantified and is not affected by the presence of significant stenoses. Their impact on diagnostic accuracy, instead, is fairly dependent on the number of significant stenoses that are present in the population. The relative impact of ECG-editing on diagnostic accuracy will depend on the number and distribution of lesions throughout the coronary tree. A population with a lower probability of disease (e.g. younger, or with less evident symptoms) would probably show a smaller variation in sensitivity than the one demonstrated in our study.

Our results suggest that from the technical point of view, heart rhythm irregularities are not an absolute limitation for proper image quality. In fact, our results exploit the flexibility of retrospective reconstruction to the limit. Other techniques already applied to non-invasive coronary artery imaging (electron-beam CT or magnetic resonance) are based on prospective ECG triggering. Even though with higher temporal resolution when compared to MDCT, for these techniques it would be impossible to compensate for the mild heart rhythm irregularities as described in our study. Prospective ECG triggering allows to acquire only one segment of the cardiac cycle without any possibility of retrospective modification.

The motion speed of the coronary vessels, especially if compared with effective temporal resolution of MDCT, remains a limitation. To compensate this limitation, slow HR and/or shorter rotation time are required.

Limitations

The patients with heart rates above 70bpm were not enrolled in this study to prevent image degradation from other sources than the ones subjects of our study.

Only mild heart rhythm irregularities could be included in the evaluation due the still limited effective temporal resolution.

The scan of patients with mild heart rhythm irregularities does not allow to use X-ray reduction software such as ECG-pulsing.[7] This is because the algorithm for dose reduction works with a prospective triggering based on the R wave. In presence of heart rate abnormalities the location of the low dose period will be variable and can fall within the diastole.

In addition, the presence of heart rhythm irregularities, with the exclusion of low heart rates, do not allow the application of multi-segmental reconstruction algorithms.[8, 9] This is because the variable diastolic filling of the heart prevents a proper interpolation between the data originating from neighbouring heart cycles.

Conclusions

Editing of the ECG in 16-row MDCT-CA reduces the negative impact of mild heart rhythm irregularities on image quality, which results in a significant increase of assessable segments and in diagnostic accuracy in a selected population of patients with stable angina. Improvements in scanner technology (e.g. faster rotation time) and software capabilities (e.g. automatic recognition and editing of heart rhythm irregularities), could allow to scan routinely patients with mild arrhythmias with a good diagnostic accuracy.

References

1. Flohr TG, Schoepf UJ, Kuettner A, Halliburton S, Bruder H, Suess C, Schmidt B, Hofmann L, Yucel EK, Schaller S, Ohnesorge BM: Advances in cardiac imaging with 16-section CT systems. Acad Radiol 2003; 10:386-401.
2. Nieman K, Cademartiri F, Lemos PA, Raaijmakers R, Pattynama PM, de Feyter PJ: Reliable noninvasive coronary angiography with fast submillimeter multislice spiral computed tomography. Circulation 2002; 106:2051-4.
3. Ropers D, Baum U, Pohle K, Anders K, Ulzheimer S, Ohnesorge B, Schlundt C, Bautz W, Daniel WG, Achenbach S: Detection of coronary artery stenoses with thin-slice multi-detector row spiral computed tomography and multiplanar reconstruction. Circulation 2003; 107:664-6.
4. Nieman K, Rensing BJ, van Geuns RJ, Vos J, Pattynama PM, Krestin GP, Serruys PW, de Feyter PJ: Non-invasive coronary angiography with multislice spiral computed tomography: impact of heart rate. Heart 2002; 88:470-4.
5. Austen WG, Edwards JE, Frye RL, Gensini GG, Gott VL, Griffith LS, McGoon DC, Murphy ML, Roe BB: A reporting system on patients evaluated for coronary artery disease. Report of the Ad Hoc Committee for Grading of Coronary Artery Disease, Council on Cardiovascular Surgery, American Heart Association. Circulation 1975; 51:5-40.
6. Achenbach S, Ropers D, Holle J, Muschiol G, Daniel WG, Moshage W: In-plane coronary arterial motion velocity: measurement with electron-beam CT. Radiology 2000; 216:457-63.
7. Jakobs TF, Becker CR, Ohnesorge B, Flohr T, Suess C, Schoepf UJ, Reiser MF: Multislice helical CT of the heart with retrospective ECG gating: reduction of radiation exposure by ECG-controlled tube current modulation. Eur Radiol 2002; 12:1081-6.
8. Dewey M, Laule M, Krug L, Schnapauff D, Rogalla P, Rutsch W, Hamm B, Lembcke A: Multisegment and halfscan reconstruction of 16-slice computed tomography for detection of coronary artery stenoses. Invest Radiol 2004; 39:223-9.
9. Halliburton SS, Stillman AE, Flohr T, Ohnesorge B, Obuchowski N, Lieber M, Karim W, Kuzmiak SA, Kasper JM, White RD: Do segmented reconstruction algorithms for cardiac multi-slice computed tomography improve image quality? Herz 2003; 28:20-31.

REDUCTION OF MOTION ARTEFACTS FROM MILD HEART RHYTHM IRREGULARITIES WITH ECG-EDITING USING MULTIDETECTOR-ROW COMPUTED TOMOGRAPHY CORONARY ANGIOGRAPHY

APPENDIX I.

MILD HEART RHYTHM IRREGULARITIES: DEFINITION AND MANAGEMENT

Following we describe the "Mild Heart Rhythm Irregularities" that we used as inclusion criteria for the study on Multidetector-row computed tomography coronary angiography (MDCT-CA). High heart rate (HR) above 70 beat-per-minute (bpm), was considered as an exclusion criteria.[10]

Electrocardiogram basics for MDCT-CA (Figure I)

As a baseline information we remind that a heart cycle is constituted by a systole and a diastole. The systole involves the contraction of the atria followed by the contraction of the ventricles. The synchronized contraction is driven by a conduction system starting in the right atrium from the sino-atrial node (SA-node). The impulse then propagates to the atrio-ventricular node (AV-node) through the walls of the atria. At the AV-node the impulse is lead into a conduction system through the septum and ventricular walls. This phenomenon is represented by the electrocardiogram (ECG) track that shows the typical sequence of waves (Figure IA): P-wave (atrial contraction), the QRS-complex (ventricular contraction), T-wave (repolarization of the ventricles). Normally the P-R interval is <0.2s, the QRS complex is <0.12s, and the Q-T interval is ~0.42s. Therefore, a complete systolic contraction with repolarization wave will last ~0.55s. This means that for a heart rate of 60bpm systole and diastole will represent roughly 50% of the cardiac cycle (Figure IB). The diastolic period will be about 0.45s.

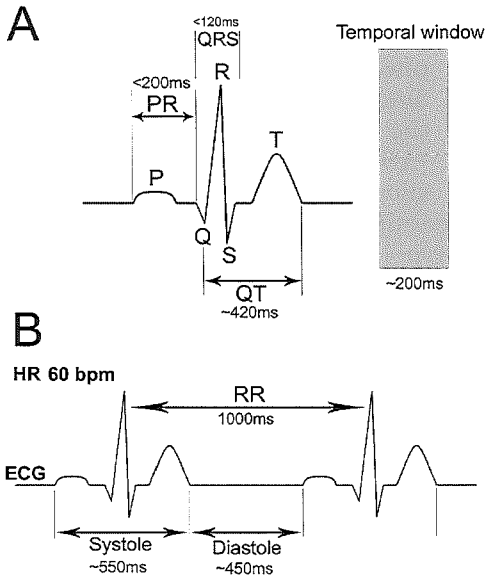

Figure I.

In this interval it is usually placed the temporal windows of ~200ms for retrospectively ECG-gated reconstruction with MDCT-CA (Figure IA). The most favourable location is usually the mid- to end-diastolic phase just prior to the P-wave.

Scan basics for MDCT-CA (Figure II)

Currently the standard technique for cardiac MDCT scanning is based on retrospective ECG gating. This means that data have to be sampled at a slow table-feed with overlapping acquisition in the z-direction throughout the cardiac cycle in order to be retrospectively synchronized. Depending on the patients heart rate and the width of the detector, a maximum table feed per second should not be exceeded. Cardiac examinations with the same CT-system at different rotation times will therefore require different pitch values to keep the table feed per second constant.

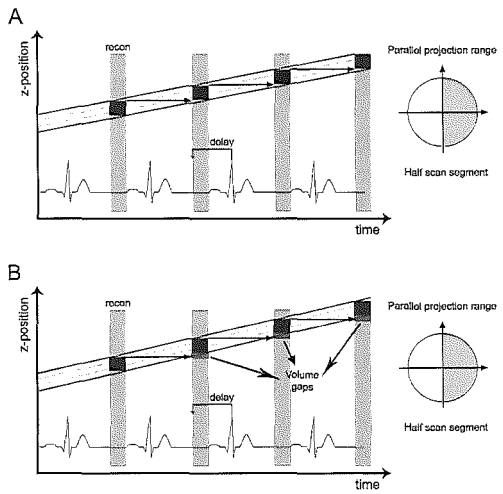

Figure II.

With 16 rows of 0.75mm width and a rotation time of 375ms, the minimum HR that can be accepted without data loss is ~40 bpm for a pitch of 0.25 (Figure IIA).

Below this threshold the software cannot find enough data between two contiguous temporal windows, and the gaps will be closed by interpolation at the expenses of a loss of spatial resolution (Figure IIB). The low pitch (e.g.: oversampling of the data) allows the scanner to cover the same z-axis position for ~1500ms with adjacent detector slices. When the RR interval, and therefore the distance between two contiguous temporal windows is >1500ms, a data gap is created and interpolation is performed to fill with information from the stack of images before and after the gap.

DEFINITION AND MANAGEMENT OF MILD HEART RHYTHM IRREGULARITIES

1. PREMATURE BEATS (PB)

Definition

A PB is a premature (compared to the previous RR interval) excitation of an area of the myocardium. This area can be located in the conduction system or in the myocardium. A PB usually results in a shorter diastolic time followed by a longer diastole. The duration of the 2 RR intervals involved in the extra-systole is usually the same as 2 RR intervals at the HR that was preceding the PB.

In MDCT-CA, even an irregularity of the heart in which, a normal heart beat happens earlier than expected based on the previous heart rate can be configured as a PB. A typical example of this is a low average heart rate around 45bpm with one or more isolated heart beats (from the SA-node) at 65bpm. For the study were included all patients with single isolated PB and a maximum number of 5 PB during the scan. Patients with bi-gemini or tri-gemini PB were excluded.

Management (Figure III)

When a PB is present in the ECG the conventional protocol for image reconstruction locates the temporal window too early in the diastolic phase when compared with previous and next heart beats (Figure IIIA – b). In this case, while all other beats are reconstructed in a late diastolic phase, the PB determines an early diastolic reconstruction. This cannot be effective for two reasons: the first is that there may be too much motion in that phase and the second that it is not the same phase as for the other beats.

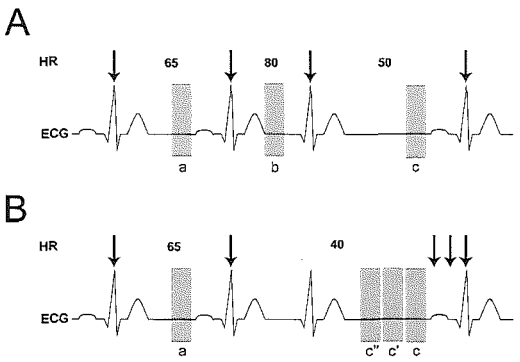

Therefore, we rule out the PB (Figure IIIB). To do that we delete temporal window applied to the PB and we fill the next diastolic interval with one or more temporal windows (Figure IIIB - 0 c' and c"). The threshold RR interval of 40bpm that avoids data gaps determines the number of additional temporal windows.

Figure III

2. ATRIAL FIBRILLATION (AF)

Definition

With AF we define an irregular and anarchic contraction of myocardial walls of the atria with hemodynamic effect. The AV-node picks up an impulse once in a while depending on its receptivity. Therefore, AV conduction is irregular. For the purpose of the study we included only patient with AF and low AV response. In these cases average HR was irregular but below 70bpm.

Management (Figure IV)

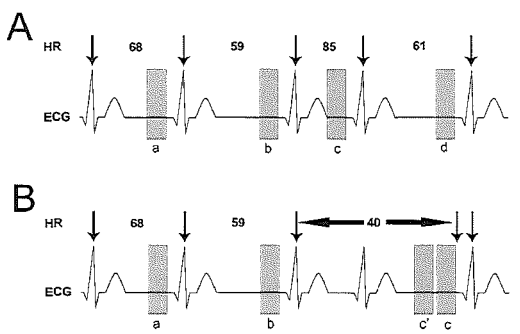

Figure IV.

The problem created in MDCT-CA by AF with low ventricular response is due the irregularity of the RR interval between contiguous heart beats. If variability remains within an acceptable range no additional editing needs to be done. When the HR in the isolated RR interval exceeds 70bpm (Figure IVA - c) that heart beat should be eliminated. If the next RR interval shows a high HR, usually the newly created RR interval is above the 40bpm

threshold. When instead the next RR shows a low HR, it will necessary to insert additional temporal windows (Figure IVB - c'), as described for PB.

3. MIS-TRIGGERING (MT)

Definition

With MS we define an event characterized by a regular or only slightly irregular HR with missed or inaccurate detection of R wave. This can happen when the ECG signal is low (e.g. small R waves, or when the waves are not usually shaped (e.g. bundle branch block, enlargement of QRS-complex). In these cases a sharp R-wave is difficult to obtain and the software can set the synchronisation point in the wrong position or miss it completely.

Management (Figure V)

The result of MT in MDCT-CA is inaccurate location of the temporal window or missing data. In the first case, the synchronisation point (thin arrows) is not on top of the R wave (Figure VA - thick arrow) and therefore the temporal window (Figure VA - b) is located later than it should, on top of the P wave. In the second case, the whole synchronisation complex is missing (Figure VB) and the RR interval is overstretched. To solve the problem it is sufficient to relocate manually the synchronisation point or insert one in the correct position (Figure VB - thick arrow).

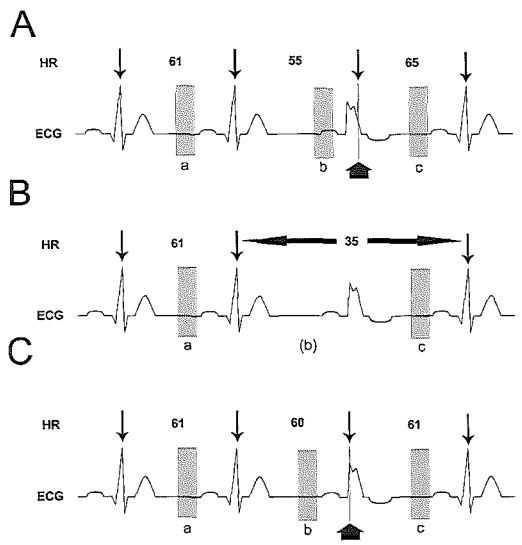

Figure V.

4. LOW HEART RATE (LHR)

Definition

A low HR for an MDCT-CA study is below 40 bpm. To solve this problem scanners currently adopt a dedicated "low heart rate" protocol, which is based on a lower pitch (e.g. ~0.20-0.15). With this protocols the HR threshold that allows to reconstruct images is lower (e.g. ~32-24bpm). Unfortunately there are a few drawbacks of this technique. The first is that a lower pitch means a longer scan time and corresponding increase in radiation exposure. The second is that usually the patient who would need this protocol present with a HR lower than average but not in the range observed during the scan. A typical example is the patient presenting with a HR of 50bpm that only during apnoea drops to 40bpm or below. A further problem is that for many of these patients with low HR we had only few cardiac cycles below a HR 40bpm.

This means that for the majority of patients with low HR using a dedicated "low heart rate" protocol would determine an unnecessary increase of radiation dose and a longer apnoea, while all the information for a proper reconstruction are available using the standard protocol.

Management (Figure VI)

Scanning patients with isolated, clustered or diffused LHR in MDCT-CA determines data gaps (see above). These gaps are present with RR intervals below 40bpm (Figure VIA - a and b). To fill the gaps the operator needs to insert additional temporal windows in order to bring the HR of the RR above 40bpm (Figure VIB - a', b' and b").

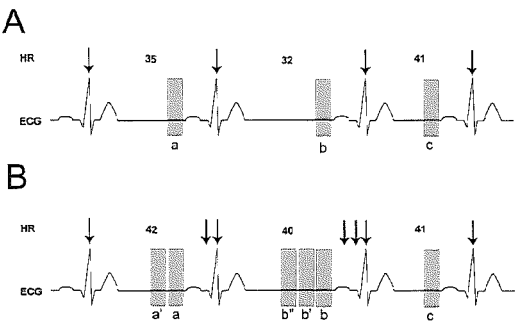

Figure VI.

5. PROCESSING

CHAPTER 5.2

STANDARD VERSUS USER-INTERACTIVE ASSESSMENT OF SIGNIFICANT CORONARY STENOSES WITH MULTISLICE COMPUTED TOMOGRAPHY CORONARY ANGIOGRAPHY

Filippo Cademartiri, MD[1]
Nico Mollet, MD[1,2]
Pedro A. Lemos, MD[2]
Eugene P. McFadden, MD, MB[2]
Riccardo Marano, MD[1]
Timo Baks, MD[1,2]
Theo Stijnen, PhD[3]
Pim J. de Feyter, MD[1,2]
Gabriel P. Krestin, MD[1]

From the Departments of Radiology[1], Cardiology[2], and Epidemiology and Biostatistics[3], Erasmus MC, University Medical Center Rotterdam, The Netherlands.

Am J Cardiol, 94:1590–1593, 2004.

Forty-four patients in sinus rhythm with suspected coronary artery disease underwent 16-row multislice computed tomography coronary angiography and conventional coronary angiography. Two protocols for image analysis were applied to the multislice computed tomographic images: standard projections versus interactive postprocessing. The diagnostic accuracy of both methods for the detection of significant lesions (>50% lumen reduction) was compared with quantitative coronary angiography. Sensitivity and specificity were 58% and 96% and 96% and 97%, for standard projections and interactive postprocessing protocol, respectively.

Sixteen-row multislice computed tomographic (MSCT) coronary angiography (CA) has shown good results in the detection of coronary artery stenoses[1,2]. To implement MSCT-CA in a clinical setting, several aspects of the technique need to be addressed. In many settings in routine radiologic practice, a technician prepares the images, which are subsequently interpreted by a radiologist. Coronary imaging may require a more interactive and "case by case" approach due to the tortuous anatomy and the small size of the vessels. This study compares the diagnostic accuracy, in a selected population of patients undergoing 16-row MSCT-CA, of 2 different protocols for image visualization: a standard projection technique and an interactive postprocessing technique.

Between April and August 2003, 44 patients (38 men; mean age 59 ± 8 years) who underwent conventional CA for suspected coronary artery disease, were retrospectively enrolled in the study. Inclusion criteria for MSCT-CA were regular heart rhythm and heart rate (HR) (spontaneous or β-blocker induced) >65 beats/min, and the ability to hold breath for 20 seconds. Exclusion criteria were: previous allergic reaction to iodine contrast media, renal insufficiency (serum creatinine >120 mmol/L), potential pregnancy, unstable clinical status, marked heart failure, previous bypass surgery or percutaneous coronary intervention, and datasets of nondiagnostic image quality. The institutional review board approved the study and patients gave written informed consent.

On arrival, the HR of the patients was measured. Patients with a prescan HR ≥65 beats/min were given 100 mg of metoprolol orally and the scan was performed 1 hour later. In all patients, a bolus (100 ml at 4 ml/s) of iodinated contrast material (Iodixanol 320 mgI/ml, Amersham Health, Little Chalfont, United Kingdom) was administered using a power injector (EnVisionCT, MedRAD, Pittsburgh, Pennsylvania) through an 18-gauge cannula, in an antecubital vein. Synchronization between the passage of contrast material and data acquisition was achieved using a realtime bolus tracking technique. The scan parameters for MSCT-CA (Sensation 16, Siemens) were: number of detectors 16, patient detector width 0.75 mm, gantry rotation time 420 ms, temporal resolution 210 ms, 120 kV, 500 mA, and feed/rotation 3.0 mm.

Three axial datasets were retrospectively reconstructed at -350, -400, and -450 ms before the next R wave with the following parameters: effective slice width 1 mm, image increment of reconstruction 0.5 mm, field of view 150 to 180 mm, and medium convolution filter (B30f). The dataset with the least motion artifacts was selected for further analysis. This dataset was transferred to a stand-alone workstation and evaluated using dedicated analysis software (Leonardo, Siemens).

Two protocols for image analysis were applied: standard projection (Figure 1; Videos 1 to 4) and interactive postprocessing (Figure 2; Video 5). An experienced radiographer prepared 5 datasets in different projections for the standard protocol. These datasets consisted of the source axial dataset (1 mm thick and 0.5 mm overlapping; Video 1), a para-axial maximum intensity projection parallel to the path of the left anterior descending artery (3 mm thick and 1.5 mm overlapping; Video 2), a parasagittal multiplanar reformat parallel to the interventricular groove to visualize the left anterior descending artery (1 mm thick and 0.5 mm overlapping; Video 3), a paracoronal multiplanar reformat parallel to the atrioventricular groove to visualize the right coronary and the left circumflex arteries (1 mm thick and 0.5 mm overlapping; Video 4), and a paracoronal maximum intensity projection parallel to the atrioventricular groove to visualize the right coronary and the left circumflex arteries (3 mm thick and 1.5 mm overlapping; Video 4). The time required to prepare the images was recorded. No image preparation was required for the interactive postprocessing protocol. In the standard protocol the observer

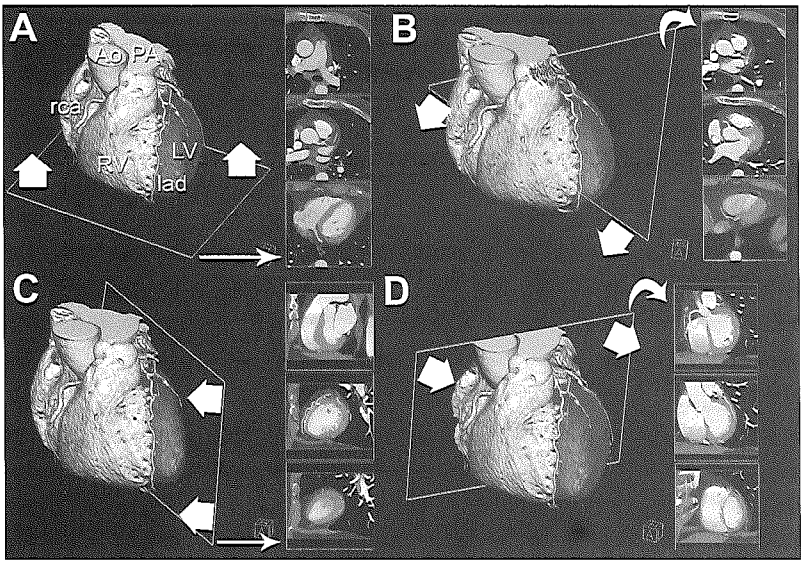

Figure 1. Imaging modalities and planes applied for the standard projections protocol. (**A**) The axial plane is displayed and sample images are shown in the right column from the bottom (caudal end) to the top (cranial end) of the dataset. (**B**) A paraaxial plane parallel to the course of left anterior descending is shown and in the right column sample images show the appearance of the origin of the left coronary artery, the right coronary artery, and the posterior descending artery, from top to bottom. (**C**) The plane is running parallel to the interventricular groove to display the left anterior descending artery and in the right column sequential images are shown. (**D**) The plane is parallel to the atrioventricular groove for the visualization of the right coronary artery and for the left circumflex artery, which are displayed in the right column. In (**A**) to (**D**), thick arrows indicate the direction of scrolling of the plane. Ao ascending aorta; lad left anterior descending; LV left ventricle; PA pulmonary artery; RV right ventricle; rca right coronary artery. (A full color version of this illustration can be found in the color section (chapter 12)).

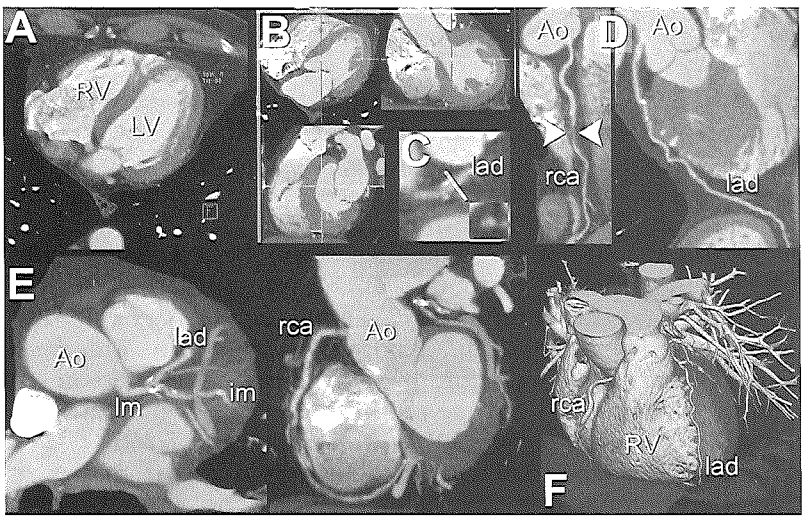

Figure 2. Imaging modalities applied for the interactive postprocessing protocol. Axial slices (**A**) and multiplanar reconstructions (**B**) are the basic tools for image assessment. Then, a multiplanar reconstruction focused on the stenosis (**C**; proximal stenosis of the left anterior descending artery) integrated with dedicated curved reconstructions along the lumen (**D**; stenosis in the midright coronary artery; arrowheads) are performed. In parallel, maximum intensity projections (**E**) and 3-dimensional volume rendering (**F**) are performed to improve panoramic perception. im intermediate branch; lm left main; other abbreviations as in Figure 1. (A full color version of this illustration can be found in the color section (chapter 12)).

Table 1. Diagnostic Accuracy of Standard Protocol Versus Interactive Protocol

				Specificity (95% CI)		Specificity (95% CI)	
AHA	Coronary segment	n	SDS (%)	S	I	S	I
1	Right proximal	44	12	83 (52 - 98)	100 (74 - 100)	88 (71 - 97)	94 (79 - 99)
2	Rightmiddle	33	16	56 (30 - 80)	100 (79 - 100)	100 (81 - 100)	88 (64 - 99)
3	Rightdistal	26	5	80 (28 - 100)	100 (48 - 100)	100 (84 - 100)	95 (76 - 100)
4	Posteriordescending	16	2	50 (1 - 99)	50 (1 - 99)	100 (77 - 100)	100 (77 - 100)
5	Leftmain	44	0	NA	NA	98 (88 - 100)	100 (92 - 100)
6	LADproximal	44	14	43 (20 - 71)	86 (57 - 98)	93 (78 - 99)	93 (78 - 99)
7	LADmiddle	41	15	53 (27 - 79)	100 (78 - 100)	100 (87 - 100)	100 (87 - 100)
8	LADdistal	38	2	100 (16 - 100)	100 (16 - 100)	100 (90 - 100)	97 (86 - 100)
9	1stdiagonal	34	2	50 (1 - 99)	100 (16 - 100)	91 (75 - 98)	94 (79 - 99)
10	2nddiagonal	36	0	NA	NA	50 (33 - 68)	100 (82 - 100)
11	LC-proximal	43	8	88 (47 - 100)	88 (47 - 100)	97 (85 - 100)	97 (85 - 100)
12	1stmarginal	37	10	20 (3 - 56)	100 (69 - 100)	96 (81 - 100)	96 (81 - 100)
13	LCmiddle	33	6	50 (12 - 88)	100 (48 - 100)	96 (81 - 100)	96 (81 - 100)
14	2ndmarginal	18	0	NA	NA	89 (65 - 99)	100 (81 - 100)
15	Posterolateral	10	1	100 (3 - 100)	100 (3 - 100)	100 (66 - 100)	100 (66 - 100)
All		478	92	58 (47 - 68)	96 (89 - 99)	96 (94 - 98)	97 (94 - 98)

AHA = American Heart Association segmental classification; CI =confidence intervals; I = interactive protocol; LAD = left anterior descending; LCx = circumflex; NA = not assessable; S = standard protocol; SDS = significantly diseased segments (>50% lumen reduction at quantitative coronary angiography).

was allowed to scroll through the images of the 5 datasets (Videos 1 to 4). In the interactive protocol, the observer used all the tools on the workstation (Video 5): axial images, multiplanar reformats, slab multiplanar maximum intensity projections, curved planar reformats, and 3-dimensional volume rendering.

Two independent observers (1 radiologist and 1 cardiologist), unaware of the results of CA, reviewed all images at the workstation. They were asked to visually identify the presence of significant stenoses (≥50% lumen reduction) on a "per segment" analysis using the American Heart Association classification of coronary segments[3]. Disagreements were resolved in by consensus. The time required to score was recorded.

Conventional CA was performed within 2 weeks of MSCT-CA using a standard technique. One experienced observer, unaware of the results of MSCT-CA, determined the diameter of all coronary branches and evaluated the presence of significant stenoses using quantitative CA (CAAS, Pie Medical Imaging, Maastricht, The Netherlands). Lesions with an average diameter stenosis of ≥50% in 2 orthogonal views were considered significant obstructions.

PPV (95% CI)		NPV (95% CI)		Accuracy (95% CI)		
S	I	S	I	S	I	Kappa
71 (42 - 92)	86 (57 - 98)	93 (78 - 99)	100 (88 - 100)	86 (73 - 95)	96 (85 - 99)	0.69
100 (66 - 100)	89 (65 - 99)	71 (49 - 87)	100 (78 - 100)	79 (61 - 91)	94 (80 - 99)	0.48
100 (40 - 100)	83 (36 - 100)	96 (77 - 100)	100 (83 - 100)	96 (80 - 100)	96 (80 - 100)	0.78
100 (3 - 100)	100 (3 - 100)	93 (68 - 100)	93 (68 - 100)	84 (70 - 100)	94 (10 - 100)	1.0
0 (0 - 98)	NA	100 (91 - 100)	100 (92 - 100)	98 (88 - 100)	100 (92 - 100)	NA
75 (35 - 97)	86 (57 - 98)	78 (61 - 90)	93 (78 - 99)	77 (62 - 89)	91 (78 - 98)	0.41
100 (63 - 100)	100 (78 - 100)	79 (61 - 91)	100 (87 - 100)	83 (68 - 83)	100 (91 - 100)	0.59
100 (16 - 100)	67 (9 - 99)	100 (90 - 100)	100 (90 - 100)	100 (91 - 100)	97 (86 - 100)	0.78
25 (1 - 81)	50 (7 - 93)	97 (83 - 100)	100 (88 - 100)	88 (73 - 97)	94 (80 - 99)	0.15
0 (0 - 19)	NA	100 (82 - 100)	100 (82 - 100)	50 (33 - 67)	100 (82 - 100)	NA
88 (47 - 100)	88 (47 - 100)	91 (85 - 100)	97 (85 - 100)	95 (84 - 99)	95 (84 - 99)	1.0
67 (9 - 99)	91 (59 - 100)	77 (59 - 89)	100 (87 - 100)	76 (59 - 88)	97 (86 - 100)	0.18
75 (19 - 99)	83 (34 - 100)	90 (73 - 98)	100 (87 - 100)	88 (72 - 97)	97 (84 - 100)	0.37
0 (0 - 84)	NA	100 (79 - 100)	100 (82 - 100)	89 (65 - 99)	100 (82 - 100)	NA
100 (3 - 100)	100 (3 - 100)	100 (66 - 100)	100 (66 - 100)	100 (69 - 100)	100 (69 - 100)	1.0
78 (66 - 87)	87 (79 - 93)	91 (87 - 93)	99 (97 - 100)	89 (86 - 91)	96 (94 - 98)	0.58

The consensus reading of the MSCT-CA was used to calculate sensitivity, specificity, positive and negative predictive values, and diagnostic accuracy with 95% confidence intervals. The agreement between the 2 image analysis protocols (standard and interactive) was evaluated by the coefficient of variation κ. Kappa values <0.4 indicate poor, and values ≥0.4, >0.6, and >0.8 indicate fair, moderate, and excellent agreement, respectively. The differences (and 95% confi- dence intervals for the difference) in sensitivity and specificity between the 2 analysis protocols were evaluated by a previously proposed method[4]. A p value <0.05 was considered significant.

Mean HR during the scan was 54 ± 8 beats/min. A total of 478 ≥2-mm segments were included in the analysis. Ninety-two segments (19%) had significant obstructions on CA. The proximal and middle right coronary artery and left anterior descending segments accounted for 63% of diseased segments (n = 57). In these segments, the sensitivity ranged from 43% to 83% for the standard protocol and from 86% to 100% for the interactive protocol. Overall, the standard protocol missed 37 significant lesions, whereas the interactive protocol missed 4 significant lesions.

Interobserver agreement was excellent for interactive protocol (κ = 0.81) and moderate for standard protocol (κ = 0.64).

The specificity did not differ significantly between the 2 protocols ($p > 0.05$); however, the interactive protocol had a significantly better sensitivity for the detection of coronary obstructions ($p < 0.05$) (Table 1).

The mean time required for the radiographer to prepare the 5 datasets for standard protocol was 6 ± 2 minutes. The mean time required for the observers to complete the analysis was 16 ± 9 minutes for the standard protocol and 23 ± 13 minutes for the interactive protocol ($p < 0.05$).

The present study assessed the diagnostic accuracy of 16-row MSCT-CA using 2 protocols for image visualization: the first protocol was based on a standard series of projections that the observer could assess using a workstation implemented in a digital archiving system. The second protocol required the interaction between the operator and the dataset using a 3-dimensional workstation equipped with all available postprocessing tools. The results show that an approach using standard projections prepared by a technician was faster. In addition, it was probably less expensive, in that image processing was performed by a radiographer and image assessment by a radiologist. However, the standard projections approach had a significantly lower diagnostic sensitivity compared with the interactive postprocessing. In particular, the proximal segments, where disease was more frequent and of greater clinical importance (the proximal left anterior descending artery alone represented of significant lesions), were the sites that showed a major and significant discrepancy between the techniques. This reflects the large number (37 of 92; 40%) of lesions that were missed using standard projections. Specificity, instead, did not differ significantly between techniques.

One limitation of our study is that patients were retrospectively enrolled and selected. Patients with severe residual motion artifacts were not enrolled. This can improve the overall diagnostic accuracy. The results cannot be extrapolated to other patient populations, such as those with stents or bypass grafts. Finally, our interactive postprocessing protocol is based on a single vendor platform.

1. Nieman K, Cademartiri F, Lemos PA, Raaijmakers R, Pattynama PM, de Feyter PJ. Reliable noninvasive coronary angiography with fast submillimeter multislice spiral computed tomography. Circulation 2002;106:2051–2054.
2. Ropers D, Baum U, Pohle K, Anders K, Ulzheimer S, Ohnesorge B, Schlundt C, Bautz W, Daniel WG, Achenbach S. Detection of coronary artery stenoses with thin-slice multi-detector row spiral computed tomography and multiplanar reconstruction. Circulation 2003;107:664–666.
3. Austen WG, Edwards JE, Frye RL, Gensini GG, Gott VL, Griffith LS, McGoon DC, Murphy ML, Roe BB. A reporting system on patients evaluated for coronary artery disease. Report of the Ad Hoc Committee for Grading of Coronary Artery Disease, Council on Cardiovascular Surgery, American Heart Association. Circulation 1975;51:5– 40.

4. Hawass NE. Comparing the sensitivities and specificities of two diagnostic procedures performed on the same group of patients. Br J Radiol 1997;70:360–366.

PART 2 - CLINICAL IMPLEMENTATION

6. CORONARY STENOSIS

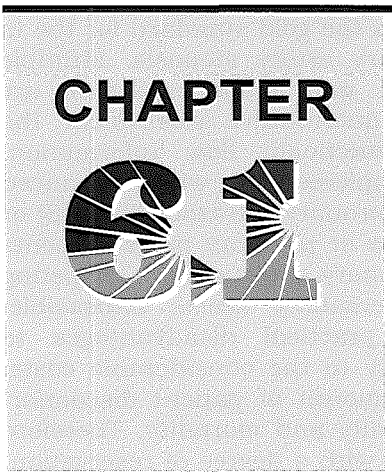

CT OF THE HEART: PRINCIPLES AND METHODS CT ANGIOGRAPHY FOR THE DETECTION OF CORONARY ARTERY STENOSIS

Koen Nieman, MD[1,2]
Filippo Cademartiri, MD[2]
Peter MT Pattynama, MD,PhD[2]
Pim J de Feyter, MD,PhD[1,2]

From the Departments of Cardiology,Thoraxcenter[1] and Radiology[2], Erasmus MC, University Medical Center Rotterdam,The Netherlands

CT of the Heart: Principles and Applications;
Edited by: U. Joseph Schoepf – pp. 321-332;

INTRODUCTION

In the past decade we have witnessed the development of non-invasive coronary imaging using different imaging modalities. Computed tomography (CT) and magnetic resonance imaging (MRI) modalities have been applied for the quantification of coronary calcium, detection of coronary and bypass graft occlusion and most recently the characterization of non-calcified plaque material. However, the decisive application of non-invasive coronary CT or MRI, which determines whether it will find widespread clinical application, will be the detection of coronary stenosis. The first comparative study between MRI and conventional coronary angiography was published in 1993,[1] and numerous studies followed using various data acquisition techniques.[2] Since 1997 a number of studies have compared ECG-triggered electron beam computed tomography (EBCT) and conventional coronary angiography, also with promising results.[3-9] In 1999 four-slice multislice spiral computed tomography (MSCT) was introduced and the first comparative publications appeared in 2001.[10-16] In 2002 the first results were published using 16-slice MSCT scanners with a sub-millemeter slice thickness and rotation time of less than a half second.[17] In this chapter we will discuss the practical considerations, diagnostic value and remaining limitations of MSCT coronary imaging for the detection of coronary stenosis. The clinical utility and future developments will be discussed, as well as a comparison with other non-invasive imaging techniques.

IMAGING REQUIREMENTS OF NON-INVASIVE CORONARY ANGIOGRAPHY

Catheter-based selective X-ray coronary angiography

Conventional X-ray coronary angiography with selective contrast enhancement of the coronary arteries remains the gold standard for the in vivo detection and quantification of coronary artery stenosis. Multiple high-contrast projections with a 0.1 x 0.1 mm image resolution are acquired each heart cycle. Besides accurate quantitative assessment, the dynamic injection of contrast provides functional flow information. Catheter-based angiography can be complemented with advanced coronary imaging techniques, such as intra-coronary ultrasound (ICUS) or optical coherence tomography (OCT), and flow or pressure measurements to determine the functional severity of a coronary obstruction. Competing with a technique of such quality and versatility seems impossible. However, there are also a number of practical disadvantages to catheter-based coronary imaging. Additionally to the considerable costs, this invasive procedure involves a certain amount of patient discomfort and a small but not negligible risk of morbidity and mortality. Therefore conventional coronary angiography is applied with a degree of reservation, when adequate supportive evidence has been obtained, such as by exercise testing, and when either percutaneous intervention or bypass surgery are anticipated.

Requirements for non-invasive coronary angiograpphy

In order to visualize the coronary arteries and find coronary artery disease at an earlier stage, and to follow-up patients with known disease, a non-invasive, and preferably less costly imaging technique would be desirable. To ensure sufficient image quality, non-invasive techniques require a high spatial resolution to image small coronary arteries, high temporal resolution to acquire motion-free images, adequate contrast to distinguish the coronary lumen from the vessel wall, and particularly in the case of computed tomography a short scan time to acquire all data within the duration of a comfortable breath hold. Finally, to maintain the advantage of a lower health risk, the non-invasive method should minimize the use of radiation and contrast media, which particularly applies to computed tomography.

Besides attempting to approximate the diagnostic quality of conventional angiography, computed tomography and magnetic resonance imaging provide additional information regarding the cardiac and three-dimensional coronary anatomy and the composition of the vessel wall.

ACQUISITION, RECONSTRUCTION, POST-PROCESSING AND EVALUATION

Data acquisition and image reconstruction

A detailed description of the general data acquisition and image reconstruction considerations for MSCT coronary angiography can be found in the previous chapters. For the assessment of the coronary arteries the highest image quality is required. This means the fastest X-source rotation speed and thinnest detector collimation possible, while

still allowing complete scanning of the entire heart within a single breath hold. Images are routinely reconstructed during the diastolic cardiac phase to minimize motion artefacts, and out of a number of reconstructions at a slightly varying reconstruction window position the most optimal data set is used for image analysis. Particularly at higher heart rates, different vessel segments are most optimally visualized during different phases.

Post-processing and data analysis

The coronary lumen can be assessed using different post-processing techniques (figure 1). Generally, maximum intensity projections MIP) of thin slabs, or multiplanar reformations (MPR), oriented parallel to the coronary of interest, are used in addition to the axial source images. MIP provides smooth high-contrast images, and has the advantage that longer sections of a vessel can be visualized in the same plane. However, when calcifications or stents are present, the coronary lumen becomes obscured by these high-attenuating structures, in which case MPR or the axial source images are more suitable. For presentation purposes and three-dimensional orientation of the referring physician, advanced post-processing techniques are available such as curved MPR, volume rendering and virtual angioscopy.

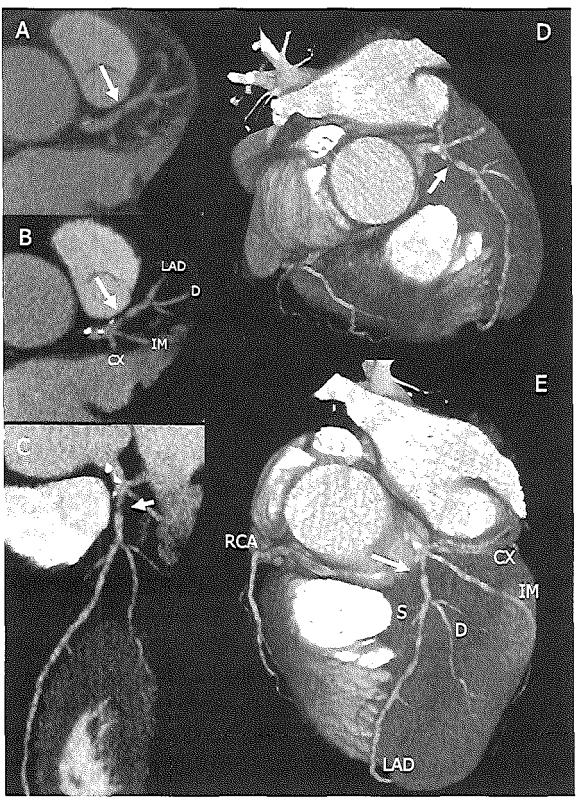

Figure 1. Post-processing techniques. A stenotic lesion (arrow) in the proximal left anterior descending coronary artery (LAD), displayed using multi-planar reformation (**A**), thin slab maximum intensity projection (**B**), curved maximum intensity projection (**C**), and volume rendering (**D and E**). Right coronary artery (RCA), diagonal (**D**), intermediate (IM), circumflex (CX) and septal branch (S).

DIAGNOSTIC PERFORMANCE OF FOUR-SLICE MSCT

MSCT compared to conventional coronary angiography

The first multislice spiral computed tomography scanners (MSCT), introduced in 1999 and equipped with four parallel detector-arrays, were the first mechanical CT scanners that allowed assessment of the coronary artery lumen. The first studies that compared MSCT coronary angiography and the gold standard of conventional X-ray coronary angiography were published in early 2001, with promising results (table 1).

Table 1. Diagnostic performance of multislice spiral CT to detect coronary stenosis, using conventional coronary angiography as the standard of reference

		β	N	Assess.	D	Prev	Excl	Se	Sp	PPV	NPV	Se[a]
Nieman[10]	4	-	31	Segment	50%	0.9	27%	81%	97%	81%	97%	68%
Achenbach[11]	4	-	64	Branch	50%	1.1	32%	85%	76%	56%	93%	55%
					70%	0.9	32%	91%	84%	59%	98%	58%
Knez[12]	4	-	43	Segment	50%	1.2	6%	78%	98%	84%	96%	51%
Vogl[13]	4	+	64	Segment	50%	NR	28%	75%	99%	92%	98%	NR
Kopp[14 b]	4	-	102	Segment	50%	1.5	15%	86%	96%	76%	98%	86%
								93%	97%	81%	99%	93%
Giesler[15 c]	4	+	100	Branch	70%	1.0	29%	91%	89%	66%	98%	49%
Nieman[16 c]	4	-	78	Segment	50%	0.9	32%	84%	95%	67%	98%	63%
Nieman[17]	16	+	58	Branch	50%	1.1	0	95%	86%	80%	97%	95%
Ropers[18]	16	+	77	Branch	50%	1.0	12	93%	81%	92%	85%	73%

Use of betablockers (b); method of assessment (assess.); Diameter reduction considered significantly stenosed (D); Number of stenotic vessel per patient (Prev.); Percentage of excluded segments / branches (Excl); Sensitivity (Se), specificity (Sp), positive (PPV) and negative predictive value (NPV) regarding the assessable segments/branches; Sensitivity including missed lesions in non-assessable segments/branches (Sea).
[b]Results by two observers, without consensus reading.
[c]Studies include patients from earlier publications.

The studies were performed with comparable techniques but varied in study design. The patient population varied between 31 and 102, and consisted of patients suspected of obstructive coronary artery disease and an indication for conventional coronary angiography. Therefore, the average number of diseased vessels varied between 0.9 and 1.5 per patient. Most studies considered a lumen diameter reduction of 50% as significant,[10,12-14,16] while others used a 70% cut-off point.[11,15] In two studies the main coronary branches: left main (LM), left anterior descending (LAD), left circumflex (LCX) and right coronary artery (RCA) were evaluated as a whole, including all >2.0 mm branches,[11,15] while the other studies assessed a predefined number of proximal, middle and distal coronary segments, according to the ACC/AHA guidelines, regardless of

the vessel diameter.[10,12-14] One study considered all coronary segments, including side-branches, with a minimal diameter of 2.0 mm.[16] All studies were performed by single centers, and all but one were based on a consensus reading by two blinded observers. The firsts three studies did not use additional beta-receptor blocking medication to reduce the patientÆs heart rate during the data acquisition.

Image interpretability

The percentage of coronary arteries or coronary segments with a subjectively adequate image quality varied between 6% and 32% in the different studies. Reasons for non-assessability mainly related to motion artifacts caused by residual cardiac motion, severe coronary calcification and voluntary patient movement, but also include the inability to discriminate the coronary artery lumen from adjacent contrast-enhanced structures, technical scanner failure and insufficient scan range (figure 2). With four-slice MSCT scanners the entire heart can be covered within the duration of a long breath hold of 35-45s. However, a scan time of up to 40

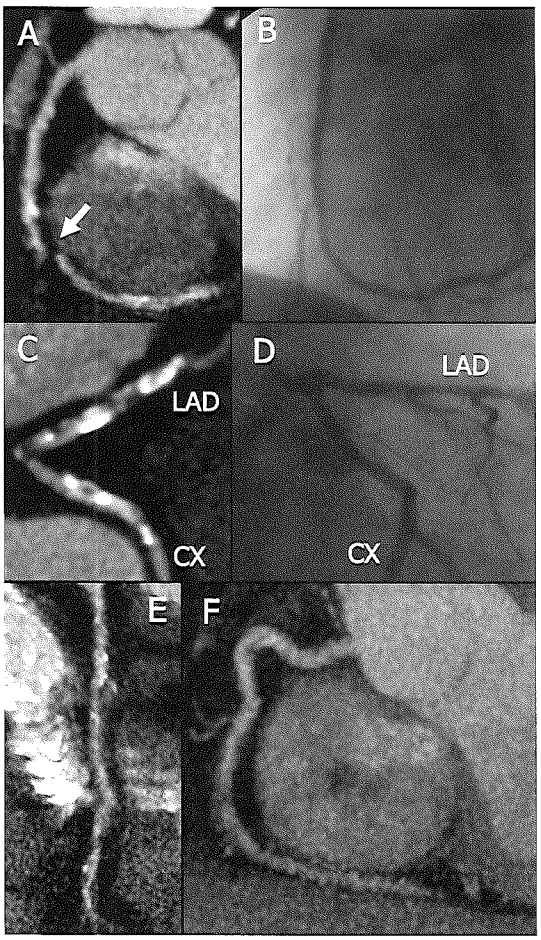

Figure 2. Image artefacts. The accuracy of MSCT can be affected by a number of artefacts. Consecutive slabs are reconstructed during different cardiac phases in the occurrence of irregular heart beats, which results in stair step artefacts or in complete discontinuity of the artery (arrow), as in this case (**A & B**). The presence of extensive calcification of the left anterior descending (LAD) and circumflex coronary artery (CX) limits the assessability due to partial volume artefacts and beam hardening (**C & D**). At faster heart rates image degrading motion artefacts occur (**E**). Particularly in overweight patients the attenuation by the surrounding tissue, such as the liver, can decrease the signal-to-noise ratio. In this case the distal RCA, which runs at the same level as the liver, is poorly assessable (**F**).

seconds proofs too long in a substantial number of patients. Other incidental causes for reduced interpretability are beam hardening artefacts from the high concentration of contrast medium in the superior caval vein or pacemaker wires. While MSCT in patients with arrhythmia is generally discouraged because of the end-diastolic volume variation, occasional premature contractions occur in many patients and can adversely affect the assessment. All studies show that the left main coronary artery can nearly always be evaluated. Of the remaining main branches the left anterior descending coronary artery (LAD) is least affected by motion artefacts. The most important cause for non-assessability in case of the LAD is the presence of extensive calcifications. The right coronary artery (RCA), which has a large motion radius and short motion-sparse period during the diastole, is branch that is most affected by motion artefacts caused by residual cardiac motion during the image reconstruction interval. The left circumflex coronary artery (LCX) also suffers from motion artefacts. Occasionally it can be difficult to distinguish the small LCX from the adjacent contrast-enhanced cardiac vein. The fact that proximal vessels are better visualized than more distal branches is only partially related to diameter size. Both the middle segment of the RCA as well as the LCX have a larger motion radius compared to the proximal segments. The more distal branches and side branches are most difficult to visualize. In a study that compared the assessability of the different coronary segments with a minimal diameter of 2.0 mm, the proximal RCA was evaluable in 88%, compared to 61% of the middle and 60% of the distal segments. While assessment of the proximal LAD was possible in 89%, compared to 77% of the middle and 75% of the distal segments. In this study the proximal and the middle segments of the LCX were equally difficult to evaluate, 57% and 56%, respectively.[19]

Detection of coronary obstruction

When considering only the coronary arteries or segments that were imaged with sufficient image quality, the sensitivity of 4-slice MSCT to detect significant coronary obstruction, defined as ≥50% lumen diameter reduction, ranges between 75% and 95%, and the specificity between 76% and 99%.[10-16] As can be expected the sensitivity and specificity are inversely correlated, as well as the number of excluded segments and the diagnostic performance in the assessable segments. The positive and negative predictive value ranged between 56% and 99%, and 93% and 99%, respectively. Compared to >50% lesions, Achenbach et al found a higher diagnostic performance for the detection of lesions with a lumen diameter reduction of at least 70%.[11] The results show that exclusion of disease in a normal vessel is less challenging than the classification of a diseased vessel as significantly stenosed or not, particularly in the presence of extensive calcification. The apparent size of the calcium deposits causes overestimation of the total plaque size, which results in false-positive assessments. According to some investigators, MSCT coronary angiography may be most valuable as a tool to exclude significant lesions in patients with a relatively low pre-test likelihood for

the presence of stenoses, and not for the staging of patients with very high likelihood and expectedly advanced coronary artery degeneration. Figures 3-8 are examples of MSCT imaging of coronary obstruction with corresponding conventional X-ray angiograms.

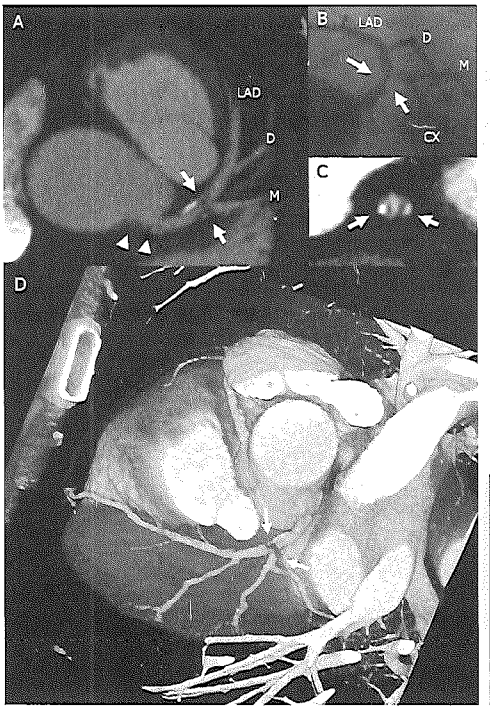

Figure 3. Lesions in the left main bifurcation. A significant lesion (arrow), consisting of two partially calcified plaques is situated at the distal part of the left main coronary artery, obstructing both the left anterior descending (LAD) as well as the left circumflex branch (CX) (**A**). The cross-section of the vessel confirms the distinct configuration of the lesions (**C**). Additionally, more non-calcified plaque material (arrow head) can be observed in the proximal part of the left main artery (arrow heads) (**A**). Diagnonal (**D**) and marginal (M) branch.(A full color version of this illustration can be found in the color section (chapter 12)).

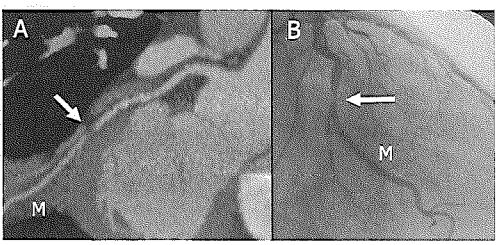

Figure 4. Significant lesion in the left circumflex coronary artery. A significant lesion (arrow) was found in the mid-segment of the left circumflex branch, just proximal of the bifurcation of a major marginal branch (M), both by MSCT (**A**) and conventional angiography (**B**).

In a study comparing the diagnostic accuracy of MSCT in relation to the proximity of the coronary segment, a sensitivity and specificity of 92% and 96% were found in the largest proximal segments (RCA1, LM, LAD6), 85% and 90% for the middle segments (RCA2, LAD7, LCX11), 71% and 94% for the distal segments (RCA3, LAD8, LCX13) and 50% and 89% for the side-branches.[19] In the study by Kopp et all, the sensitivity to detect stenotic lesions significantly increased, to 97%/99%, by selectively assessing he proximal and middle coronary segments.[14]

The segments and vessels that were excluded from analysis because of inadequate image quality contained a substantial number of undetected lesions. If these lesions in non-evaluable vessels are included in the analysis, as false-negative interpretations, the sensitivity is much lower in most studies, between 49% and 93%.[10-16]

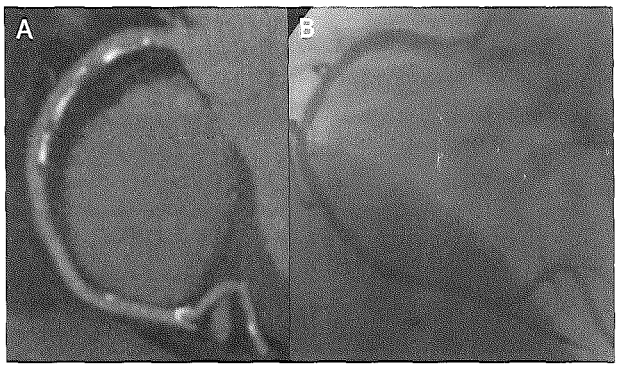

Figure 5. Diffuse coronary artery disease. This right coronary artery shows extensive atherosclerotic degeneration, with calcified and non-calcified plaque material along the entire length of the proximal inner curve, and separate lesions more distally (**A**). Although the MSCT shows no severe stenosis, the absence of significant lesions was more straightforward on the conventional angiogram.

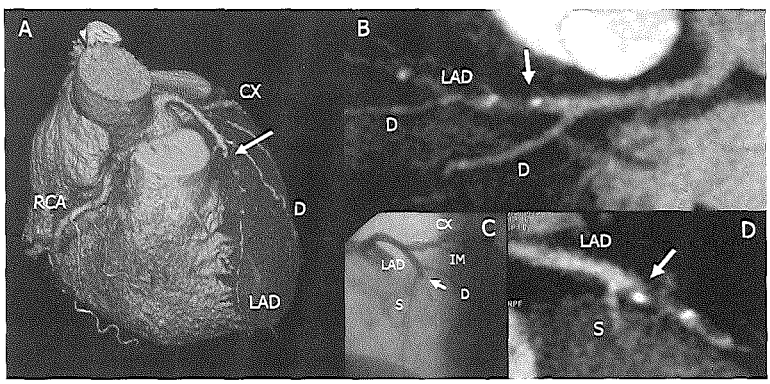

Figure 6. Occlusion of the left anterior descending coronary artery. Three-dimensional reconstruction (**A**) and curved multiplanar reconstruction (**B**) of a CT coronary angiogram showing an occluded (arrow) left anterior descending coronary artery (LAD) (**B**), which was confirmed by conventional by conventional coronary angiography (**C**). A saggital cross-section shows in detail the different plaque components, both calcified and non-calcified, as well as some residual contrast enhancement within the obstructed segment (**D**). Right coronary artery (RCA), diagonal (**D**), intermediate (IM) and circumflex branch (CX).(A full color version of this illustration can be found in the color section (chapter 12)).

SIXTEEN-SLICE CORONARY ANGIOGRAPHY

To date two studies has been published comparing MSCT and conventional coronary angiography using 16-slice MSCT.[17,18] The advantages offered by this new technique are a faster rotation time of 0.42 s, an extended number of thinner detector-rows (0.75 mm), and shorter total scan time of approximately 20 seconds. For the ECG-gated protocol, the 12 central detector-rows were applied. To optimise the image quality, consistent heart rate control was incorporated into both protocol. In the study by Nieman et al, patients with a pre-scan heart rate over 65 beats per minute were given an oral dose of 100 mg metoprolol one hour prior to

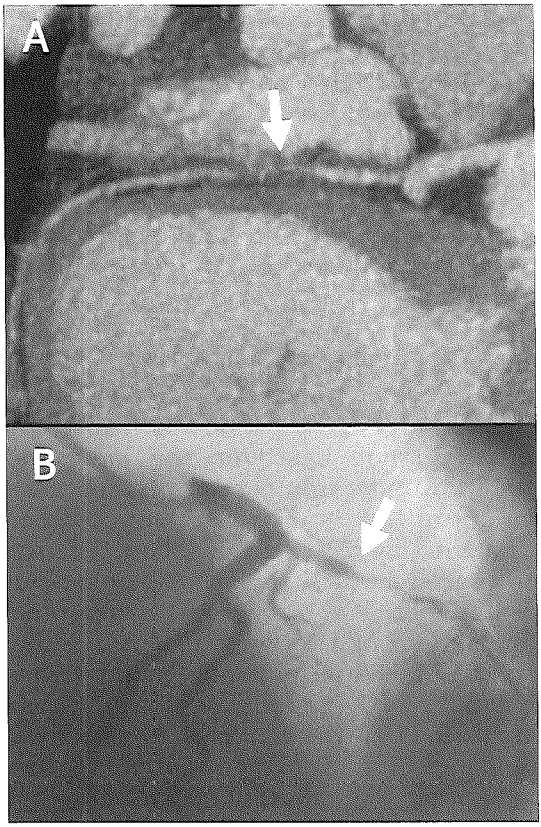

Figure 7. Occlusion of the left circumflex coronary artery. Curved maximum intensity projection (MIP) of a predominantly non-calcified occlusion (arrow) of the left circumflex branch (**A**), confirmed by conventional coronary angiography (**B**). the distal segment is filled by collaterally by the left anterior descending coronary artery.

the examination, decreasing the average heart to 57 b.p.m.. Ropers et al, used 50 mg of atenolol to decrease the heart rates of all patients with >60 b.p.m., down to an average heart rate of 62 b.p.m. Only 7% and 12% of the coronary branches contained sections with a poor image quality. Compared to the other branches the right coronary artery was still most vulnerable to image quality degradation. Nieman et al, irrespectively of the image quality, evaluated all branches with a minimal lumenal diameter of 2.0 mm, and found a

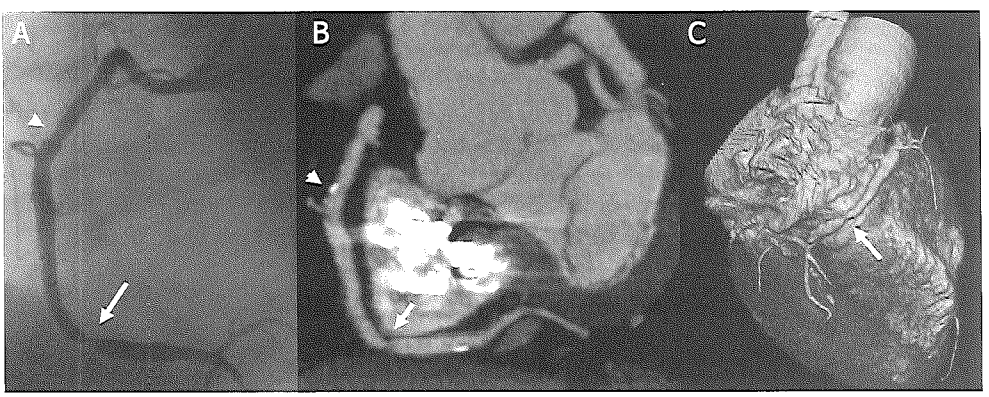

Figure 8. Stenosis of the distal right coronary artery. Using thin slab maximum intensity projection (MIP), a stenotic lesion (arrow) is demonstrated in the distal right coronary artery (**A**). Also minor wall irregularities, caused by small calcified lesions (arrow heads), can be observed, and were confirmed by conventional angiography (**B**).(A full color version of this illustration can be found in the color section (chapter 12)).

sensitivity and specificity of 95% and 86% to detect significantly stenosed branches. The positive and negative predictive value were 80% and 97%.[17] All four missed lesions were located in the LCX and marginal branches, no lesions were missed in the left main, left anterior descending or right coronary artery. The twenty overestimations included seven lesions with a sub-significant (40-49%) diameter reduction, according to quantitative coronary angiography. Including only the evaluable (88%) vessels (minimal diameter 1.5 mm), Ropers et al found a sensitivity and specificity of 92% and 93% to detect significant stenoses. Without exclusion of non-evaluable lesions the sensitivity was 73%.[18]

PATIENT-BASED ASSESSMENT

Understanding that different methods of data analysis and presentation were used is important to compare the results of the previously mentioned studies. For instance, by using an evaluation based on the individual coronary segments, the relative and absolute number of non-diseased segments is much larger, compared to the number of non-diseased branches in case of a main branch based analysis. One of the consequences is that for the segment-based studies, the specificity is often better compared to the branch-based studies. Perhaps a more comparable indicator towards the clinical applicability of MSCT coronary angiography is the diagnostic accuracy based on the individual patients. Using 4-slice MSCT Giesler et al showed that in 39 out of 100 patients (39%) all vessels could be evaluated.[15] In the study by Knez et al, the accuracy to detect no, single, double or triple vessel disease was 74% (32/43 patients) after exclusion of the non-assessable segments.[12] Nieman et al, reported a 56% (45/78 patients) accuracy to distinguish no, single or multi-vessel disease, without the exclusion of non-assessable segments.[16] A high heart rate affects also the diagnostic accuracy per patient in a negative way.[16] By 16-slice MSCT, Nieman et al reported a patient-based accuracy to distinguish no, single or multi-vessel disease of 78% (table 2).[17] In this study the number of diseased vessels was overestimated in a number of patients, but none with significant coronary stenoses were falsely evaluated as normal, without exclusion of non-assessable segments. Ropers et al, correctly assessed 85% as having one or more lesions.[18]

CONSIDERATIONS AND LIMITATIONS

TEMPORAL RESOLUTION AND THE HEART RATE

Coronary motion

The coronary arteries are in constant motion and therefore an infinitely short acquisition or reconstruction time is required to acquire completely motionless images. Angiography studies have shown that during diastole a brief moment of near-immobility occurs.[20] The moment and duration of this window of imaging opportunity varies per person and per vessel, but always shortens at higher heart rates. Generally, the right coronary artery moves at a wider radius and has a shorter motion-sparse period compared

Table 2. Patient-based diagnostic performance of MSCT coronary angiography

	4-slice MSCT[19] Segment-based (N=53)		16-slice MSCT[17] Vessel-based (N=58)	
	Accuracy	Predictive value	Accuracy	Predictive value
No lesions	9/14 (64%)	9/19 (47%)	7/7 (100%)	7/8 (88%)
Single lesion/vessel	9/23 (39%)	9/15 (60%)	12/16 (75%)	12/20 (60%)
Multiple lesions/vessel	11/16 (69%)	11/19 (58%)	26/35 (74%)	26/30 (87%)
Overall	29/53 (55%)	29/53 (55%)	45/58 (78%)	45/58 (78%)

to the left coronary artery. The right coronary artery is therefore most vulnerable to motion artefacts caused by cardiac motion (Figure 2).

Temporal resolution

The temporal resolution of 4-slice MSCT scanners is 250 ms at low heart rates. At a heart rate of 50 b.p.m. the duration of the heart cycle measures 1200 ms, of which 21% is required for the reconstruction of a set of axial slices. At a heart rate of 80 b.p.m. ratio is 33% and at 120 b.p.m. the ratio is 50%, thereby increasing the occurrence of motion artifacts. Considering the fact that the shortening of the diastolic phase at higher heart rates is more substantial than the shortening of the systolic phase, the negative effect of a fast heart rate on the image quality is even more profound. At higher heart rates multi-segment reconstruction algorithms can improve the effective temporal resolution by combining data from consecutive heart cycles. However, this reduction is highly dependent on the actual heart rate, and does not always result in an improvement of image quality. Using a bi-segmental reconstruction algorithm at a rotation time of 500 ms, a heart rate of 68 b.p.m. results in an effective temporal resolution of 125 ms, while at 80 b.p.m. the non-complementary configuration of the X-ray source and detector array allows no reduction at all, maintaining a 250 ms effective temporal resolution. Up to approximately 75 b.p.m. the relative temporal resolution, the ratio of the image reconstruction interval to the RR-interval, is less than 30%. The use of more than two segments for reconstruction of a set of slices, which potentially reduces the duration of the image reconstruction interval per cycle to less than 100 ms, requires a very slow table propagation, resulting in an increased radiation exposure to the patient.

Motion artefacts

Motion artefacts are probably the most important limitation of MSCT coronary angiography and lead to substantial numbers of non-assessable investigations. The high number of non-assessable vessels reduces the clinical applicability of the technique. Two studies evaluated the diagnostic accuracy of MSCT in relation to the heart rate of the patient. Giesler et al, divided 100 patients into four groups and showed in patients with a heart

rate below 60 b.p.m. motion artefacts occurred in only 8% of the coronary arteries, compared to 18% at a heart rate between 61 and 70 b.p.m., 41% at a heart rate between 71 and 80 b.p.m., and 22% at a heart rate of more than 80 b.p.m.. The respective percentage of non-assessable vessels: 22%, 23%, 50% and 24%, resulted in a degrading overall sensitivity to detect >70% coronary diameter narrowing: 67%, 55%, 35% and 22%, for the respective heart-rate groups.[15] In a study by Nieman et al, 78 patients were equally divided into 3 groups according to the average heart rate during MSCT coronary angiography. In the low-heart-rate group (56±4 b.p.m.), intermediate-heart-rate group (67±3 b.p.m.), and high-heart-rate group (82±9 b.p.m.), the number of assessable segments were 78%, 73% and 54%, resulting in an overall sensitivity to detect >50% lumenal stenosis of 82%, 61% and 32%, respectively. The accuracy of MSCT to classify patients as having no, single or multivessel disease, without exclusion of non-assessable segment, was 73%, 54% and 42%, for each respective group.[16] Based on these and other experiences, many centers have introduced the administration of anti-chronotropic medication, such as beta-blockers, particularly in patients with higher heart rates, to reduce the occurrence of motion artefacts, and improve the accuracy of MSCT coronary angiography.

State-of-the-art scanners now have a rotation time below 500 ms, and combined with sufficient heart rate control, the reliability of MSCT has substantially improved (table 1). It needs to be established up till what heart rate these faster scanners can acquire motion-sparse images, but is seems unlikely that a rotation time of 400 ms or more provides sufficient image quality in the majority of patients with a heart rate over 80 b.p.m., when the coronary arteries are concerned.

Respiration and the scan time

Respiratory motion is suppressed during scanning by maintaining an inspiratory breath hold. Using four-slice scanners the relatively long scan time of 35-45 seconds, that is required to scan the entire heart at a thin collimation, can be too long in a substantial number of patients. In addition to respiratory motion artefacts, the long breath hold increases the patientÆs heart rate, resulting in an increased occurrence of cardiac motion artifacts. The new generation MSCT scanners are equipped with up to 16 slices and have a faster rotation, which results in a total scan time below 20s. A breath hold of 20s can be performed by most patients, and does not result in a significant acceleration of the heart rate.

Arrhythmia

Inappropriate ECG-synchronization results in inter-slice discontinuity (Figure 2). Contrary to prospectively ECG-triggered modalities, such as electron-beam computed tomography and most magnetic resonance imaging sequences, ECG-gated spiral CT image reconstruction allows for retrospective editing of the ECG. This can be useful to correct for inappropriate interpretation of the ECG by the reconstruction algorithm and provides an opportunity to manually insert R-wave indicators in case of ECG noise. Patients with continuous arrhythmia, editing of the ECG will

suffice. For instance, during atrial fibrillation, the end-diastolic volume constantly varies because of the alternating filling time. Thereby, the heart will be displaced and have a different shape and position at each consecutive heart cycle and acquisition. Apart from cardiac motion artefacts, this results in severe, and non-correctable inter-slice discontinuity and non-interpretable results. On the other hand, non-sinus rhythm, delayed conduction or otherwise unusual configuration of the ECG is no contra-indication for MSCT, as long as the RR-interval variation is within an acceptable range.

HIGHLY ATTENUATING MATERIAL

Stents and surgical material

Material with strong X-ray attenuating characteristics, such as metal and calcium, cause beam hardening and partial volume artefacts. Because stents are positioned within the coronary, adjacent to the lumen, assessment of the lumen diameter is impaired. In patients who underwent bypass grafting, sternal wires and vascular clips can cause streak artefacts that hamper proper assessment of the bypass grafts as well as coronary arteries. Both patient groups will be discussed in more detail in following chapters. Occasionally, pacemaker wires in the right heart can cause identical artefacts obscuring the right coronary artery. In case of bi-ventricular pacing systems, with wires positioned in the cardiac veins, assessment of the left circumflex and the left anterior descending coronary arteries are severely hampered.

Calcifications

Calcium deposits also cause a strong attenuation of the X-ray and are the most frequent cause of high-density artefacts, such as partial voluming and beam hardening artefacts. Partial volume artefacts are directly, but not solely related to the size of the voxel, or three-dimensional image elements. The direct result is that calcified plaque material appears larger than it actually is, thereby increasing the apparent severity of the lumen narrowing and complicating accurate assessment (Figure 2). By experience most reviewers will take the overestimation into account when assessing the lumen diameter of a calcified lesion. Nevertheless, an accurate (semi-)quantitative assessment of coronary arteries with extensive coronary calcification remains less reliable, and patients with suspected or known advanced coronary artery disease are therefore not the most suitable candidates for CT coronary angiography.

All studies comparing MSCT and conventional coronary angiography report that extensive calcification of the coronary arteries prevented assessment of a substantial number of segments and resulted in a number of false-positive or false-negative interpretations of significant stenoses.[10-19] In order to avoid contrast-enhanced CT angiography in these individuals, some proposed to perform a low-dose non-enhanced scan in all patients prior to angiography to determine the amount of calcium in the coronary arteries, and exclude unsuitable candidates.

EBCT coronary angiography

In 1997 the first studies comparing electron beam computed tomography (EBCT) with conventional angiography were published. All but one study were performed using an 1.0 mm overlapping 3.0 mm slice thickness.[3-5,7-9] In one study a non-overlapping 1.5 mm detector collimation was applied.[6] The non-mechanical EBCT is a sequential CT scanner. Prospectively triggered by the patients electrocardiogram (ECG) a single slice is acquired, after which the table advanced to the next slice position. The acquisition is performed during the diastolic phase and the exact timing of the electron generation is based on the preceding heart cycles. Due to the lack of mechanically rotating elements, the slice acquisition time is very short: 100 ms. The one-slice sequential scan design requires a long scan time, and breath hold, to cover the entire heart. To increase the scan coverage atropine can be injected to increase the heart rate, and consequently the number of slices that can be acquired within a certain breath hold time.[6]

Comparative studies against conventional angiography

Table 3 lists the results from the comparative publications between contrast-enhanced EBCT and conventional coronary angiography for the purpose of the detection of significant coronary artery obstruction.

Table 3. Diagnostic performance of electron-beam CT to detect coronary stenosis, using conventional coronary angiography as the standard of reference

		A	N	Assess.	D	Prev	Excl.	Se	Sp	PPV	NPV	Se[a]
Nakanishi[3]	3.0	-	37	Vessel	50%	0.8	-	74%	94%	68%	93%	74%
Reddy[4]	3.0		23	Vessel	50%	1.3	10%	88%	78%	65%	94%	77%
Schmermund[5]	3.0	+	28	Segment	50%	1.1	28%	82%	88%	57%	96%	70%
Rensing[6]	1.5	+	37	Segment	50%	1.1	81%	77%	94%	73%	95%	63%
Achenbach[7]	3.0		125	Vessel	70%	0.8	25%	92%	94%	78%	98%	70%
Budoff[8]	3.0	-	52	Vessel	50%	≥1.1	11%	78%	91%	78%	91%	NR
Achenbach[9]	3.0	-	36	Vessel	75%	≥1.0	20%	92%	94%	85%	92%	NR

Use of atropine (A); method of assessment (Assess.); Diameter reduction considered significantly stenosed (D); Number of stenotic vessel per patient (Prev.); Percentage of excluded segments/branches (Excl.); Sensitivity (Se), specificity (Sp), positive (PPV) and negative predictive value (NPV) regarding the assessable segments/branches; Sensitivity including missed lesions in non-assessable segments/branches (Sea). Not reported (NR).

The study populations ranged from 23 to 125 patients. The use of atropine to increase the number of acquisitions per breath hold was reported in two studies.[6,7] At low heart rates, breath hold durations of >50s were reported. In one study no segments were excluded,[3] in the others between 10% and

28% of the segments and vessels were excluded due to impaired image quality. Similar to MSCT non-interpretability was caused by motion artefacts and extensive calcification. Considering the assessable segments and vessels, the sensitivity to detect significant lumenal narrowing ranged from 74% to 92%. The specificity ranged from 63% to 94%. The positive and negative predictive value ranged from 57% to 85% and 91% and 98%, respectively. If lesions in non-assessable vessels were included as false-negative results the overall sensitivity decreased to 63% and 77%, although these figures were only reported in five studies. Contrary to the MSCT studies, the many of the EBCT studies were limited to the proximal and middle coronary segments.[6,7]

Future developments

A recently introduced generation of EBCT scanners acquires two slices simultaneously, and is capable of scanning several times during one heart cycle, which increases the radiation exposure, but allows for retrospective selection of the dataset at the most optimal phase. The slice acquisition time has been decreased to 50 ms which will further improve the image quality with regard to motion artefacts. Whether the use of thinner slices and faster scan times has a negative effect on the contrast-to-noise is currently unknown. Future studies will need to determine the incremental diagnostic value of this new EBCT technology.

Magnetic Resonance Imaging

Due to the lack of X-radiation and use of less harmful and optional contrast media, magnetic resonance imaging is an attractive modality for non-invasive imaging, including coronary angiography. Various scanning techniques and data acquisition sequences have been explored, and compared to conventional coronary angiography. The first experiences in 1993 were very promising, reporting a sensitivity and sensitivity to detect significant coronary stenosis of 90% and 92% in 39 patients.[1] Currently respiratory gated volumetric acquisitions of the entire heart are acquired, or smaller targeted volumes are acquired during single breath-hold acquisitions. Intravenous injection of contrast media can be applied but is not mandatory to image the coronary artery lumen. Many comparative studies using different two- and three-dimensional techniques have been published with widely varying results.[2] Between 4% and 48% of the vessels and segments needed to be excluded because of insufficient image quality. The sensitivity and specificity to detect significant coronary obstruction ranges from 38% to 93% and 54% to 97%, respectively.[2] A recent multicenter trial using a respiratory-gated free-breathing scan protocol and a study population of 109 patients has been published by Kim et al in 2001.[21] The investigators reported a sensitivity of 93% and specificity of 42% to detect significant lesions in the assessable (84%) proximal and middle coronary segments. The overall sensitivity, including lesions in non-assessable segments, was not reported.

Despite it's benign nature MR coronary angiography is complicated by a relatively low three-dimensional image resolution of rarely less than 1

mm^3, long scanning time and inconsistent image quality. Compared to CT, the acquisition of the coronary MR is time-consuming and requires dedicated scanners and image sequences as well as experienced operators.

Discussion

Multi-slice spiral CT is currently the most accurate non-invasive angiographical modality for the detection of coronary stenosis. Despite the use of radiation and contrast media, MSCT coronary angiography is a relatively safe and simple procedure. All data can be acquired within 20 seconds, often providing predictable image quality, depending on the heart rate and the coronary calcium status of the patient. The contrast-to-noise ratio is high and the three-dimensional resolution of the current generation scanners is less than 0.3 mm^3. This high spatial resolution allows imaging of small branches, often neglected in the MR and EBCT studies.

Clinical implementation of MSCT coronary angiography

MSCT coronary angiography will, however, not within the foreseeable future replace coronary angiography as the reference coronary imaging tool. Conventional angiography is being performed without severe complications in the vast majority of patients. Conventional angiography consistently provides high-quality data, with an excellent spatial resolution that allows quantitative assessment of the severity of the stenotic lesion. Apart from motion artefacts, image noise or calcium-related artefacts, with a slice thickness between 0.5 and 1.0 MSCT can not be expected to provide comparable quantitative assessments. Conventional angiography can also be complemented by functional flow assessment and advanced plaque imaging techniques. Finally, conventional angiography can immediately be followed by a percutaneous interventional procedure to treat the obstructive problem.

In patients with a modest heart rate MSCT could, however, provide a useful and reliable alternative to diagnostic catheter-based angiography for the initial detection and localization of coronary stenoses. Additionally, because of it's non-invasive nature, MSCT coronary angiography can be introduced into the diagnostic work-up of patients with anginal complaints at an earlier stage, when catheter-based angiography is not yet indicated. Potential applications are the exclusion of an acute coronary obstruction in patients with atypical chest pain at the emergency ward, coronary artery stenosis in patients who need major (non-cardiac) surgery, or obstructive disease in patients with inconclusive stress test. MSCT may also be valuable when repeated angiographic follow-up is indicated, or after percutaneous coronary intervention or coronary artery bypass surgery (table 4).

Additional value of MSCT coronary angiography

Besides being a non-invasive alternative to conventional coronary angiography, MSCT provides additional and possible valuable information with respect to the coronary artery wall, that is not provided by standard X-ray coronary angiography (Figures 1, 3, and 5).

Table 4. Potential applications of CT coronary angiography

Early detection of stenoses in non-symptomatics	
Exclusion of coronary disease:	high-risk patients
	prior to major (non-cardiac) surgery
Detection and/or exclusion of stenoses:	Atypical (unstable) chest pain
	Non-conclusive stress tests
Substitution for diagnostic X-ray coronary angiography:	Prior to percutaneous coronary intervention
	High risk patients: aortic disease
Adjuvant to coronary angiography:	Plaque characterization
	Complicated coronary intubation
Follow-up:	Percutaneous coronary intervention
	Bypass surgery

Non-stenotic atherosclerotic material is visualized well and the value of plaque characterizing by MSCT is currently being investigated and will be discussed in the following chapters.[22] Furthermore, MSCT presents a three-dimensional depiction of the coronary arteries, which can be useful when a coronary anomaly is suspected.[23] Diseased vessels can easily be related to an infracted, or perfusion depleted myocardial segment. Besides the coronary arteries, the MSCT scan includes high quality volumetric information of the entire heart and lower lungs, resulting in (accidental) early detection of abnormalities, including pericardial disease, intra-cardiac thrombi, morphologic valvular disease (calcifications, thickening), lung tumours, etc. Finally, the raw MSCT data can be used for reconstruction of different cardiac phases, to evaluate the ventricular performance: ventricular cavity volumes, ejection fraction and regional myocardial wall thickening.[24]

Further improvement

To further improve the quality and quantitative potential of MSCT coronary angiography, the fundamental characteristics, such as the spatial and temporal resolution need to be further optimised. Evaluation of three-dimensional MSCT angiograms may become more efficient, and better reproducible with dedicated post-processing tools. More sophisticated tools that combine an accurate reproducible assessment with presentable overviews are currently being developed, and will improve the clinical implementation of MSCT coronary angiography as a non-invasive tool to localize obstructive coronary artery disease.

REFERENCES

1. Manning WJ, Li W, Edelman RR, et al. A preliminary report comparing magnetic resonance coronary angiography with conventional angiography. N Engl J Med. 1993;328-832.
2. Fayad ZA, Fuster V, Nikolaou K, et al. Computed tomography and magnetic resonance imaging for noninvasive coronary angiography and plaque imaging. Current and potential future concepts. Circulation 2002 106:2026-2034.
3. Nakanishi T, Ito K, Imazu M, et al.Evaluation of coronary artery stenoses using electron-beam CT and multiplanar reformation. J Comput Assist Tomogr. 1997;21:121-127.
4. Reddy G, Chernoff DM, Adams JR, et al. Coronary artery stenoses: assessment with contrast-enhanced electron-beam CT and axial reconstructions. Radiology 1998;208:167û172.
5. Schmermund A, Rensing BJ, Sheedy PF, et al. Intravenous electron-beam computed tomographic coronary angiography for segmental analysis of coronary artery stenoses. J Am Coll Cardiol. 1998;31:1547û1554.
6. Rensing BJ, Bongaerts A, van Geuns RJ, et al. Intravenous coronary angiography by electron beam computed tomography: a clinical evaluation. Circulation 1998;98:2509û2512.
7. Achenbach S, Moshage W, Ropers D, et al. Value of electron-beam computed tomography for the noninvasive detection of high-grade coronary-artery stenoses and occlusions. N Engl J Med. 1998;339:1964-1971.
8. Budoff MJ, Oudiz RJ, Zalace CP, et al. Intravenous three-dimensional coronary angiography using contrast-enhanced electron beam computed tomography. Am J Cardiol. 1999;83:840û845.
9. Achenbach S, Ropers D, Regenfus M, et al. Contrast enhanced electron beam computed tomography to analyse the coronary arteries in patients after acute myocardial infarction. Heart. 2000;84:489-493.
10. Nieman K, Oudkerk M, Rensing BJ, et al., Coronary angiography with multi-slice computed tomography. Lancet 2001;357:599-603.
11. Achenbach S, Giesler T, Ropers D, et al. Detection of coronary artery stenoses by contrast-enhanced, retrospectively electrocardiographically-gated, multislice spiral computed tomography. Circulation 2001;103:2535-2538.
12. Knez A, Becker CR, Leber A, et al. Usefulness of multislice spiral computed tomography angiography for determination of coronary artery stenoses. Am J Cardiol. 2001;88:1191-1194.
13. Vogl TJ, Abolmaali ND, Diebold T, et al. Techniques for the detection of coronary atherosclerosis: multi-detector row CT coronary angiography. Radiology 2002;223:212-220.
14. Kopp AF, Schr÷der S, K³ttner A, et al. Non-invasive coronary angiography with high resolution multidetector-row computed tomography: results in 102 patients. Eur Heart J. 2002;23:1714-1725.
15. Giesler T, Baum U, Ropers D, et al. Noninvasive visualization of coronary arteries using contrast-enhanced multidetector CT: influence of heart rate on image quality and stenosis detection. AR Am J Roentgenol. 2002;179:911-916.
16. Nieman K, Rensing BJ, van Geuns RJ, et al.Non-invasive coronary angiography with multislice spiral computed tomography: impact of heart rate. Heart. 2002;88:470-474.
17. Nieman K, Cademartiri F, Lemos PA, et al. Reliable noninvasive coronary angiography with fast submillimeter multislice spiral computed tomography. Circulation 2002;106:2051-2054.

18. Ropers D, Baum U, Pohle K, et al. Detection of coronary artery stenoses with thin-slice multi-detector row spiral computed tomography and multiplanar reconstruction. Circulation 2003 (in press).
19. Nieman K, Rensing BJ, van Geuns RJM, Munne A, Ligthart JMR, Pattynama PMT, Krestin GP, Serruys PW, de Feyter PJ. Usefulness of multislice computed tomography for detecting obstructive coronary artery disease. Am J Cardiol. 2002;89:913-918.
20. Wang Y, Watts R, Mitchell I, et al. Coronary MR angiography: selection of acquisition window of minimal cardiac motion with electrocardiography-triggered navigator cardiac motion prescanning--initial results. Radiology 2001;218:580-585.
21. Kim WY, Daniel PG, Stuber M, et al. Coronary magnetic resonance angiography for the detection of coronary stenoses. N Engl J Med. 2001;345:1863-1869.
22. Schroeder S, Kopp AF, Baumbach A, et al. Noninvasive detection and evaluation of atherosclerotic coronary plaques with multislice computed tomography. J Am Coll Cardiol. 2001;37:1430-1435.
23. Ropers D, Gehling G, Pohle K, et al. Anomalous course of the left main or left anterior descending coronary artery originating from the right sinus of Valsalva. Identification of four common variations by electron beam tomography. Circulation 2002;105:e42-e43.
24. Dirksen MS, Bax JJ, de Roos A, Jukema JW, van der geest RJ, Geleijns K, Boersma E, van der Wall EE, Lamb HJ. Usefulness of dynamic multislice computed tomography and left ventricular function in unstable angina pectoris and comparison with echocardiography. Am J Cardiol. 2002;90:1157-1160.

6. CORONARY STENOSIS

CHAPTER 6.2

RELIABLE NONINVASIVE CORONARY ANGIOGRAPHY WITH FAST SUBMILLIMETER MULTISLICE SPIRAL COMPUTED TOMOGRAPHY

Koen Nieman, MD [1,2]
Filippo Cademartiri, MD [2]
Pedro A. Lemos, MD [1]
Rolf Raaijmakers, RT [2]
Peter M.T. Pattynama, MD, PhD [2]
Pim J. de Feyter, MD, PhD [1,2]
From the Thoraxcenter,
Departments of Cardiology[1] and Radiology[2]
Erasmus Medical Center, Rotterdam, the Netherlands.

Circulation, 106:2051-2054, 2002.

Background
Multislice spiral computed tomography (MSCT) is a promising technique for noninvasive coronary angiography, although clinical application has remained limited because of frequently incomplete interpretability, caused by motion artifacts and calcifications.

Methods and Results
In 59 patients (53 male, aged 58±12 years) with suspected obstructive coronary artery disease, ECG-gated MSCT angiography was performed with a 16-slice MSCT scanner (0.42-s rotation time, 12 x 0.75-mm detector collimation). Thirty-four patients were given additional β-blockers (average heart rate: 56±6 min^{-1}). After contrast injection, all data were acquired during an approximately 20-s breath hold. The left main (LM), left anterior descending (LAD), left circumflex (LCX), and right coronary artery (RCA), including ≥2.0-mm side branches, were independently evaluated by two blinded observers and screened for ≥50% stenoses. The consensus reading was compared with quantitative coronary angiography. MSCT was successful in 58 patients. Eighty-six of the 231 evaluated branches were significantly diseased. Without exclusion of branches, the sensitivity, specificity and positive and negative predictive value to identify ≥50% obstructed branches was 95% (82/86), 86% (125/145), 80% (82/102), and 97% (125/129), respectively. The overall accuracy for the LM, LAD, RCA, and LCX was 100%, 91%, 86%, and 81%, respectively. No obstructed LM, LAD, or RCA branches remained undetected. Classification of patients as having no, single, or multivessel disease was accurate in 78% (45/58) of patients and no patients with significant obstructions were incorrectly excluded.

Conclusions
Improvements in MSCT technology, combined with heart rate control, allow reliable noninvasive detection of obstructive coronary artery disease.

During the past decade, considerable progress has been achieved in the field of noninvasive coronary imaging with MRI, electron beam computed tomography (EBCT), and, most recently, multislice spiral computed tomography (MSCT). With the use of 4-slice MSCT scanners, promising results have been published; however, cardiac motion and calcium deposits in the coronary artery wall rendered a substantial number of scans incompletely interpretable.[1-3]

Motion artifacts limit proper assessment, particularly at higher heart rates.[4] Recently, a new generation of MSCT scanners, equipped with more and thinner detector rows and increased rotation speed, have been introduced. The purpose of the present study is to evaluate the diagnostic accuracy of noninvasive coronary angiography with the latest-generation MSCT scanner, combined with effective heart-rate control.

METHODS

Study Population

Fifty-nine patients (53 male, aged 58±12 years) who had suspected coronary obstructions and were scheduled for elective conventional angiography participated in the study. Criteria for exclusion included previous bypass graft surgery, irregular heart rate, allergy to iodine contrast media, and renal insufficiency (serum creatinine >120 $mmol/L^{-1}$). Significant coronary obstructions were absent in 8 patients. Single-vessel disease was found in 20 patients, 2-vessel disease in 25 patients, 3-vessel disease in 4 patients, and 4-vessel disease in 1 patient. Eight patients previously underwent PTCA with stent implantation. The average interval between MSCT and conventional angiography was 21±17 days. Thirty-seven patients (64%) used β receptor-blocking medication at the time of the examination. The study was approved by the ethics committee of the university medical center, and all participating patients gave informed consent.

Scan Protocol and Image Reconstruction

CT angiography was performed with the use of a 16-slice MSCT scanner with a 0.42-s rotation time (Sensation 16, Siemens). For cardiac protocols, the 12 inner detector rings are applied. Thirty-four patients (58%), 22 of whom already used β-blockers, had a prescan heart rate >65 min^{-1}, and were given a single oral dose of 100 mg metoprolol one hour before the examination in the absence of contraindications. A bolus of 120 to 140 mL iodixanol (320 mgI/ml^{-1}) was intravenously injected (4 to 5 mL/s^{-1}). As soon as the signal density level in the ascending aorta, which was monitored at a 1.25-s interval, reached a predefined threshold of 100 Hounsfield units, the patient was automatically instructed to maintain an inspiratory breath hold (20.5±1.4 s), during which the CT data and ECG trace were acquired. Scan parameters: detector collimation 12 x 0.75 mm, table feed 6.7 mm/s^{-1}, tube voltage 120 kV, 400 or 450 mAs (depending on the patient size), and estimated radiation exposure between 8 and 9 mSv. After this feature became available, prospectively ECG-controlled roentgen

tube modulation was applied in patients (n=15) with a reliable ECG trace to decrease the roentgen output during systole and reduce the exposure by half at low heart rates.[5]

Synchronized to the recorded ECG, axial slices were reconstructed from the acquired MSCT data with the use of an algorithm that uses only the data from a half gantry rotation per slice, resulting in a temporal resolution of ≤210 ms.[6] The continuous data acquisition allows slice reconstruction at different time positions within the cardiac cycle. Three image data sets were reconstructed during the mid-to-end diastolic phase, during which coronary artery displacement is relatively small, with reconstruction window positions starting at 350, 400, and 450 ms before the next R wave. If indicated, additional window positions were explored, although 400 and 450 ms generally provided nearly motion-free results.

MSCT Image Interpretation

Two blinded reviewers independently evaluated the MSCT scans by assessment of the axial slices and with case-dependent application of postprocessing tools, such as multiplanar reconstruction and thinslab maximum intensity projection. Vessel wall calcification was classified as either calcium spots (small isolated eccentric lesions) or severe calcification (large high-density lesions, extending along the wall, causing partial volume and beam hardening artifacts). The image interpretability was classified as good, adequate, or poor. The 4 main coronary branches-left main (LM), left anterior descending (LAD), left circumflex (LCX), and right coronary artery (RCA), including side branches with a diameter of ≥2.0 mm-were screened for significant narrowing (≥50% diameter reduction) of the lumen. Cases of disagreement were settled by a joined consensus reading. Because of the known low interpretability of small coronary stents, the in-stent lumen was not included in the analysis.

X-Ray Coronary Angiography

Conventional selective coronary angiography was performed with standard techniques and evaluated by a blinded reviewer with the use of quantitative coronary angiography (CAAS, Pie Medical), catheterderived image calibration, and automated vessel contour detection, to determine the diameter of all coronary branches. The diameter stenosis, as a percentage of the reference diameter, was determined in two orthogonal directions and the average between the two determined the stenosis severity.

Statistical Analysis

The diagnostic accuracy of MSCT to detect significant stenoses in ≥2.0-mm-diameter segments was evaluated regarding QCA as the standard of reference. All vessels, regardless of the image quality, were included. If a coronary branch contained more than one lesion, the most severe lesions in the most proximal branch determined the diagnostic accuracy of the assessment.

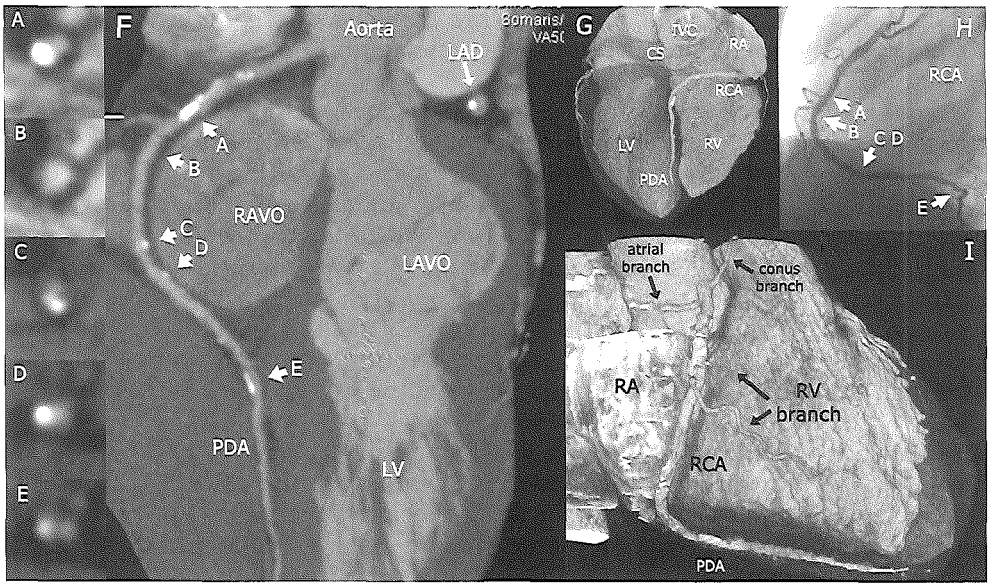

Figure 1. H, MSCT and conventional angiogram of an atherosclerotic RCA without significant stenoses. **A and F**, Blooming artifacts around the bright calcifications suggest stenosis. Cross-sections **A through E** are indicated in panel **F** (curved MSCT reconstruction along the course of the RCA) and **H. G**, Three-dimensional representations from an inferior and **I**, right-oblique angle, show the PDA and side branches. RAVO/LAVO indicates right/left atrioventricular orifices; PDA, posterior descending; LV/RV, right/left ventricles; CS, coronary sinus; RA, right atrium; and IVC, inferior vena cava. (A full color version of this illustration can be found in the color section (chapter 12)).

Standard descriptive statistics were calculated for each observer and the precision of the overall parameters was expressed with a 95% confidence interval. Concordance between observers was calculated and expressed by the κ value.

RESULTS

The average heart rate was 56±6 min^{-1} (range 45 to 70 min^{-1}). One scan that was prematurely triggered by contrast medium detection in the superior vena cava was excluded from the study because of insufficient contrast enhancement. In the absence of a ≥2.0-mm RCA in a single patient, 231 vessels were available for evaluation. Calcified lesions were present in 61% of the branches, half of which limited to small calcified nodules (Figure 1). All coronary branches included, the overall sensitivity and specificity to detect significantly stenosed branches was 95% (82/86) and 86% (125/145) (Figure 2). Of the vessels containing ≥70% stenoses, 97% (62/64) were identified (Table 1).

All undetected stenoses (n=4), 2 of which were moderate (51% and 55%), were located in the LCX and marginal branches. Twenty false-positive

assessments involved seven 40% to 49% lesions. Seven misinterpreted vessel segments contained extensive calcification, and 8 contained calcium spots. Concordance between both MSCT observers was reasonably good (κ value 0.69).

Table 1. Diagnostic Accuracy to Detect Significantly Stenosed Coronary Arteries*

	All Branches	RCA	LM	LAD	CX
≥50% stenosed branches	86	22	3	37	24
Well assessable	160 (69)	32 (56)	52 (90)	38 (66)	38 (66)
Adequately assessable	54 (23)	18 (32)	5 (9)	15 (26)	16 (28)
Poorly assessable	17 (7)	7 (12)	1 (2)	5 (9)	4 (7)
No detectable calcium	89 (39)	23 (40)	29 (50)	9 (16)	28 (48)
Small calcified nodules	74 (32)	14 (25)	19 (33)	26 (45)	15 (26)
Marked calcification	68 (29)	20 (35)	10 (17)	23 (40)	15 (26)
Sensitivity	82/86 (95, 89–98)	22/22 (100)	3/3 (100)	37/37 (100)	20/24 (83)
Specificity	125/145 (86, 83–88)	27/35 (77)	55/55 (100)	16/21 (76)	27/34 (79)
Negative predictive value	82/102 (80, 75–83)	22/30 (73)	3/3 (100)	37/42 (88)	20/27 (74)
Positive predictive value	125/129 (97, 93–99)	27/27 (100)	55/55 (100)	16/16 (100)	27/31 (87)

Values are n (%, 95% confidence interval).
RCA, LM, LAD, and LCX indicate right, left main, left anterior descending, and left circumflex coronary artery, respectively.
* ≥50% lumen diameter reduction, in ≥2.0 mm diameter vessels, consensus reading.

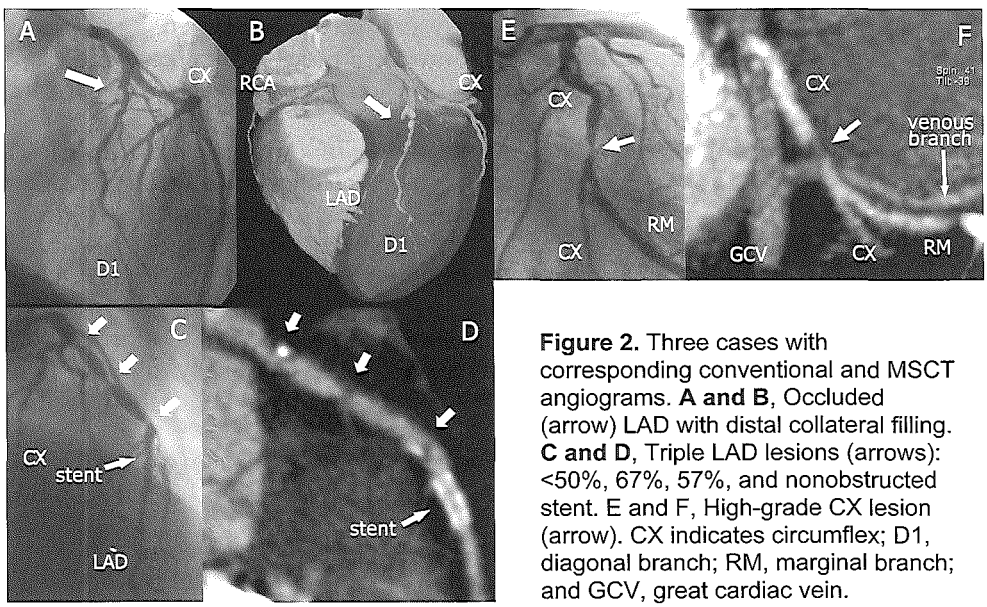

Figure 2. Three cases with corresponding conventional and MSCT angiograms. **A and B**, Occluded (arrow) LAD with distal collateral filling. **C and D**, Triple LAD lesions (arrows): <50%, 67%, 57%, and nonobstructed stent. E and F, High-grade CX lesion (arrow). CX indicates circumflex; D1, diagonal branch; RM, marginal branch; and GCV, great cardiac vein.

Contrast medium was detected within all 11 stents, and patency was confirmed by conventional angiography. One case of in-stent restenosis (85%) in the distal LAD was not recognized by MSCT.

The predictive value of MSCT angiography to detect patients with no, single, or multivessel disease was 100% (7/7), 75% (12/16), and 74% (26/35), respectively (overall predictive value 78% [45/58]). Seven out of 8 patients without significant lesions were correctly identified. No incorrect exclusion of patients with significant lesions occurred.

Discussion

Four-slice MSCT scanners showed promising results but were not robust enough to consistently produce reliable coronary imaging because of insufficient spatial and temporal resolution.[1–4] Generally, 20% to 30% of the proximal and middle coronary segments were noninterpretable because of insufficient image quality.[1,3] The use of a scanner with thinner slices and faster rotation, combined with β-blocking, improved the image quality and diagnostic accuracy of MSCT to detect significant disease in all ≥2.0-mm coronary segments. Advantages of the shorter scan time are a more comfortable breath hold (approximately 20 s), less venous contrast enhancement, and a lower contrast dose. The welltolerated examination can be performed within 15 minutes and requires no hospital admission. Currently, MSCT coronary angiography is not reliable in patients with arrhythmias, high heart rates, or severely calcified vessels. Disadvantages are the still considerable radiation dose and frequently required use of β-blockers, which were well tolerated but require observation and a prolonged stay of the patient.

For alternative noninvasive coronary imaging modalities, such as EBCT and MRI, good diagnostic results were reported. However, assessment was usually limited to proximal and middle main branches, and ≤25% of these branches were excluded because of insufficient image quality.[7,8] Development of both techniques is ongoing, and although no direct comparisons have been performed, they seem at this moment outperformed by 12-slice MSCT with respect to stenosis detection. MSCT will not soon equal the versatility or quantitative accuracy of catheter-based imaging techniques, but it does allow noninvasive detection and exclusion of coronary obstructions.

In what clinical setting CT coronary angiography is of most value for the early detection of coronary artery disease, or evaluation of chest pain, should be the focus of future studies.

References

1. Achenbach S, Giesler T, Ropers D, et al. Detection of coronary artery stenoses by contrast-enhanced, retrospectively electrocardiographicallygated, multislice spiral computed tomography. *Circulation.* 2001;103: 2535–2538.

2. Knez A, Becker CR, Leber A, et al. Usefulness of multislice spiral computed tomography angiography for determination of coronary artery stenoses. *Am J Cardiol.* 2001;88:1191–1194.
3. Nieman K, Rensing BJ, van Geuns RJ, et al. Usefulness of multislice computed tomography for detecting obstructive coronary artery disease. *Am J Cardiol.* 2002;89:913–918.
4. Nieman K, Rensing BJ, van Geuns RJM, et al. Non-invasive coronary angiography with multislice spiral CT: the impact of heart rate. *Heart.* 2002;88:470–474.
5. Jakobs TF, Becker CR, Ohnesorge B. Multislice helical CT of the heart with retrospective ECG gating: reduction of radiation exposure by ECG-controlled tube current modulation. *Eur Radiol.* 2002;12: 1081–1086.
6. Ohnesorge B, Flohr T, Becker C, et al. Technical aspects and applications of fast multislice cardiac CT. In: Reiser MF, Takahashi M, Modic M, Bruening R, eds. *Medical Radiology–Diagnostic Imaging and Radiation Oncology.* Berlin, Germany: Springer; 2001:121–130.
7. Achenbach S, Moshage W, Ropers D, et al. Value of electron-beam computed tomography for the noninvasive detection of high-grade coronary-artery stenoses and occlusions. *N Engl J Med.* 1998;339: 1964 –1971.
8. Kim WY, Danias PG, Stuber M, et al. Coronary magnetic resonance angiography for the detection of coronary stenoses. *N Engl J Med.* 2001;345:1863–1869.

6. CORONARY STENOSIS

CHAPTER 23

MULTISLICE SPIRAL COMPUTED TOMOGRAPHY CORONARY ANGIOGRAPHY IN PATIENTS WITH STABLE ANGINA PECTORIS

Nico R. Mollet, MD,[1,2]
Filippo Cademartiri, MD,[2]
Koen Nieman, MD,[1]
Francesco Saia, MD,[1]
Pedro A. Lemos, MD,[1]
Eugene P. McFadden, MB,[1]
Peter M. T. Pattynama, MD,[2]
Patrick W. Serruys, MD, FACC,[1]
Gabriel P. Krestin, MD,[2]
Pim J. de Feyter, MD, FACC[1,2]

From the Departments of Cardiology[1] and Radiology[2]
Erasmus MC, University Medical Center Rotterdam,
The Netherlands

Journal of the American College of Cardiology,
Vol. 43, No. 12, 2265-2270, 2004.

Objectives. This study was designed to prospectively evaluate the diagnostic performance of multislice spiral computed tomography (msct) coronary angiography for the detection of significant lesions in all segments of the coronary tree potentially suitable for revascularization.

Background. Noninvasive msct coronary angiography is a promising coronary imaging technique.

Methods. Sixteen-row msct coronary angiography was performed in 128 patients (89% men, mean age 58.9 11.7 years) in sinus rhythm with stable angina pectoris scheduled for conventional coronary angiography. Sixty percent (77 of 128) of patients received pre-scan oral betablockers, resulting in a mean heart rate of 57.7 7.7 beats/min. The diagnostic performance of msct for detection of significant lesions (50% diameter reduction) was compared with that of quantitative coronary angiography (qca).

Results. The sensitivity of msct for detection of significant lesions was 92% (216 of 234, 95% confidence interval [ci]: 88 to 95). Specificity was 95% (1,092 of 1,150, 95% ci: 93 to 96), positive predictive value 79% (216 of 274, 95% ci: 73 to 88), and negative predictive value 98% (1,092 of 1,110, 95% ci: 97 to 99). Two 50% lesions were missed because of motion artifacts and two because of severe coronary calcifications. The rest (78%, 14 of 18) were detected but incorrectly classified as 50% obstructions. All patients with and 86% (18 of 21) of patients without significant lesions on qca were correctly classified by msct. All patients with significant left main disease or total occlusions were correctly identified on msct.

Conclusions. Sixteen-row msct coronary angiography permits reliable detection of significant obstructive coronary artery disease in patients with stable angina in sinus rhythm.

Multislice spiral computed tomography (MSCT) coronary angiography is a promising noninvasive technique for the detection of obstructive epicardial coronary artery disease (CAD), and 16-row MSCT scanners have the potential to further improve its diagnostic performance.[1] Complete visualization of all clinically important coronary segments is a prerequisite for MSCT coronary angiography to become an accepted clinical tool for the assessment of patients with suspected CAD. Previous studies performed in relatively small numbers of patients showed high sensitivity and specificity for the detection of significant obstructive lesions.[2,3] However, in one study, a significant number of coronary segments were excluded because of poor image quality, and neither report presented a comprehensive lesion-by-lesion comparative analysis.

We prospectively evaluated the diagnostic accuracy of MSCT coronary angiography for the detection of signifi- cant lesions in coronary segments potentially amenable to revascularization (≥2 mm in diameter).

METHODS

Study population. During a period of six months, we studied 128 patients (113 men, 15 women, mean age 58.9±11.7 years) with stable angina pectoris scheduled for conventional coronary angiography. Only patients in sinus rhythm able to perform a 20-s breath-hold were included. Exclusion criteria were contraindications to iodinated contrast (e.g., known allergy, serum creatinine >120 mmol/l, and thyroid disorders), patients with previous bypass surgery, and patients presenting with an acute coronary syndrome. No patients of the previously reported studies were included in the present study.

The institutional review board of our institution approved the study and all patients gave written, informed consent.

Patient preparation

A single oral dose of 100 mg metoprolol (Selokeen, AstraZeneca Pharmaceutics, London, United Kingdom) was administered 1 h before the scan if the heart rate was ≥65 beats/min.

Scan protocol and image reconstruction

All scans were performed using a 16-row MSCT scanner (Sensation 16, Siemens, Germany). Scan parameters were: detector collimation 16 x 0.75 mm, tube rotation time 420 ms, table feed 3 mm/rotation, tube voltage 120 kV, and tube current 400 to 450 mAs. Prospectively triggered X-ray tube current modulation was applied in patients with a heart rate below 60 beats/min and in the absence of any rhythm disturbances during a monitoring period of approximately 1 min. This feature reduces the radiation output of the X-tube during the less important systolic phase, thereby decreasing the total radiation dose by 40% to 50% in patients with low heart rates.[4,5] A bolus of 100 ml of contrast (Visipaque 320, Amersham Health, Forchheim, United Kingdom) was injected intravenously at a flow rate of 4 ml/s. An automated bolus tracking system was used to synchronize the arrival of the contrast material with initiation of the scan. All data were acquired during a single breath-hold of approximately 20 s,

and images were reconstructed using retrospective ECG gating. To obtain motion-free images, standard reconstruction windows were selected during the mid-toend diastolic phase (350, 400, and 450 ms before the next R-wave). Additional image reconstruction windows were explored when deemed necessary. The reconstruction algorithm uses data obtained in half gantry rotation time, resulting in a temporal resolution of up to 210 ms. In case of a heart rate of >70 beats/min, a bi-segmental reconstruction algorithm is applied that uses data obtained from two consecutive heartbeats, reducing the effective reconstruction interval per heart cycle down to 105 ms, depending on the heart rate.[1]

Quantitative coronary angiography (QCA)

The mean (SD) interval between the MSCT scan and conventional coronary angiography was 19.1±10.4 days. The coronary arteries were divided into segments according to the American Heart Association classification.[6] A single observer, unaware of the MSCT results, classified all coronary segments as <2 and ≥2 mm in diameter using a QCA algorithm (CAAS, Pie Medical, Maastricht, Netherlands). Only segments classified as ≥2 mm were considered for comparison with MSCT. The severity of coronary stenoses was quantified in two orthogonal views, and a stenosis was classified as significant if the mean lumen diameter reduction was ≥50%.

MSCT image evaluation

Two observers blind to the results of conventional coronary angiography independently evaluated all of the MSCT scans. Thin-slab maximum intensity projections with a slice thickness of 2 to 6 mm, depending on the presence of adjacent structures or coronary calcifications, were used to screen for coronary stenoses. Multiplanar reconstructions were used to obtain more detailed information.

All main branches as well as large (≥2 mm in lumen diameter) side branches of the coronary tree were evaluated for the presence of significant (≥50% diameter reduction) obstructive stenoses. Segments with stents were excluded from analysis because beam-hardening artifacts and partial volume effects hamper reliable visualization of the coronary lumen. Image quality of all segments was classified as good, adequate, or poor. Good image quality was classified as the absence of any image-degrading artifacts related to motion, noise, or calcification. In the presence of image-degrading artifacts, image quality was classified as adequate or poor. Adequate image quality allowed the assessment of significant lesions with moderate confidence, whereas poor image quality allowed the assessment of significant lesions with only a low confidence.

The presence of calcium in the coronary wall was systematically assessed. Each segment was classified as noncalcified, moderately calcified (small isolated eccentric highdensity lesions in the coronary wall), or heavily calcified (high-density lesions extending longitudinally along the coronary wall, causing beam hardening and partial volume artifacts). Disagreements were resolved by consensus.

Statistical analysis

The diagnostic performance of MSCT coronary angiography for the detection of significant obstructive lesions, with QCA as the standard of reference, is presented as sensitivity, specificity, and negative and positive predictive value. These diagnostic parameters are expressed with a 95% confidence interval calculated with binomial expansion. On a lesion-by-lesion analysis, inter- and intraobserver variability for the detection of significant lesions was calculated and expressed as kappa values. The most proximal significant stenosis was considered as the predominant lesion in the vessel-based analysis.

RESULTS

Sixty percent (77 of 128) of the patients received a betablocker before the MSCT scan and 42 of these patients were already receiving beta-blockers. The mean (±SD) heart rate was 57.7±7.7 during the scan procedure. The total scan time was 18.2±1.4 s. One scan could not be evaluated because of technical failure. Prospectively triggered X-tube modulation was applied in 64% (81/127) of the remaining patients.

Conventional coronary angiography revealed no signifi- cant stenoses in 17% (21 of 127), one-vessel disease in 35% (44 of 127), two-vessel disease in 35% (44 of 127), and three-vessel disease in 14% (18 of 127) of patients. Six patients had significant left main stenosis.

Lesion-by-lesion analysis: overall performance of MSCT

A total of 1,384 non-stented segments with a diameter ≥2 mm were analyzed for the detection of significant obstructive coronary stenoses (37 segments with stents were excluded). Per patient, we included 10.9±1.9 segments for analysis. Image quality was classified as good in 75% (1,049 of 1,384) of segments, adequate in 18% (243 of 1,384) of segments, and poor in 7% (92 of 1,384) of segments. Causes of poorly assessable segments were motion artifacts (63%, 58 of 92), severe calcification (30%, 28 of 92), and low contrast-to-noise ratio (7%, 6 of 92). Motion artifacts were most frequently located in the midright coronary artery. Inter- and intraobserver variability for the detection of significant lesions had kappa values of 0.71 and 0.79, respectively.

The sensitivity was 92% (216 of 234, 95% confidence interval [CI]: 88 to 95), the specificity was 95% (1,092 of 1,150, 95% CI: 93 to 96), the positive predictive value was 79% (216 of 274, 95% CI: 73 to 88), and the negative predictive value was 98% (1,092 of 1,110, 95% CI: 97 to 99) (Table 1) for the detection of significantly obstructed lesions.

Nineteen percent (268 of 1,384) of all segments were classified as heavily calcified, 31% (430 of 1,384) as moderately calcified, and 50% (686 of 1,384) as noncalcified. The diagnostic performance of MSCT coronary angiography for detection of significant obstructive lesions in noncalcified, moderately calcified, and heavily calcified segments is tabulated in Table 2.

Table 1. Results: Detection of Significant (≥50%) Stenoses With 16-Row Multislice Spiral Computed Tomography Coronary Angiography

Coronary Segment	N	TP	TN	FP	FN	Sensitivity	Specificity	PositivePV	Negative PV
All segments	1,384	216	1,092	58	18	92% (216/234)	95% (1,092/1,150)	79% (216/274)	98%(1,092/1,110)
LM	124	6	118	0	0	100% (6/6)	100% (118/118)	100% (6/6)	100% (118/118)
LAD	473	90	350	27	6	94% (90/96)	93% (350/377)	77% (90/117)	98% (350/356)
Proximal	124	37	74	10	3	93% (37/40)	88% (74/84)	79% (37/47)	96% (350/353)
Middle	111	41	65	5	0	100% (41/41)	93% (65/70)	89% (41/46)	100% (65/65)
Distal	102	5	94	3	0	100% (5/5)	97% (94/97)	63% (5/8)	100% (94/94)
Side branches	136	7	117	9	3	70% (7/10)	93% (117/126)	44% (7/16)	98% (117/120)
CX	395	49	325	12	9	84% (49/58)	96% (325/337)	80% (49/61)	97% (325/334)
Proximal	111	16	90	3	2	89% (16/18)	97% (90/93)	84% (16/19)	98% (90/92)
Middle	102	13	81	4	4	76% (13/17)	95% (81/85)	76% (13/17)	95% (81/85)
Side branches	182	20	154	5	3	87% (20/23)	97% (154/159)	80% (49/61)	98% (154/157)
RCA	392	71	299	19	3	96% (71/74)	94% (299/318)	79% (71/90)	99% (299/302)
Proximal	120	30	81	9	0	100% (30/30)	90% (81/90)	77% (30/39)	100% (30/30)
Middle	103	31	63	8	1	97% (31/32)	89% (63/71)	79% (31/39)	98% (63/64)
Distal	91	8	80	2	1	89% (8/9)	98% (80/82)	80% (8/10)	99% (80/81)
PDA	78	2	75	0	1	67% (2/3)	100% (75/75)	100% (2/2)	99% (75/76)

CX = circumflex coronary artery; FN = false negative; FP = false positive; LAD = left anterior descending coronary artery; LM = left main coronary artery; PDA = posterior
descending artery; RCA = right coronary artery; PV = predictive value; TN = true negative; TP = true positive.

Table 2. Diagnostic Performance of Multislice Spiral Computed Tomography Coronary Angiography for the Detection of Significant Obstructive Lesions

Segments	N	TP	TN	FP	FN	Sensitivity	Specificity	Positive PV	NegativePV
Non-calcified	686	60	602	15	9	87% (76–97)	98% (96–98)	80% (69–91)	90% (97–99)
Moderately calcified	430	64	342	17	7	90% (80–97)	95% (92–97)	79% (68–90)	98% (95–99)
Heavily calcified	268	92	148	26	2	98% (92–94)	85% (78–90)	78% (69–86)	99% (95–99)
Overall	1,384	216	1,092	58	18	92% (88–95)	95% (93–96)	79% (73–88)	98% (97–99)

Noncalcified = complete absence of coronary calcification; moderately calcified = Small isolated eccentric calcified deposits; Heavily calcified = Large deposits of calcium expanding longitudinally along the coronary wall, causing partial volume effects and beam-hardening artifacts. Abbreviations as in Table 1.

Lesion-by-lesion analysis: false-negative results on MSCT

Eighteen significantly obstructed segments with a mean diameter reduction of 61.1±7.5% (range 51% to 72% using QCA) were missed on the MSCT scan. The majority of the missed lesions were located in the circumflex coronary artery or in smaller side branches (13 of 18, 72%). Two lesions were missed because of severe calcifications and two because

of motion artifacts; the severity of the stenosis was underestimated in the remaining 14 lesions.

Lesion-by-lesion analysis: false-positive results on MSCT

Fifty-eight segments were incorrectly classified as significantly obstructed because of overestimation of the severity of the lesion. Fifteen noncalcified and 17 moderately calcified lesions (mean diameter reduction 41.2±5.1%, range 30% to 48%) were overestimated. Twenty-six heavily calcified lesions were overestimated; in the majority of these lesions conventional angiography revealed only minor wall irregularities. Overestimation of heavily calcified lesions was likely related to beam-hardening artifacts and partial volume effects resulting in blooming of the coronary calcifications.

Vessel-based analysis

The sensitivity for classification of vessels with or without CAD was 94% (177 of 188, 95% CI: 89 to 95); specificity was 91% (298 of 329, 95% CI: 86 to 93), positive predictive value was 85% (177 of 208, 95% CI: 79 to 91), and negative predictive value was 96% (298 of 309, 95% CI: 93 to 98). All significantly obstructed left main coronary arteries (n=6) and total occlusions (n=60) were correctly identified on the MSCT scan.

Patient-based analysis

Multislice spiral computed tomography coronary angiography correctly identified 18 of 21 (86%) patients without significant stenoses on angiography. No patient with single-vessel disease (n=44) on angiography was incorrectly classified as having no significant coronary disease on MSCT; however, 15 patients were classified as having multivessel disease. Fifty-five patients with multivessel disease (n=62) on angiography were correctly classified on MSCT; the remaining seven patients were classified as having single-vessel disease.

Overall, all patients with a significant stenosis in one or more vessels were correctly classified as patients with CAD. Sensitivity for classification of patients with or without CAD was 100% (106 of 106, 95% CI: 96 to 100), specificity was 86% (18 of 21, 95% CI: 63 to 96), positive predictive value was 97% (106 of 109, 95% CI: 92 to 98), and negative predictive value was 100% (18 of 18, 95% CI: 81 to 100).

DISCUSSION

Complete visualization of all clinically important coronary segments is a prerequisite for MSCT coronary angiography to become an accepted clinical tool for the assessment of patients with suspected CAD. Previous studies in relatively small cohorts showed high sensitivity and specificity for the detection of significant obstructive lesions (2,3). The major finding of the present study, which compared MSCT with QCA, is that 16-row MSCT is a robust tool for assessing the presence of significantly obstructed coronary artery in the clinically important part of the coronary tree (Figs. 1 and 2). All MSCT segments corresponding to angiographic segments with a diameter above 2 mm on QCA were analyzed, without any prespecified exclusion criteria based on the quality of the MSCT images. This resulted in 10.9 1.9 available segments per patient. For the

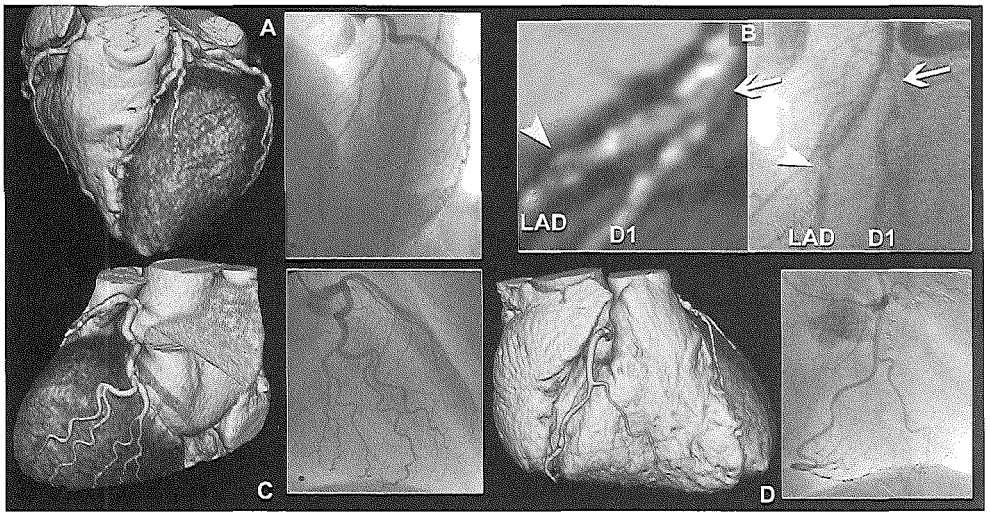

Figure 1. Volume-rendered multislice spiral computed tomography images (left) and corresponding conventional angiography images (right) of the left anterior descending (LAD) (**A**), circumflex (**C**), and right coronary artery (**D**) in a 69-year-old woman with stable angina and a positive bicycle test. Significant lesions were found in the proximal part of the LAD coronary artery (arrowhead) and first diagonal (D1) (arrow), which are demonstrated on the inlay (**B**).(A full color version of this illustration can be found in the color section (chapter 12)).

segmentbased analysis, both the overall sensitivity and specificity were found to be above 90% (92% and 94%, respectively). Image quality was classified as poor in 7% of the segments. However, these segments were included in the comparative analysis with QCA.

The current-generation 16-slice scanners have a higher spatial and temporal resolution when compared with previous scanners, resulting in an improvement in the diagnostic accuracy of MSCT angiography.[7–10]

One-half of the segments contained calcified deposits in the coronary wall. Calcifications are high-density structures causing beam-hardening artifacts and partial volume effects on computed tomography. These artifacts have an important impact on the evaluation of calcified lesions. Only two lesions in the present study were missed because of severe calcifications, but 26 heavily calcified lesions were overestimated. The majority of these lesions appeared as wall irregularities on conventional angiography.

Another 32 overestimated lesions with a mean diameter reduction of 40% on QCA (range between 30% and 48%) were noncalcified or moderately calcified. This probably reflects the semiquantitative nature of the evaluation of coronary lesions with MSCT.

One-third of the missed ≥50% lesions were located in the circumflex and a further one-third in smaller side branches. The circumflex coronary artery is more difficult to evaluate, probably because of its tortuous course

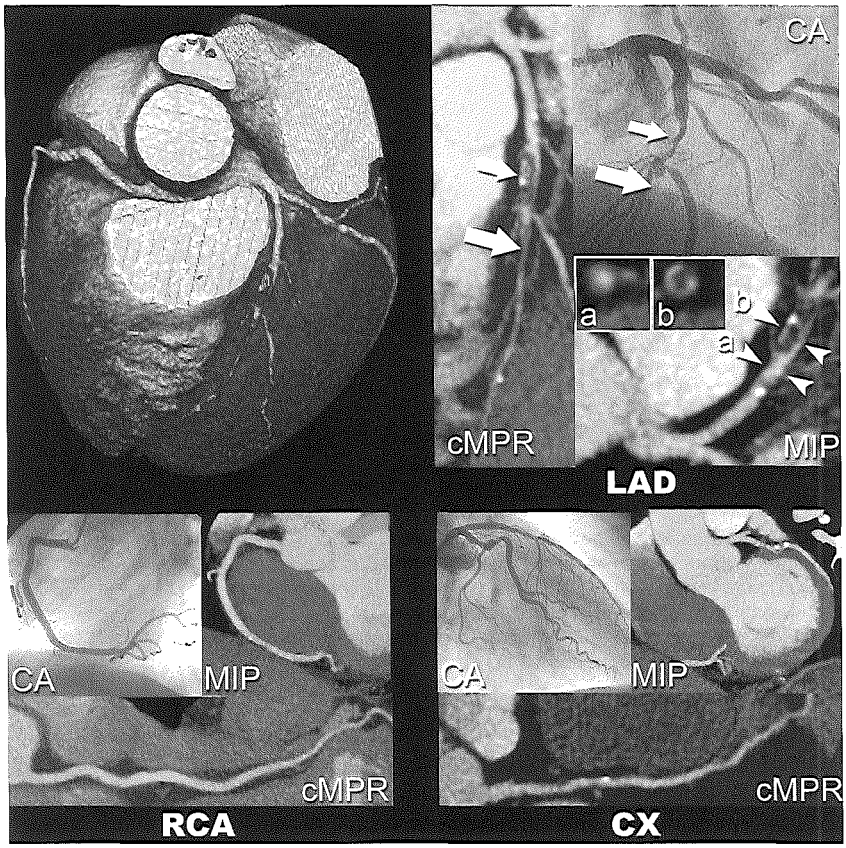

Figure 2. Colored image volume rendered multislice spiral computed tomography (MSCT) image providing an overview of the anatomy of the main coronary arteries. Black and white images MSCT (curved multiplanar reconstructions [cMPR] and maximum intensity projections [MIP]) and conventional coronary angiography (CA) images of the four main coronary arteries (left main/left anterior descending [LAD], circumflex coronary artery [CX], right coronary artery [RCA]) of a single patient. The small arrows highlight a high-grade stenosis and the large arrows an occlusion located at the midpart of the LAD. The arrowheads indicate cross-sectional images proximal (inlay a) and within the occlusion (inlay b). Inlay b shows calcified (displayed as white) and noncalcified (displayed as black) plaque tissue components. (A full color version of this illustration can be found in the color section (chapter 12)).

and overlapping structures, whereas the relatively high number of missed lesions in smaller side branches suggest a lower diagnostic performance of MSCT angiography in branches toward the threshold of 2 mm.

All patients with at least one significant obstruction on QCA were correctly classified as having CAD with MSCT. This suggests that the current generation of scanners may be a suitable tool to triage patients with stable angina who are being considered for revascularization. Further studies are needed to determine the role of this technique in the clinical workup of patients with other presentations of coronary disease or who are being evaluated to exclude significant disease.

Study limitations

Only patients with stable angina were included in this study. Whether a broader group of patients might benefit from this technique (excluding patients with severe arrhythmia) must be explored, but there are no reasons to believe that results would differ in patients with acute coronary syndromes.

In our study we noted that the sensitivity of detection for noncalcified obstructive lesions tended to be lower. This is caused by the fact that these lesions have a relatively low tissue contrast and may be missed, especially in small vessel segments. This may be problematic in younger patients with a lower likelihood of lesion calcification. Dedicated automatic software that is able to detect and calculate the degree of coronary stenoses would improve diagnostic accuracy.

The high radiation exposure during MSCT coronary angiography, which is reported between 6.7 and 13.0 mSv,[5,11,12] remains a matter of concern. Further fine-tuning of the prospective X-ray tube current modulation and development of new features lowering radiation exposure is highly desirable.

CONCLUSIONS

Multislice spiral computed tomography coronary angiography permits reliable detection of CAD in a population of patients in sinus rhythm with stable angina.

REFERENCES

1. Flohr TG, Schoepf UJ, Kuettner A, et al. Advances in cardiac imaging with 16-section CT systems. Acad Radiol 2003;10:386–401.
2. Nieman K, Cademartiri F, Lemos PA, Raaijmakers R, Pattynama PM, de Feyter PJ. Reliable noninvasive coronary angiography with fast submillimeter multislice spiral computed tomography. Circulation 2002;106:2051–4.
3. Ropers D, Baum U, Pohle K, et al. Detection of coronary artery stenoses with thin-slice multi-detector row spiral computed tomography and multiplanar reconstruction. Circulation 2003;107:664–6.
4. Jakobs TF, Becker CR, Ohnesorge B, et al. Multislice helical CT of the heart with retrospective ECG gating: reduction of radiation exposure by ECG-controlled tube current modulation. Eur Radiol 2002;12:1081–6.
5. Trabold T, Buchgeister M, Kuttner A, et al. Estimation of radiation exposure in 16-detector row computed tomography of the heart with retrospective ECG-gating. Rofo Fortschr Geb Rontgenstr Neuen Bildgeb Verfahr 2003;175:1051–5.
6. Austen WG, Edwards JE, Frye RL, et al. A reporting system on patients evaluated for coronary artery disease. Report of the Ad Hoc Committee for Grading of Coronary Artery Disease, Council on Cardiovascular Surgery, American Heart Association. Circulation 1975;51:5–40.
7. Nieman K, Oudkerk M, Rensing BJ, et al. Coronary angiography with multi-slice computed tomography. Lancet 2001;357:599–603.
8. Achenbach S, Giesler T, Ropers D, et al. Detection of coronary artery stenoses by contrast-enhanced, retrospectively electrocardiographicallygated, multislice spiral computed tomography. Circulation 2001;103: 2535–8.

9. Knez A, Becker CR, Leber A, et al. Usefulness of multislice spiral computed tomography angiography for determination of coronary artery stenoses. Am J Cardiol 2001;88:1191–4.
10. Vogl TJ, Abolmaali ND, Diebold T, et al. Techniques for the detection of coronary atherosclerosis: multi-detector row CT coronary angiography. Radiology 2002;223:212–20.
11. Morin RL, Gerber TC, McCollough CH. Radiation dose in computed tomography of the heart. Circulation 2003;107:917–22.
12. Hunold P, Vogt FM, Schmermund A, et al. Radiation exposure during cardiac CT: effective doses at multi-detector row CT and electron-beam CT. Radiology 2003;226:145–52.

6. CORONARY STENOSIS

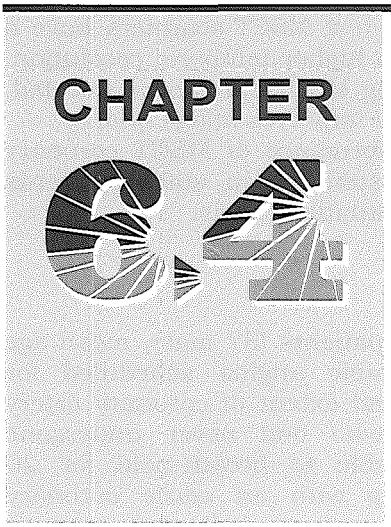

IMPROVED DIAGNOSTIC ACCURACY WITH 16-ROW MULTISLICE CT CORONARY ANGIOGRAPHY TOMOGRAPHY

Nico R. Mollet, MD[1,2]
Filippo Cademartiri, MD[2]
Gabriel P. Krestin, MD[2]
Eugène P. Mc Fadden, MB, FACC[1]
Chourmouzios A. Arampatzis, MD[1]
Patrick W. Serruys, MD, FACC[1]
Pim.J. de Feyter, MD, FACC[1,2]

Departments of Cardiology[1] and Radiology[2]
Erasmus MC, University Medical Center Rotterdam,
The Netherlands

J Am College of Cardiology, in press-online

ABSTRACT

Objectives: To compare the diagnostic value of Multislice Computed Tomography (MSCT) coronary angiography to detect significant stenoses (≥50% lumen diameter reduction) with that of invasive coronary angiography.

Background: The latest 16-row MSCT scanner has a faster rotation time (375 ms) and permits scanning with a higher X-ray tube current (500-600 mAs) during MSCT coronary angiography when compared to previous scanners.

Methods: We studied 51 patients (37 men, mean age 58.9±10.0 years) with stable angina or atypical chest pain. Patients with pre-scan heart rates ≥70 beats/minute received oral β-blockade. The heart was scanned after intravenous injection of 100 ml contrast (iodine content: 400 mg/ml). Mean scan-time was 18.9±1.0 seconds. The MSCT-scans were analysed by 2 observers unaware of the results of invasive angiography and all available ≥2mm coronary branches were included.

Results: Invasive coronary angiography demonstrated normal arteries in 16% (8/51), non-significant disease in 21% (11/51), single-vessel disease in 37% (19/51), and multi-vessel disease in 26% (13/51) of patients. There were 64 significant lesions. Sensitivity, specificity, positive and negative predictive value for detection of significant lesions on a segment-based analysis were 95% (61/64, 95% CI 86-99), 98% (537/546, 95% CI 96-99), 87% (61/70, 95% CI 76-98), and 99% (537/540, 95% CI 98-99) respectively. All patients with angiographically normal coronary arteries or significant lesions were correctly identified. Three of 11 patients with <50% lesions were incorrectly classified as having single vessel disease.

Conclusions: 16-row MSCT coronary angiography reliably detects significant coronary stenoses in patients with atypical chest pain or stable angina pectoris.

INTRODUCTION

Ongoing significant advances in MSCT technology in recent years prompted us to re-evaluate the clinical potential of non-invasive coronary angiography (CA).[1-9] The latest generation 16-row MSCT-scanners have a faster X-ray tube rotation speed that provides higher temporal resolution. In addition, a higher X-ray tube current during MSCT-CA can be selected, which increases the contrast-to-noise ratio and improves image quality.

We now report the current diagnostic performance of MSCT coronary angiography to detect significant coronary stenoses in stable patients referred for conventional angiography on an outpatient basis.

METHODS

Study Population

During a period of 7 months, we studied 51 patients (37 male, mean age 58.9±10.0) with atypical chest pain or stable angina scheduled for conventional-CA to determine the presence and extent of coronary artery disease. Only patients in sinus rhythm, who had never undergone angioplasty or bypass surgery and were able to breath-hold for 20 seconds, were included. Patients presenting with an acute coronary syndrome or in whom administration of intravenous iodinated contrast material was contraindicated (e.g. known allergy, impaired renal function, or thyroid disorders) were excluded. Our institutional review board approved the study protocol and all patients gave written informed consent.

Patient Preparation

Patients with a heart rate above 70 beats/minute received, unless contraindicated, a single oral dose of 100mg metoprolol one hour before the scan.

Scan protocol and Image Reconstruction

All patients were scanned on a 16-row MSCT scanner (Sensation16 Straton®, Siemens, Forchheim, Germany). Scan parameters: 16 x 0.75 mm detector collimation, rotation time 375 ms, table feed 3.0 mm/rotation, tube voltage 120 kV, effective mAs: 500-600, CTDIvol 51,0 mGy, no X-ray tube modulation. The estimated radiation exposure using this scan protocol is 11.8-16.3 mSv (Male-Female). A bolus of 100 ml contrast material with an iodine content of 400 mg/ml (iomeprol, Iomeron® 400, Bracco, Milan, Italy) was injected through an arm vein (rate: 4 ml/s). A bolus-tracking technique was used to synchronize the arrival of contrast in the coronary arteries with the initiation of the scan. Data was acquired during a single breath-hold of 18.9±1.0 s.

ECG-gated images were standard reconstructed during mid-to-end diastole to obtain optimal image quality. Additional reconstruction windows (e.g. early diastole) were explored when deemed necessary. Generally, best image quality was obtained when the reconstruction windows were positioned -350 ms before the next R-wave, or at 60% of the R-R interval. The reconstruction algorithm uses data of a single heartbeat,

obtained during half a rotation time, resulting in a temporal resolution of up to 188 ms.

Quantitative Coronary Angiography (QCA)

All scans were performed within 2 weeks prior to the conventional diagnostic angiogram. A single observer, unaware of the MSCT results, identified coronary segments according to the AHA classification,[10] and classified them as <2 and ≥2mm using a quantitative coronary angiography algorithm (CAAS, Pie Medical, The Netherlands). All available ≥2mm segments were included for comparison with MSCT-CA. Segments were classified as normal (smooth parallel or tapering borders), as having non-significant disease (luminal irregularities or <50% stenosis), or as having significant stenoses. Stenoses were evaluated in two orthogonal views, and classified as significant if the mean lumen diameter reduction was ≥50%.

MSCT Image Evaluation

All scans were analysed independently by a cardiologist and a radiologist, unaware of the results of conventional-CA. All main coronary arteries and large (≥2 mm) side branches were evaluated. Maximum intensity projections were used to identify coronary lesions and multi-planar reconstructions to classify lesions as significant or non-significant. Disagreement between observers was resolved by consensus.

Statistical Analysis

The diagnostic performance of MSCT-CA for detection of significant lesions in ≥2 mm coronary arteries with QCA as the standard of reference is presented as sensitivity, specificity, positive and negative predictive value with the corresponding 95% confidence intervals. Comparison between MSCT and QCA was performed on 3 levels: segment-by-segment, vessel-by-vessel (no or any disease per vessel), and patient-by-patient (no or any disease per patient). Coronary segments were scored irrespective of the score in other segments or vessels within the same patient, therefore independence between the analyses was assumed. The most proximal coronary lesion determined the diagnostic performance in the vessel-based analysis in coronary branches with >1 significant lesions.

RESULTS

Conventional-CA revealed normal coronary arteries in 16% (8/51), non-significant disease in 21% (11/51), and significant coronary artery disease in 63% (32/51) of patients. Nineteen patients had single- and 13 patients multi-vessel disease; Five patients had significant left main disease. The mean number of included segments per patient was 12.0±1.9. All proximal and mid coronary segments were included in the analysis. Mean heart rate during scanning was 57.1±1.0 (range 43 to 80) beats/minute. A β-blocker was administered before the scan in 25 of the 51 patients; most (80%) were already receiving long-term β-blockade. Inter- and intra-observer variability for detection of significant lesions had κ-values of 0.73 and 0.80.

Diagnostic Performance of MSCT Coronary Angiography

The diagnostic performance of MSCT-CA for detection of significant lesions is detailed in Table 1. Two significant (52% and 57% lumen diameter reduction) lesions on QCA, located in the proximal and mid circumflex coronary artery (CX), were incorrectly classified as non-significant on MSCT. A single significant (67% lumen diameter reduction) lesion in the distal right coronary artery (RCA) was not visualised on the MSCT scan due to motion artifacts. No significant lesions were missed in the left main (LM) or left anterior descending (LAD) coronary arteries. Nine non-significant lesions on QCA were incorrectly classified as ≥50% lesions on MSCT. On conventional-CA 4 of these were non-significant lesions (mean lumen reduction 40%, range 38-42%), and the other 5 were lumen irregularities. The majority (n=7) of these lesions were calcified.

On a vessel-based analysis, two significantly obstructed vessels were missed on MSCT: one RCA and one CX. Six vessels without ≥50% lesions were incorrectly classified as significantly obstructed.

Table 1. Diagnostic performance of MSCT-CA for detection of ≥50% stenoses

	N	Sensitivity	Specificity	Positive PV	Negative PV
Segment-based	610	61/64 (95,86-99)	537/546 (98,96-99)	61/70 (87,76-98)	537/540 (99,98-99)
LM (1)	51	5/5 (100,47-100)	46/46 (100,92-100)	5/5 (100,47-100)	46/46 (100,92-100)
LAD (3-5)	205	24/24 (100,85-100)	175/181 (97,92-98)	24/30 (80,61-96)	175/175 (100,97-100)
CX (3-5)	172	15/17 (88,63-99)	154/155 (99,96-99)	15/16 (94,69-99)	154/156 (99,95-99)
RCA (3-4)	182	17/18 (94,72-99)	162/164 (99,95-99)	17/19 (90,66-99)	162/163 (94,96-99)
Vessel-based	202	51/53 (96,87-99)	143/149 (96,91-98)	51/57 (90,78-97)	143/145 (99,95-99)
LM	51	5/5 (100,47-100)	46/46 (100,92-100)	5/5 (100,47-100)	46/46 (100,92-100)
LAD	51	16/16 (100,79-100)	31/35 (89,73-96)	16/20 (80,56-95)	31/31 (100,88-100)
CX	50	13/14 (93,66-99)	35/36 (97,85-99)	13/14 (93,66-99)	35/36 (97,85-99)
RCA	50	17/18 (94,72-99)	31/32 (97,83-99)	17/18 (94,72-99)	31/32 (97,83-99)
Patient-based	51	31/31 (100,88-100)	17/20 (85,62-96)	31/34 (91,76-97)	17/17 (100,80-100)

PV = Predictive Value. Values are n (%, 95% confidence interval)

All patients with normal coronary angiograms were classified as having neither significant nor non-significant stenosis on MSCT. All patients with significant coronary artery disease were correctly identified on MSCT as having at least single-vessel disease, whereas 3 patients without ≥50% lesions were classified as single-vessel disease. Two examples comparing the results of MSCT-CA with conventional-CA are shown in Figures 1-2.

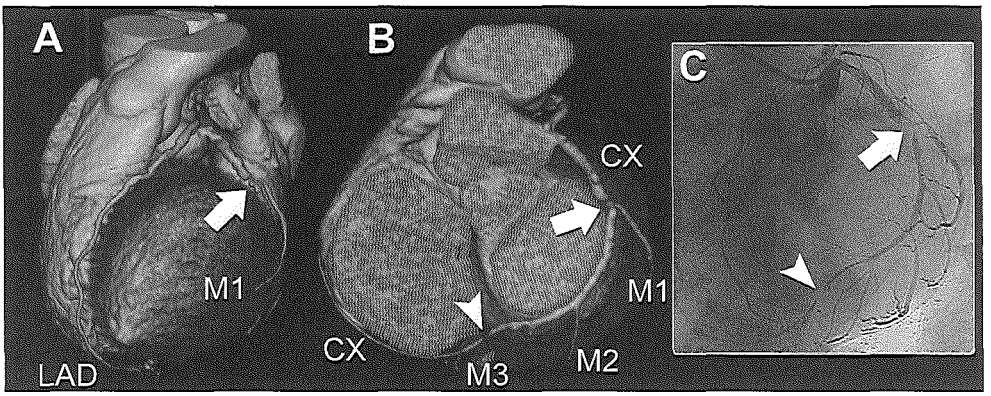

Figure 1a. Volume rendered CT images (**A, B**) reveal the presence of 2 significant stenoses (arrow, arrowhead) located at the circumflex coronary artery (CX), which was confirmed on the conventional angiogram (**C**).
LAD: left anterior descending coronary artery, M: marginal branch.
(A full color version of this illustration can be found in the color section (chapter 12)).

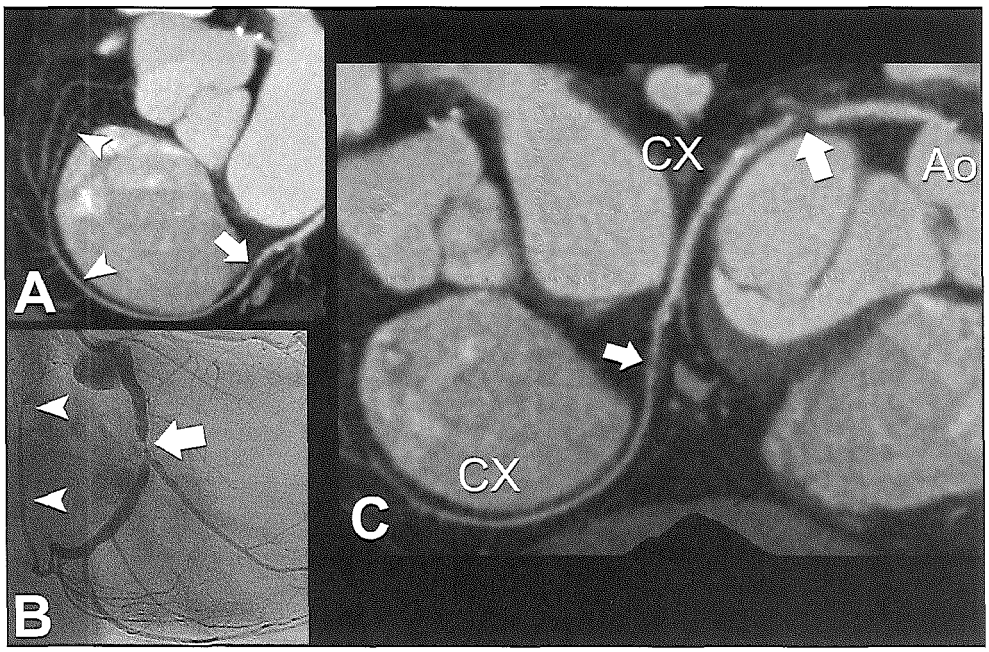

Figure 1b. Maximum intensity projected (**A**) and curved multiplanar reconstructed (**C**) CT images showing the trajectory of the circumflex coronary artery (CX), which ends almost at the right coronary sinus. The arrows indicate the stenoses. These findings were confirmed on the conventional angiogram (**B**).
Ao: Aorta.

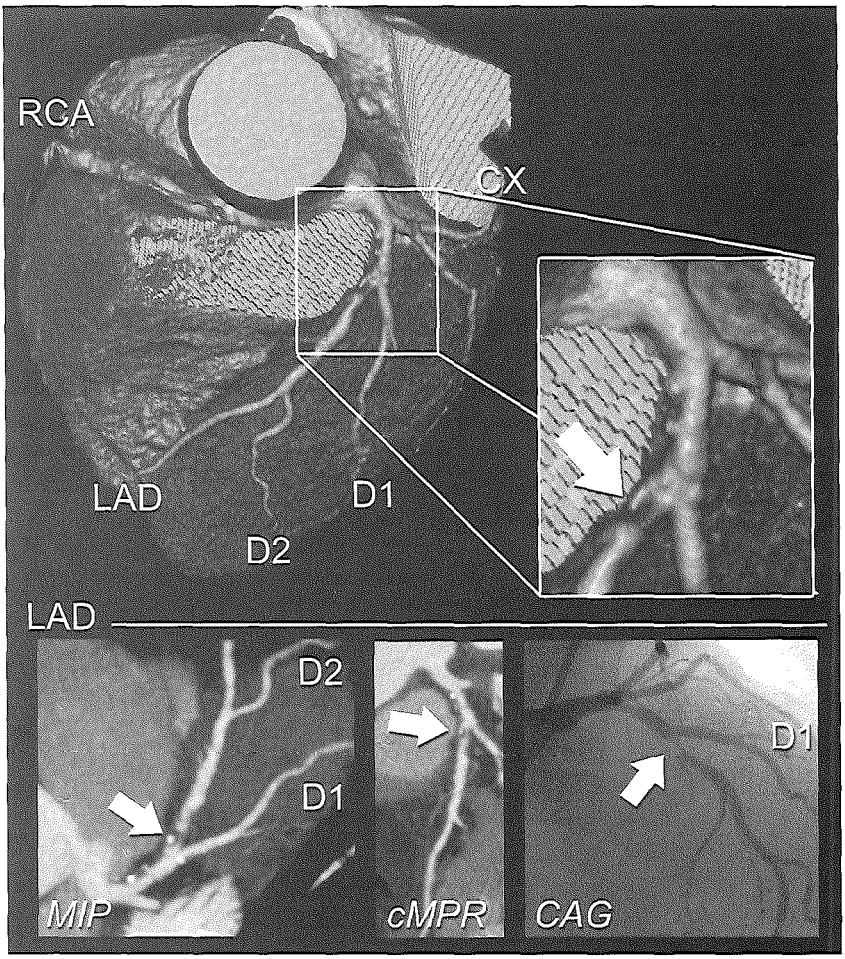

Figure 2. Volume rendered (coloured images), maximum intensity projected (MIP), and curved multiplanar reconstructed (cMPR) CT images demonstrate a significant stenosis (arrow) of the left anterior descending coronary artery (LAD), which was confirmed on the conventional angiogram (CAG).
CX: circumflex coronary artery, D: diagonal branch, RCA: right coronary artery.
(A full color version of this illustration can be found in the color section (chapter 12)).

DISCUSSION

Conventional-CA is currently the standard technique for evaluation of patients with suspected coronary atherosclerosis. It is used both to exclude coronary atherosclerosis as a cause of symptoms and to evaluate the extent and severity of atherosclerosis with a view to referral for revascularization. Previous reports demonstrated that earlier generations of MSCT scanners showed promise for the non-invasive detection of coronary artery stenoses.[1-9] Those scanners acquire fewer slices simultaneously[1-8] (4, 8, or 12 vs. 16 slices) and are equipped with a lower

X-ray tube rotation speed[1-9] (500 or 420 ms vs. 375 ms) compared to the latest generation 16-row MSCT scanners. An additional advantage of the new MSCT scanner is the ability to scan with a higher X-ray tube output, which increases the contrast-to-noise ratio and therefore image quality. These technical developments result in a markedly improved diagnostic performance when compared to the results reported with previous scanner generations.

Our study found that non-invasive CA can detect significant stenoses with a sensitivity of 95%, a specificity of 98% and positive and negative predictive values of 87% and 99% respectively, when compared to conventional-CA. Furthermore, all patients with normal coronary arteries on conventional-CA were classified as having neither significant nor non-significant stenosis on MSCT. These results were obtained in patients with atypical chest pain or stable angina pectoris who had varying degrees of coronary artery disease ranging from no detectable significant obstructive disease to 1, 2, 3 vessel disease or left main disease.

MSCT-CA will not equal either the resolution or real-time imaging capabilities of conventional-CA in the foreseeable future; however, its non-invasive nature renders the technique more patient-friendly and reduces the risk of iatrogenic injury. This technique may open new avenues for research and contribute to the development of novel management algorithms in selected patients. Potential applications include the evaluation of asymptomatic individuals at high risk of atherosclerosis or assessment of disease progression in patients with known coronary artery disease.

Limitations

We did not investigate patients with an acute coronary syndrome, because of safety and logistic issues associated with the examination of these patients in a setting outside the coronary care unit. However, we do expect that the diagnostic performance of MSCT would be similar in these patients.

The limited spatial resolution of current MSCT scanners only allows qualitative, therefore user-dependent, assessment of coronary stenoses. Development of reliable software able to detect and quantify the degree of coronary stenoses would make MSCT-CA a more robust and reproducible technique.

The estimated radiation dose during MSCT-CA using this scan protocol (11.8-16.3 mSv [Male-Female]) is higher when compared to previously reported doses using older scanner generations (6.7-13.0 mSv)[11,12] or conventional-CA (3-5 mSv). Radiation exposure should be reduced by technical adjustments such as prospective X-ray tube current modulation, which limits the radiation exposure with nearly 50% in patients with low heart rates.[11] However, we did not apply this feature because it limits reconstruction of images during the early-diastolic phase, which can be of importance for evaluation of the RCA.

Persistent irregular heart rhythm such as atrial fibrillation and frequent extra-systoles precludes MSCT-CA. However, in some cases, motion

artifacts due to an occasional extra-systole can be corrected by ECG-editing. Severe coronary calcification obscures the coronary lumen and can lead to overestimation of the severity of lesions due to blooming artifacts. In fact, the vast majority of false-positive lesions were calcified (7/9). Improvements in spatial resolution and dedicated post-processing algorithms may diminish the problem.

Motion artifacts associated with higher heart rates may be resolved by faster X-ray tube rotation time or sophisticated reconstruction algorithms that use data obtained from multiple, consecutive heartbeats.

Conclusion

MSCT-CA is a reliable technique to non-invasively detect coronary stenoses in patients with stable angina and atypical chest pain. More studies are needed in other patient groups with different prevalences of disease to show that these initial favourable results are reproducible on a wider scale.

References

1. Nieman K, Oudkerk M, Rensing BJ, et al. Coronary angiography with multi-slice computed tomography. Lancet. 2001;357:599-603.
2. Achenbach S, Giesler T, Ropers D, et al. Detection of coronary artery stenoses by contrast-enhanced, retrospectively electrocardiographically-gated, multislice spiral computed tomography. Circulation. 2001;103:2535-8.
3. Knez A, Becker CR, Leber A, et al. Usefulness of multislice spiral computed tomography angiography for determination of coronary artery stenoses. Am J Cardiol. 2001;88:1191-4.
4. Vogl TJ, Abolmaali ND, Diebold T, et al. Techniques for the detection of coronary atherosclerosis: multi-detector row CT coronary angiography. Radiology. 2002;223:212-20.
5. Kopp AF, Schroeder S, Kuettner A, et al. Non-invasive coronary angiography with high resolution multidetector-row computed tomography. Results in 102 patients. Eur Heart J. 2002;23:1714-25.
6. Nieman K, Cademartiri F, Lemos PA, et al. Reliable noninvasive coronary angiography with fast submillimeter multislice spiral computed tomography. Circulation. 2002;106:2051-4.
7. Ropers D, Baum U, Pohle K, et al. Detection of coronary artery stenoses with thin-slice multi-detector row spiral computed tomography and multiplanar reconstruction. Circulation. 2003;107:664-6.
8. Kuettner A, Kopp AF, Schroeder S, et al. Diagnostic accuracy of multidetector computed tomography coronary angiography in patients with angiographically proven coronary artery disease. J Am Coll Cardiol. 2004;43:831-9.
9. Mollet NR, Cademartiri F, Nieman K, et al. Multislice Spiral CT Coronary Angiography in Patients With Stable Angina Pectoris. J Am Coll Cardiol. 2004;43:2265-70.
10. Austen WG, Edwards JE, Frye RL, et al. A reporting system on patients evaluated for coronary artery disease. Report of the Ad Hoc Committee for Grading of Coronary Artery Disease, Council on Cardiovascular Surgery, American Heart Association. Circulation. 1975;51:5-40.

11. Trabold T, Buchgeister M, Kuttner A, et al. Estimation of Radiation Exposure in 16-Detector Row Computed Tomography of the Heart with Retrospective ECG-gating. Rofo Fortschr Geb Rontgenstr Neuen Bildgeb Verfahr. 2003;175:1051-5.
12. Hunold P, Vogt FM, Schmermund A, et al. Radiation exposure during cardiac CT: effective doses at multi-detector row CT and electron-beam CT. Radiology. 2003;226:145-52.

7. CORONARY STENTS

CHAPTER 7.1

NONINVASIVE ANGIOGRAPHIC EVALUATION OF CORONARY STENTS WITH MULTI-SLICE SPIRAL COMPUTED TOMOGRAPHY

NICHTINVASIVE ANGIOGRAPHISCHE BEURTEILUNG VON KORONARSTENTS MIT DEM MULTI-SLICE-SPIRAL-CT

Koen Nieman[1,2]
Filippo Cademartiri[2]
Rolf Raaijmakers[2]
Peter Pattynama[2]
Pim de Feyter[1,2]

From the Departments of Cardiology[1] and Radiology[2], Erasmus MC, University Medical Center Rotterdam, The Netherlands.

Herz, 28:136–42, 2003.

Background: The number of patients with obstructive coronary artery disease, who undergo coronary angioplasty with implantation of stents, is ever increasing. As an alternative to catheter-based angiography, ECG-gated multi-slice spiral computed tomography (MSCT) allows noninvasive imaging of the coronary arteries. However, coronary stents have been notoriously difficult to assess by CT.
Methods and Results: In vitro experiments were performed, using varying detector collimations, contrast concentrations, stent positions and stent diameters, to evaluate the feasibility and image characteristics of stents. The stent-related highdensity artifacts expand the apparent size of the stent struts.This blooming effect is a fairly constant phenomenon, and therefore relatively less evident in larger-diameter stents. The in vivo images show the same artifacts, but assessment is further complicated by motion, lower contrast-to-noise, and vessel wall calcifications.
Conclusions: The clinical value of CT after percutaneous coronary intervention currently remains largely limited to the detection of stent occlusion, and the progression of coronary artery disease in the remaining nonstented segments. Subtle in-stent abnormalities cannot be reliably imaged. Some relief will be offered by improvements in scanner technology, but the use of less radiopaque stent material would be more effective.
Hintergrund: Die Anzahl von Patienten mit stenosierender koronarer Herzerkrankung, bei denen eine Stentimplantation erfolgte, steigt stetig an. Als Alternative zur Katheter-basierten Angiographie, kann die EKG-gesteuerte Multi-Slice-Spiral- Computertomographie (MSCT) nichtinvasiv die Koronararterien darstellen. Die Beurteilung von Koronarstents mittels CT ist jedoch schwierig.
Methoden und Ergebnisse: Um die Bildcharakteristik der Stents zu evaluieren, wurden In-vitro-Untersuchungen mit unterschiedlichen Kollimationen, Konzentrationen der Kontrastmittel, Stentpositionen und Stentdurchmessern

durchgeführt. Die stentbedingten Artefakte bei hohen Dichten überschätzen die wahre Größe der Stents. Dieser „Blooming"- Effekt ist ein ziemlich konstantes Phänomen und steht bei größeren Stentdurchmessern weniger stark im Vordergrund. Die In-vivo-Bilder zeigen die gleichen Artefakte, die Beurteilung der Stents ist jedoch durch die Bewegung, das niedrigere Kontrast-zu-Untergrund-Verhältnis und Kalzifizierungen der Gefäßwand komplexer.

Schlussfolgerung: Der klinische Wert der CTs nach Koronarinterventionen bleibt gegenwärtig zur Erkennung eines Stentverschlusses bzw. einer Progression der koronaren Herzerkrankung im nicht gestenteten Segment limitiert. Eine Feindiagnostik innerhalb des Stents kann nicht zuverlässig durchgeführt werden. Möglicherweise können diese Probleme durch neuere Technologien reduziert werden-effektiver jedoch wäre die Verwendung von weniger kontrastreichen Stents.

INTRODUCTION

Over the last decade the management of refractory angina has changed dramatically with the introduction of percutaneous coronary angioplasty. More than 1 million percutaneous coronary interventions are performed each year, and the majority of these procedures involve the placement of one or more stents. Unfortunately, angioplasty is not permanently curative, and most patients will eventually develop recurrent symptoms at some time after the procedure. Until the introduction of the coated stents, neointimal hyperplasia caused clinically significant restenosis in at least 20%.[2,4] Although the occurrence of restenosis may be significantly reduced by these drug-eluting stents, progression of atherosclerotic degeneration in the remaining vessels is not affected.

Multi-slice spiral computed tomography (MSCT) allows contrastenhanced angiography of the coronary arteries. The diagnostic accuracy of this noninvasive technique to detect coronary stenoses is good, particularly in the absence of extensive vascular calcification and in patients with low heart rates.[1,3,5–7] Patients, who undergo percutaneous coronary intervention (PCI) with stent placement, are likely to develop recurrent anginal complaints in the period after the procedure and will often need repeated angiographic evaluation of the coronary arteries. In the event of in-stent restenosis or newly developed coronary obstruction, therapeutic options remain available, even in case of a compromising physical condition of the patient: advanced age, cardiac or noncardiac comorbidity. A noninvasive technique to visualize the coronary arteries in this patient group would be highly desirable. Potential clinical indications for angiography could include suspected early (thrombotic) occlusion of stents after the procedure, or later for the detection of in-stent restenosis and progression of coronary artery disease in the nonstented vessel segment.

Coronary Stents

Stents are small expandable devices that are delivered through small catheters and, either directly or after balloon dilatation, expanded in coronary arteries. The purpose of the stent is to maintain the lumen diameter after dilatation or to restore the endothelial integrity after a

dissection. The devices are expected to sustain considerable inward radial force, while maintaining longitudinal flexibility. Over the years the designs of stents have evolved, and the currently used types are laser-cut stainless-steel meshes that are well expandable, strong, flexible, and well visualized on conventional angiography. Recent developments in stent design include stents coated with pharmaceuticals to prevent restenosis, biodegradable stents, nonmetallic and/or MR-compatible stents.

In Vitro Coronary Stent

Imaging To study the image characteristics of stents, we expanded several types of stainless-steel stents (by a number of manufacturers), with a diameter of 3.0 or 4.0 mm, in silicon tubes of corresponding diameter. The tubes were filled with a diluted contrast medium and scanned with two different detector collimations: 4 x 1.0 mm and 2 x 0.5 mm. The stents were placed both in a longitudinal (parallel to the scan direction) and transverse position (perpendicular to the scan direction). The stationary stents were scanned without the use of an ECG-synchronized protocol.

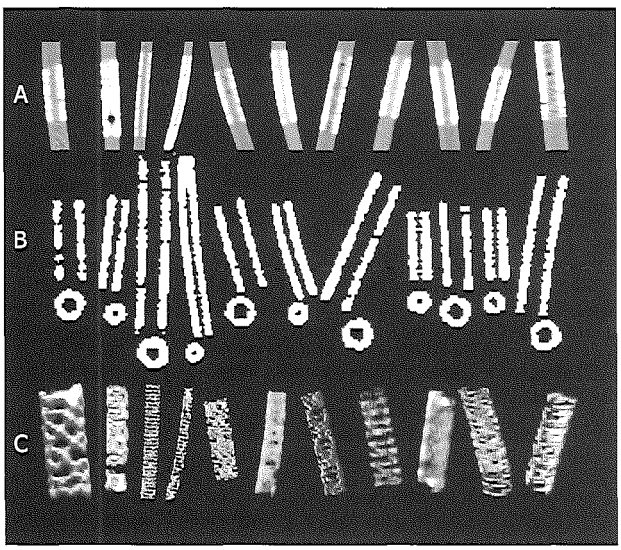

Figures 1A to 1C. In vitro imaging of coronary stents. The first series (sliding-window settings) shows longitudinal 2-D cross sections of the stents and the contrast-enhanced lumen within the stents (A). The second series shows the long- and short-axis view of the stents with a zerowindow and level setting depending on the maximum stent density value (B). The 4.0-mm stents have a lumen of 1–2 mm, unaffected by partial volume effects. The smaller 3.0-mm stents show a near occluded lumen, indicating increased density values throughout the instent lumen. The last series shows the 3-D appearance of the stents (C). The second stent contains an air bubble. The imaged stents are, from left to right: Seaquence 4.0 and 3.0 mm (Nycomed Amersham, Paris, France), Multilink RX Tristar 4.0 and 3.0 mm (Guidant ACS, Temecula, USA), Synthesis Star 4.0 and 3.0 mm (CardioVascular Dynamics, Irvine, USA), Crossflex LC 4.0 mm (Cordis, Miami, USA), Multilink RX Penta 4.0 mm (Guidant), Crossflex 4.0 mm (Cordis), Multilink RX Tetra 3.0 mm (Guidant), Multilink Duet 4.0 mm (Guidant).

Abbildungen 1A bis 1C. In-vitro-Bilder von Koronarstents: Die erste Serie (mit gleitendem Fenster) zeigt Längsschnitte der Stents und des kontrastverstärkten Lumens innerhalb der Stents (A). Die zweite Serie zeigt die Längs- und Kurzachsen der Stents mit einem Fenster von 0 und weiteren Einstellungen in Abhängigkeit von der maximalen Stentdichte (B). Die 4,0-mm- Stents haben ein Lumen von 1–2 mm und bleiben vom Partialvolumeneffekt unbeeinflusst. Die kleineren 3,0-mm-Stents erscheinen nahezu verschlossen als Hinweis für die erhöhten Dichtewerte innerhalb des Lumens. Die letzte Serie zeigt die 3-D-Rekonstruktion der Stents (C). Der zweite Stent beinhaltet ein Luftbläschen. Die abgebildeten Stents sind (von links nach rechts): Seaquence 4,0 und 3,0 mm (Nycomed Amersham, Paris, France), Multilink RX Tristar 4,0 und 3,0 mm (Guidant ACS, Temecula, USA), Synthesis Star 4,0 und 3,0 mm (CardioVascular Dynamics, Irvine, USA), Crossflex LC 4,0 mm (Cordis, Miami, USA), Multilink

The experiments have shown that, despite the lack of cardiac motion and the use of very thin slices, highdensity artifacts cause the stent struts to appear much larger than they actually are (Figure 1). The density of the

stents is inhomogeneous and depends on the distribution of the thin struts throughout the 3-D image matrix, but the maximum values range from 600 to > 1,500 Hounsfied Units (HU). The partial volume artifacts and beam hardening result in a higher average CT density value within the in-stent lumen. While a small (1 mm) region of artifact-free lumen remains in the central instent lumen of the 4.0-mm stents, there is density elevation throughout the 3.0-mm stents, an observation that was consistent for all types of stents we evaluated (Figure 2). The contrast medium concentration, within the clinically used range, did not significantly influence this phenomenon (Figure 3).

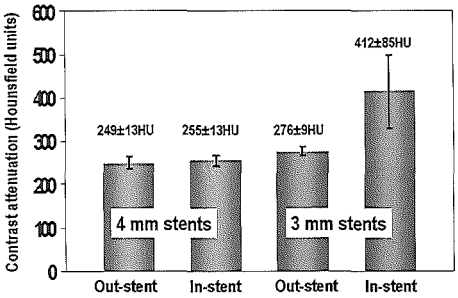

Figure 2. The in-stent density value (Hounsfield Units [HU]) of 4.0-mm stents approximately equals that outside the stents. In 3.0-mm stents, partial volume effects cause elevation of the density values throughout the in-stent lumen.

Abbildung 2. Die Stentdichtewerte (Hounsfield-Einheiten, HU) eines 4,0-mm-Stents gleichen nahezu denen außerhalb des Stents. In einem 3-mm-Stent führt der Partialvolumeneffekt sogar zu einer Zunahme der Dichtewerte innerhalb des Stentlumens.

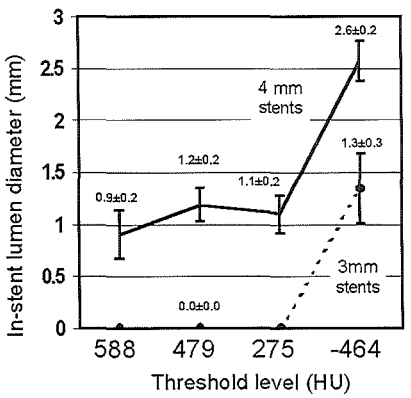

Figure 3. For three clinically relevant concentrations of contrast medium: 588 Hounsfield Units (HU), 479 HU, and 275 HU, no significant differences between the measured artifact-free areas (mm2) were measured. Without contrast medium (–464 HU), the artifact-free lumen was substantially larger.

Abbildung 3. Dichtewerte für drei klinisch relevante Konzentrationen von Kontrastmittel: 588 Hounsfield-Einheiten (HU), 479 HU und 275 HU; keine signifikanten Unterschiede zwischen den gemessenen artefaktfreien Flächen (mm2). Ohne Kontrastmittel (–464 HU) war das artefaktfreie Lumen substantiell größer.

The 3-D reconstructions of the larger stents show distinct patterns, unique to the stent type (Figure 4). The appearance depends on the stent design, but also displays the interaction of the strut configuration, the pathway of the X-ray beam, and spatial resolution of the scanner. This is illustrated in Figure 5, which shows the 3-D representation of a stent scanned in two different directions.

These experiments show that even under in vivo conditions, without cardiac motion or surrounding tissues and using thin detector collimation (0.5 mm), the imaging of particularly small stents is difficult.

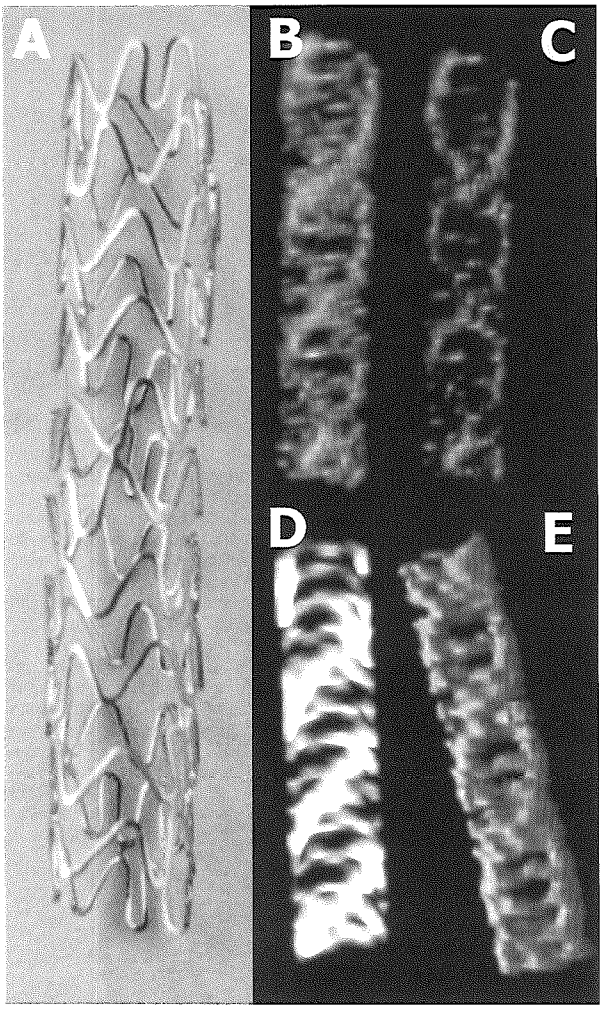

Figures 4A to 4E. MSCT appearance of a 4.0-mm Crossflex LC stent (Cordis, Miami, USA). The strut design of the stent is too detailed to be represented well by MSCT. However, due to locally increased densities of struts and metal, the appearance of a double helix is created on the 3-D images.

Abbildungen 4A bis 4E. MSCT-Bilder eines 4,0-mm-Crossflex LCStents (Cordis, Miami, USA). Das Strebenmuster des Stents ist zu detailliert, um exakt mit dem MSCT erkannt zu werden. Durch die erhöhte Dichte der Stentstreben entsteht das Muster einer Doppelhelix in den 3-D-Rekonstruktionen.

In Vivo Coronary Stent Imaging

In the presence of stents, the standard contrast-enhanced ECG-gated MSCT protocol is used with a 4 x 1.0 mm and, more recently, 12 x 0.75 mm detector collimation.[5, 6] The density of stents is higher than any other material in or around the heart, including the contrast-enhanced lumen, which is why these devices are easily recognized on both nonenhanced and contrast-enhanced CT images (Figure 6). In vivo imaging of stents is complicated by the same image- degrading artifacts as those that were encountered in the in vitro experiments (Figure 7 and Table 1). In noncoronary vessels with a larger diameter, beam hardening and partial volume effects are present, but limited to the proximity of the stent wall (Figures 8 and 9). In the coronary arteries, the artifacts are of the same magnitude, but because of the small diameter, there is only little

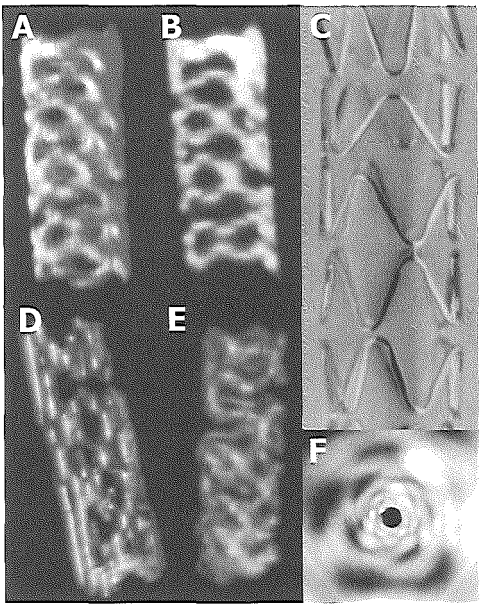

Figures 5A to 5F. MSCT appearance of a 4.0-mm Seaquence stent (Nycomed Amersham, Paris, France; C). The 3-D images show the enlarged stent struts compared to the actual stent dimensions (A to C). Changing appearance when scanned either in a transverse or longitudinal position (D and E). Endoscopic view of the stent (F).

Abbildungen 5A bis 5F. MSCT-Bilder eines 4,0 mm Seaquence-Stents (Nycomed Amemsham, Paris, Frankreich); C) Die dreidimensionalen Bilder zeigen im Vergleich zu den aktuellen Stentdimensionen (A–C) „vergrößerte" Stentstreben. Die unterschiedliche Erscheinungsform zeigt sich sowohl in den transversalen als auch longitudenalen Schnitten (D und E). F) zeigt die endoskopischen Bilder des Stents.

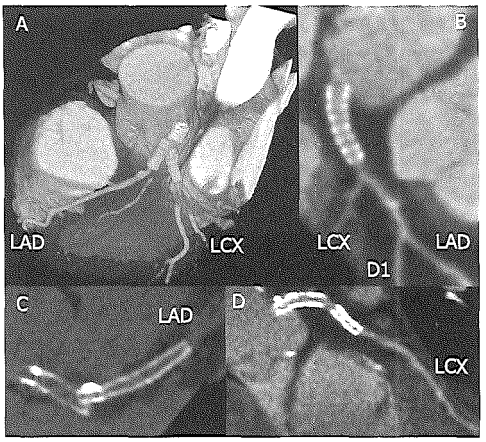

Figures 6A to 6D. Three stents in the left main coronary artery, left anterior descending coronary artery (LAD), and left circumflex coronary artery (LCX; A). A patent low-density stent in the left main coronary artery (B). Nonenhanced scan of two stents in the left main coronary artery and LCX (C). A patent 4.0-mm diameter stent in the left main coronary artery and a less assessable 3.0 mm stent in the LCX (D). Diagonal branch (D1).

Abbildungen 6A bis 6D. Drei Stents im Hauptstamm, im Ramus interventricularis anterior (LAD) und Ramus circumflexus (LCX; A). Man erkennt den offenenen Stent niedriger Dichte im Hauptstamm (B). Bilder ohne Kontrastmittelverstärkung von zwei Stents im Hauptstamm und LCX (C). Ein offener 4,0-mm-Stent im Hauptstamm und ein weniger gut beurteilbarer 3,0-mm-Stent im LCX (B). D1 = Diagonalast.

artifact-free lumen left that can be assessed reliably. Apart from the small vessel and stent size, partial volume effects and beam-hardening artifacts, there are additional complications. The tissues surrounding the heart cause X-ray scattering, and a reduction of the contrast- to-noise. Finally, residual cardiac motion is one of the major causes of nonassessability in MSCT coronary angiography, particularly in patients with high heart rates. The use of β-blockers, in order to reduce the heart rate and prevent the occurrence of residual motion artifacts, significantly improves the interpretability of MSCT coronary angiography.

Coronary Stent Imaging in Clinical Practice

Despite these limitations, MSCT may still be useful in patients who underwent coronary stenting. Stents with thinner struts cause less artifacts and are therefore better assessable (Figure 6). Occlusion, or the presence of a severe stenosis, is generally detectable by CT (Figure 10).

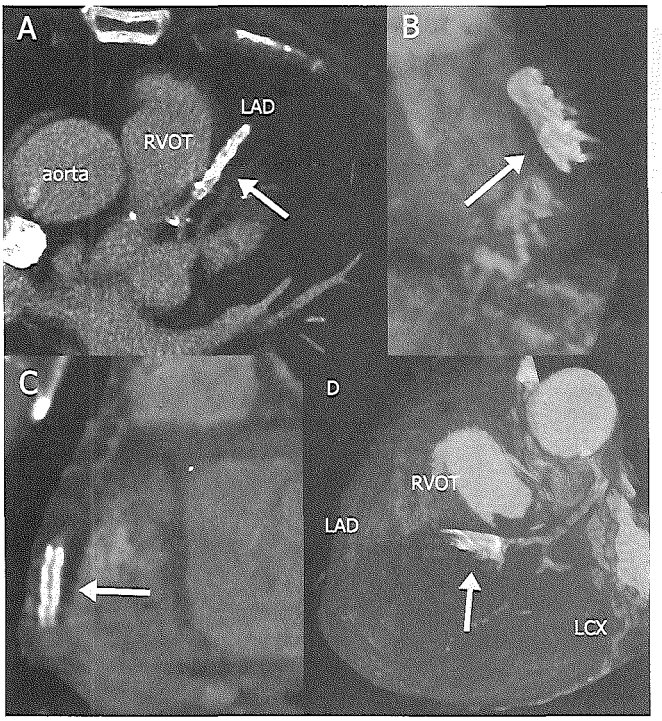

Figures 7A to 7D. Complicated imaging of coronary stents. High-density stent in a calcified left anterior descending coronary artery (LAD; A). Motion and a high-density stent in the right coronary artery (B). A high-density stent in the mid right coronary artery (C). A high-density stent and motion in the LAD (D). Left circumflex coronary artery (LCX), right ventricular outflow tract (RVOT).

Abbildungen 7A bis 7D. Komplexe Bildgebung von Koronarstents. Stent mit hoher Dichte in einer kalzifizierten Läsion des Ramus interventricularis anterior (LAD; A). Bewegungsartefakte bei einem Stent hoher Dichte in der rechten Koronararterie (B). Ein Stent hoher Dichte im mittleren Abschnitt der rechten Koronararterie (C). Ein Stent hoher Dichte und Bewegungsartefakte in der LAD (D). LCX = Ramus cirumflexus, RVOT = rechtsventrikulärer Ausflusstrakt.

However, nonsignificantly stenotic neointimal hyperplasia, stent malapposition, tissue prolaps, and other subtle irregularities in the proximity of the stent wall are usually lost in the metal artifacts. Examination of small stents in distal branches and patients with a high heart rate rarely provides satisfactory results. Finally, patients who underwent angioplasty are at risk for recurrent symptoms due to progression of obstructive disease in the native, nonstented, coronary vessels, which can be detected by MSCT.

Table 1. Limitations in coronary stent imaging. SSP: slice sensitivityprofile.
Tabelle 1. Limitationen der Bildgebung von Koronarstents.

Characteristic	Complication
High-density stent material (steel)	High-density artifacts or blooming
Small stent and vessel size	Small artifact-free lumen
Limited spatial resolution	
Spiral scan mode	Wide-based SSP, increased partial voluming
Heterogeneous X-ray spectrum	Beam-hardening artifacts
Residual cardiac motion	Motion artifacts
Location within the chest	Increased image noise

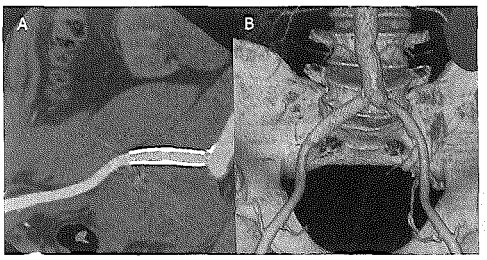

Figures 8A and 8B. Curved multiplanar reconstruction (A) and 3-D volume- rendered reconstruction (B) of a stent in the proximal right iliac artery.

Abbildungen 8A und 8B. „Curved MPR"-Rekonstruktion (A) und dreidimensionale Volumenrekonstruktion (B) eines Stents in der proximalen rechten Arteria iliaca.

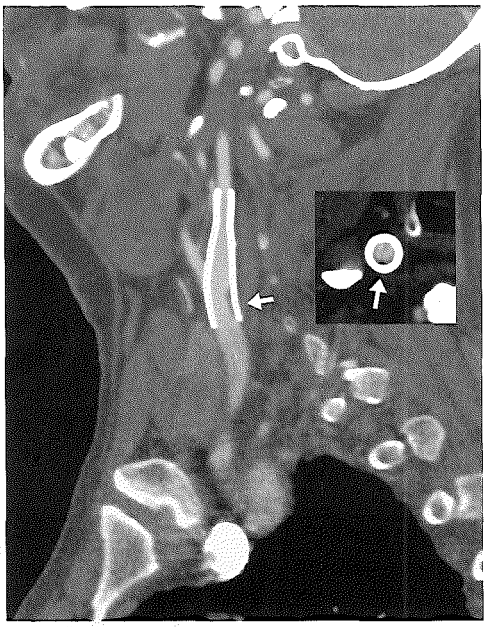

Figure 9. Curved reconstruction and cross section (inset) of a carotid stent with nonstenotic neointimal hyperplasia.

Abbildung 9. „Curved" Rekonstruktion und Querschnitt (Bildeinschub) eines Karotisstents mit nicht stenosierender Neointimahyperplasie.

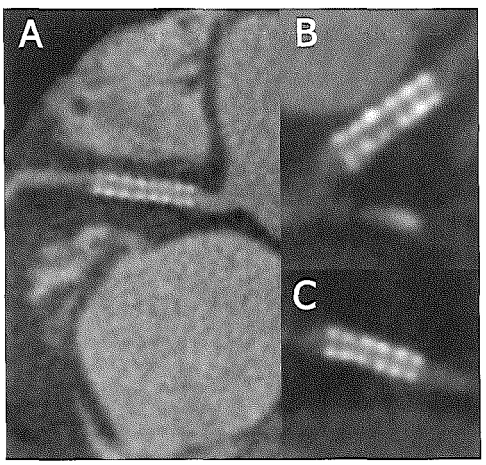

Figures 10a to 10C. Two small (3.0 mm diameter) stents in the proximal right (A) and proximal left anterior descending coronary artery in an axial (B) and longitudinally reconstructed cross section (C). In both stents the stent struts can be distinguished.

Abbildungen 10A bis 10C. Zwei kleine (3,0 mm Durchmesser) Stents in der proximalen rechten Koronararterie und im proximalen Ramus interventricularis anterior in den axialen (B) und longitudinal rekonstruierten Querschnitten (C). In beiden Stents können die einzelnen Streben erkannt werden.

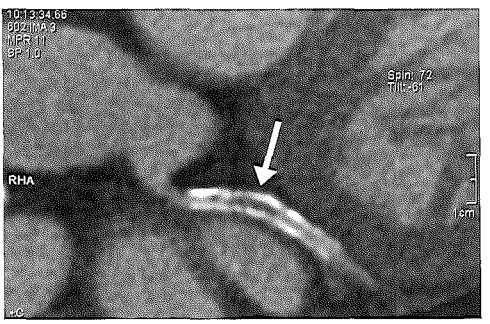

Figure 11. In-stent occlusion (arrow) of a device in the proximal left circumflex coronary artery. The distal vessel segment is most likely contrast- enhanced by collateral filling.

Abbildung 11. Stentverschluss (Pfeil) im proximalen Ramus circumflexus. Der distale Gefäßabschnitt ist wahrscheinlich mit Kontrastmittel über Kollateralen gefüllt.

Requirements for Reliable Coronary Stent Imaging

To better image the coronary arteries, MSCT scanners need thinner detectors to reduce partial volume effects. 16-slice MSCT scanners are equipped with an extended number of thinner slices, rotate at a higher speed, and show significant improvement in image quality and diagnostic accuracy to detect stenotic coronary artery disease.[5] Recent experience with this new technology also suggests improved assessability of coronary stents (Figures 10 and 11). Some correction of the high-density artifacts could be provided by the development of more dedicated data filtering.

Yet, perhaps the most straightforward way to improve stent imaging is, first and foremost, to implant stents without metal artifacts. Current stents consist of thinner struts, but use of low-density nonmetallic material would even be more efficient. Additionally, the development of temporary biodegradable stents also preserves the option of noninvasive follow-up by MSCT coronary angiography.

CONCLUSIONS

In the recent year considerable progress has been made in noninvasive imaging of the coronary arteries. Although advancements in scanner technology will expectedly improve the assessment of coronary arteries with stents, the role of MSCT after percutaneous coronary intervention is, for the time being, limited to the exclusion of complete stent obstruction and evaluation of coronary artery disease in the remaining nonstented segments.

REFERENCES

1. Achenbach S, Giesler T, Ropers D, Ropers D, Ulzheimer S, Derlien H, Schulte C, Wenkel E, Moshage W, Bautz W, Daniel WG, Kalender WA, Baum U. Detection of coronary artery stenoses by contrast- enhanced, retrospectively electrocardiographically-gated, multislice spiral computed tomography. Circulation 2001;103: 2535–8.
2. Kiemeneij F, Serruys PW, Macaya C, Rutsch W, Heyndrickx G, Albertsson P, Fajadet J, Legrand V, Materne P, Belardi J, Sigwart U, Colombo A, Goy JJ, Disco CM, Morel MA. Continued benefit of coronary stenting versus balloon angioplasty: five-year clinical followup of Benestent-I trial. J Am Coll Cardiol 2001;37:1598–603.
3. Knez A, Becker CR, Leber A, Ohnesorge B, Becker A, White C, Haberl R, Reiser M. Usefulness of multislice spiral computed tomography angiography for determination of coronary artery stenoses. Am J Cardiol 2001;88:1191–4.
4. Morice MC, Serruys PW, Sousa JE, Fajadet J, Ban Hayashi E, Perin M, Colombo A, Schuler G, Barragan P, Guagliumi G, Molnar F, Falotico R. A randomized comparison of a sirolimus-eluting stent with a standard stent for coronary revascularization. N Engl J Med 2002;346:1773–80.
5. Nieman K, Cademartiri F, Lemos P, Raaijmakers R, Pattynama P, de Feyter P. Reliable non-invasive coronary angiography using sub-millimetre multislice spiral CT. Circulation 2002;106:2051–4.
6. Nieman K, Rensing BJ, van Geuns RJM, Vos J, Pattynama PMT, Krestin GP, Serruys PW, de Feyter PJ. Non-invasive coronary angiography with multislice spiral CT: impact of heart rate. Heart 2002;88:470–4.

7. Vogl TJ, Abolmaali ND, Diebold T, Engelmann K, Ay M, Dogan S, Wimmer-Greinecker G, Moritz A, Herzog C. Techniques for the detection of coronary atherosclerosis: multi-detector row CT coronary angiography. Radiology 2002;223:212–20.

7. CORONARY STENTS

CHAPTER 7.2

MULTISLICE COMPUTED TOMOGRAPHY CORONARY ANGIOGRAPHY TO ASSESS IN-STENT RESTENOSIS

Filippo Cademartiri[1], MD
Nico Mollet[1,2], MD
Pedro A Lemos[2], MD
Eugene P McFadden[2], FCRPI,FACC
Patrick W Serruys[2], MD,PhD,FACC
Gabriel P Krestin[1], MD,PhD
Pim J de Feyter[1,2], MD,PhD,FACC

Departments of Radiology[1] and Cardiology[2],
Erasmus MC, University Medical Center Rotterdam,
The Netherlands

American Journal of Cardiology (in press).

ABSTRACT

Objective: Establishment of the diagnostic accuracy of multislice computed tomography (MSCT) coronary angiography to evaluate in-stent restenosis.

Background: Multislice spiral computed tomography (MMSCT) is a promising technique for non-invasive coronary angiography.

Methods: 51 patients (42 males, aged 59.8 ± 11.6 years) with previous stent-implantation underwent, ECG-gated MSCT angiography with a 16-slice MSCT scanner (375ms rotation time, 16x0.75mm detector collimation, 600mAs).

The left main (LM), left anterior descending (LAD), left circumflex (LCX), and right coronary artery (RCA), including ³2.0-mm side branches, were independently evaluated by two observers and screened for in-stent restenosis (³50%) and occlusion. The consensus reading was compared with quantitative coronary angiography.

Results: Six (3 restenosis; 3 occlusions) of the 74 (8.1%) evaluated stents were significantly diseased. The sensitivity, specificity and positive and negative predictive value to identify was 83.3% (CI: 35.9-99.6), 98.5% (CI: 92.1-100), 83.3% (CI: 35.9-99.6), and 97.3% (CI: 92.1-100), respectively. One in-stent re-stenosis remained undetected.

Conclusions: MSCT coronary angiography allows the detection of in-stent re-stenosis in a selected population of patients with low and regular heart rate.

INTRODUCTION

Stent-implantation has significantly reduced the occurrence of restenosis compared to balloon angioplasty.[1,2]

Drug-eluting stents have further reduced the frequency of in-stent restenosis compared to bare stent implantation.[3-5]

Traditionally, in-stent restenosis had been assessed by invasive coronary angiography. The latest generation of MSCT scanners is a promising non-invasive alternative to evaluate in-stent restenosis.[6]

We report the diagnostic performance of MSCT to identify in-stent restenosis compared to invasive coronary angiography.

METHODS

Study Population

Fifty-one patients (42 males, aged 59.8±11.6 years) who were referred for evaluation of in-stent restenosis were retrospectively enrolled in the study. The average time interval between previous stent implantation and MSCT coronary angiography was 5.8±1.5 months. The average interval between MSCT and conventional angiography was 4±16 days. A total of 76 stents (mean 1.5±0.7 stent per patient) were implanted.

Table 1. Demographic and angiographic characteristics of assessable segments (n=51 pts; 76 stented segments).

Demographics		Demographics	
age	59.8 ± 11.6	***Stents***	
males	83%	segments*	
previous MI	22%	prox rca	11%
previous CABG	4%	mid rca	9%
previous PCI	16%	distal rca	8%
hypertension	26%	LMC	5%
current smoking	36%	prox LAD	25%
diabetes	13%	mid LAD	13%
Angiographic		distal LAD	3%
single vessel disease	56%	diagonal	9%
double vessel disease	27%	prox LCx	5%
triple vessel disease	18%	marginals and intermediate	9%
hypercholesterolemia	53%	SVG	1%

*count may not sum 100% due to rounding

The site of stent implantation was: saphenous vein graft (SVG) in 1 (1%), right coronary artery (RCA) in 22 (29%), left main coronary (LMC) in 4 (5%), left anterior descending (LAD) in 38 (50%), and left circumflex (LCx) in 11 (15%).

The ethics committee of the university medical center approved the study, and all participating patients gave informed consent.

Scan Protocol and Image Reconstruction

MSCT angiography was performed using a 16-row MSCT scanner with a 0.37s rotation time (Sensation 16®, Siemens). Thirty-four patients (58%) had a pre-scan heart rate (HR) ≥65bpm, and were given a single oral dose of 100 mg metoprolol one hour before the examination in the absence of contraindications. A bolus of 100ml iomeprol (400 mgI/ml; Iomeron®, Bracco) was intravenously injected (4ml/s). To trigger the start of the scan a real-time bolus tracking technique was used. During the scan performed in inspiratory breath hold (18.3±1.4s) the MSCT data and ECG trace were acquired. Scan parameters: detector collimation 16x0.75mm, table feed 8.0mm/s, tube voltage 120kV, 600mAs, and estimated radiation exposure between 11.8-16.3mSv (male-female).

Reconstruction parameters: effective slice width 0.75mm, increment 0.4mm, standard and sharp heart view convolution filters.

Axial slices synchronized to the recorded ECG, were reconstructed from the acquired MSCT data with the use of an algorithm that uses only the data from a half gantry rotation per slice, resulting in a temporal resolution of ≥188ms.

The continuous data acquisition allows slice reconstruction at any time position within the cardiac cycle. An image data set was reconstructed during the mid-to-end diastolic phase, during which coronary artery displacement is relatively little, with reconstruction window positions starting at 400ms before the next R wave. If indicated, additional window positions were explored (usually, 350 and 450ms before the next R wave).

MSCT Image Interpretation

Two observers independently evaluated the MSCT scans by assessment of the axial slices, multiplanar and curved reconstructions. Both reviewers were blinded to the angiographic findings.

Sites with multiple stents in the same vessel were evaluated as a single stent, while stents in bifurcations were evaluated separately as main vessel stent and branch stent.

A stent was considered occluded when the lumen inside the stent was darker than the contrast-enhanced vessel before the stent. This may be associated with absence of vessel lumen opacification distal to the stent. Non-occlusive in-stent re-stenosis was defined if the lumen inside the stent showed a darker rim (eccentric or concentric non-contrast enhanced neo-intimal hyperplasia) between the stent and the contrast-enhanced vessel lumen with a lumen diameter reduction ≥50% (Figure 1, 2, 3). Disagreement was settled by a joined consensus reading.

X-Ray Coronary Angiography

Conventional selective coronary angiography was performed with standard techniques and evaluated by a blinded reviewer with the use of quantitative coronary angiography system (CAAS II, Pie Medical, Maastricht, The Netherlands). The percentage in-stent diameter stenosis, was determined in two orthogonal projections and the percentage stenosis was taken as average of the 2 values.

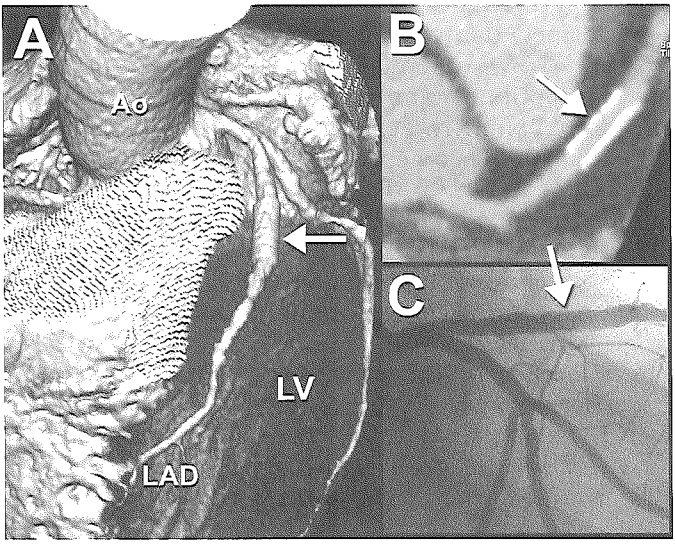

Figure 1. Patent stent in LAD. **A**: three-dimensional volume rendering of the heart showing the left coronary artery and a stent in of the proximal LAD (arrow). **B**: a multiplanar reconstructions showing the left main and the LAD with the patent stent (arrow). The contrast enhancement in the lumen of the stent is comparable with the one before and after the stent. **C**: the corresponding diagnostic coronary angiogram with no in-stent restenosis.
Abbreviations: Ao= ascending aorta; LAD= left anterior descending; LV= left ventricle. (A full color version of this illustration can be found in the color section (chapter 12)).

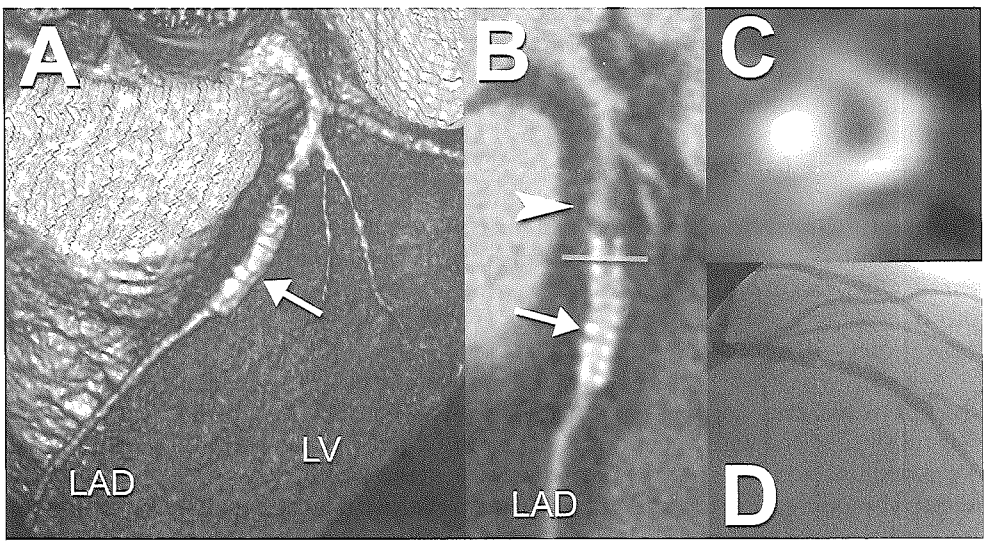

Figure 2. In-stent restenosis in a LAD stent. **A**:three-dimensional volume rendering of the heart showing the left coronary artery and a stent in the proximal LAD (arrow). **B**:a curved reconstructions shows the left main and the LAD with the stent (arrow). An obstructive plaque beginning at the proximal edge of the stent (arrowhead) and continuing within the proximal segment of the stent is visualized. A cross section performed at the level of the proximal segment of the stent (C) shows the in-stent restenosis appearing as hypoattenuating tissue within the stent. The bright zone represents the remaining lumen and on the right side a stent strut. **D**: the corresponding diagnostic angiogram Abbreviations: LAD= left anterior descending; LV= left ventricle. (A full color version of this illustration can be found in the color section (chapter 12)).

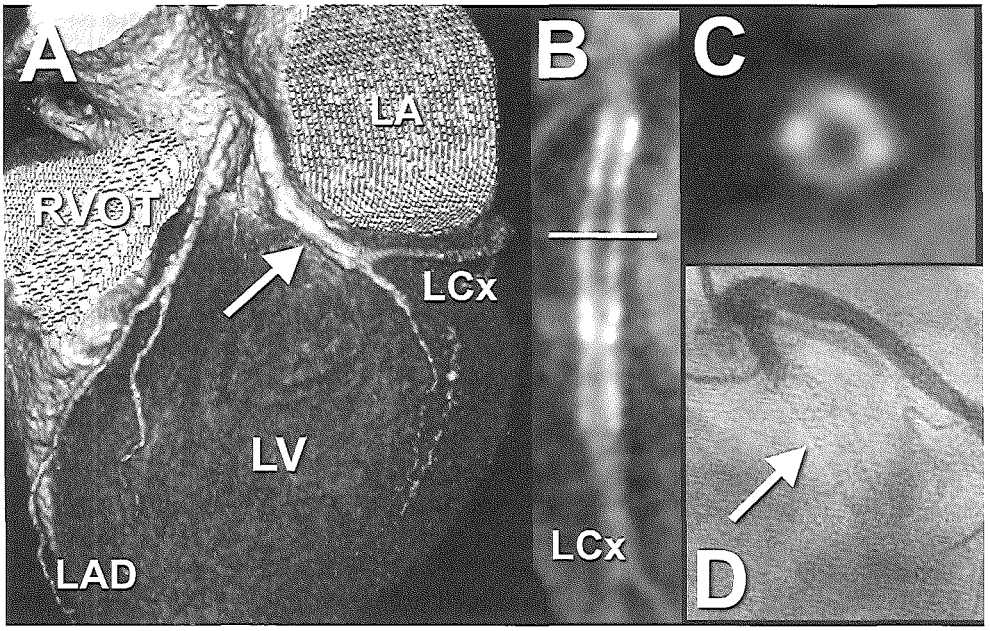

Figure 3. Occluded stent in LCx. **A**: a three-dimensional volume rendering of the left coronary artery, showing a stent in the proximal segment of the the LCx (arrow). **B**: a curved multiplanar reconstruction along the lumen of the LCx, shows the in-stent occlusion appearing as a hypoattenuating region, occupying the whole in-stent lumen. An orthogonal view performed at this level (C) shows the lack of contrast enhancement (dark zone) within the lumen of the occluded stent. **D**: the corresponding diagnostic angiogram. It should be noticed that with CT coronary imaging the distal segment of LCx appears patent (due to collateral retrograde flow), while at conventional coronary angiography there is only faint distal filling of the occluded vessel. Abbreviations: LAD= left anterior descending; LCx= left circumflex; LV= left ventricle; RVOT= right ventricle outflow tract. (A full color version of this illustration can be found in the color section (chapter 12)).

Statistical Analysis

The diagnostic accuracy of MSCT to detect in-stent re-stenosis (≥50%) and occlusion inside the stents was evaluated regarding QCA as the standard of reference. Standard descriptive statistics were calculated for each observer and the precision of the overall parameters was expressed with a 95% confidence interval. Concordance between observers was calculated and expressed by the κ value.

RESULTS

The average HR was 57.1±2.7bpm. In total, 74 stents were available for evaluation. Two stented segments (1.3%) were considered uninterpretable due to residual motion. The incidence of significant intra-stent luminal obstructions (non-occlusive in-stent restenosis[3] and total stent occlusions[3] was 8.1% (6/74), as assessed by conventional angiography.

The overall sensitivity, specificity, positive and negative predictive value to detect significant intra-stent obstructions was 83.3% (CI: 35.9-99.6), 98.5% (CI: 92.1-100), 83.3% (CI: 35.9-99.6), and 98.5% (CI: 92.1-100), respectively (Table 2).

Table 2. Crosstable MSCT vs. angio for the classification of restenosis (n=51 pts; 76 stented segments).

		Angio		
		without restenosis	with restenosis	Total
MSCT	without restenosis	67	1	68
	with restenosis	3	5	6
	with occlusion	3		
	Total	68	6	74

One undetected in-stent re-stenosis was located in the first diagonal (segment 9) and one false positive was located in distal circumflex. In both cases the diameter of the vessel was 2mm. Concordance between both MSCT observers was good (κ value 0.75).

DISCUSSION

Stents are difficult to visualize with CT because the metallic struts cause a severe artifact due to the "blooming effect".[7] This results in an enlarged appearance of the stent struts that affects the capability to visualize the lumen. The artefact depends on the material and design of the stent: (the higher the density the larger the "blooming"). This effect is less important in large vessels, such as the aorta and its abdominal branches, but it impairs the visualization of the lumen in smaller vessels such as coronary arteries.[7]

An earlier study with electron beam CT reported a sensitivity of 78% and specificity of 98% to identify coronary stent patency.[8] In this study assessment of patency was achieved with, a dynamic multisection analysis assessing the attenuation profile proximal and distal of the coronary stent during contrast-enhancement coronary angiography.[8]

In vitro studies have shown that 16 row - MSCT scanners offer a better delineation of the stent struts and of the presence of in-stent restenosis (9). However, in-vivo in-stent lumen evaluation with CT remained difficult and by using a 4-row MSCT scanner it was not possible to visualize stent lumen.[10] In a recent report with 16-row MSCT scanner a sensitivity and specificity of 78% and 100% was reported for the assessment of stent-patency.[6] However, only fifty (77%) of the 65 included stents were assessable due to insufficient image quality.[6]

In that study patency of the stent was defined if the vessel distal to the stent was contrast opacified. However, we have noted in a few instances that that criterion is not full-proof and that collaterals can retrogradely opacify the entire vessel distal to the stent occlusion. We therefore defined in-stent restenosis as the presence of a darker, non-contrast enhanced rim of tissue within the stent-lumen and occlusion as a dark non-opacified occluded region within the stent. In addition an occlusion may be associated with a non-contrast-enhanced vessel distal to the stent. Our first experience with coronary in-stent restenosis evaluation is promising. We were able to visualize both in-stent restenosis and re-occlusion in the

majority of the cases. However, the technique is not sufficiently reliable to allow clinical implementation.

Limitations

The size of the study population is reasonable but due to the use of drug eluting stents the number of patients with an in-stent restenosis or occlusion is rather low. Only patients with stable rhythm and heart rates below 75 bpm were included. The high radiation exposure estimated between 8 to 12 mSv during MSCT coronary angiography remains a matter of concern.

CONCLUSION

Multislice computed tomography coronary angiography allows detection of in-stent restenosis and occlusion with reasonable diagnostic accuracy. The highly attenuating material of stent struts remains an obstacle for optimal visualisation and quantification of in-stent restenosis, in particular in smaller stents. Therefore, higher spatial resolution of new MSCT scanners and use of different stent material (less dense) would improve stent visualisation.

REFERENCES

1. Serruys PW, de Jaegere P, Kiemeneij F, et al. A comparison of balloon-expandable-stent implantation with balloon angioplasty in patients with coronary artery disease. Benestent Study Group. N Engl J Med 1994;331:489-95.
2. Fischman DL, Leon MB, Baim DS, et al. A randomized comparison of coronary-stent placement and balloon angioplasty in the treatment of coronary artery disease. Stent Restenosis Study Investigators. N Engl J Med 1994;331:496-501.
3. Moses JW, Leon MB, Popma JJ, et al. Sirolimus-eluting stents versus standard stents in patients with stenosis in a native coronary artery. N Engl J Med 2003;349:1315-23.
4. Morice MC, Serruys PW, Sousa JE, et al. A randomized comparison of a sirolimus-eluting stent with a standard stent for coronary revascularization. N Engl J Med 2002;346:1773-80.
5. Stone GW, Ellis SG, Cox DA, et al. A polymer-based, paclitaxel-eluting stent in patients with coronary artery disease. N Engl J Med 2004;350:221-31.
6. Schuijf JD, Bax JJ, Jukema JW, et al. Feasibility of assessment of coronary stent patency using 16-slice computed tomography. Am J Cardiol 2004;94:427-30.
7. Maintz D, Juergens KU, Wichter T, Grude M, Heindel W, Fischbach R. Imaging of coronary artery stents using multislice computed tomography: in vitro evaluation. Eur Radiol 2003;13:830-5.
8. Pump H, Mohlenkamp S, Sehnert CA, et al. Coronary arterial stent patency: assessment with electron-beam CT. Radiology 2000;214:447-52.
9. Maintz D, Seifarth H, Flohr T, et al. Improved coronary artery stent visualization and in-stent stenosis detection using 16-slice computed-tomography and dedicated image reconstruction technique. Invest Radiol 2003;38:790-5.

10. Kruger S, Mahnken AH, Sinha AM, et al. Multislice spiral computed tomography for the detection of coronary stent restenosis and patency. Int J Cardiol 2003;89:167-72.

7. CORONARY STENTS

CHAPTER 7.3

NEOINTIMAL HYPERPLASIA IN CAROTID STENT DETECTED WITH MULTISLICE COMPUTED TOMOGRAPHY

Filippo Cademartiri, MD[1]
Nico Mollet, MD[1,2]
Koen Nieman, MD[1,2]
Gabriel P. Krestin, MD, PhD[1]
Pim J. de Feyter, MD, PhD[1,2]

From the Departments of Radiology[1] and Cardiology[2]
Erasmus MC, University Medical Center Rotterdam, The Netherlands.

Circulation, 108:e147, 2003.

Movies I through VII are available in the online-only Data Supplement at http://www.circulationaha.org.

The latest generation of 16-row multislice computed tomography (MSCT) scanner offers high temporal and submillimeter spatial resolution, which allows the visualization of carotid artery atherosclerosis.

At present, carotid artery obstructions are increasingly treated with stent implantation. However, in-stent restenosis may occur within 6 months after stent implantation. MSCT allows the presence and extent of intimal hyperplasia to be monitored.

A 65-year-old symptomatic man with high-grade right carotid artery stenosis underwent wall stent implantation. The stent was positioned in the common carotid artery and internal carotid artery. After 11 months, the patient underwent 16-row MSCT (Sensation 16, Siemens Medical Solutions, Forchheim, Germany) (Figure). A rim of in-stent neointimal hyperplasia was shown, demonstrating the feasibility of using noninvasive MSCT to image in-stent neointimal hyperplasia. The density of the tissue was 75.6 ± 5.6 Hounsfield units, which suggested the presence of fibrotic tissue.

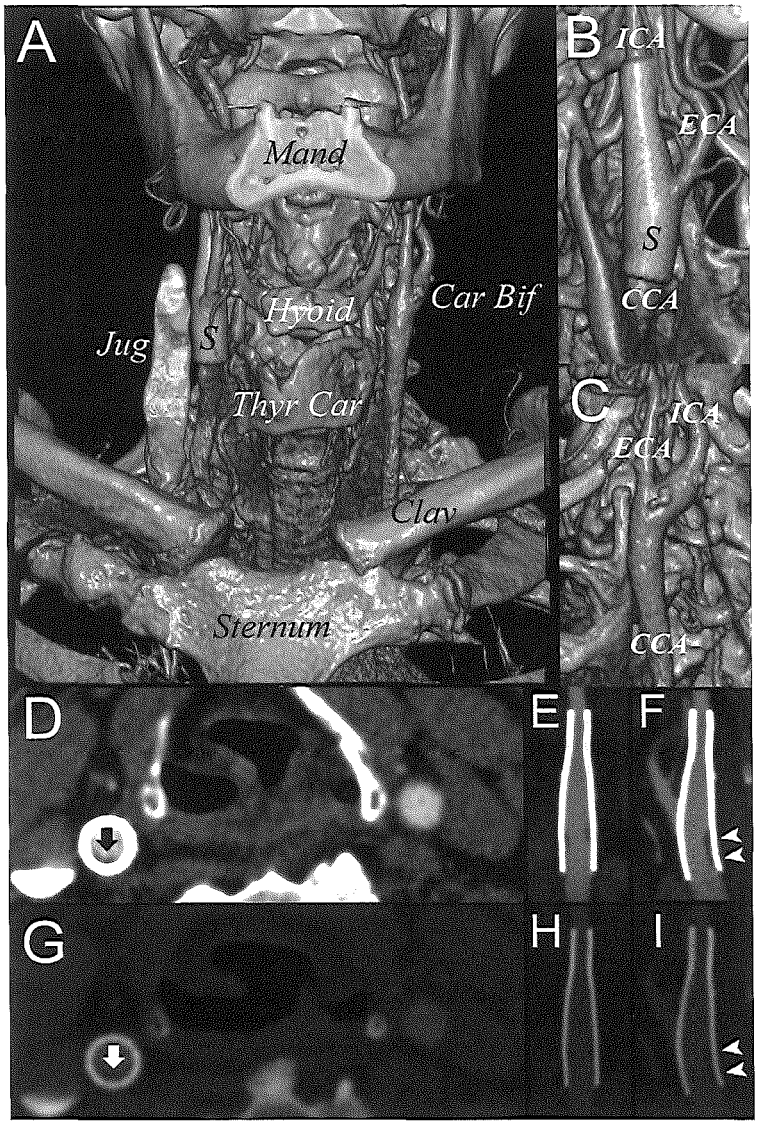

Direct 3-dimensional volume rendering (**A**, **B**, and **C**) shows the anatomy of the arteries of the neck at the level of the carotid bifurcation (Car Bif) (**see also Movies IV, V, and VI**). Clav indicates clavicle; Hyoid, hyoid bone; Jug, jugular vein; Mand, mandible; and Thyr Car, thyroid cartilage. A magnified view of the right (**B**) and left (**C**) carotid bifurcations permits recognition of the common carotid artery (CCA), the internal and external carotid arteries (ICA and ECA), and the wall stent (S) at the right side. The left carotid bifurcation (**C**) is patent but is slightly dilated at the origin of ICA. A few calcified spots also are present. Note the backflow of iodinated contrast material into the right jugular vein (Jug in **A**). Multiplanar reformats (**D** through I) show the lumen of the stent. One window setting is used for the visualization of soft tissue (**D**, **E**, and **F**), and another window setting permits the visualization of high-density structures such as stents (**G**, **H**, and **I**). Intimal hyperplasia can be appreciated in Movie I and in sagittal reformats (arrowheads in **F** and **I**; **Movie II**). Because of the spatial orientation of the intimal hyperplasia, the coronal reformats (**E** and **H**; **Movie III**) do not allow an optimal visualization. (A full color version of this illustration can be found in the color section (chapter 12)).

7. CORONARY STENTS

CHAPTER 7.4

IN-STENT NEO-INTIMAL HYPERPLASIA WITH 16-ROW MULTISLICE CT CORONARY ANGIOGRAPHY

Nico R. Mollet, MD[1,2]
Filippo Cademartiri, MD[2]

from the Departments of Cardiology, Thoraxcenter[1] and Radiology[2], Erasmus MC, University Medical Center Rotterdam, The Netherlands

Circulation, 110, e514, 2004.

CASE DESCRIPTION

A 55-year-old woman was admitted with unstable angina pectoris. She had no risk factors for coronary disease. The admission ECG showed ST-depression in leads I, II, aVL, aVF, V2-V6. Serial Troponin T and cardiac enzyme measurements were normal. Multislice CT (MS-CT) coronary angiography, using a 16-row MS-CT scanner, showed a high-grade stenosis of the left main coronary artery with no other significant lesions (Figure 1a-c, Video 1). Conventional angiography was performed the same day and confirmed the diagnosis. Immediate percutaneous intervention was undertaken and a bare-metal stent (diameter 5.0 mm, length 18 mm) was successfully implanted from the left main into the left anterior descending coronary artery with excellent final angiographic result.

Follow-up MSCT coronary angiography four months later showed moderate neo-intimal hyperplasia within the stent (Figure 2 a-b, Video 2), which was confirmed by conventional angiography (Figure 2 c-d).

MSCT coronary angiography is a useful clinical tool for diagnosis and in-stent neo-intimal hyperplasia assessment of left main coronary artery disease.

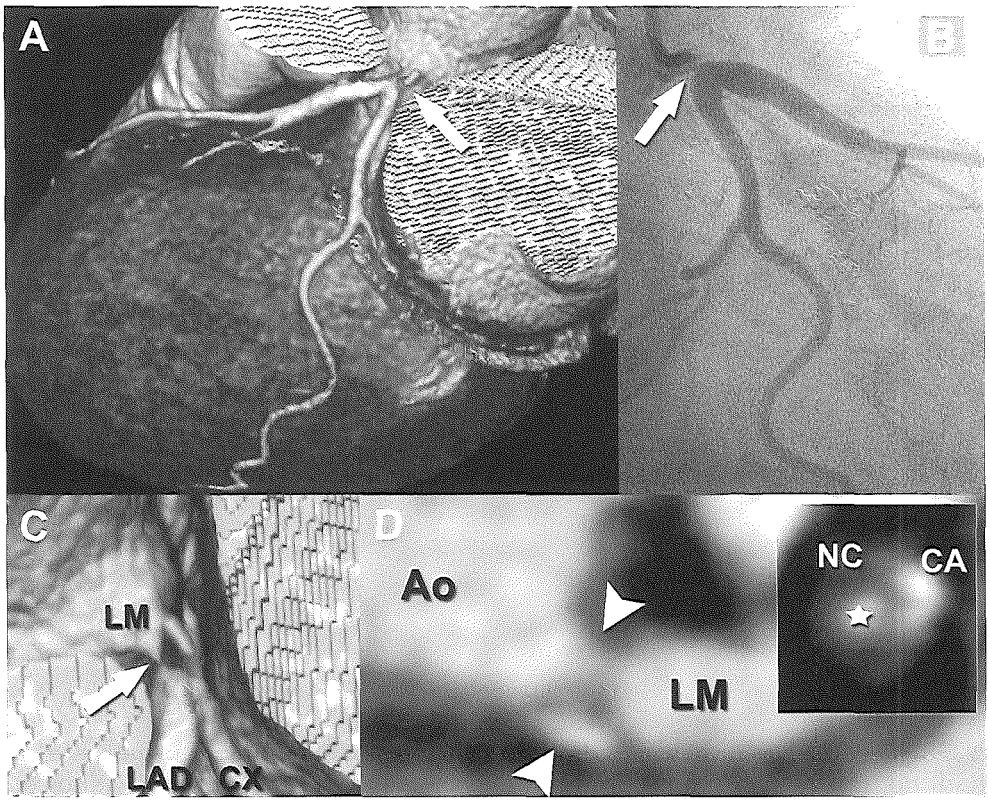

Figure 1. Volume Rendered (**A, B**) and Multiplanar Reconstruction (**C**) images show a high-grade stenosis of the left main coronary artery (arrows), afterwards confirmed on conventional angiography (arrow, **D**). A cross-sectional image of the lesion (inlay) shows calcified (CA) and non-calcified (NC) plaque tissue components surrounding the lumen (asterisk). (A full color version of this illustration can be found in the color section (chapter 12)).

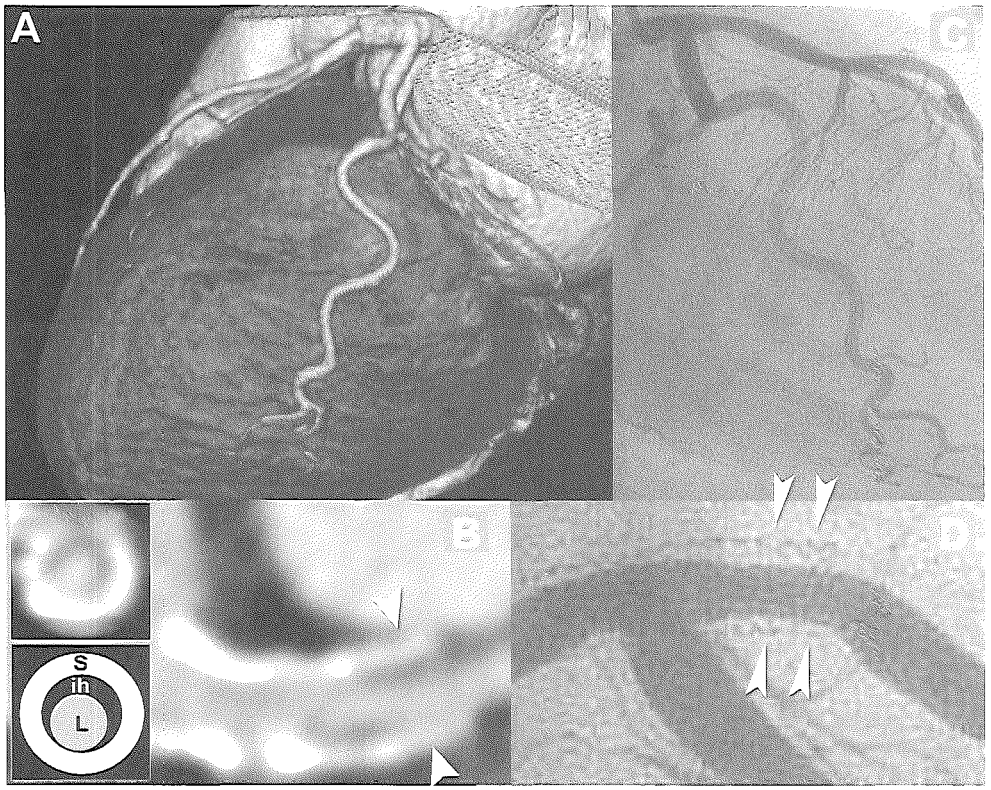

Figure 2. Volume Rendered image (**A**) and corresponding conventional angiography image (**D**) after 4 months follow-up. Figure **B** (including inlays) show moderate neo-intimal hyperplasia (ih) presenting as a dark rim surrounding the lumen (L), located at the distal part of the stent (S), afterwards confirmed on conventional angiography (arrowheads, **D**). (A full color version of this illustration can be found in the color section (chapter 12)).

8. CORONARY PLAQUES

CHAPTER 8.1

MULTISLICE COMPUTED TOMOGRAPHY: ASSESSMENT OF CORONARY PLAQUE BURDEN

Nico R. Mollet, MD[1,2]
Filippo Cademartiri, MD[2]
Koen Nieman, MD,PhD[1,2]
Fransesco Saia, MD[1]
Eugene P. McFadden, MD[1]
Pedro A. Lemos, MD[1]
Peter M.T. Pattynama, MD, PhD[2]
Patrick W. Serruys, MD, PhD[1]
Gabriel P Krestin, MD, PhD[2]
Pim J. de Feyter, MD, PhD[1,2]

from the Departments of Cardiology, Thoraxcenter[1] and Radiology[2], Erasmus MC, University Medical Center Rotterdam, The Netherlands

Am J Cardiol, (in press)

ABSTRACT

Background: Recent technical advances in Multislice Computed Tomography (MSCT) permit more detailed assessment of coronary plaques.

Methods: Coronary plaque imaging with 16-row MSCT was performed to evaluate plaque burden, composed as: plaque extent (number of diseased coronary segments), size (small and large), distribution ≥plaque in left main (LM), left anterior descending (LAD), left circumflex (LCX), and right coronary artery (RCA), and type (calcified, non-calcified, or mixed).

Of 83 patients included, 78 (94%) had fully evaluable MSCT scans of the entire coronary tree, including major and side-branches (≥2mm) comprising a total of 855 segments. These 78 patients (92% male, mean age 57±6.6) had stable angina pectoris, regular heart rhythm, and a heart rate <70 b.p.m. (spontaneous or medically induced).

Results: Plaque was present in 57% (487/855) of all segments. The number of segments with a plaque per patient was 6.2±3.9. A large plaque was present in 33% and predominantly located in proximal and mid LAD and RCA, and a small plaque in 67%. Plaques were located preferentially in proximal and mid LAD (80% and 78% resp.), RCA (78% and 77% resp.), LCx (66% and 46% resp.), and LM (51%). Calcified plaques were present 65%, non-calcified 24%, and mixed 11%.

Conclusions: MSCT coronary imaging of clinically relevant coronary segments allows non-invasive assessment of the coronary plaque burden in selected patients with stable angina.

INTRODUCTION

Coronary calcium is a definite marker of coronary atherosclerosis.[1-3] Electron Beam Tomography (EBT) can accurately quantify coronary calcium. The amount of coronary calcium highly correlates with the amount of atherosclerosis, but severely underestimates the histological measured coronary plaque burden.[1,4,5] EBT and spiral Multislice Computed Tomography (MSCT) scanners can also non-invasively assess presence and location of coronary obstructions.[6-9] The most recent scanner, the 16-row MSCT scanner, has an improved resolution, which does permit more detailed imaging of coronary plaques. Non-invasive assessment of coronary plaques may further enhance our understanding of the development of atherosclerosis. In this study we assessed the coronary plaque burden in patients with stable angina pectoris.

METHODS

Subjects

Over an 8-month period, 83 consecutive patients with stable angina pectoris underwent 16-row MSCT coronary angiography and conventional coronary angiography. Patients were eligible for inclusion if they had a stable heart rhythm, a heart frequency less than 70 b.p.m. (spontaneous or medically induced), and were able to breath hold for 20 seconds. Excluded were patients with known intolerance to iodinated contrast material, serious renal or pulmonary dysfunction, unstable angina or acute coronary syndrome, previous bypass graft surgery, stent implantation or pregnant women.

The study was approved by the local medical ethics committee, and all patients gave written informed consent.

Patient preparation

The majority of the patients already used a β-blocker (70%, 58/83). Forty-eight percent (40/83) of the patients received 100 mg metoprolol-tartraat (Selokeen®, AstraZeneca Pharmaceutics, UK) orally one hour before the examination because of a pre-scan heart rate of >65 b.p.m.

MSCT data acquisition and image reconstruction

All MSCT examinations were performed using a 16-detector row MSCT scanner (Sensation 16, Siemens Medical Solutions, Forcheim, Germany). A bolus of 120 ml of iodinated contrast material (Visipaque® 320, Amersham Health, Little Chalfont, UK) was administered through an antecubital vein (4 ml/s). Scan parameters: detector collimation 16 x 0.75 mm, table feed 3.0 mm/rotation, gantry rotation time 0.42 s, tube voltage 120 kV and 400-500 mAs. Prospective X-ray tube modulation was applied in 53% (41/78) of the patients, which has been estimated to reduce the radiation dose by 30 to 50%.[10,11] To obtain motion-free image quality, axial slices were reconstructed within the mid- to end-diastolic phase. Three datasets were reconstructed with a reconstruction window starting at 350, 400 and 450 ms prior to the next R-wave, and the most optimal high-quality dataset (least motion artifacts) was selected and sent to a dedicated

workstation (Leonardo, Siemens Medical Solutions, Forcheim, Germany) for evaluation. Additional reconstruction windows were explored when this was deemed necessary.

Conventional X-ray coronary angiography

Conventional coronary angiography was performed within 3 weeks after the MSCT scan using standard techniques. The coronary arteries were divided in segments according to the AHA classification.[13] Unaware of MSCT results, the diameters of all coronary segments and branches were measured, using a quantitative coronary angiography (QCA) algorithm (CAAS, Pie Medical Imaging, Maastricht, The Netherlands). Only branches of ≥2mm were included for comparison with MSCT. Coronary lesions were quantified by QCA and were classified as significantly obstructive if an average lumen diameter reduction of ≥50% in two orthogonal views was present.

MSCT image interpretation

The MSCT-scans were evaluated by two observers, independently, and blinded to the diagnostic coronary angiography data. Disagreements were resolved by consensus after consultation with a third observer. The coronary tree segments were evaluated using dedicated post-processing techniques such as multiplanar reconstructions and thin-slab maximum intensity projections to detect and to classify plaques.

MSCT image classification

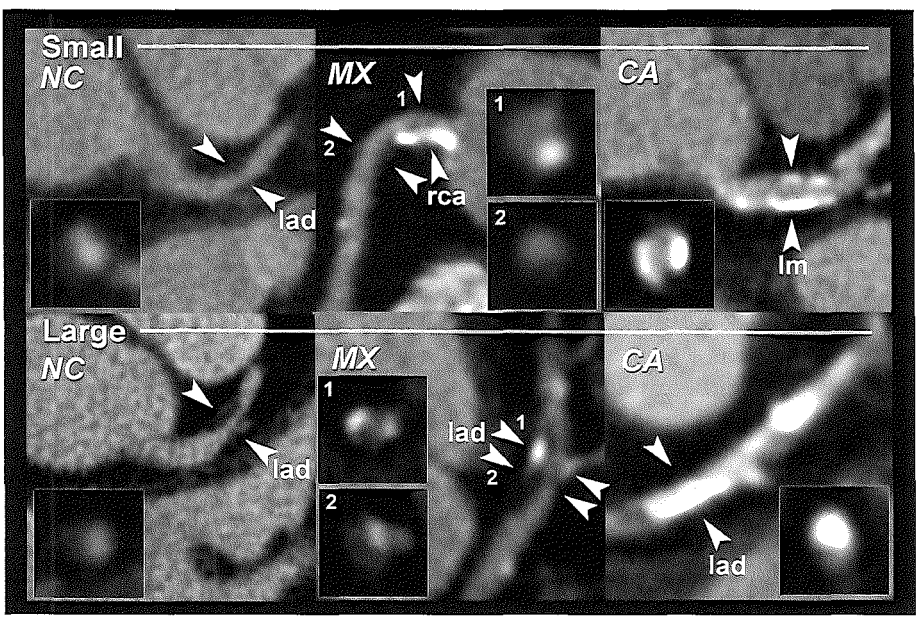

Figure 1. Plaque type and size. Arrowheads indicate the location of the corresponding cross-sectional images (inserts).
NC : non-calcified plaque; MX : mixed plaque; CA : calcified plaque;. LAD: left anterior descending coronary artery. RCA: right coronary artery. LM : left main.

Plaque burden was defined as an overall assessment of plaque extent, plaque distribution, plaque size (small or large), and plaque type (calcified, non-calcified, mixed plaque) with MSCT. Plaque extent was defined as the number of coronary segments with the presence of a plaque. Plaque distribution was defined as the occurrence of a plaque in the proximal, middle and distal coronary segments of left anterior descending (LAD), left coronary circumflex (CX), right coronary artery (RCA), large side branches, and the left main (LM). Plaques were classified according to their size into small and large plaques.

Small plaques were defined as plaques with <50% lumen reduction, and plaques with ≥50% lumen reduction as large. A calcified plaque was defined as a high-density lesion and a non-calcified plaque was defined as a soft-tissue-density lesion clearly distinguishable from the adjacent epicardial fat and the coronary lumen. A mixed plaque was defined as a combination of a non-calcified and a calcified plaque (figure 1).

Statistical analysis

Inter- and intra-observer variability of MSCT readers were calculated for plaque extent, distribution, and size for the first 30 patients by use of κ-statistics. The κ-value for inter- and intra-observer agreement regarding plaque extent and distribution were 83% and 87% respectively, whereas the κ-values regarding plaque size was 72% and 74% respectively.

The diagnostic accuracy of MSCT coronary angiography to detect significant coronary obstructions was determined regarding QCA as the reference standard. Precision of the overall parameters regarding to stenoses detection was expressed with a 95% confidence interval.

RESULTS

Over an 8-month period, 83 eligible patients with stable angina underwent MSCT. MSCT was not of diagnostic quality in 4 patients due to motion artifacts and technical failure in one case. Thus, 78 patients had evaluable scans. The majority of these patients (92%, 76/84) were men. Risk factors for atherosclerosis were hypercholesterolemia 62% (48/78), hypertension 59% (46/78), smoking 33% (26/78), BMI >27kg/m^2 32% (25/78), and diabetes mellitus 22% (17/78). Conventional coronary angiography showed non-significant stenoses in 9 patients, one vessel disease in 27 patients, and multi-vessel disease in 42 patients.

The mean heart rate was 57±6.6 b.p.m. during the scan procedure. After exclusion of all segments distal to an occlusion and small (<2mm) segments, a total of 855 segments were included for further analysis.

MSCT coronary plaque burden (table 1)

More than half of the evaluated coronary segments contained a plaque (57%, 487/855). Twenty-four percent of the plaques were classified as non-calcified, 11% as mixed, and 65% as calcified (figure 2). Thirty-four percent of the plaques were large and 66% were small plaques. The frequency of large plaques was higher in mixed plaques when compared with non-calcified and calcified plaques (82% vs. 46% and 49%). Large plaques were preferentially located at the proximal and mid part of the

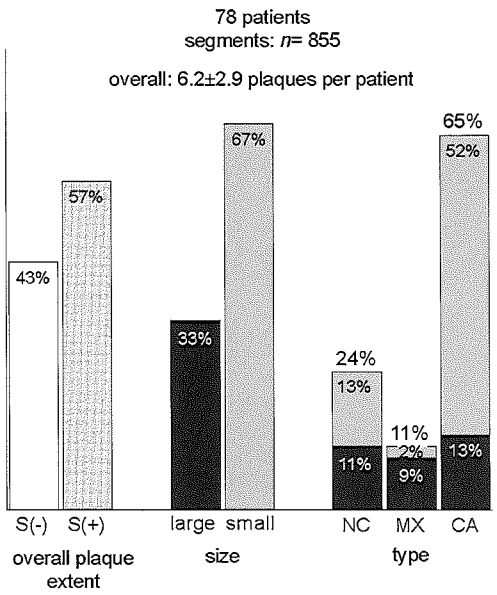

Figure 2. Plaque extent, size, and type.
S(-):segments without plaque; S(+): segments with plaque; NC: non-calcified plaque; MX: mixed plaque; CA: calcified plaque. L: large plaque ; S: small plaque.

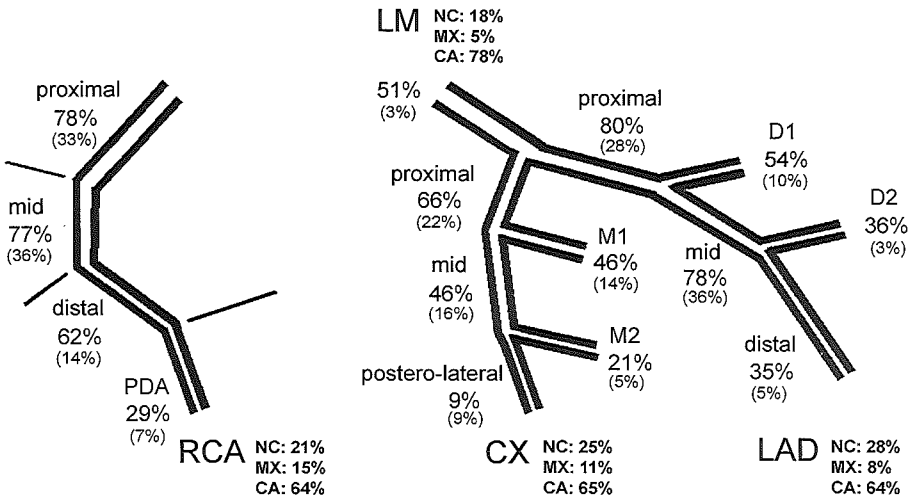

Figure 3. Plaque distribution and size. Percentage of segments with plaque, and percentage of large plaques (?50% lumenal obstruction, between brackets). LM : left main. RCA : right coronary artery. CX : circumflex coronary artery. LAD : left anterior descending coronary artery.
PDA: posterior descending artery; M1: first marginal branch; M2: second marginal branch; D1: first diagonal branch; D2: second diagonal branch.

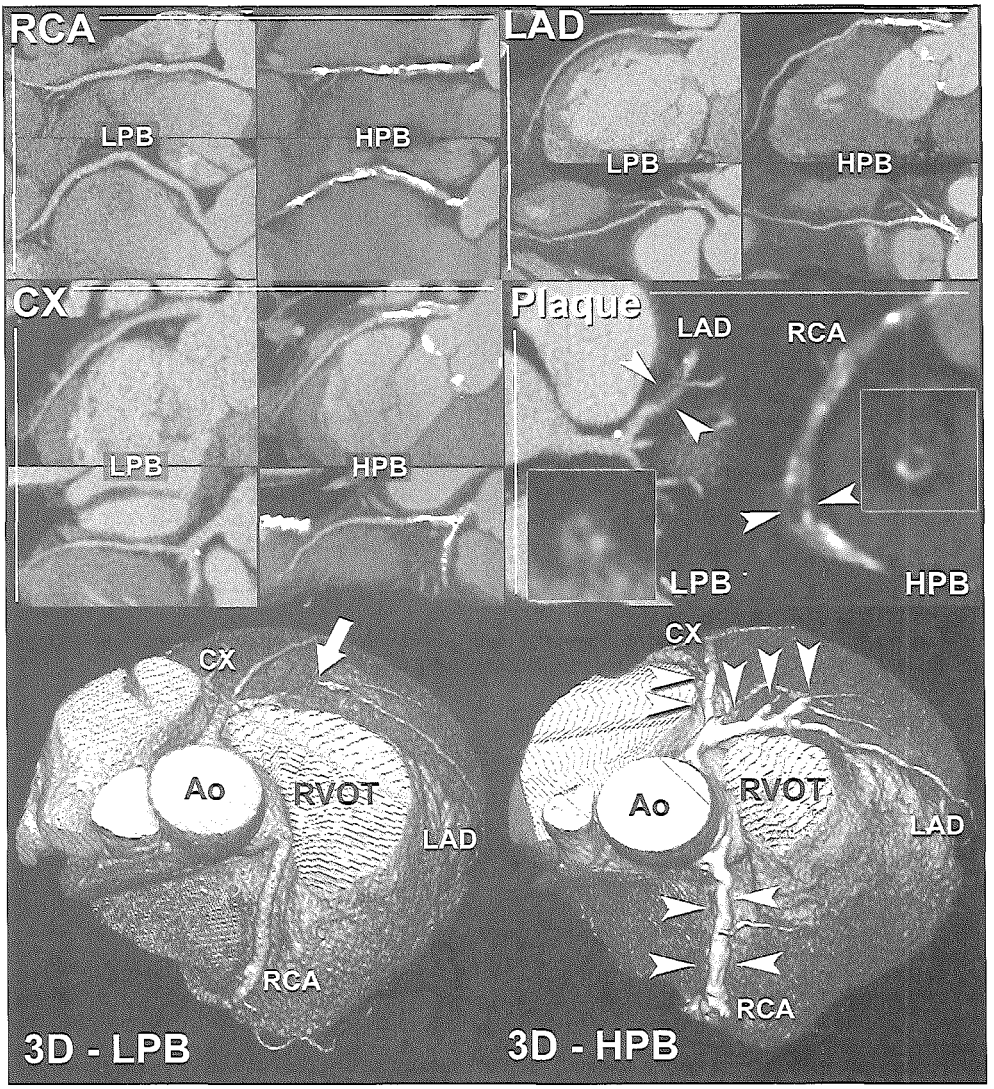

Figure 4. Low coronary plaque burden versus high coronary plaque burden. **Upper panels and left middle panel** demonstrate curved multiplanar reconstruction of low versus high plaque burden in RCA, LAD and CX in two orthogonal projections. The **middle right panel** shows multiplanar reconstructions of a large plaque in the proximal LAD (**left**), and a total occlusion of mid RCA. Arrowheads indicates the location of the corresponding cross-sectional images (**small panels**). The 3D images in the lower panel are reconstructed using a volume rendering technique. The arrow in the **left panel** indicates a large plaque of the LAD in a patient with an overall low plaque burden, and the arrowheads in the **right panel** indicate various plaques in a patient with a high plaque burden.
LPB : low plaque burden; HPB: high plaque burden; Ao: aorta; RVOT: right ventricular outflow tract. 3D : 3-dimensional.
(A full color version of this illustration can be found in the color section (chapter 12)).

Table 1. MSCT coronary plaque burden: plaque extent, type, size, and distribution.

LCA	n segments	plaques(%)	large(%)	non-calcified(%)	mixed(%)	calcified(%)
LM	78	40(51)	2(3)	7(18)	2(5)	31(78)
LAD proximal	78	62(80)	22(28)	17(27)	9(15)	36(58)
LAD mid	72	56(78)	27(38)	19(34)	3(5)	34(61)
LAD distal	63	22(35)	3(5)	2(9)	3(14)	17(77)
1st diagonal	59	32(54)	7(12)	9(28)	0(-)	23(72)
2nd diagonal	31	11(36)	1(3)	4(36)	0(-)	7(64)
LAD overall	303	183(60)	60(20)	51(28)	15(8)	117(64)
CX proximal	68	45(66)	15(22)	7(16)	6(13)	32(71)
CX mid	62	30(46)	10(16)	6(20)	3(10)	21(70)
1st marginal	65	30(46)	8(12)	8(27)	3(10)	19(63)
2nd marginal	39	8(21)	3(8)	6(75)	0(-)	2(25)
postero-lateral	11	1(9)	1(9)	1(100)	0(-)	0(-)
CX overall	245	114(47)	37(15)	28(25)	12(11)	74(65)
RCA	n segments	plaques(%)	large(%)	non-calcified(%)	mixed(%)	calcified(%)
RCA proximal	76	59(78)	29(38)	15(25)	9(15)	35(59)
RCA mid	62	48(77)	24(39)	10(21)	10(21)	28(58)
RCA distal	50	31(62)	7(14)	4(13)	1(3)	26(84)
PDA	41	12(29)	2(5)	3(25)	2(17)	7(58)
RCA overall	229	150(66)	62(27)	32(21)	22(15)	96(64)
Overall	n segments	plaques(%)	large(%)	non-calcified(%)	mixed(%)	calcified(%)
All vessels	**855**	**487(57)**	**161(33)**	**118(24)**	**51(11)**	**318(65)**

LCA, left coronary artery; RCA, right coronary artery; LM, left main; LAD, left anterior descending; CX, circumflex; PDA, posterior descending.

LAD and the RCA. The plaque extent, distribution, size, and type are tabulated in table 1. The segmental distribution of plaques, shows that the proximal and mid segments of the LAD, RCA, and LCx are most frequently affected (figure 3,4). In more than half of the patients a plaque was detected in the left main. The distribution of the type of plaques in each coronary vessel is shown in figure 3.

Diagnostic accuracy of MSCT coronary angiography for detection of significant stenoses

The MSCT coronary angiography results were compared with the conventional coronary angiography results. MSCT coronary angiography correctly detected 147 of 154 significant obstructive plaques. Seven plaques were detected with MSCT but incorrectly classified as non-significant (QCA: mean diameter reduction 61.0±6.4%). Fourteen plaques, of which 13 were heavily calcified, were incorrectly classified by MSCT as significantly obstructed (QCA: mean diameter reduction 30.5±11.5%). Overall sensitivity, specificity, positive predictive value and negative predictive value were calculated as 96% (95% CI: 90-98), 98% (95% CI: 96-98), 91% (95% CI: 85-95), and 99% (95% CI: 97-99) respectively.

Discussion

The ultimate objective of non-invasive imaging of the coronary arteries is to identify significant lumenal stenoses and to identify plaques that may, in the future, be responsible for an acute coronary syndrome. Earlier studies have shown that non-invasive calcium quantification with EBT correlated well with the extent of atherosclerosis, but seriously under-estimated the total coronary plaque burden.[1-5] Correlation with histology revealed that the amount of calcium detected by EBT was only about one-fifth of the measured atherosclerotic plaque burden1. The newest 16-detector row MSCT technology has improved sensitivity to detect obstructive and non-obstructive lesions and permits to detect both calcified and non-calcified plaques.[12,13] Non-calcified plaques may consist of lipid accumulation or fibrous tissue. It has been suggested that on the basis of differences in the X-ray beam attenuation properties of these tissues expressed as differences in Hounsfield units, one could distinguish between lipid and fibrous tissue.[14] We have not further subdivided non-calcified coronary plaques because we noted considerable intra-plaque variability in the measured Hounsfield units, which precluded the distinction between lipid and fibrous plaques. In our study we observed that 24% of the total number of plaques were non-calcified and 11% were mixed (combination of non-calcified and calcified). The MSCT overall plaque burden assessment is a significant expansion compared to the established EBT calcium quantification and may more closely correlate with the total measured atherosclerotic plaque burden as determined by histology. However, one should take into account that the resolution of the current MSCT scanners does not allow to assess the earlier phases of atherosclerosis, thus underestimation of the total coronary plaque burden still remains. Especially detection of small non-calcified plaques remains challenging, while the higher tissue contrast difference of small calcified plaques allows more easy detection and explains why the majority of small plaques were calcified. Further technical advances resulting in higher spatial resolution and more heart-rate independent data acquisition, are needed for more accurate detection and classification of small plaques.

The MSCT coronary plaque distribution is similar to the distribution shown in pathology and angiographic studies.[15-19] The most frequently affected segments were the proximal and mid segments of the left anterior descending coronary artery and the right coronary artery.

The diagnostic performance of current 16-row MSCT scanners was fairly high to detect obstructive coronary plaques. The sensitivity has been reported to be between 92 and 95% with a specificity ranging between 86% and 93%,[12,13] when compared to invasive conventional coronary angiography. Our study was not designed to evaluate the diagnostic accuracy of 16-detector row MSCT to detect significant coronary stenoses. However, in a subanalysis we presented the data to provide a sense of the image quality of current MSCT scanners. In this study the sensitivity was 96% and the specificity was 98%, but these numbers should be interpreted with caution because only patients with high quality images

were included into the analysis while 6% of patients with insufficient image quality were excluded.

Limitations

The outcome of the study should be interpreted with caution because the patient population in this study was selective. Only patients with stable angina, stable heart rhythm and slow heart rate (less than 70 b.p.m. either spontaneous or β-blocker included), which are variables predictive of high-quality CT-scan imaging, were included into the study. The results of the study may be different in asymptomatic individuals, or patients with acute coronary syndromes.

The high radiation exposure of the patient during MSCT coronary angiography which is reported between 7.1 and 10.9 mSv remains a matter of concern.[10,11,20,21] The radiation exposure can be reduced by 30% to 50% using the prospective X-ray tube current modulation setting.[10,11] In our experience, this setting can only be used in patients with a very stable heart rhythm and a heart rate less than 60 b.p.m., which was the case in approximately 50% of the procedures.

CONCLUSION

MSCT assessment of the coronary plaque burden is feasible and may be a useful addition to the diagnostic armamentarium to increase our understanding of the development of coronary atherosclerosis. It may carry additional prognostic information and is expected to improve management of patients with coronary atherosclerosis.

REFERENCES

1. Rumberger JA, Simons DB, Fitzpatrick LA, Sheedy PF, Schwartz RS. Coronary artery calcium area by electron-beam computed tomography and coronary atherosclerotic plaque area. A histopathologic correlative study. Circulation 1995; 92:2157-62.
2. Simons DB, Schwartz RS, Edwards WD, Sheedy PF, Breen JF, Rumberger JA. Noninvasive definition of anatomic coronary artery disease by ultrafast computed tomographic scanning: a quantitative pathologic comparison study. J Am Coll Cardiol 1992; 20:1118-26.
3. Sangiorgi G, Rumberger JA, Severson A, et al. Arterial calcification and not lumen stenosis is highly correlated with atherosclerotic plaque burden in humans: a histologic study of 723 coronary artery segments using nondecalcifying methodology. J Am Coll Cardiol 1998; 31:126-33.
4. Baumgart D, Schmermund A, Goerge G, et al. Comparison of electron beam computed tomography with intracoronary ultrasound and coronary angiography for detection of coronary atherosclerosis. J Am Coll Cardiol 1997; 30:57-64.
5. Schmermund A, Baumgart D, Adamzik M, et al. Comparison of electron-beam computed tomography and intracoronary ultrasound in detecting calcified and noncalcified plaques in patients with acute coronary syndromes and no or minimal to moderate angiographic coronary artery disease. Am J Cardiol 1998; 81:141-6.

6. Rensing BJ, Bongaerts A, van Geuns RJ, van Ooijen P, Oudkerk M, de Feyter PJ. Intravenous coronary angiography by electron beam computed tomography: a clinical evaluation. Circulation 1998; 98:2509-12.
7. Achenbach S, Moshage W, Ropers D, Nossen J, Daniel WG. Value of electron-beam computed tomography for the noninvasive detection of high-grade coronary-artery stenoses and occlusions. N Engl J Med 1998; 339:1964-71.
8. Achenbach S, Giesler T, Ropers D, et al. Detection of coronary artery stenoses by contrast-enhanced, retrospectively electrocardiographically-gated, multislice spiral computed tomography. Circulation 2001; 103:2535-8.
9. Nieman K, Oudkerk M, Rensing BJ, et al. Coronary angiography with multi-slice computed tomography. Lancet 2001; 357:599-603.
10. Jakobs TF, Becker CR, Ohnesorge B, et al. Multislice helical CT of the heart with retrospective ECG gating: reduction of radiation exposure by ECG-controlled tube current modulation. Eur Radiol 2002; 12:1081-6.
11. Trabold T, Buchgeister M, Kuttner A, et al. Estimation of Radiation Exposure in 16-Detector Row Computed Tomography of the Heart with Retrospective ECG-gating. Rofo Fortschr Geb Rontgenstr Neuen Bildgeb Verfahr 2003; 175:1051-5.
12. Ropers D, Baum U, Pohle K, et al. Detection of coronary artery stenoses with thin-slice multi-detector row spiral computed tomography and multiplanar reconstruction. Circulation 2003; 107:664-6.
13. Nieman K, Cademartiri F, Lemos PA, Raaijmakers R, Pattynama PM, de Feyter PJ. Reliable noninvasive coronary angiography with fast submillimeter multislice spiral computed tomography. Circulation 2002; 106:2051-4.
14. Schroeder S, Kopp AF, Baumbach A, et al. Noninvasive detection and evaluation of atherosclerotic coronary plaques with multislice computed tomography. J Am Coll Cardiol 2001; 37:1430-5.
15. Vieweg WV, Alpert JS, Johnson AD, et al. Distribution and severity of coronary artery disease in 500 patients with angina pectoris. Cathet Cardiovasc Diagn 1979; 5:319-30.
16. McNamara JJ, Norenberg RG, Goebert HW, 3rd, Soeter JR. Distribution and severity of atherosclerosis in the coronary arteries. J Thorac Cardiovasc Surg 1976; 71:637-40.
17. Halon DA, Sapoznikov D, Lewis BS, Gotsman MS. Localization of lesions in the coronary circulation. Am J Cardiol 1983; 52:921-6.
18. Warnes CA, Roberts WC. Comparison at necropsy by age group of amount and distribution of narrowing by atherosclerotic plaque in 2995 five-mm long segments of 240 major coronary arteries in 60 men aged 31 to 70 years with sudden coronary death. Am Heart J 1984; 108:431-5.
19. Roberts WC. The coronary arteries in coronary heart disease: Morphologic observations. Pathobiol Annu 1975; 5:249-82.
20. Hunold P, Vogt FM, Schmermund A, et al. Radiation exposure during cardiac CT: effective doses at multi-detector row CT and electron-beam CT. Radiology 2003; 226:145-52.
21. Morin RL, Gerber TC, McCollough CH. Radiation dose in computed tomography of the heart. Circulation 2003; 107:917-22.

8. CORONARY PLAQUES

CHAPTER 8.2

INFLUENCE OF INTRACORONARY ATTENUATION ON CORONARY PLAQUE MEASUREMENTS USING MULTISLICE CT: OBSERVATIONS IN AN EX–VIVO MODEL OF CORONARY CT ANGIOGRAPHY

Filippo Cademartiri, MD[1]
Nico R Mollet, MD[1,2]
Giuseppe Runza, MD[3]
Nico Bruining, PhD[2]
Ronald Hamers, MD[2]
Pamela Somers, MSc[4]
Michiel Knaapen, PhD[4]
Stefan Verheye, MD, PhD[5]
Massimo Midiri, MD[3]
Gabriel P Krestin, MD[1]
Pim J de Feyter, MD[1,2]

From the Departments of Radiology[1], and Cardiology[2], Erasmus MC, University Medical Center Rotterdam,The Netherlands
Department of Radiology[3], DIBIMEL, University of Palermo, Palermo, Italy
Department of Pathology[4], Middelheim Hospital, Antwerp, Belgium
Department of Cardiology[5], Middelheim Hospital, Antwerp, Belgium

European Radiology, (in press)

ABSTRACT

Purpose: assessment of attenuation (HU) of human coronary plaques using multislice CT (MSCT) in an ex–vivo model.

Material and methods: in three ex–vivo specimens of left coronary arteries into oil, MSCT was performed after intracoronary injection of 4 solutions of contrast material (Iomeprol 400mgI/ml). The four solutions were diluted: 1/∞, 1/200, 1/80, and 1/20. All scans were performed with the following parameters: slices/collimation 16/0.75mm, rotation time 375ms. Each specimen was scored for the presence of atherosclerotic plaques. In each plaque the HU was measured in 4 ROIs for: lumen, plaque (non calcified thickening of the vessel wall), calcium, and surrounding (oil surrounding the vessel). The results were compared with one-way ANOVA–test and correlated with Pearson's test.

Results: there were no significant differences in the HU of calcium and oil in the 4 solutions. The mean HU in the 4 solutions for lumen (35±10HU; 91±7HU; 246±18HU; 511±89HU) and plaque (22±22HU; 50±26HU; 107±36HU; 152±67HU) was significantly different between each decreasing dilution ($p<0.001$). The mean HU of lumen and plaque of coronary plaques showed high correlation while the values were significantly different ($r = 0.73$; $p<0.001$).

Conclusion: intracoronary HU modifies significantly the HU of plaques assessed with MSCT.

INTRODUCTION

Several studies reported that atherosclerotic plaque composition and morphology are important predictors of plaque stability and clinical behaviour when compared to the degree of vessel stenosis.[1-3]

Quantitative and qualitative information (e.g. lumen diameter, wall thickness, and morphology) can be obtained using intra-coronary ultrasound (ICUS), which has been approved by Food and Drug Administration (FDA) as the standard for the in-vivo evaluation of coronary plaques.[4-6] This technique cannot be used for routine evaluation of plaque characteristics because of its invasiveness and cost.

Several non-invasive techniques have been tested for the visualisation and characterisation of coronary plaques. Preliminary reports using Magnetic resonance imaging (MRI) report the ability to detect and characterize the lipid-pool in atherosclerotic plaques at the level of the carotid arteries,[7] and in the coronary arteries.[8-10]

Multislice Computed Tomography (MSCT) coronary angiography has showed a good potential in the detection, quantification, and characterization of coronary artery plaques.[11-16] Nevertheless, several aspects concerning the methodology for the assessment of coronary plaques with MSCT coronary angiography remain unexplored.

With this study we address the issue of the variability of coronary plaque attenuation as measured with MSCT in an ex–vivo model with varying intracoronary attenuation.

MATERIAL AND METHODS

Specimens

Three left coronary arteries were dissected during autopsy. The dissected arteries were sampled 1 cm proximal of the bifurcation of the LCx and covered a length of 4 cm. For orientation the anterior side of the arteries were inked in black and the left side of the artery in green. Two patients (both males with an age of 78 and 63 years) died of non-cardiovascular diseases. One patient (female with an age of 73 years) died of ischaemic heart disease. The study was approved by the Medical Committee of the Middelheim Hospital.

The specimens were prepared and scanned separately. Each specimen was prepared with two sheaths. The sheaths were introduced and fixed at the proximal end (in the left main coronary artery) and at the distal end (in the anterior descending artery) of the specimens. The left circumflex was, previously, closed at its end with a wire.

Contrast material

Four saline solutions with decreasing dilution of contrast material (Iomeprol 400 mgI/mL, Bracco, Italy) were used: $1/\infty$, 1/200, 1/80, and 1/20. The attenuation values of the 4 solutions obtained in a 10ml syringe after dilution were 3.2±4.5HU ($1/\infty$; defined as Saline; no contrast material was diluted), 144.7±8.6HU (1/200; defined as Low), 298.4±3.4HU (1/80; defined as Medium), and 588.0±6.0HU (1/20; defined as High).

Experimental settings

The experimental settings included a box that was filled with vegetal oil. Prior to positioning the specimen into oil, saline was instilled through the sheaths to washout as much as possible. The specimens were put into oil as a mean to simulate the epicardial fat. Once the specimen was sunk into oil, the solution was injected through the sheath using a 10ml syringe from the sheath positioned at the proximal end of the specimen. The injection was finished when the solution was observed leaking out of the specimen. The leaking solution was removed from the specimen using an empty syringe. The specimen was not mobilized between the scans.

Scan parameters

A MSCT scan (Sensation 16, Siemens, Germany) was performed after intracoronary injection with increasing concentration of CM. After each scan the coronary arteries were washed out with saline before the injection of the following solution and the leaking solution was removed from the specimen using an empty syringe.

All scans were performed with the following parameters: slices/collimation 16/0.75mm, rotation time 375ms, feed/rotation 3.0mm (pitch 0.25), kV 120, mAs 400, effective slice thickness 1mm, reconstruction increment 0.5mm, field of view (FOV) 100mm, convolution filter medium smooth (B30f). The scan geometry was based on a retrospective ECG gated protocol (the same used for in-vivo MSCT coronary angiography). This protocol is based on a low pitch that allows a retrospective reconstruction of multiple phases within the cardiac cycle. In this case, a demo ECG was switched on and the scan was performed as if the heart rate was 71bpm. The reconstruction algorithm uses 180° of rotation bringing the effective temporal resolution down to 187ms.

Data preparation

In order to analyse the specimen with the same settings an experienced operator loaded the datasets into a dedicated workstation (Leonardo, Siemens, Germany) and performed a stack of orthogonal views in each solutions for all the specimens with the following parameters: slice thickness 1mm, increment 0.5mm, FOV 50mm.

Data collection

One observer performed all the measurements. Each specimen was evaluated for the presence of coronary atherosclerotic plaques. A coronary atherosclerotic plaque was defined as a thickening of the coronary wall clearly distinguished from the surrounding hypo-attenuating oil and from the lumen after injection of the solution with the lowest dilution of contrast material (e.g. high). Plaques where targeted regardless their size.

The operator loaded the 4 datasets for each dilution of the same specimen onto a workstation screen divided 2 x 2 scrolling the datasets in parallel with standard window settings (window width = 700HU; window center = 140HU). Once a plaque was detected in the 4 solutions, the operator draw 4 regions of interest (ROIs) for contrast material in the lumen of the vessel (defined as lumen), the soft tissue of the coronary plaque (defined as plaque), the calcification within the coronary artery wall

(defined as calcium), and the oil immediately surrounding the plaque (defined as surrounding). These 4 ROIs were defined as structures. The first drawing of the ROI was performed in the dataset with lowest dilution of contrast material because the lumen was easier to identify. The ROIs were drawn as large as possible but avoiding the borders of each structure in order to limit the effect of interpolation and partial volume on the measurement. Once the 4 ROIs of the structures were draw the operator could copy and paste the ROIs into the other stacks of images corresponding to different solutions. Therefore, the position of the ROIs was mirrored in each orthogonal slice with a plaque for each solution. The mean attenuation in each ROI was collected.

Statistical Analysis

The values of attenuation are presented as means and standard deviations. Statistical evaluation was performed with a dedicated software (SPSS 10.1, SPSS Inc., Chicago, Illinois). The attenuation measurements in each solution within the structure and clustered per structure were compared with one-way ANOVA–test and correlated with Pearson's test. For each structure (e.g. lumen, plaque, calcium, and surrounding), the attenuation values obtained in the 4 solutions were plotted in order to obtain a slope. The mean slope of each structure was tested for significant differences. For all tested comparisons a $p<0.05$ was considered significant.

RESULTS

Overall 109 levels containing plaque were measured. At each level 4 solutions were available (436 slices) and in each slice 4 ROIs were sampled (1744 samples). Results are summarized in Table I.

Table 1.

			Solutions (HU)			
	Overall (HU)	Slope	Saline	Low	Medium	High
Lumen	223.0±186.5*	153.4±30.7*	35.2±9.7**	90.6±6.7**	246.2±17.8**	511.0±88.7**
Plaque	86.1±71.5*	45.7±25.7*	21.9±22.4**	49.9±26.3**	106.7±35.6**	152.0±67.2**
Calcium	640.7±533.7*	8.0±31.5*	354.1±152.2	343.6±167.7	356.6±150.0	351.3 ±164.3
Surrounding	–123.9±11.1*	0.9±6.2*	–129.6±6.9	–127±12.2	–122±6.6	–115±7.1

Summary of the attenuation values measured in the different solutions in each slice (*for $p<0.05$ and **for $p<0.01$). Abbreviations: HU= Hounsfield Units; SD= Standard Deviation.

The mean attenuation obtained for all samples was: 223±187HU for the lumen, 86±71HU for the plaque, 641±534HU for the calcium, and -124±11HU for the surrounding. Values were all significantly different ($p<0.05$).

The mean slopes obtained for all the 4 structures were: 153±31 for the lumen, 46±26 for the plaque, 8±31 for the calcium, and 1±6 for the surrounding. Values were all significantly different between the structures ($p<0.05$).

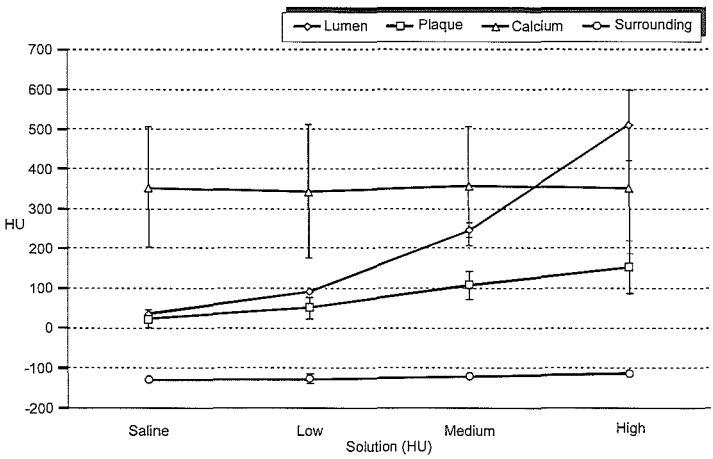

Figure 1. Plot of the mean attenuation of the 4 structures in the 4 solutions. The plot shows how the increasing attenuation in the lumen affects mainly the attenuation of the plaque. The calcium and the surrounding are, instead, almost not affected.

The mean attenuation in the 4 solutions for the 4 structures are displayed in Table 1 and Figure 1. The attenuation values of the lumen and of the plaques were significantly different in each structure ($p<0.01$). The attenuation values of the calcium and of the surrounding were not significantly different in each structure ($p>0.05$).

After clustering the paired attenuation values obtained for the 4 structures in all the 4 solutions the correlation between the structures was good ($r = 0.733$) only between the attenuation values of the lumen and the plaque (Table 2 and Figure 2).

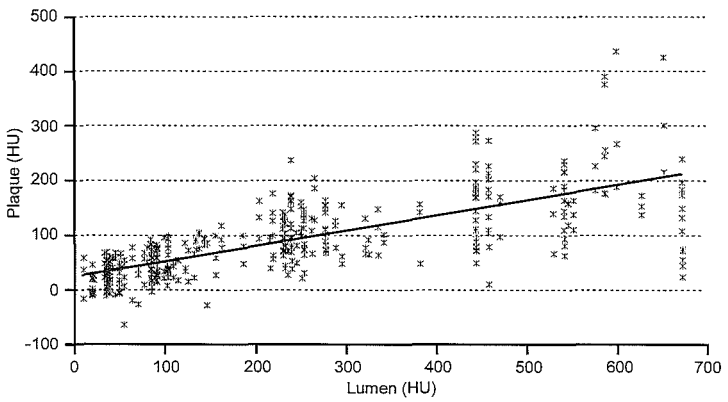

Figure 2. Lumen attenuation vs. plaque attenuation. All the attenuation values measured within the lumen and the plaque are plotted. The distribution is clearly linear demonstrating a correlation between the two variables ($r = 0.73$).

Table 2.

	Lumen vs. Plaque	Lumen vs. Calcium	Lumen vs. Surrounding	Plaque vs. Calcium	Plaque vs. Surrounding	Calcium vs. Surrounding
r	0.733**	0.063	0.106*	0.178**	0.166**	0.060

Correlation between the clustered attenuation values in each structure (*p<0.05; **p<0.01).

DISCUSSION

Several studies reported the ability of MSCT to visualize coronary atherosclerotic plaque.[12,14,15,17-20]

A study in-vivo by Kopp et al. compared MSCT vs. ICUS in the characterization of coronary plaques.[11] The plaques were divided for the attenuation values in soft (6±28HU and -5±25HU; two plaques), intermediate (83±17HU and 51±19HU; two plaques) and calcified (489±372HU and 423±111HU; two plaques). The MSCT criteria based on attenuation values showed an excellent correspondence with the ICUS criteria.

In a study in-vivo Schroeder et al. analyzed the composition of 34 plaques comparing MSCT vs. ICUS.[12] The Authors found that plaque echogenicity as determined by ICUS corresponds well to plaque attenuation as measured by MSCT.

Leber et al. in a study in-vivo showed that lesion echogenicity correlates well with MSCT attenuation measurements in coronary plaques.[16] The attenuation values for hypoechoic, hyperechoic, and calcified plaques were 49HU, 91HU, and 391HU, respectively. The MSCT attenuation values reflect the predominant plaque composition (e.g. a plaques with a large lipid core with a low echogenicity on ICUS might be identified on the basis of low attenuation value).

Becker et al. investigated 11 human cadaver heart specimens and compared the atherosclerotic lesions detected by MSCT (n=40) with the histopathological macroscopic characterization according to American Heart Association (AHA) criteria.[13] The Authors concluded that MSCT is a promising tool for the characterization of atherosclerotic coronary lesions.
From the literature resumed above it appears that MSCT can provide data and characterize coronary artery plaques, based on the attenuation values.

In a phantom study, Schroeder et al. measured the attenuation of two plaques made of rubber material after injection within a tube (simulating a coronary artery) of three decreasing concentrations of contrast material: 1:30 (336 HU), 1:40 (280 HU), and 1:50 (258 HU).[17] The increased attenuation of contrast material determined an increase in the measured attenuation of the plaque. Based on this observation we studied the influence of intravascular attenuation on the assessment of coronary plaques with MSCT.

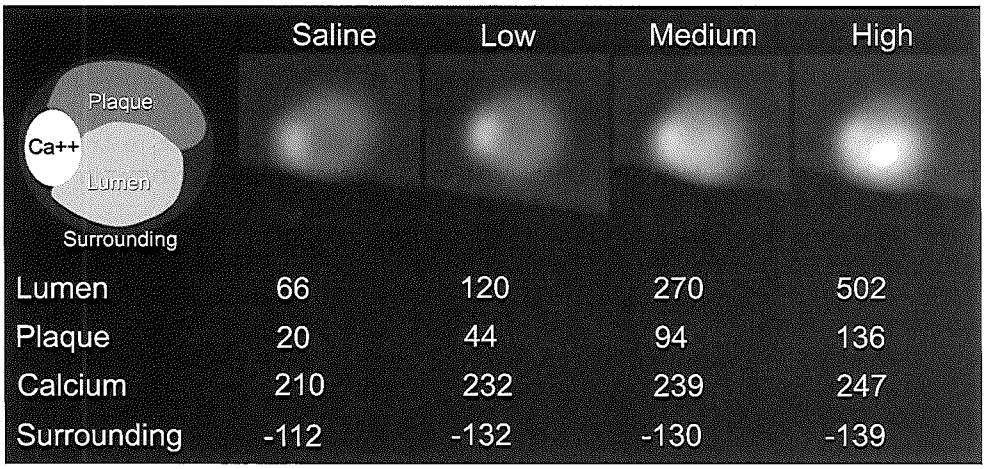

Figure 3. Example of plaque in the 4 solutions. The scheme in the upper left corner shows the configuration of the plaque in orthogonal cut performed with multislice CT. The 4 solutions producing a progressive increase in lumen attenuation are displayed from left to right in the upper part of the figure. Below, the related attenuation are displayed for every structure.

In our experimental study we showed that lumen attenuation measured by MSCT significantly affects the measured plaque attenuation (Figure 3). The higher the lumen attenuation, the higher plaque attenuation. Calcium attenuation and surrounding fat attenuation are, instead not significantly affected. Based on this finding, it is difficult to identify absolute ranges of attenuation that relates with the specific plaque characteristics.

Several factors and parameters affect the accuracy of the attenuation measurement. Partial volume and interpolation modify the profiles of attenuation in the range of the soft tissues. This is particularly important when there are calcifications in the plaque and contrast material in the lumen in contiguity with the region of interest. Therefore, absolute plaque attenuation values determined in the various studies are not comparable.
Our observation has a potential impact on the approach to plaque measurements with MSCT. In fact, since the attenuation within the lumen affects the attenuation within the plaque, further studies should probably focus on the relationship between these two variables. Based on our results the relationship appears to be close to linear. Thus, a coefficient could be introduced when plaque measurements are performed in order to compare the different studies.

One of the most important feature of the vulnerable plaque is the lipid core. The usual location of the lipid core within the atherosclerotic plaque is just below the thin cap. This means that it is also very close to the attenuation of the lumen as displayed in MSCT. In this area the attenuation measurements will be affected the most by intravascular attenuation.

There are several limitations in our study. The first one is due to the lack of motion in the specimens. The artefacts derived from the heartbeat were not present and/or reproduced. The second limitation is related to

the low number of specimens. Nevertheless, the high sampling rate using cross-sectional views of the vessels balanced this. The third limitation is that an excised coronary specimen does not necessarily represents the reality of a coronary vessel. The last limitation is inherent to the lack of a histopathological correlation. Yet, the aim of our study was not to correlate histopathology with MSCT, but to assess the influence of intracoronary attenuation on overall plaque attenuation measurements.

In conclusion, intravascular attenuation modifies significantly the attenuation of the coronary atherosclerotic plaques assessed with MSCT. Therefore, the characterization of the plaque on the basis of absolute attenuation values should be reported with caution. When plaque attenuation is measured, intraluminal attenuation should also be reported. Probably, a calibration factor will be introduced in the future to address this issue.

REFERENCES

1. Fuster V, Badimon L, Badimon JJ, Chesebro JH (1992) The pathogenesis of coronary artery disease and the acute coronary syndromes (1). N Engl J Med 326:242-50.
2. Fuster V, Badimon L, Badimon JJ, Chesebro JH (1992) The pathogenesis of coronary artery disease and the acute coronary syndromes (2). N Engl J Med 326:310-8.
3. Virmani R, Kolodgie FD, Burke AP, Farb A, Schwartz SM (2000) Lessons from sudden coronary death: a comprehensive morphological classification scheme for atherosclerotic lesions. Arterioscler Thromb Vasc Biol 20:1262-75.
4. Stone GW, Hodgson JM, St Goar FG, Frey A, Mudra H, Sheehan H, Linnemeier TJ (1997) Improved procedural results of coronary angioplasty with intravascular ultrasound-guided balloon sizing: the CLOUT Pilot Trial. Clinical Outcomes With Ultrasound Trial (CLOUT) Investigators. Circulation 95:2044-52.
5. Schroeder S, Baumbach A, Haase KK, Oberhoff M, Marholdt H, Herdeg C, Athanasiadis A, Karsch KR (1999) Reduction of restenosis by vessel size adapted percutaneous transluminal coronary angioplasty using intravascular ultrasound. Am J Cardiol 83:875-9.
6. Bruining N, Sabate M, de Feyter PJ, Kay IP, Ligthart J, Disco C, Kutryk MJ, Roelandt JR, Serruys PW (1999) Quantitative measurements of in-stent restenosis: A comparison between quantitative coronary ultrasound and quantitative coronary angiography. Catheter Cardiovasc Interv 48:133-42.
7. Shinnar M, Fallon JT, Wehrli S, Levin M, Dalmacy D, Fayad ZA, Badimon JJ, Harrington M, Harrington E, Fuster V (1999) The diagnostic accuracy of ex vivo MRI for human atherosclerotic plaque characterization. Arterioscler Thromb Vasc Biol 19:2756-61.
8. Stuber M, Botnar RM, Danias PG, Sodickson DK, Kissinger KV, Van Cauteren M, De Becker J, Manning WJ (1999) Double-oblique free-breathing high resolution three-dimensional coronary magnetic resonance angiography. J Am Coll Cardiol 34:524-31.
9. Bunce NH, Pennell DJ (1999) Coronary MRA--a clinical experience in Europe. J Magn Reson Imaging 10:721-7.

10. Worthley SG, Helft G, Fuster V, Zaman AG, Fayad ZA, Fallon JT, Badimon JJ (2000) Serial in vivo MRI documents arterial remodeling in experimental atherosclerosis. Circulation 101:586-9.
11. Kopp AF, Schroeder S, Baumbach A, Kuettner A, Georg C, Ohnesorge B, Heuschmid M, Kuzo R, Claussen CD (2001) Non-invasive characterisation of coronary lesion morphology and composition by multislice CT: first results in comparison with intracoronary ultrasound. Eur Radiol 11:1607-11.
12. Schroeder S, Kopp AF, Baumbach A, Meisner C, Kuettner A, Georg C, Ohnesorge B, Herdeg C, Claussen CD, Karsch KR (2001) Noninvasive detection and evaluation of atherosclerotic coronary plaques with multislice computed tomography. J Am Coll Cardiol 37:1430-5.
13. Becker CR, Nikolaou K, Muders M, Babaryka G, Crispin A, Schoepf UJ, Loehrs U, Reiser MF (2003) Ex vivo coronary atherosclerotic plaque characterization with multi-detector-row CT. Eur Radiol 13:2094-8.
14. Nikolaou K, Sagmeister S, Knez A, Klotz E, Wintersperger BJ, Becker CR, Reiser MF (2003) Multidetector-row computed tomography of the coronary arteries: predictive value and quantitative assessment of non-calcified vessel-wall changes. Eur Radiol 13:2505-12.
15. Achenbach S, Moselewski F, Ropers D, Ferencik M, Hoffmann U, MacNeill B, Pohle K, Baum U, Anders K, Jang IK, Daniel WG, Brady TJ (2004) Detection of calcified and noncalcified coronary atherosclerotic plaque by contrast-enhanced, submillimeter multidetector spiral computed tomography: a segment-based comparison with intravascular ultrasound. Circulation 109:14-7.
16. Leber AW, Knez A, Becker A, Becker C, von Ziegler F, Nikolaou K, Rist C, Reiser M, White C, Steinbeck G, Boekstegers P (2004) Accuracy of multidetector spiral computed tomography in identifying and differentiating the composition of coronary atherosclerotic plaques: a comparative study with intracoronary ultrasound. J Am Coll Cardiol 43:1241-7.
17. Schroeder S, Flohr T, Kopp AF, Meisner C, Kuettner A, Herdeg C, Baumbach A, Ohnesorge B (2001) Accuracy of density measurements within plaques located in artificial coronary arteries by X-ray multislice CT: results of a phantom study. J Comput Assist Tomogr 25:900-6.
18. Leber AW, Knez A, White CW, Becker A, von Ziegler F, Muehling O, Becker C, Reiser M, Steinbeck G, Boekstegers P (2003) Composition of coronary atherosclerotic plaques in patients with acute myocardial infarction and stable angina pectoris determined by contrast-enhanced multislice computed tomography. Am J Cardiol 91:714-8.
19. Schoenhagen P, Tuzcu EM, Stillman AE, Moliterno DJ, Halliburton SS, Kuzmiak SA, Kasper JM, Magyar WA, Lieber ML, Nissen SE, White RD (2003) Non-invasive assessment of plaque morphology and remodeling in mildly stenotic coronary segments: comparison of 16-slice computed tomography and intravascular ultrasound. Coron Artery Dis 14:459-62.
20. Nikolaou K, Becker CR, Muders M, Babaryka G, Scheidler J, Flohr T, Loehrs U, Reiser MF, Fayad ZA (2004) Multidetector-row computed tomography and magnetic resonance imaging of atherosclerotic lesions in human ex vivo coronary arteries. Atherosclerosis 174:243-52.

9. SUMMARY/SAMENVATTING

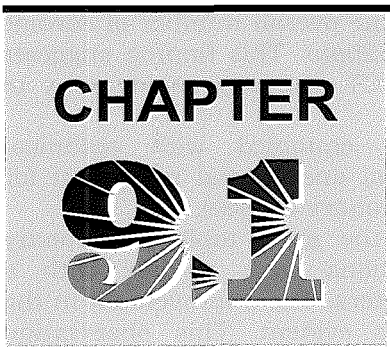

SUMMARY AND CONCLUSIONS

Multislice computed tomography (MSCT) has showed great potential for the imaging of the heart and coronary arteries. Preliminary studies reported promising results for the detection of significantly obstructive coronary stenoses. However, optimisation of several technical aspects is mandatory to allow this non-invasive technique to become part of the routine diagnostic armamentarium.

The correct use of contrast material is of paramount importance for a high quality MSCT angiography. In this thesis, problems associated with intravenous administration of contrast material were discussed and effective solutions were provided. As a result of our experience, higher rates and iodine concentrations should be used for MSCT coronary angiography to improve intra-vascular enhancement. The use of a saline bolus chaser administered immediately after the main angiographic bolus results in a more effective utilization of contrast material. It allows a reduction of 35% in the volume of administered contrast material.

The anatomy of coronary vessels have been reviewed and exposed in a way that should become familiar to both Radiologist and Cardiologist. The volumetric approach that is typical of MSCT should push the operator towards a comprehensive three-dimensional evaluation characterized by the use of several post-processing techniques (e.g. multiplanar reconstructions, maximum intensity projections, curved planar reconstructions, and volume rendering). This thesis demonstrates that the use of standardized projections to evaluate coronary arteries, limits significantly the diagnostic accuracy in the detection of significant stenosis. This observation shows that MSCT coronary angiography is an operator-dependent technique. Further developments may allow this technique to become less user-dependent, but for the time being highly trained operators should perform the evaluation to maintain the diagnostic quality of the report.

An important source of operator-dependency in MSCT coronary angiography is related to the presence of mild irregularities of cardiac rhythm (e.g. the presence of pre-mature beat/extra-systole). Currently, such an event is thought to be source of data loss in MSCT coronary

angiography. However, this thesis shows that the problems related to mild heart rhythm irregularities can be overcome, as long as the operator is allowed to edit the ECG pattern of temporal window position, the number of pre-mature beats is not exceeding 1/3 of the overall number of cardiac cycles and the average heart rate is below 65bpm. This finding suggests one of the possible future solutions for MSCT coronary angiography in patients with arrhythmia.

The latest 16-row MSCT scanners are equipped with technical improvements resulting in increased temporal and spatial resolution for the evaluation of small and rapidly moving coronary arteries.

In the field of coronary artery evaluation the main topic is coronary stenosis. Several different patient populations were studied with a progressively optimised protocols and parameters. The improvement in the results in terms of diagnostic accuracy is evident. This observation suggests that the direction for the next development in the field of MSCT scanners should aim at an increased tube power and gantry rotation speed, with a concomitant reduction in slice thickness.

The follow-up of coronary stent could be one of the main fields of application for MSCT coronary angiography. Interventional cardiology is progressively substituting major coronary bypass surgery even in more advanced three-vessel disease patients, especially after the introduction of drug-eluting stents.

Earlier generations of MSCT scanners showed relevant problems when facing the challenge of stent patency visualisation. In addition MSCT is not capable of displaying the dynamic distribution of contrast material along the vessel as conventional coronary angiography. Therefore, a direct visualisation of stent lumen should be obtained for MSCT to be a reliable diagnostic tool.

The main issue for MSCT in the visualisation of stent lumen was the high density of the metal struts. This high density produces two artefacts in MSCT: volume averaging towards higher densities within the same and neighbouring voxels, and interpolation. In the images these artefacts appear like a "blooming" of the stent (e.g. the stent strut appears much larger than it really is). The "blooming" effect severely limits the ability to directly visualize the lumen inside the stent. With 4-row MSCT scanners spatial resolution was insufficient to determine stent patency in stents with a diameter of 3mm or less. After the introduction of 16-row MSCT scanners, we could challenge MSCT in the direct visualisation of stent lumen and compare the performance for the detection of in-stent restenosis with the gold standard. Yet, the high density remains a problem that can be partially solved increasing spatial resolution and improving convolution filtering (i.e. reducing the "blooming" effect). Nevertheless, a final solution would be the modification of stent strut material with a MSCT-compatible material and/or with re-absorbable stents.

Non-invasive visualisation of coronary artery lumen is only the beginning of the exploration that can be performed with MSCT. The coronary artery

wall is the true key for the future developments in the field of coronary artery disease.
Multislice CT coronary angiography can detect and classify significant coronary plaques into calcified and not calcified, providing a unique in-vivo assessment of the extent and distribution of coronary artery disease.
In this thesis a preliminary experience of plaque burden quantification is reported in patients with stable angina. The information provided seems to be consistent with previously reported pathology studies and shows unequivocally the location and importance of coronary artery disease at the level of proximal coronary arteries.
Previous and current literature claims that the absolute density measurements performed in the non-calcified regions of coronary plaques is a mean for the characterization of lipid vs. fibrotic atherosclerotic plaques. Based on our experience and on our knowledge of MSCT physics we were sceptic on this finding.
In an ex-vivo study we focused on the modification in non-calcific plaque attenuation due to the variable amount of attenuation derived from intra-coronary contrast material. The variability is significant and the higher the attenuation in the lumen the higher the range of attenuation achieved by the non-calcific plaque. This finding has several methodological implications for future studies in the field of plaque imaging with MSCT. In fact, absolute density values in non-calcific plaques should not be used as means for the characterization of coronary plaques. A calibration factor based on lumen density may be introduced to compare current literature and to develop a reproducible methodology for plaque characterisation with MSCT coronary angiography.
Looking at the potential of MSCT in cardiovascular imaging one could expect that in less than 5 years this technique will mature into a routine imaging modality for diagnostic coronary angiography in selected populations of patients. Potential populations of patients suitable for this application are: patients with low probability of disease (e.g. young women, atypical chest pain, functional test non conclusive), patients with no other option prior to conventional catheter coronary angiography (e.g. functional tests not completed), patients in which significant obstructive coronary artery disease should be excluded (e.g. pre-operative in valve surgery), follow-up of coronary artery stents, follow-up of coronary artery bypass grafts.
An application of MSCT coronary angiography that will modify completely our perception of coronary artery disease is plaque imaging. At present, being an MD, we all know that coronary atherosclerosis in most of the cases starts very early in our life and symptoms are only the last evidence of a long lasting disease. One thing is to know it, another one is to see the disease while we are still asymptomatic. Most of us, seeing our own coronary arteries with some calcifications and some soft plaque along the proximal left anterior descending would surely modify our lifestyle. Images are an important part of our life (given that ¼ of our brain cortex is

devoted to this function). We read less and we use our eyes more and more. Television, mobile phones, PDA's are all providing tools that are mainly visual. As a language, the visual one is more powerful and easy to use.
Medicine is no exception. When imaging is performed, the Radiologist is often asked: "Did you see anything?". Whenever possible, as humans, we try to make the message as visual as possible. Less words and less numbers is better, also in presentations. We tend to believe in what we can see. I believe that the ability to show coronary artery disease will not only become a useful tool from the scientific standpoint but will also modify the perception of coronary artery disease in the people.
Apart from these elective diagnostic applications, an extremely interesting field in which MSCT will play a relevant role is acute chest pain. The chance to scan all the vessels of the thorax in less than 20s is very attractive from the clinical point of view, considering that with the same scan the operator could perform the differential diagnosis between pulmonary embolism, aortic dissection and acute myocardial infarction (and many other thoracic diseases). Currently, there are no evidences on the feasibility of such a protocol but it is reasonable to expect that future developments will allow to complete such an investigation. The time required to triage acute chest pain could be dramatically reduced allowing structures with poorer logistics to perform on-site the diagnosis a therefore to stratify/filter the patients for major referral centres.
From the technical point of view, the race is just at the beginning. While writing this summary we are already using for more than a month a 64-slice CT scanner with a rotation speed of 330ms and an isotropic voxel of 0.43mm. Images are improved, we can evaluate more of the coronary tree, plaques are better displayed and more easily evaluated, and so forth. The potential of the technique presented in this thesis will be soon outdated by newer technology. Nevertheless, by putting the basis for the next step we will be able to improve both our knowledge and our understanding of coronary artery disease and use more properly newer MSCT scanners generations.
In conclusion, the introduction of electrocardiographic-gated multislice computed tomography is probably one of the most important innovations in cardiovascular imaging of this decade. It will change the way we look at coronary artery disease. It will provide new tools and earlier diagnosis. It will shed light on several questions, and it will raise new problems, as it always happens in research.

9. SUMMARY/SAMENVATTING

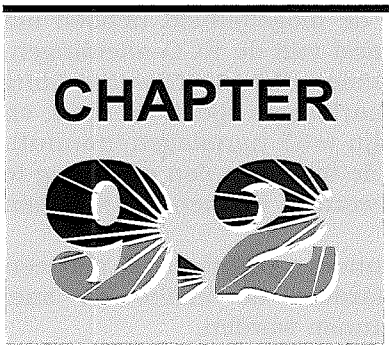

SAMENVATTING EN CONCLUSIES

Multislice computed tomography (MSCT) is een veelbelovende, niet-invasieve techniek om het hart en de kransslagvaten af te beelden. De eerste studies met deze techniek lieten goede resultaten zien betreffende het opsporen van belangrijke vernauwingen op de kransslagvaten. De techniek moet echter nog aangescherpt worden voordat dit onderzoek routinematig uitgevoerd kan worden.
De correcte toediening van een contrast middel is van groot belang om de kransslagvaten goed af te beelden op de MSCT-scan. Problemen gerelateerd aan de intraveneuze toediening van dit contrast middel en direct toepasbare oplossingen werden in deze thesis besproken. Uit onze ervaring blijkt dat de beste resultaten worden verkregen als het contrast middel een hoog Jodium gehalte heeft en snel in een vene wordt ingespoten. Door het gebruik van een zoutoplossing, die direct na toediening van het contrast middel wordt ingespoten, kan de hoeveelheid contrast middel met 35% teruggebracht worden.
De anatomie van de kransslagvaten op de MSCT-scan en de manier waarop deze vaten beoordeeld moeten worden, is besproken en in de toekomst zou iedere Radioloog en Cardioloog dit moeten weten. Evaluatie van de MSCT-scan zou op een volledig 3-dimensionele aanpak gebaseerd kunnen worden, waarbij de arts die de scan analyseert gebruik zou moeten maken van verschillende postprocessing technieken zoals zgn. "Multi-planar reconstructies", "maximum intensity projecties", "curved planar reconstructies" en "volume rendering". Gebruik makend van deze informatie zou de scan niet beoordeeld moeten worden met behulp van standaard, 2-dimensionele projecties. Deze thesis laat zien dat deze laatste aanpak leidt tot een minder goede beoordeling van de scan. De uitkomst van de scan is dus sterk afhankelijk van de arts die de scan beoordeelt. Mogelijk komt hier in de toekomst verandering in, maar om deze reden zou op dit moment dit onderzoek alleen beoordeeld moeten worden door uitvoerig getrainde artsen.
Een verkeerd beoordeelde scan kan het gevolg zijn een onregelmatige hartslag tijdens de opname van de scan. Een onregelmatige hartslag kan

het gevolg zijn van een premature slag (extrasystole). Aanwezigheid van een premature slag werd vroeger gezien als een oorzaak van een onbeoordeelbare scan. Deze thesis laat zien dat dit niet het geval hoeft te zijn onder enkele voorwaarden: de arts moet de mogelijkheid hebben om de datapunten zelfstandig te kiezen aan de hand van de ECG-afleidingen, premature hartslagen mogen niet vaker voorkomen dan in een verhouding van 1 op 3, vergeleken met het totaal aantal hartslagen tijden de scan, en de basisfrequentie van het hart moet rustig zijn (<65 hartslagen/minuut). Deze bevinding kan als leidraad dienen om in de toekomst een oplossing te vinden hoe een MSCT-scan uitgevoerd kan worden in mensen met een onregelmatig hartritme.
De laatste versies van de 16-detector CT scanners zijn uitgerust met een betere temporele en spatiele resolutie waardoor de kleine en snel bewegende kransslagvaten beter beoordeeld kunnen worden.
Het belangrijkste onderdeel tijdens de beoordeling van de kransslagvaten is het opsporen van belangrijke vernauwingen. Verschillende patiëntengroepen werden onderzocht met deze techniek, waarbij de verschillende scanners steeds meer mogelijkheden boden en de techniek steeds verder ontwikkeld werd. Als gevolg hiervan worden belangrijke vernauwingen veel beter vastgesteld op de MSCT-scan. Deze bevindingen suggereren dat toekomstige ontwikkelingen op dit gebied zich zouden moeten richten op de ontwikkeling van een sterkere en sneller roterende röntgenbuis en de ontwikkeling van smallere detectorelementen.
Het opvolgen van stents in de kransslagvaten kan in de toekomst een belangrijke indicatie zijn voor het uitvoeren van een MSCT coronair angiogram. Behandeling van ernstige vernauwingen op de kransslagvaten wordt steeds vaker via een dotterbehandeling uitgevoerd in plaats van een bypass operatie, zelfs in patiënten met vergevorderde kransslagaderverkalking. Deze trend wordt gestimuleerd door de recente ontwikkeling van de zgn. "drug-eluting" stents.
Het vaststellen of een stent in een van de kransslagvaten voldoende open is, was moeilijk te beantwoorden met de eerdere generaties MSCT scanners. Bovendien geeft een MSCT coronair agiogram geen informatie met betrekking tot de bloedstroom, waardoor directe visualisatie van het lumen van het kransslagvat binnenin de stent een vereiste is om te beoordelen of een stent open of dicht is.
Een belangrijke limitatie voor het evalueren van het lumen was gerelateerd aan het radio-opake materiaal waarvan de stent gemaakt is. Dit veroorzaakt twee belangrijke artefacten op het MSCT coronair angiogram, zgn. "volume-averaging" en interpolatie. Door deze artefacten wordt de stent groter afgebeeld dan hij in werkelijk is. Dit effect wordt "blooming" genoemd en hindert in belangrijke mate de evaluatie van het lumen in de stent. De spatiele resolutie van de 4-detector MSCT scanners was niet toereikend om te bepalen of kleinere (<3 mm diameter) stents open of dicht waren. Met de introductie van de 16-detector MSCT scanner, werd de directe visualisatie van het lumen in de stent mogelijk. We hebben de diagnostische capaciteit van deze techniek om belangrijke vernauwingen

in een stent op te sporen vergeleken met het conventionele angiogram, de gouden standaard. Tot op heden vormt het radio-opake materiaal waarvan de stent gemaakt is een limitatie. Dit probleem kan deels opgelost worden door een verbeterde spatiele resolutie en filtering die dat zgn. "blooming"-effect tegen gaan. Desalniettemin, de uiteindelijke oplossing ligt in het maken van stents die speciaal gefabriceerd zijn om een betere CT evaluatie mogelijk te maken en/of bio-afbreekbare stents.
Niet-invasieve evaluatie van het lumen van de kransslagvaten is slechts het begin van wat er mogelijk is met MSCT. De evaluatie van de wand van de kransslagvaten vormt de echte uitdaging in toekomstige ontwikkelingen met betrekking tot kransslagaderverkalking.
Multislice CT coronair angiografie kan belangrijke plaques detecteren en onderverdelen in verkalkte en niet-verkalkte plaques, wat een unieke in-vivo evaluatie met betrekking tot de uitgebreidheid en distributie van kransslagaderverkalking toelaat.
In deze thesis wordt een studie gepresenteerd waarin de hoeveelheid plaque wordt gekwantificeerd in patiënten met stabiele angina pectoris. Deze bevindingen lijken vergelijkbaar te zijn met eerder gepubliceerde pathologie-studies die lieten zien dat de meeste kransslagaderverkalking plaatsvindt in de het proximale gedeelte van de kransslagvaten.
Eerdere, maar ook meer recente studies claimen dat niet-verkalkte plaques onderverdeeld kunnen worden in Lipid of fibreuze plaques op basis van absolute densiteit waarden op de CT scan. Gebaseerd op onze ervaringen als wel onze kennis van de fysica van MSCT waren we erg sceptisch met betrekking tot deze bevindingen.
In een ex-vivo studie hebben we ons gericht op de variabiliteit in densiteitmetingen van niet verkalkte plaques als gevolg van een variabele hoeveelheid contrast middel in de kransslagvaten. Deze variabiliteit is significant en hoe hoger de hoeveelheid contrast in het vat is, des te hoger zijn de waarden gemeten in de niet-verkalkte plaque. Deze bevinding heeft verscheidene methodologische implicaties voor toekomstige studies die het proces van kransslagaderverkalking willen onderzoeken met behulp van MSCT. Absolute densiteits metingen zouden niet gebruikt moeten worden om plaques onder te verdelen. Er zou een correctiewaarde ingevoerd moeten worden die het toelaat om de verschillende studies te vergelijken en om een reproduceerbare methode te ontwikkelingen die het toelaat plaques te karakteriseren.
Rekening houdend met de potentie van MSCT op het gebied van de cardiovasculaire beeldvorming, is het goed mogelijk dat deze techniek routinematig uitgevoerd zal worden voor het opsporen van ernstige vernauwingen op de kransslagvaten in een geselecteerde patiëntenpopulatie. Verschillende patiënten populaties kunnen baat hebben aan deze techniek, zoals: patiënten met een lage kans op kransslagaderverkalking (bvb. jonge vrouwen, patiënten met atypische pijn op de borst en patiënten waarin functionele testen niet eenduidig geïnterpreteerd kunnen worden), patiënten waarbij functionele test niet uitgevoerd kunnen worden, patiënten waarbij belangrijke vernauwingen op

de kransslagvaten moeten worden uitgesloten (bvb. preoperatief onderzoek voorafgaand aan een hartklepvervanging), het opvolgen van patiënten na een dotterbehandeling waarbij een stent werd geplaatst en het opvolgen van patiënten na een bypassoperatie.
Een toepassing van MSCT coronair angiografie die onze perceptie van het proces van kransslagaderverkalking volledig zal veranderen is het visualiseren van plaques. Als arts weten we allemaal dat het proces van kransslagaderverkalking reeds vroegtijdig tijdens ons leven plaatsvindt en symptomen slechts het gevolg zijn van een reeds lang bestaande ziekte. De aanname dat kransslagaderverkalking plaatsvindt is een ding, maar het zien van kransslagaderverkalking terwijl we nog geen klachten hebben betekent nog iets anders. De meeste van ons die geconfronteerd worden met het beelden waarop verkalkte en niet-verkalkte plaques te zien zijn, zullen geneigd zijn hun levensstijl aan te passen. Beelden zijn een belangrijk onderdeel van ons leven (rekening houdend met het feit dat ongeveer ¼ van onze hersencortex gebruikt wordt voor deze functie). We lezen minder en gaan steeds meer af op wat we zien. Televisie, mobiele telefoons, PDA's zijn slechts enkele voorbeelden van apparaten die voor een belangrijk deel visuele informatie verschaffen. Het visuele is een sterke taal en eenvoudig te gebruiken.
Geneeskunde vormt hierop geen uitzondering. Wanneer de beeldverwerking is uitgevoerd, wordt de Radioloog vaak gevraagd: "Heb je iets gezien?". Wanneer mogelijk probeert de mens een zo visueel mogelijke boodschap door te geven. Minder woorden en minder getallen is beter, wat ook opgaat voor het houden van presentaties. We neigen er naar te geloven wat we zien. Ik geloof dat de mogelijkheid om kransslagaderverkalking visueel zichtbaar te maken niet alleen wetenschappelijk gebruikt zal worden, maar ook om mensen beter bewust te maken van het proces van kransslagaderverkalking.
Behalve voor diagnostische indicaties die gepland kunnen worden, kan MSCT mogelijks een rol spelen in patiënten met acute pijn op de borst. De mogelijkheid om alle vaten in de thorax af te beelden in minder dan 20 seconden biedt veel klinische mogelijkheden, gezien de arts met behulp van een scan onderscheidt kan maken tussen longembolieën, dissecties van de grote slagader en een acuut hartaanval (en vele andere ziektes van de thorax). Momenteel is er nog geen hard bewijs dat zo'n protocol inderdaad uitgevoerd kan worden, maar het is redelijk om aan te nemen dat dit in de toekomst mogelijk wordt. De tijd die nodig is om te bepalen welke behandeling een patiënt die zich presenteert met acute pijn op de borst moet krijgen, kan hiermee drastisch afnemen. Dit maakt het mogelijk voor minder uitgeruste centra om de diagnose on-site te stellen, waarna de patiënt verwezen wordt naar grotere, beter uitgeruste centra voor het uitvoeren van een bepaalde behandeling.
Vanuit technisch oogpunt is de race nog maar net begonnen. Terwijl ik deze samenvatting schrijf, hebben we al meer dan een maand de beschikking over de nieuwe 64-slice CT scanner, die uitgerust is met een rotatietijd van 330 ms en een isotropische beeldkwaliteit met voxels van

0.4 mm3. Beelden worden verbeterd, we kunnen de kransslagvaten in zijn geheel beter beoordelen, plaques worden meer accuraat afgebeeld en geëvalueerd, enz. De potentie van deze techniek die gepresenteerd wordt in deze thesis zal snel achterhaald zijn door nieuwere technologie. Desalniettemin, door de volgende stap te zetten zal onze kennis en begrip met betrekking tot het proces van kransslagaderverkalking toenemen en zullen we de kwaliteiten van toekomstige CT scanners meer optimaal kunnen benutten.
Waarschijnlijk is de introductie van het aan het ECG gekoppelde MSCT coronair angiogram een van de meest belangrijke uitvindingen van de laatste 10 jaar. Het zal de manier waarop we naar kransslagaderverkalking kijken danig veranderen. Het zal nieuwe mogelijkheden en een snellere diagnose bieden. Het zal antwoord geven op diverse vragen, maar tegelijkertijd, zoals zo vaak in wetenschappelijk onderzoek, nieuwe vragen oproepen.

10. ACKNOWLEDGEMENTS

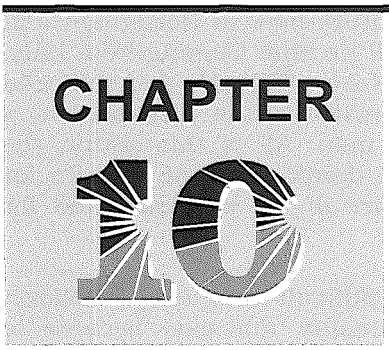

This book represents more or less (definitely "more" than "less") the completion of the first part of my life. If somebody would have told me 6 years ago during my medical school that I would become an expert of Cardiac MSCT (by the way, at that time people was still believing that MRI could make it on coronaries...) in one of the most important University Medical Center of the world,... I would have started laughing... very very loud.

This is a dream come true that started by chance. There was no planning, no intention to do something like this. Several people and events played key roles (without actually knowing it) and in the end, everything happened (almost) flawlessly.

I was a resident at the first year in Radiology in Parma (my hometown very famous for ham, "parmigiano" cheese, Barilla,... sadly also for Parmalat), and it came to my girlfriend's minds the idea to go abroad for a period. The aim was to develop a new experience and to see something different. There were several scholarships of 6-12 months available, we got two and we left for Rotterdam EMC. The choice of Rotterdam was totally random.

Once here we learned how different the medical reality can be, between two countries. Several things I had to learn, and several things I discovered I already knew.

The first person I met was Marja. She is a cornerstone of my life in The Netherlands, always helpful, pragmatic and positive. One of the key persons of this adventure was not available that day therefore I was "given" to Jacqueline van Holten, which gave me the tour of the Department. Too many people, places and faces to remember. Anyway, everybody was kind but for me it was a little bit of overload.
Shortly after, I met my first supervisor, Aad van der Lugt. Aad is a wonderful person with a wonderful family that I had the honour and the pleasure to meet. He is an example for me and a wise voice that I could

hear when I was here alone in my first months. Thanks Aad, this book is also very much of yours.

Then I met the person that determined my future here in Rotterdam and the feasibility of this thesis, Prof. Dr. Gabriel P Krestin. Coming from Italy, I was used to a King-to-slave relationship between everybody and the head of the Department. What I found in Prof. Krestin was a nice person, a smart and pragmatic colleague, and a wise man. All of this within the same human being was luck,... much luck. I thank you Prof. Krestin for being such a complete person, for taking care of my problems and for letting me do my job for you.

Starting the work in the Department was difficult and easy. Difficult because I was coming from such a different reality, and easy because of the good organization that I found. Things were available and I could learn and improve my knowledge under the guide of Aad van der Lugt. Multislice CT was immediately my favourite, even though I asked to see more MRI. I was already an "addict" of spiral CT but to see multislice CT in action was paradise on earth.

I felt appreciation from many sides until I was asked to give a lecture on post-processing. I remember it was 21st of February 2001. A lot of stress, a lot of preparation, but I think a good result.

After that, Prof. Krestin offered me to take care of the Sensation 16 project here at the EMC. That was a lot bigger than I ever expected and very quick. Almost without thinking I accepted, even though the decision was not completely up to me. In fact, I had to finish my residency program as a Radiologist in Italy. "My Italian Boss" (which already sounds dangerous!) Prof. Pellegrino Bassi had to give me the authorization to spend more time in Rotterdam during my residency. That was tough (!!!), but the help of the local Associate Professor and friend Paolo Pavone was the key to solve the problem in a smooth way. Thank you Paolo for the support in this and in other situations.

In July 2001 we left Rotterdam to go back to Italy.

After that I kept contacts with Rotterdam waiting for the new scanner to be developed and installed. This took longer than expected. In the meantime I had the unique chance to spend one month in Forchheim (Germany) at Siemens CT factory to see, learn and perform the first tests and scans on a prototype of the future scanner.

There I had the honour and pleasure to meet the cardiac CT team of Siemens: Stefan Schaller, Thomas Flohr, Bernd Ohnesorge, Karl Stierstorfer and many others. They taught me the technical issues and the solutions adopted by Siemens in the 16-slice generation of CT scanners. I grew a lot during that month guys, and I thank all of you at Siemens. There is a lot of your input in this book.

Of the Siemens guys I really want to thank some people in particular. Bernd Ohnesorge for the help in all our projects, Marco Silvestrini for the humor, the help and the "patience", Luigi Moramarco for the kindness and support.

In February 2002 I came back to EMC to start the tests with one of the first worldwide clinical installation of the new 16-slice scanner from Siemens.

At this point the 16-slice cardiac experience started for real. The team was small.
Beside myself...
Koen Nieman: great scientist, Japanese food/culture/woman lover and producer (Lisa), reliable colleague. Thanks Koen, You kick started my cardiac passion and this is priceless because it will be part of my life forever.

Rolf Raaijmakers: great CT tech, great friend, we did not work together long enough. Thanks Rolf, you taught me a lot about CT. I miss you as tech and I hope you are happy in Philips.

At this stage there was only an idea for the PhD.
Now I want to deeply thank my other promoter: Prof. Dr. Pim de Feyter.
Pim is a pure gentleman. I had the honour to work with and for you long enough to be able to know you as a person. I appreciate your soft touch even when you have to say things that someone might not like. Your insight and balance was and will always be an example for me. You made me love more and more the world of cardiology.
I like very much the way you describe Italian people...

After the first 3-4 months of hard work the PhD of Koen was finished, the first paper was out and I was really seeing my future in cardiac imaging. Therefore, in the summer of 2002 I planned with Prof. Krestin this thesis. From this point everything started and the book is the end of it.

During the summer of 2002 the successor of Koen was enrolled. I was very lucky!

Nico Mollet: still I do not know if you are Belgian or not (are you?), nevertheless you are good friend, good scientist, outstanding barbeque-man...

We spent so much time together, so many patients, so many images, so many slides, so many movies (and codecs), so many working weekends,.. You have been very close to me, helped me whenever it was possible.
You have only two problems: you don't drink coffee (which is almost impossible for me to understand!!!), and you wear green trousers (which is definitely impossible for me to understand!!!). I cannot write here why the first problem is severe but the second is worse. Anyway, thanks Nico.

Thanks a lot to our techs. First of all Marcel Dijkshoorn who has helped the cardiac people very well with proper organization and open mind. Thanks to Berend and Marieke for their help and patience when working with us.

Thanks a lot to Timo Baks and Robert-Jan van Geuns who let me think with them on the MR side of cardiac imaging.

Now I want to thank people that contributed in some way to this thesis. Pedro before and Francesco later were two important supporters. They believed in CT and in me, Koen and Nico. We shared beers, images, papers. The cooperation is undergoing and I really hope it will keep going. Thanks to both of you and good luck in your countries.

Special thanks have to go to Piotr Wielopolski, Shaid Hussain, Remy Geenen, Jan-Willem Kuiper, Lukas van Dijk, and Prof. Peter Pattynama, because of the cooperation, support and kindness.

Special thanks also to the people of the cath-lab: Eugene McFadden, Carlos van Meighem, George Sianos, Akis Arampatzis, Marco Valgimigli,... in several and different ways they all helped me to learn and better understand the world of cardiology.

Special thanks to the people of the 23rd floor of the EMC tower. Namely, Marc Kock, Mika Vogel, Adriaan Moelker, and Ruzica Maksimovic. You all were close to me in different ways.

Special thanks to Karin ten Wolde, Teun Rijsdijk, and MASSIVE THANKS to Andries Zwamborn. This book is made with their work and dedication. These people also made the nice posters I could present in Congresses around the world winning a lot prizes. Thanks a lot from the bottom of my heart.

During my PhD I had the possibility to work with other people who came to learn from me. This is an honour and a pleasure. I started also realizing how teaching is a way of learning.

The first one who came and stayed for 5 months to learn from our work was Riccardo Marano. Thanks Riccardo, to you and your nice family. For me it was Italy coming back and your help in several matters was really important.

Then Giuseppe Runza was here at EMC from Palermo (Sicily, which by the way is in Italy and the source of ¼ of my blood). I was again lucky to meet you. You wanted to learn and work hard to help me achieving good results. Thank you for your time, support and advice.

With Manuel Belgrano (from Trieste, Italy) I was again lucky. You are smart and hard worker. Thanks for your work and energies.

Latest arrivals and co-workers were Bob Meijboom and Patrizia Malagutti. Hard workers and nice people.

In the background of my activities other people played different roles. I want to mention them because of their help and their input in several different ways: Prof. Ottavio Alfieri, Prof. Paolo Maria Fioretti, Prof. Lorenzo Bonomo, Prof. Patrick Serruys, Prof. Massimo Midiri, Prof. Roberto Lagalla, Prof. Paolo Coruzzi, Dr. Massimo Gualerzi, Dr. Lorenzo Brambilla, Dr. Valerio Brambilla, Dr. Joseph Schoepf, Prof. Rossella Fattori, Dr. Giancarlo Casolo, Prof. Armando Rossi, Prof. Mario Sianesi, Dr. Sergio Venturi.

A special thank to two very good friends and colleagues with whom I shared a lot in my professional life until now. Giacomo Luccichenti and Vincenzo Lucidi, thank you for the advices, the support and the help.

In the period of my PhD I also had to work with other people on side projects. They all let me learn something new and different. This was all part of the thesis in a way.

Thanks to Jack Haitsma, Jozef Kesecioglu, Dinis Dos Reis Miranda, Prof. Lachmann, and all the guys of the 23rd floor Experimental Anaesthesiology. We "scanned" a lot of sheep and pigs while having fun.
Thanks to Edward Leter (Radiation Oncology) for the ideas and the will to carry them on. It was complex and difficult to realize your project but we all learned a lot from it.

I thank my family, Bianca, and God in the end just because I can take my time to focus and use the good words. It is easier for me to express this in Italian.

Grazie Mamma e Papá. Siete la forza che mi porto dentro da sempre. Stando lontano ho capito quanta me ne avete data durante la vita. Questo libro è per voi. Vi voglio bene, sempre.

Grazie Ludovico. Sei un fratello speciale, unico e coraggioso. Fai sempre quello che il cuore ti spinge a fare.

Bianca ti ringrazio per avere avuto pazienza, per avermi aiutato e ti chiedo scusa se le mie scelte hanno fatto sì che il tempo per noi fosse poco. Ti voglio bene.

Ringrazio Dio per essere parte costante della mia vita per mezzo delle persone che mi stanno accanto.

11. CURRICULUM VITAE AND LIST OF PUBLICATIONS

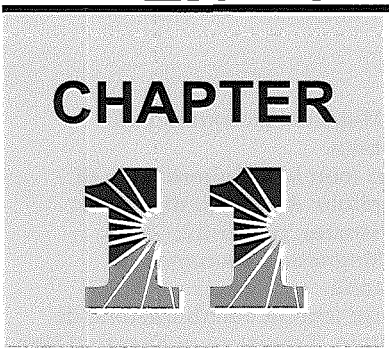

Curriculum Vitae

Filippo Cademartiri was born in Parma, Italy on June the 22nd 1973. He completed high-school at Liceo Scientifico "G. Ulivi", Parma (Italy) in July 1991. He obtained his medical degree "cum laude and honours" at the University of Parma (Italy) in May 1998. He completed his training in Radiology "cum laude" at the Department of Radiology of the University of Parma (Italy) in October 2002. Since November 2002 he is researcher in the Department of Radiology of the Erasmus Medical Center, Rotterdam (The Netherlands).

Between March 2002 and September 2002 he has been in charge of the project for the installation of the new 16-slice Computer Tomography scanner (Sensation 16 – Siemens Medical Solutions, Forchheim, Germany) at the Erasmus Medical Center, Rotterdam (The Netherlands). Between April 2003 and October 2003 he has been in charge of the project for the installation of the new 16-slice Computer Tomography scanner (Sensation 16 STRATON – Siemens) at the Erasmus Medical Center, Rotterdam. Between June 2004 and December 2004 he has been in charge of the project for the installation of the new 64-slice Computer Tomography scanner (Sensation 64 – Siemens) at the Erasmus Medical Center, Rotterdam.

He is member of the Italian Society of Radiology (SIRM), of the European Society of Cardiac Radiology (ESCR), and of the European Congress of Radiology/European Association of Radiology (ECR-EAR).

Since 1st January 2005 he is member of the Scientific Editorial Board of Cardiac section of the Journal "European Radiology".

Since 1st January 2005 he is in charge of the Non-invasive Cardiovascular Imaging Unit at the Academic Hospital of Parma, Italy.

Scientific output

He is author or co-author of 283 publications divided as follows: 1 book, 11 book chapters, 107 papers in scientific journals (67 published and the remaining "in press"), 63 oral scientific presentations at international congresses, and 101 poster presentations at international congresses.

LIST OF PUBLICATIONS

Book

Computed Tomography of the Coronary Arteries. Editors: Pim J de Feyter, Gabriel P Krestin, Filippo Cademartiri, Nico R Mollet, Koen Nieman. Publisher: Taylor & Francis, A Martin Dunitz Book, 2005. ISBN: 184184439X.

BOOK CHAPTERS

Year 2000

1. In:"Risonanza Magnetica in Gastroenterologia (Magnetic Resonance in Gastroenetrology)" Poletto Editore – Bologna – Italia.
   Paolo Pavone, Andrea Laghi, Filippo Cademartiri (con la collaborazione di Giacomo Luccichenti e Valeria Panebianco). Capitolo: Apparato digerente: Visceri cavi (Gastrointestinal tract and hollow viscera); pp 25-32; 2000.
2. In:"Risonanza Magnetica in Gastroenterologia (Magnetic Resonance in Gastroenetrology)" Poletto Editore – Bologna – Italia.
   Paolo Pavone, Andrea Laghi, Giacomo Luccichenti (con la collaborazione di Filippo Cademartiri e Valeria Panebianco). Capitolo: Trapianto di Fegato (Liver Transplantation); pp 81-88;2000.

Year 2001

3. In:"Endoscopia Toracica. Attualità e Prospettive (Thoracic Endoscopy. The present and future perspectives)" - SIET/Società Italiana di Endoscopia Toracica (Italian Society of Thoracic Endoscopy) - Giovanni Ferrante e Michele Loizzi con Giulio Deodato, Giuseppe Gotti e Francesco Gianpaglia. Publisher: Giuseppe De Nicola Editore. Napoli. Italy. 2001. (www.denicolaeditorecom).
   Giacomo Luccichenti, Filippo Cademartiri, Daniele Caporale, Antonio Bobbio, Leonardo Cattelani, Paolo Carbognani, Luigi Fecci, Paolo Pavone, Michele Rusca, Paolo Bobbio. "La Ricostruzione Tridimensionale ed Endoscopia Virtuale delle Stenosi Tracheali non Neoplastiche (Chapter: Three-dimensional reconstruction and virtual endoscopy on non-neoplastic tracheal stenosis)" - pp. 245-250.

Year 2003

4. In:"Syllabus 3rd International Workshop on: Multislice CT, 3D imaging, Virtual Endoscopy" – Editori: Paolo Pavone e Jorg F Debatin, Co-Editori: Andrea Laghi, Carlo Catalano. Publisher: Springer Verlag. Milano. Italy.
   Paolo Pavone, Giacomo Luccichenti, Filippo Cademartiri. "Three-dimensional reconstruction techniques: from MPR to Volume Rendering" - pp 3-6.
5. In:"Multislice CT - A practical guide: Proceedings of the of the 6th International SOMATOM CT scientific user conference Tuebingen" – Editors: Claussen CD, Fishman EK, Maricek B, Reiser M. Publisher: Sprinter-Verlag Inc. Heidelberg. Germany. ISBN: 3540047611.
   Gabriel P Krestin, Filippo Cademartiri. "Multislice CT angiography of the abdominal visceral arteries" – pp 137-146.
6. In:"Prostate and renal cancer, benign prostatic hyperplasia, erectile dysfunction and basic research: an update" - Proceedings of 7th Congress PACIOU/Progress and Controversies in Oncological Urology VII – Editors: CH Bangma and DWW Newling - Co-Editors: JLHR Bosh, PCMS Verhagen, GR Dohle, GW Jenster, FH Schroeder. Publisher: The Parthenon Publishing Group, New York and London, 2003. ISBN: 1-84214-196-1.
   Gabriel P Krestin and Filippo Cademartiri. "High-tech diagnostic procedures in renal cell carcinoma: promise and practice" - pp. 304-309.

Year 2004

7. In:"EuroPCR04 – The Paris Course on Revascularization" – Editors: Jean Marco, Patrick Serruys, Giancarlo Biamino, Jean Fajadet, Pim J de Feyter, Marie Claude Morice, William Wijns, Bernard de Bruyne, Alec Vahanian, Barry Katzen, Felix Mahler, Marc van Sambeek. Publisher: EUROPA Edition may 2004. ISBN: 2-913628-16-8.
   Koen Nieman, Nico R Mollet, Filippo Cademartiri, Pim J de Feyter. "Coronary spiral Computed Tomography" – pp. 197-202.
8. In:"Handbook of Vulnerable Plaque" – Editor: Ron Waksman and Patrick W Serruys. Publisher: Taylor & Francis, A Martin Dunitz Book, USA, 2004. ISBN: 1841843237.
   Pim J De Feyter, Nico R Mollet, Karen Nieman, Filippo Cademartiri, Peter Pattynama, Patrick W Serruys. "Non-invasive visualization of coronary atherosclerosis with multislice computed tomography" – pp. 237-253.
9. In:"CT of the Heart: Principles and Applications" – Editor: U. Joseph Schoepf. Publisher: Humana Press 2004. USA. ISBN: 1-59259-818-8.
   Robert J van Geuns, Filippo Cademartiri. "Anatomy of the Coronary Arteries and Veins in CT imaging" – pp. 219-228.
10. In:"CT of the Heart: Principles and Applications" – Editor: U. Joseph Schoepf. Publisher: Humana Press 2004. USA. ISBN: 1-59259-818-8.
    Filippo Cademartiri, Koen Nieman. "Contrast Material Injection Techniques for CT Angiography of the Coronary Arteries" – pp. 237-246.
11. In:"CT of the Heart: Principles and Applications" – Editor: U. Joseph Schoepf. Publisher: Humana Press 2004. USA. ISBN: 1-59259-818-8.
    Koen Nieman, Filippo Cademartiri. "CT Angiography for the Detection of Coronary Artery Stenosis" – pp. 321-332.

ARTICLES

Year 1999

1. Ferrozzi F, Cademartiri F Perforazione sigmoidea da vasculite farmaco-indotta: quadro con Tomografia Computerizzata (Iatrogenic sigmoid perforation: CT features in a case). Radiologia Medica 1999;97(5): 438-9.
2. Ferrozzi F, Cademartiri F, Zuccoli G, Izzi G. Sindrome di Pepper. Quadro con Risonanza Magnetica in un caso (Pepper Syndrome: MR features in a case). Radiologia Medica 1999; 97(6): 548-50.
3. Ferrozzi F, Cademartiri F, Tognini G. Lipoma bilaterale della parotide. Aspetti con Tomografia Computerizzata (Bilateral Parotid Lipoma: CT features in a case). Radiologia Medica 1999; 98(4); 317-8.
4. Ferrozzi F, Cademartiri F, Tognini G. Idatidosi Surrenalica. Quadro con Tomografia Computerizzata in un caso (Adrenal Idatidosis: CT features in a case). Radiologia Medica 1999; 98(5); 430-1.

Year 2000

5. Pavone P, Laghi A, Luccichenti G, Panebianco V, Cademartiri F, Spaggiari E. Cholangiopancréatographie par résonance magnétique (Magnetic Resonance CholangoPancreatography). ACTA Endoscopica 2000; 30(4); 453-464.
6. Pavone P, Luccichenti G, Cademartiri F, Laghi A, Panebianco V, Lucidi V. Virtual CT endoscopy. ACTA endoscopica 2000; 30(3) 299-428.
7. Luccichenti G, Cademartiri F, Pedrazzini M, Armaroli S, Lucidi V, Cusmano F, Pavone P. Ricostruzione tridimensionale (3D) in ambito osteo-articolare (Three-dimensional reconstruction in muscolo-skeletal applications). ACTA Bio-Medica Ateneo Parmense 2000; 71(6); 209-213.

8. Sianesi M, Del Rio P, Cademartiri F, Arcuri MF, Bertocchi A, Robuschi G. Gli Incidentalomi Surrenalici (Adrenal incidentalomas). ACTA Chirurgica Italica 2000; 56(2); 103-108.

Year 2001

9. Ferrozzi F, Tognini G, Zuccoli G, Cademartiri F, Pavone P. Peliosis hepatis with pseudotumoral and hemorrhagic evolution: CT and MR findings. Abdominal Imaging 2001 Mar;26(2):197-199. (0.866)
10. Cademartiri F, Luccichenti G, Salamousas BV, Lucidi V, Zuccoli P, Pavone P. Colonna gassosa nella vena cava inferiore: un caso con Tomografia Computerizzata (Computed Tomography of gas column inside the inferior vena cava: a case). Radiologia Medica (Torino) 2001 Jul-Aug;102(1-2):87-9.
11. Cademartiri F, Luccichenti G, Ferrozzi F, Lucidi V, Pavone P. Tumore maligno gastrico mesenchimale a differenziazione simil-leiomiomatosa: un caso con Tomografia Computerizzata (Stromal malignant gastric cancer with smooth muscle differentiation. CT features in a case). Radiologia Medica (Torino) 2001 Jul-Aug;102(1-2):80-1.
12. Pavone P, Luccichenti G, Cademartiri F Improving the results of virtual colonoscopy: what the future will bring. Seminars in Ultrasound CT and MR 2001; 22(5):400-2. (0,797)
13. Pavone P, Luccichenti G, Cademartiri F. From maximum intensity projection to volume rendering. Seminars in Ultrasound CT and MR 2001; 22(5):413-9.

Year 2002

14. Pavone P, Catalano C, Cademartiri F, Luccichenti G, Passariello R. Improvement of vascular signal intensity in contrast-enhanced MRA with Gd-BOPTA: comparison with Gd-DTPA. Academic Radiology 2002; 9 (Suppl 1):S134.
15. Pavone P, Luccichenti G, Cademartiri F, Ugolotti U. Influence of contrast media dose in elliptical ordered MR angiography image quality of the carotid arteries: preliminary results. Academic Radiology 2002; 9 (Suppl 2): S417-20.
16. Cademartiri F, van der Lugt A, Luccichenti G, Pavone P, Krestin GP. Parameters affecting bolus geometry in CTA: a review. JCAT Journal Computer Assisted Tomography 2002; 26(4) Jul-Aug; 598-607.
17. Nieman K, Cademartiri F, Lemos PA, Raaijmakers RHJM, Pattynama PMT, de Feyter PJ. Reliable non-invasive coronary angiography using fast sub-millimetre multislice spiral CT. Circulation 2002; 106: 2051-2054.
18. Cademartiri F, Luccichenti G, Rossi A, Pavone P. La TC spirale idro-dinamica nella valutazione del carcinoma del colon-sigma (Spiral hydro-CT in the evaluation of colo-sigmoideal cancer). Radiologia Medica (Torino) 2002 Oct; 104(4): 295-306.

Year 2003

19. Luccichenti G, Cademartiri F, Dake MD, Larini P, Pavone P. The value of three-dimensional reconstruction in evaluating thoracic aortic aneurysms. Circulation 2003 Feb 11;107(5):E34-5.
20. Nieman K, Cademartiri F, Raaijmakers R, Pattynama P, de Feyter PJ. Non-invasive angiographic evaluation of coronary stents with multi-slice spiral computed tomography. Herz 2003 Feb;28(2):136-42.
21. Cademartiri F, Nieman K, Raaijmakers RHJM, de Feyter PJ, Flohr T, Alfieri O, Krestin GP. Non-invasive demonstration of coronary artery anomaly performed with 16-slice multidetector spiral Computed Tomography. Italian Heart Journal 2003 Jan;4(1):56-9.

22. Luccichenti G, Cademartiri F, Ugolotti U, Marchesi G, Pavone P. Angiografia a Risonanza Magnetica con ordinamento centrico e triggerig fluoroscopico delle arterie renali (Magnetic resonance angiography with elliptical ordering and fluoroscopic triggering of the renal arteries). Radiologia Medica (Torino) 2003 Jan-Feb;105(1-2):42-7.
23. Luccichenti G, Cademartiri F, Lucidi V, Marchesi G, Ugolotti U, Pavone P. MR angiography of the carotid arteries: parameters affecting image quality. Academic Radiology 2003 May;10:520-26.
24. Cademartiri F, Nieman K, Mollet N. An unusual case of chest murmur demonstrated with three-dimensional volume rendering with 16-row multislice spiral computed tomography. Heart 2003 Jun;89(6):586.
25. Luccichenti G, Cademartiri F, Pavone P. Assessment of organ volume with different techniques using a living liver model. European Radiology 2003 Jun;13(6):1286-90.
26. Cademartiri F, Nieman K, Raaijmakers R, de Feyter PJ, Alfieri O, Krestin GP. Three-dimensional Volume Rendering with Multislice Computed Tomography in the evaluation aortic coarctation. Italian Heart Journal 2003 Apr;4(4):286-7.
27. Cademartiri F, Nieman K, Mollet NR. The dynamics of an ascending aorta dissection by 16-row multislice computed tomography. Heart 2003 Sep; 89(9): 970.
28. van Dijk LC, van Sambeek M, Cademartiri F, Pattynama PM. Partial Blockage of the Renal Artery Ostium After Stent-Graft Placement: Detection and Treatment. Journal of Endovascular Therapy 2003 Jun;10(3):684.
29. Luccichenti G, Cademartiri F, Ugolotti U, Pavone P. Tecniche di acquisizione e di timing in angiografia con Risonanza Magnetica (Technique and timing in contrast-enhanced MR angiography). Radiologia Medica (Torino) 2003 May-Jun;105(5-6):471-481.
30. de Feyter PJ, Serruys PW, Nieman K, Mollet N, Cademartiri F, van Geuns RJ, Slager C, ven der Steen AFW, Krams R, Schaar JA, Wielopolski P, Pattynama PMT, Arampatzis A, van der Lugt A, Regar E, Lightart J, Smits P. Imaging of coronary atherosclerosis and identification of the vulnerable plaque. Netherlands Heart Journal 2003 Sep; 11(9): 347-356.
31. Cademartiri F, Aad van der Lugt, Krestin GP. 16-slice CT tackles cerebrovascular disorders. Multidetector CTA offers one-stop-shop for stroke assessment. Diagnostic Imaging Europe 2003 October: 21-27.
32. Cademartiri F, Nieman K, Mollet N, Flohr TG, Alfieri O, de Feyter PJ, Krestin GP. Un anno di esperienza con coronarografia non invasiva mediante tomografia computerizzata spirale multistrato a 16 linee di detettori (Non-invasive 16-row spiral multislice computed tomography coronary angiography after one year of experience). Italian Heart Journal 2003 Jul;4(7 Suppl):587-93.
33. Cademartiri F, Nieman K, Mollet N, Alfieri O, de Feyter PJ, Krestin GP. Images in cardiovascular medicine. Sixteen-row multislice computed tomography of tuberculous pericardial abscess. Italian Heart Journal 2003 Aug;4(8):575-6.
34. Luccichenti G, Cademartiri F, Fecci L, Carbognani P, Rusca M, Pavone P. Alterazioni non neoplastiche della trachea: paragone tra broncoscopia virtuale mediante TC e broncoscopia a fibre ottiche (Non-neoplastic tracheal alterations: comparison between CT virtual bronchoscopy and fiber-optic bronchoscopy). Radiologia Medica 2003 Sep;106(3):147-153.

35. Cademartiri F, Luccichenti G, Marano R, Nieman K, Mollet N, de Feyter PJ, Krestin GP, Pavone P, Bonomo L. Angio-TC con apparecchiature spirali ad uno, quattro e sedici strati: nota tecnica (Spiral CT-angiography with one, four and 16 slice scanners: technical note). Radiologia Medica 2003 Oct;106(4):269-283.
36. Cademartiri F, Luccichenti G, Marano R, Nieman K, Mollet N, de Feyter PJ, Krestin GP, Bonomo L. Angiografia coronarica non invasiva con tomografia computerizzata spirale multistrato: stato dell'arte e prospettive future (Non-invasive coronary angiography with multislice spiral computed tomography: state of the art and future perspectives). Radiologia Medica 2003 Oct;106(4):284-296.
37. Cademartiri F, Stojanov D, Dippel DWJ, van der Lugt A, Thange H. Non-invasive detection of a ruptured aneurysm at a basilar artery fenestration with sub-millimeter multislice CT angiography. American Journal of Neuroradiology 2003 Nov/Dec; 24: 2009-2010.
38. de Feyter PJ, Mollet N, Cademartiri F, Nieman K, Pattynama P. MS-CT coronary imaging. Journal of Interventional Cardiology 2003 Dec;16(6): 465-468.
39. Cademartiri F, Mollet N, Nieman K, Krestin GP, de Feyter PJ. Neo-intimal hyperplasia in carotid stent detected with Multislice Computed Tomography. Circulation 2003 Nov;108(21); e147.
40. Luccichenti G, Cademartiri F, Pavone P. MR angiography of the Carotid arteries. Highlights in MRI 2003; 1(1);1-4.
41. Cademartiri F. Imaging coronarico non invasivo: stato dell'arte e prospettive future (Non-invasive coronary imaging: state of the art and future perspectives). Cardio Vascular Therapy and Prevention 2003:3(1);7-13.
42. Mollet N, Nieman K, Cademartiri F, Raaijmakers R, Pattynama PMT, de Feyter PJ. MSCT coronary angiography: present and future. Applied Radiology 2003:Dec;22-25.
43. Cademartiri F, Pavone P. Advantages of retrospective ECG-gating in cardio-thoracic imaging with 16-row multislice computed tomography (Vantaggi del gating elettrocardiografico retrospettivo nell'imaging cardio-toracico mediante tomografia computerizzata multistrato a 16 canali). Acta Biomedica Ateneo Parmense 2003 Dec;74(3):126-30.

Year 2004

44. Geenen RW, Hussain SM, Cademartiri F, Poley JW, Siersema PD, Krestin GP. CT and MR Colonography: Scanning Techniques, Postprocessing, and Emphasis on Polyp Detection. Radiographics 2004 Jan-Feb; 24(1): e18. Epub 2003 Oct 03.
45. de Feyter PJ, Mollet N, Nieman K, Arampatzis A, Cademartiri F, Pattynama P, Serruys P. Noninvasive visualisation of coronary atherosclerosis with multislice computed tomography. Cardiovascular Radiation Medicine 2004 Jan-Mar;5(1):49-56.
46. Cademartiri F, Mollet NR, van der Lugt A, Nieman K, Pattynama PMT, de Feyter PJ, Krestin GP. Non-invasive 16-row multislice computed tomography coronary angiography: usefulness of saline chaser. European Radiology 2004 Feb;14(2):178-183. Epub 2003 Dec 19.
47. Cademartiri F, Nieman K, Mollet N, de Feyter PJ, Krestin GP. Pseudo-aneurysms of the ascending aorta demonstrated with «motion-free» multislice computed tomography. Circulation 2004 Feb 17;109(6):e42-3.

48. Cademartiri F, Marano R, Luccichenti G, Mollet N, Nieman K, de Feyter PJ, Krestin GP, Bonomo L. Anatomia normale del circolo coronarico con tomografia computerizzata multistrato a 16 canali (Normal anatomy of coronary vessels with 16-rows multislice computed tomography). Radiologia Medica 2004 Jan-Feb;107(4):11-23.
49. Cademartiri F, Luccichenti G, Marano R, Pavone P. Tecniche per ottimizzare l'opacizzazione coronarica in angiografia non invasiva con TC multistrato a 16 detettori (Techniques for the optimisation of coronary artery opacification in non-invasive angiography with a 16-row multislice computed tomography). Radiologia Medica 2004 Jan-Feb;107(4):24-34.
50. Cademartiri F, Luccichenti G, van der Lugt A, Pavone P, Pattynama PM, de Feyter PJ, Krestin GP. 16-row Multislice Computed Tomography: basic concepts, protocols and enhanced clinical applications. Seminars in Ultrasound CT and MRI 2004 Feb:25(1); 2-16.
51. Cademartiri F, Mollet N, Nieman K, Alfieri O, Krestin GP. Motion-free ECG-gated 16-row multislice Computed Tomography in the follow-up of Aortic Coarctation with Three-Dimensional Volume Rendering. Italian Heart Journal 2004 Feb;5(2):167-68.
52. Maksimovic R, Cademartiri F, Scholten M, Jordaens LJ, Pattynama PM. Sixteen-row multislice computed tomography in the assessment of pulmonary veins prior to ablative treatment: validation vs conventional pulmonary venography and study of reproducibility. European Radiology 2004 Mar;14(3):369-74. Epub 2003 Nov 14.
53. Cademartiri F, van Geuns RJ, Nieman K, Meijeboom F, de Feyter PJ. Multislice computed tomography for the evaluation and follow-up of stenting of aortic coarctation. Circulation 2004 Apr 6;109(13):e176.
54. Cademartiri F, Mollet NR, Nieman K, Szili-Torok T, de Feyter PJ. Right coronary artery arising from the left circumflex demonstrated with multislice computed tomography. Circulation 2004 Apr 20;109(15):e185-186.
55. Cademartiri F, Pavone P. Computed Tomography coronary angiography with a 16-row multislice scanner: early experience and technical considerations (Angiografia coronarica con Tomografia Computerizzata spirale multistrato a 16 canali: esperienza preliminare e considerazioni tecniche). Acta Biomedica Ateneo Parmense 2004 Apr;75(1):63-68.
56. Cademartiri F, Luccichenti G, Marano R, Gualerzi M, Brambilla L, Coruzzi P. Confronto tra tecnica monofasica e tecnica bifasica di somministrazione del mezzo di contrasto in coronarografia non invasiva mediante TC multistrato a 16 canali (Comparison of monophasic vs. biphasic administration of contrast material in non-invasive coronary angiography using a 16-row multislice computed tomography). Radiologia Medica 2004 May-Jun;107(5-6):489-96.
57. Cademartiri F, Luccichenti G, Marano R, Runza G, Midiri M. Utilizzo della soluzione salina nella somministrazione endovenosa del mezzo di contrasto in coronarografia non invasiva con TC multistrato a 16 detettori (Use of saline chaser in the intravenous administration of contrast material in non-invasive coronary angiography with 16-row multislice computed tomography). Radiologia Medica 2004 May-Jun;107(5-6):497-505.
58. Mollet NR, Cademartiri F, Nieman K, Saia F, Lemos PA, McFadden EP, Pattynama PM, Serruys PW, Krestin GP, de Feyter PJ. Multislice Computed Tomography coronary angiography in stable angina pectoris. Journal of the American College of Cardiology 2004 Jun 16;43(12):2265-2270.

59. Cademartiri F, Raaijmakers RHJM, Kuiper JW, van Dijk LC, Pattynama PMT, Krestin GP. Role of non-invasive angiography with 4 and 16-multidetector-row CT in the evaluation of patients with Abdominal Angina. Radiographics 2004 Jul-Aug; 24(4): 969-84.
60. Galia M, Lo Casto A, Midiri M, Bellia M, Bartolotta TV, Cademartiri F, De Maria M, Lagalla R. Broncoscopia virtuale in pazienti stenosi endobronchiali centrali. Ottimizzazione tecnica con TC a singolo strato (Virtual bronchoscopy in patients with central endobronchial stenosing lesions. Technique optimisation with single slice spiral CT. Radiologia Medica (Torino) 2004 Jul-Aug; 108(1-2):28-38.
61. Cademartiri F, Luccichenti G, Laganà F, Brevi B, Sesenna E, Pavone P. Effective clinical outcome of a mandibular distraction device using three-dimensional CT with volume rendering in Pierre-Robin sequence. Acta Biomedica Ateneo Parmense 2004 Aug; vol. 75(2): 122-125.
62. Luccichenti G, Cademartiri F, Pizzigallo A, Cusmano F, Bastianello S. Semiologia TC e RM dei carcinomi della lingua (Computed Tomography and Magnetic Resonance features of carcinoma of the tongue). Radiologia Medica 2004 Oct 108; 394-403.
63. Cademartiri F, Nieman K, van der Lugt A, Raaijmakers RH, Mollet N, Pattynama PMT, de Feyter PJ, Krestin GP. Intravenous contrast administration at 16-Detector Row Helical CT coronary angiography: Test Bolus vs. Bolus Tracking. Radiology 2004 Dec;233(3):817-23. Epub 2004 Oct 29.
64. Mollet N, Cademartiri F. In-Stent Neo-Intimal Hyperplasia with 16-row Multislice Computed Tomography Coronary Angiography. Circulation 2004 Nov 23; 110 (21): e514.
65. Cademartiri F, Mollet N, Lemos PA, McFadden EP, Marano R, Baks T, Stijnen T, de Feyter PJ, Krestin GP. Standard vs. user-interactive post-processing for the detection of significant coronary artery stenosis with 16-row multislice computed tomography. American Journal of Cardiology 2004 Dec 15; 94(12): 1590-3.
66. Bartolotta TV, Midiri M, Quaia E, Bertolotto M, Galia M, Cademartiri F, Lagalla R. Liver haemangiomas undetermined at grey-scale ultrasound: contrast-enhancement patterns with SonoVue and pulse-inversion US. European Radiology 2004 Dec 21; [Epub ahead of print].
67. Mollet N, Cademartiri F, Krestin GP, McFadden EP, Arampatzis A, Serruys PW, de Feyter PJ. Non-invasive Multislice Computed Tomography coronary angiography with improved temporal resolution. Journal of the American College of Cardiology 2005 Jan 4;45(1): 128-132.

MAIN IN PRESS PUBLICATIONS

68. Luccichenti G, Cademartiri F, Sianesi M, Roncoroni L, Pavone P, Krestin GP. Radiological assessment of recto-sigmoidal cancer pre and post neo-adjuvant radiation therapy: comparison between conventional unidimensional and three-dimensional quantitation techniques. American Journal of Roentgenology (in press).
69. Mollet NR, Cademartiri F, de Feyter PJ. Non-invasive multislice-CT coronary imaging. Heart (in press) 2005.
70. Cademartiri F, Mollet NR, van der Lugt A, McFadden EP, Stijnen T, de Feyter PJ, Krestin GP. IV contrast administration for CT coronary angiography on a 16-multidetector-row helical CT scanner: impact of iodine concentration. Radiology (in press).

71. Mollet NR, Cademartiri F, de Feyter PJ. Imaging the coronary vasculature (using Multislice Computed Tomography). Heart and Metabolism (in press) 2004.
72. De Monye C, Cademartiri F, de Weert T, Siepman DAM, Dippel DWJ, van der Lugt A. CT angiography of the carotid arteries with 16-row multislice computed tomography scanner: comparison of different amounts of contrast material with and without bolus chaser. Radiology (in press).
73. Mollet NR, Hoye A, Lemos PA, Cademartiri F, Sianos G, McFadden EP, Krestin GP, Serruys PW, de Feyter PJ. Value of pre-procedure Multislice CT coronary angiography to predict failed percutaneous recanalization of chronic total occlusions. American Journal of Cardiology January 2005 (in press).
74. Maksimovic R, Scholten M, Cademartiri F, Jordaens LJ, Pattynama PM. 16-row Multi Slice Computed Tomography of the Pulmonary Veins: Three months follow-up after treatment of paroxysmal atrial fibrillation with cryothermal ablation. European Radiology (in press).
75. Cademartiri F, Mollet NR, Lemos PA, Saia F, Runza G, Midiri M, Krestin GP, de Feyter PJ. Impact of coronary calcium score on diagnostic accuracy for the detection of significant stenosis with multislice computed tomography coronary angiography. American Journal of Cardiology (in press).
76. Cademartiri F, Mollet NR, Runza G, Bruining N, Hamers R, Somers P, Knaapen M, Verheye S, Midiri M, Krestin GP, de Feyter PJ. Influence of intracoronary attenuation on coronary plaque measurements using multislice CT: observations in an ex–vivo model of coronary CT angiography. European Radiology (in press).
77. Mollet NR, Cademartiri F, Nieman K, Saia F, Lemos PA, McFadden EP, Pattynama PM, Serruys PW, Krestin GP, de Feyter PJ. Multislice computed tomography: assessment of coronary plaque burden. American Journal of Cardiology (in press).
78. Cademartiri F, Mollet NR, Runza G, Midiri M, McFadden E, Ohnesorge B, Flohr TG, de Feyter PJ, Krestin GP. Reduction of motion artefacts from mild heart rhythm irregularities with ECG-editing using multislice computed tomography coronary angiography. American Journal of Roentgenology (in press).
79. Cademartiri F, Mollet NR, Lemos PA, McFadden EP, Krestin GP, de Feyter PJ. Multislice computed tomography coronary angiography to assess in-stent restenosis. American Journal of Cardiology (in press).

Colour images section

CHAPTER 12

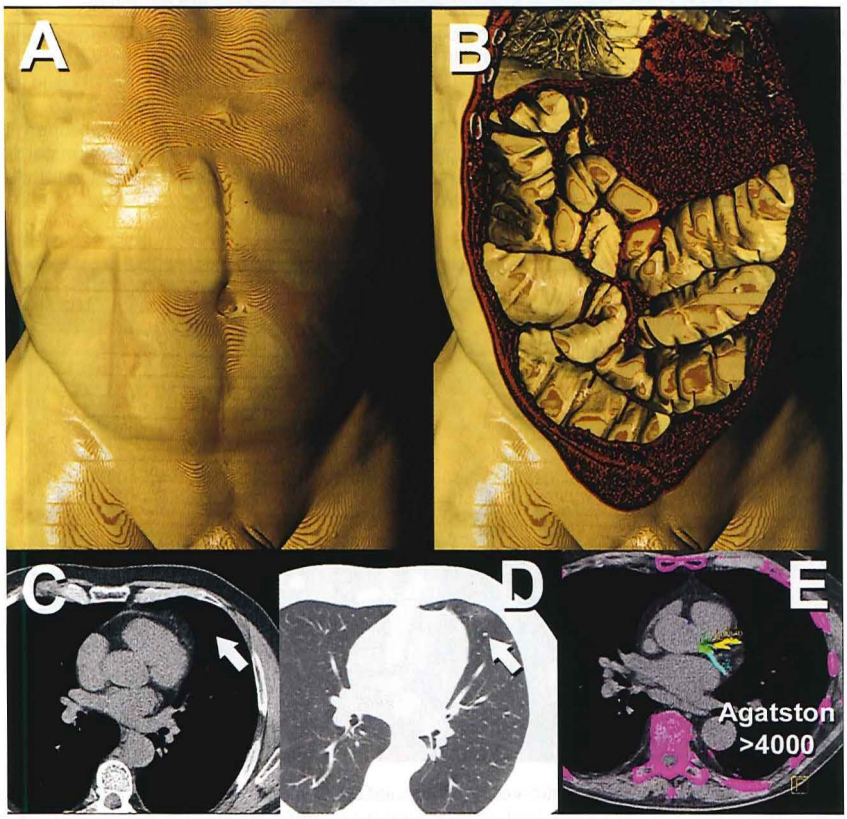

Chapter 2.1, Page 26; Figure 6. Screening MSCT applications. The main screening applications for MSCT are colon cancer (**A** and **B**), lung cancer (**C** and **D**), and coronary artery disease (**E**). Virtual colonography with MSCT shows considerable potential because of its high resolution but mostly because of the demonstrated progression from polyp to colon cancer that takes up to 10 years. The early detection of lung nodules, even though feasible with low-dose MSCT, has not yet provided good evidences of a low cost-to-benefit ratio. The biology of lung cancer and the high rate of false positives and collateral findings raise concerns about the widespread use of this technique. The main problem remains the management of small lung nodules (arrow in **C** and **D**). Coronary artery calcium score is a well-established technique to assess risk for coronary events (**E**). The experience was gained with electron-beam tomography (EBT)-based trials and it is expected that the same or similar outcomes will be obtained with MSCT.

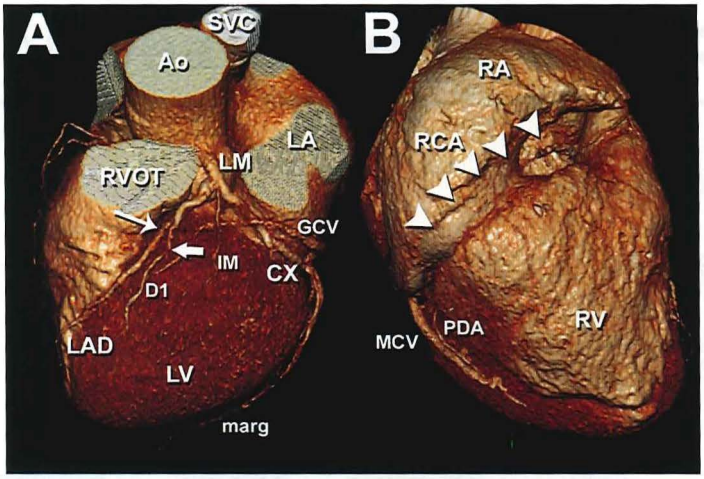

Chapter 2.1, Page 36; Figure 9. Coronary angiography with 16-row MSCT. Three-dimensional volume rendering images. (A) In an oblique right anterolateral view, a diseased left anterior descending (LAD; thin arrow) and a stenosis of the first diagonal branch (D1; thick arrow) are shown. (B) In the oblique left lateral view an occluded right coronary artery (RCA) is displayed (arrowheads). Abbreviations: Ao ascending aorta; CX circumflex; D1 first diagonal branch; GCV great cardiac vein; IM intermediate branch; LAD left anterior descending; LM left main; LV left ventricle; marg marginal branch; MCV median cardiac vein; PDA posterior descending artery; RA right atrium; RCA right coronary artery; RV right ventricle; RVOT right ventricle outflow tract; VSC superior vena cava.

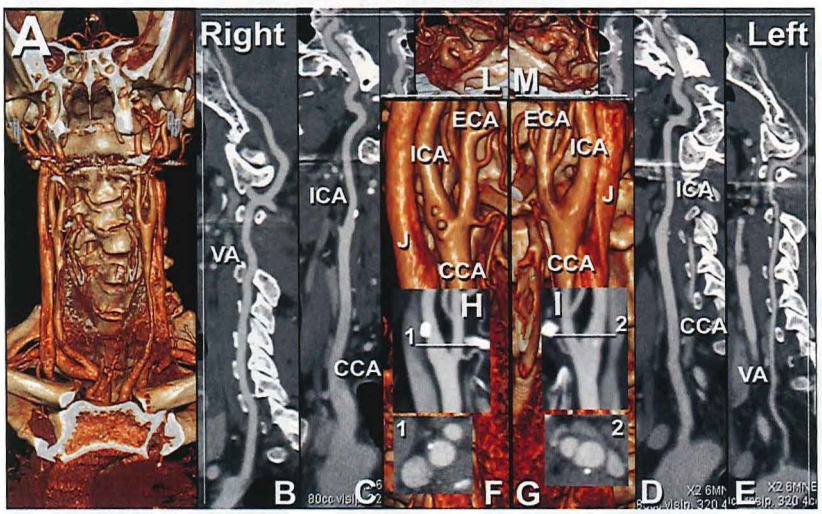

Chapter 2.1, Page 37; Figure 10. Carotid-vertebral circulation examined with 16-row MSCT angiography. (**A**) The panoramic view, with 3-dimensional volume rendering, demonstrates the whole scan range from the aortic arch to the circle of Willis. (**B-E**) To study both the carotid and vertebral arteries, curved MPR can be performed throughout the dataset. (**F** and **G**) To study the carotid bifurcation, 3-dimensional volume rendering can be used; but to evaluate patency and plaque morphology, MIPs (**H** and **I**) are required, and targeted axial cuts (1 and 2) are especially useful. (**L** and **M**) The intracranial portion of the internal carotid artery can be easily studied with 3-dimensional volume rendering (**L** and **M**; inner images) and curved MPR (**L** and **M**; lateral images). Abbreviations: CCA common carotid artery; ECA external carotid artery; ICA internal carotid artery; J jugular vein.

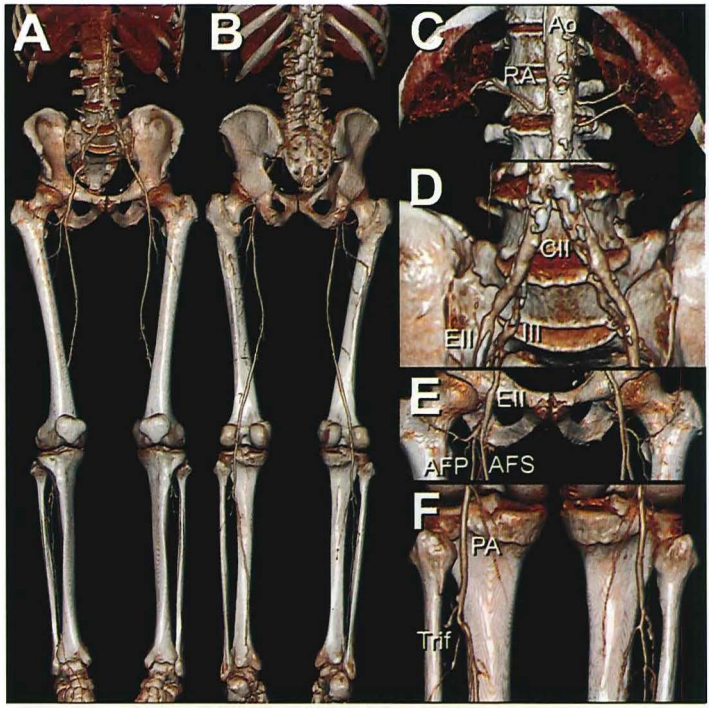

Chapter 2.1, Page 38; Figure 11. Peripheral run-off with 16-row MSCT angiography. The anterior (**A**) and posterior (**B**) views of the entire scan range for a peripheral run-off study are displayed with 3-dimensional volume rendering in a diffusely diseased patient. Magnified images show the level of the renal artery (**C**), where accessory vessels are present on both sides, the level of aortic bifurcation (**D**), the level of femoral bifurcation (**E**), and the level of popliteal trifurcation (**F**). Abbreviations: Ao aorta; CII common iliac arteries; EII external iliac arteries; IIA internal iliac arteries; AFP arteria femoralis profunda; AFS arteria femoralis superficialis; PA popliteal artery; trif trifurcation.

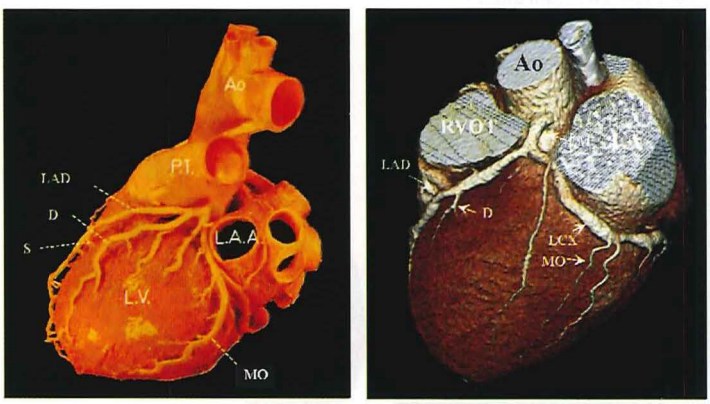

Chapter 4.1, Page 108; Figure 4. (**A**) Anatomical view of the left coronary artery (reproduced with permission from [13]). The auricle of the left atrium (L.A.A.) overlapping the circumflex coronary artery is removed. The left main (LM) artery divides beneath the L.A.A. in the left anterior descending (LAD) and circumflex (LCx) coronary arteries. From the LAD artery diagonal branches (D) arise. The margo obtusus (MO) arises from the LCx artery. (**B**) A comparable noninvasive coronary angiogram with computed tomography. Ao, aorta; PT, pulmonary trunk; LA, left atrium, after removal of the auricle; LV, left ventricle; RVOT, right ventricular outflow track.

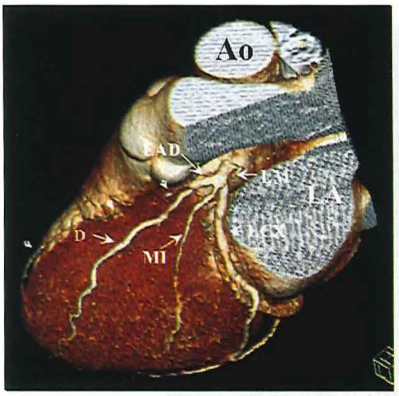

Chapter 4.1, Page 108; Figure 5. Coronary CT angiography, trifurcation of the left main artery into left anterior descending (LAD), circumflex (LCx), and intermediate (MI) arteries. The LAD is occluded after the first diagonal branch (D) but shows some contrast filling through collateral vessels (arrowheads).

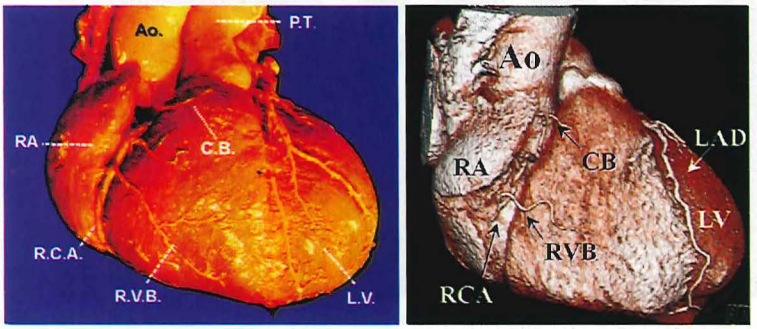

Chapter 4.1, Page 109; Figure 7. (**A**) A pressure-fixed anatomical specimen showing the proximal and middle right coronary artery (RCA) with its side branches (conus branch [CB] and right ventricular branch [RVB]). Reproduced from McAlpine (13) with permission of Springer-Verlag. (**B**) A 3-D rendering of the right coronary artery. Because of the small size, only the proximal part of the conus branch can be seen. The RCA shows atherosclerotic disease over its full length. At the right side of the picture, the left anterior descending (LAD) coronary artery can be clearly seen. Ao, ascending aorta; PT, pulmonary trunk; LV, left ventricle; RV, right ventricle; RA, right atrium.

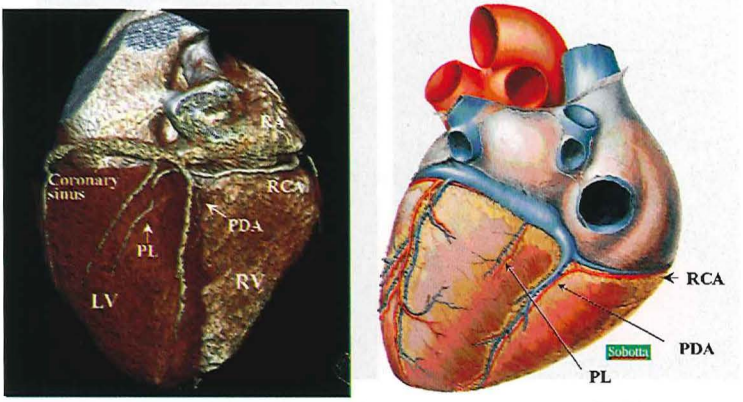

Chapter 4.1, Page 110; Figure 8. Distal right coronary artery (RCA), diaphragmatic view. (**A**) Coronary CT angiography. At the crux the RCA divides into the posterodescending artery (PDA) and postero-lateral (PL) branch over the inferior wall of the left ventricle (LV). RV, right ventricle; RA, right atrium. (**B**) Anatomical view. (Reproduced with permission from the Medical Illustration Library, Williams & Wilkins, Baltimore.)

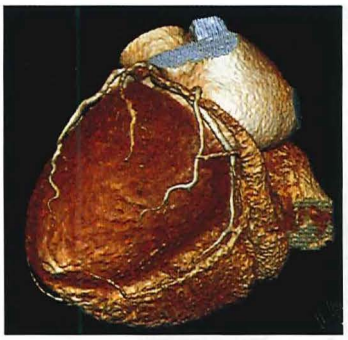

Chapter 4.1, Page 110; Figure 9. Left coronary artery dominance. Posterior descending artery (PDA) and postero-lateral (PL) branch originate from the circumflex (LCx) coronary artery. LV, left ventricle; RV, right ventricle.

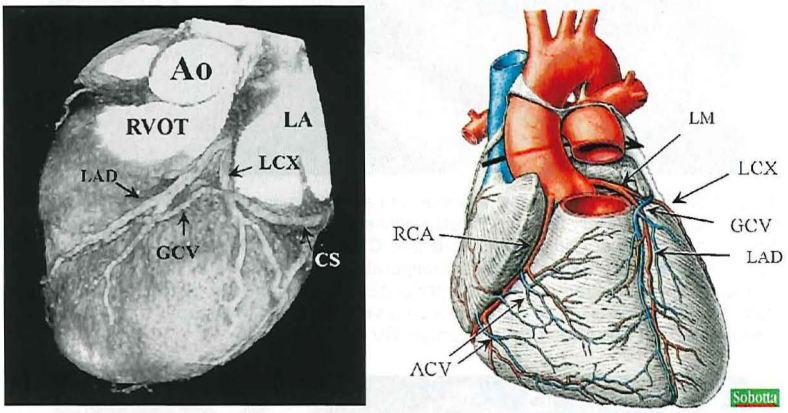

Chapter 4.1, Page 112; Figure 11. The great cardiac vein (GCV) turns from the anterior interventricular groove into the atrioventricular groove, crossing all the branches of the left coronary artery and forming the triangle of Brocq and Mouchet together with the left anterior descending (LAD) and circumflex (LCx) coronary arteries. (**A**) CTA: the view at the LCx artery is obstructed by the GCV. (**B**) Comparative anatomical view (reproduced with permission from the Medical Illustration Library, Williams & Wilkins, Baltimore). LM, left main artery; RCA, right coronary artery; ACV, anterior cardiac veins.

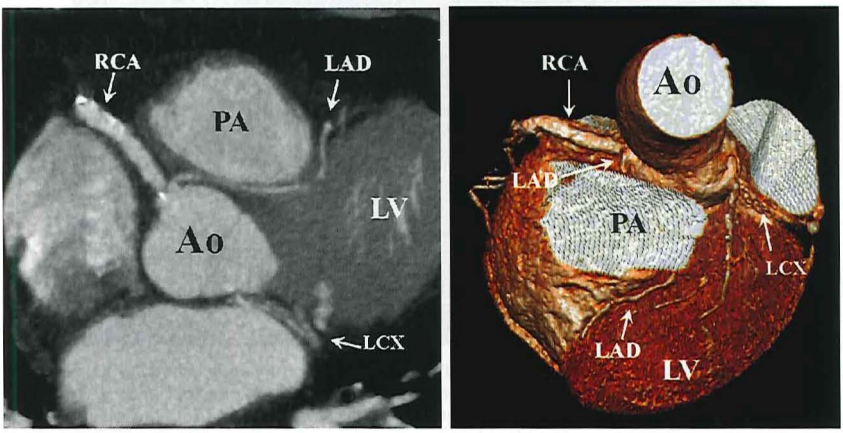

Chapter 4.1, Page 115; Figure 15. Left anterior descending (LAD) coronary artery from right coronary cusp. (**A**) Curved axial MIP demonstrating the inter-arterial course of the LAD between the pulmonary artery (PA) and the aorta (Ao). (**B**) VRT image. The proximal and distal LAD are clearly visible; the interarterial course is covered by the PA. LCx, left circumflex coronary artery; RCA, right coronary artery; LV, left ventricle.

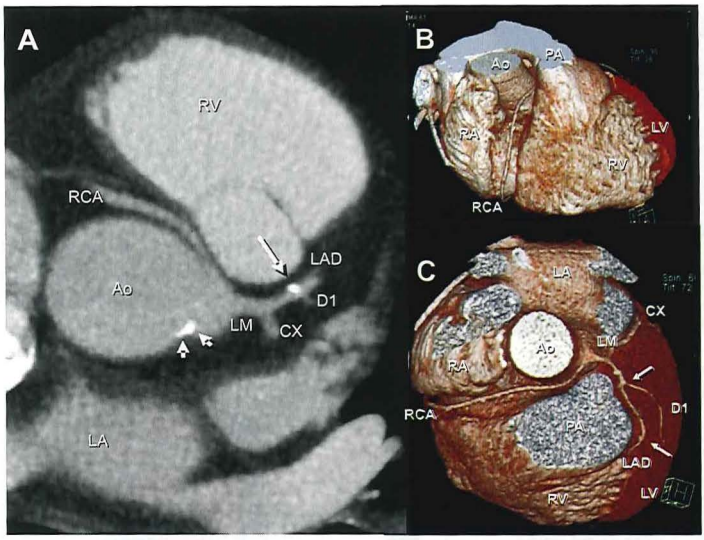

Chapter 4.2, Page 120; Figure 1. In **A** an axial image with a multiple intensity projection algorithm is displayed. The origin of the right coronary artery (RCA) is located between the anterior wall of the ascending aorta (Ao) and the posterior wall of the pulmonary artery (PA). In **B** and **C** the data-set is displayed with a three-dimensional volume rendered algorithm. The proximal and mid configurations of the RCA are displayed. A few atherosclerotic lesions with calcification may be seen on the left anterior descending coronary artery (LAD) (arrows) and at the level of the aortic wall (arrowheads). CX = circumflex coronary artery; D1 = diagonal 1; LA = left atrium; LM = left main coronary artery; LV = left ventricle; RA = right atrium; RV = right ventricle.

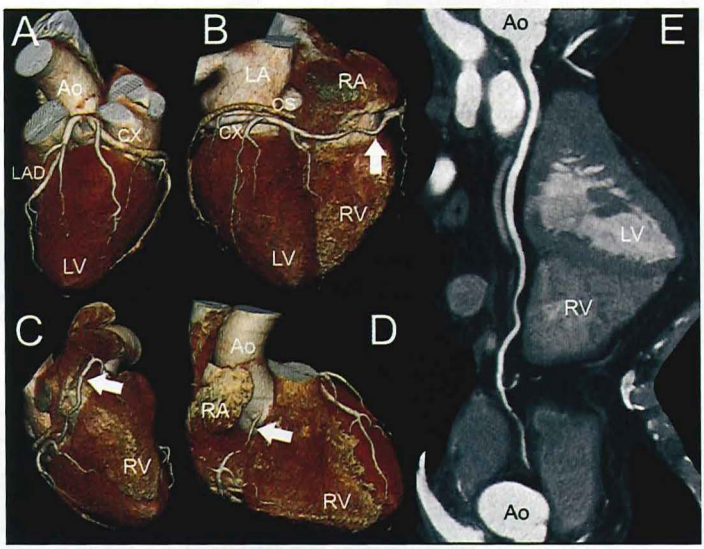

Chapter 4.3, Page 126; Figure 1. Multislice computed tomography coronary angiography. A 3D volume rendering is applied to the dataset in **A** through **D**, whereas a curved planar reconstruction is performed along the lumen of the left circumflex in **E**. The multislice computed tomography scan shows a split origin of the left coronary artery (**A**; Movie I). Therefore, this anomaly cannot be identified as a "single" coronary artery. The left circumflex runs first in the left atrioventricular groove (**A**), crosses the crux (**B**, arrow), and then goes further in the right atrioventricular groove (**C**, arrow), ending 1 cm before the wall of the ascending aorta (**D**, arrow) on the opposite side of its own origin (**E**; Movie I). No ostium of the right coronary artery in the region of the right Valsalva sinus was detected (**D** and **E**; Movie I). Ao indicates ascending aorta; CS, coronary sinus; CX, circumflex; LAD, left anterior descending; LA, left atrium; LV, left ventricle; RA, right atrium; and RV, right ventricle.

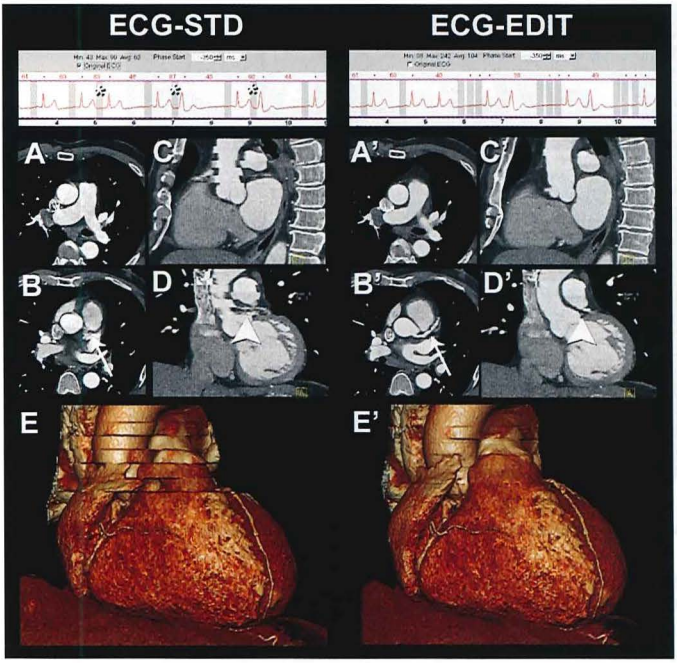

Chapter 5.1, Page 130;
Figure 2. Correction of artefacts from premature beats. Example of dataset with premature beats before (left panel) and after (right panel) ECG editing. The ECG of the left panel shows three premature beats (asterisks) in a background heart rate of ~45bpm. The dataset resulting from a reconstruction performed without any editing shows motion artefacts at the level of the pulmonary artery (**A**) and at the origin of the left coronary artery (**B** - arrow). Sagittal and coronal reconstructions (**C** and **D**) show the impact of these three premature beats on the ascending aorta and on the origin of the left coronary artery (**D** - arrowhead). In **E** a frontal view of the dataset with three-dimensional volume rendering shows the misalignment of the stacks of images in the cranial part of the dataset. After ECG-editing, the artefacts are ruled out and coronary vessels are assessable (**A'-E'**). A significant stenosis of proximal left anterior descending was missed because of the artefacts (**B'** - arrow; **D'** - arrowhead).

Chapter 5.1, Page 131;
Figure 3. Correction of artefacts from mis-triggering. Example of dataset with mis-triggering before (left panel) and after (right panel) ECG editing. The ECG on the left panel shows an anomaly of the conduction for one heart beat that result in a missing synchronisation point and very long RR interval. The appearance of this event is showed by the arrow in three-dimensional volume rendering (**A**), a dedicated double oblique MIP for the right coronary artery (**B**), a coronal MIP (**C**), and two curved reconstructions: one for the right coronary artery (**D**), and one for the left main-left anterior descending (**E**). The data are missing because the RR interval is too large, and two coronary segments have to be considered not assessable. After ECG editing by means of inserting the synchronisation point in the correct position (ECG in the right panel), all the images are recovered (**A'-E'**).

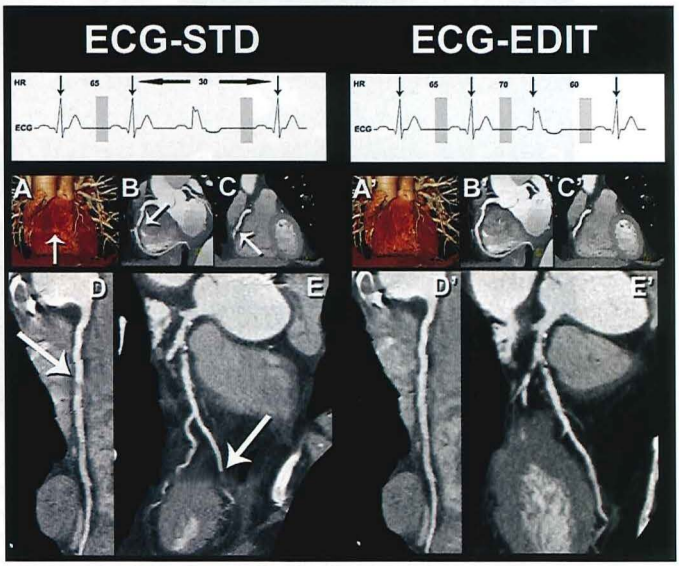

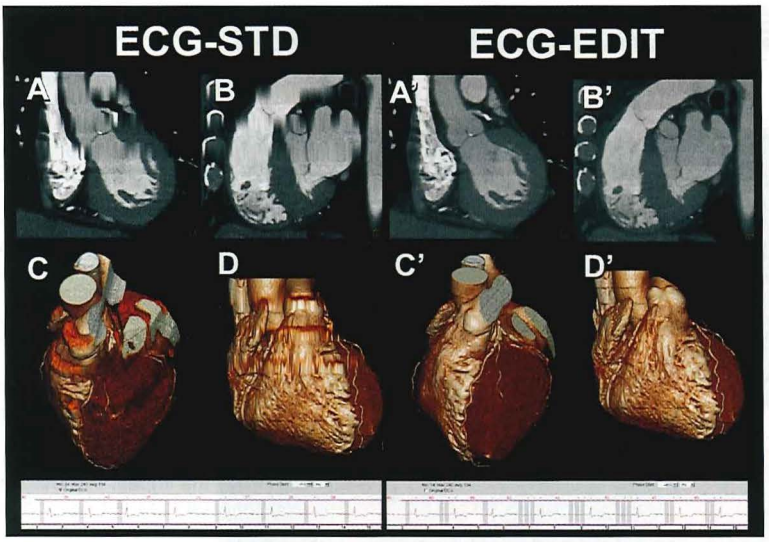

Chapter 5.1, Page 132; Figure 4. Correction of artefacts from low heart rate. Example of dataset with low heart rate before (left panel) and after (right panel) ECG editing. The ECG on the left panel shows a very low heart rate almost always below 40bpm. This determines data gaps that appear in coronal (**A**), sagittal (**B**), and three-dimensional reconstructions (**C** and **D**), as blurring of stacks of images. After ECG editing by means of inserting additional synchronisation points (ECG in the right panel), all the images are recovered (**A'-D'**).

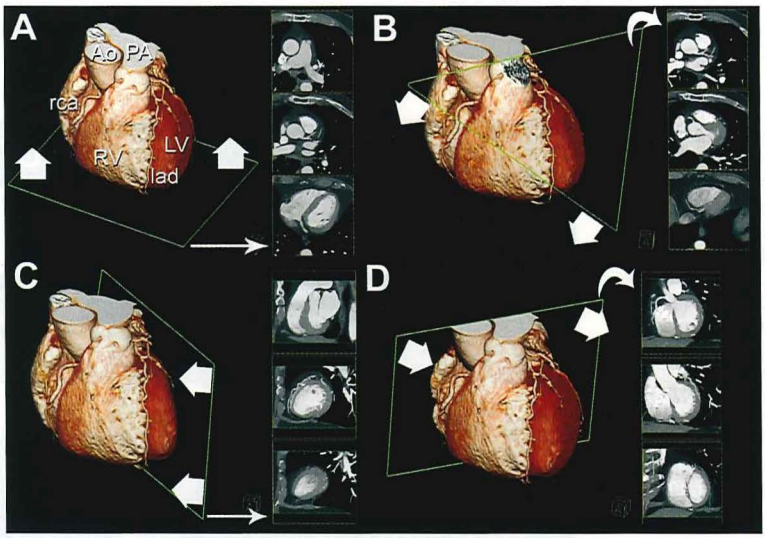

Chapter 5.2, Page 147; Figure 1. Imaging modalities and planes applied for the standard projections protocol. (**A**) The axial plane is displayed and sample images are shown in the right column from the bottom (caudal end) to the top (cranial end) of the dataset. (**B**) A paraaxial plane parallel to the course of left anterior descending is shown and in the right column sample images show the appearance of the origin of the left coronary artery, the right coronary artery, and the posterior descending artery, from top to bottom. (**C**) The plane is running parallel to the interventricular groove to display the left anterior descending artery and in the right column sequential images are shown. (**D**) The plane is parallel to the atrioventricular groove for the visualization of the right coronary artery and for the left circumflex artery, which are displayed in the right column. In (**A**) to (**D**), thick arrows indicate the direction of scrolling of the plane. Ao ascending aorta; lad left anterior descending; LV left ventricle; PA pulmonary artery; RV right ventricle; rca right coronary

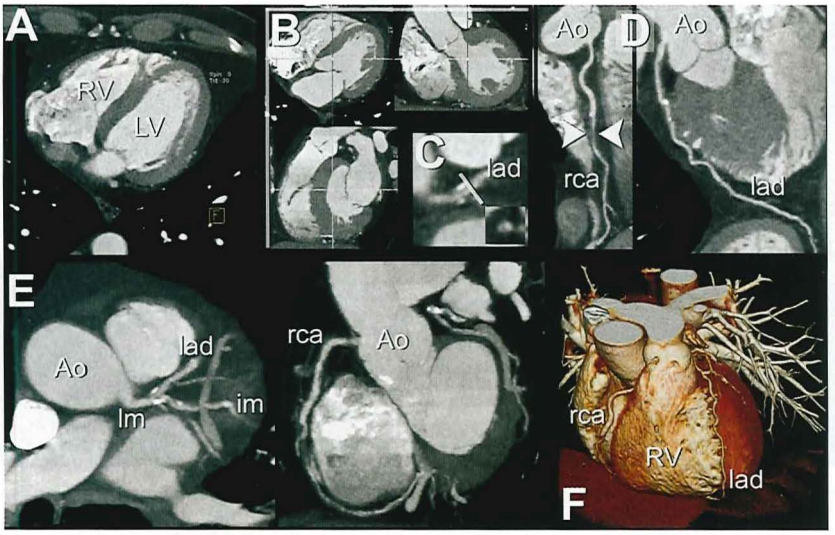

Chapter 5.2, Page 147; Figure 2. Imaging modalities applied for the interactive postprocessing protocol. Axial slices (**A**) and multiplanar reconstructions (**B**) are the basic tools for image assessment. Then, a multiplanar reconstruction focused on the stenosis (**C**; proximal stenosis of the left anterior descending artery) integrated with dedicated curved reconstructions along the lumen (**D**; stenosis in the midright coronary artery; arrowheads) are performed. In parallel, maximum intensity projections (**E**) and 3-dimensional volume rendering (**F**) are performed to improve panoramic perception. im intermediate branch; lm left main; other abbreviations as in Figure 1.

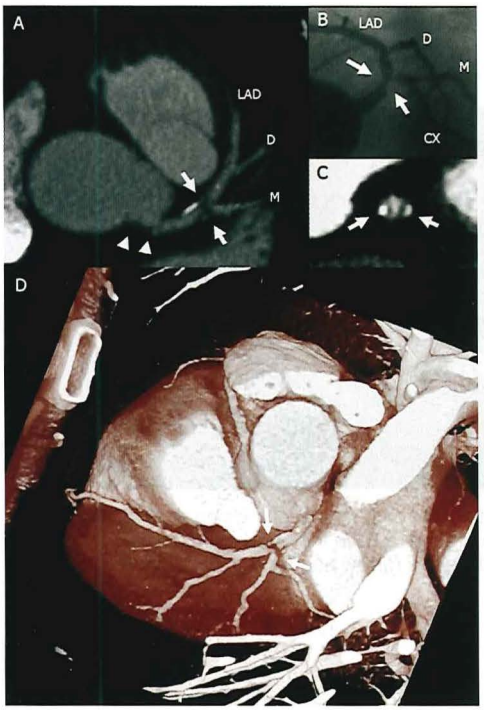

Chapter 6.1, Page 161; Figure 3. Lesions in the left main bifurcation. A significant lesion (arrow), consisting of two partially calcified plaques is situated at the distal part of the left main coronary artery, obstructing both the left anterior descending (LAD) as well as the left circumflex branch (CX) (**A**). The cross-section of the vessel confirms the distinct configuration of the lesions (**C**). Additionally, more non-calcified plaque material (arrow head) can be observed in the proximal part of the left main artery (arrow heads) (**A**). Diagnonal (D) and marginal (M) branch.

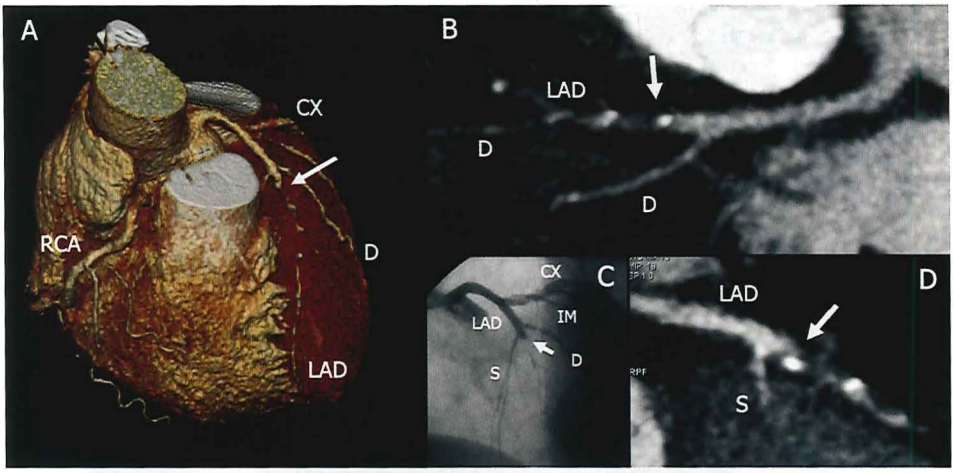

Chapter 6.1, Page 162; Figure 6. Occlusion of the left anterior descending coronary artery. Three-dimensional reconstruction (**A**) and curved multiplanar reconstruction (**B**) of a CT coronary angiogram showing an occluded (arrow) left anterior descending coronary artery (LAD) (**B**), which was confirmed by conventional by conventional coronary angiography (**C**). A saggital cross-section shows in detail the different plaque components, both calcified and non-calcified, as well as some residual contrast enhancement within the obstructed segment (**D**). Right coronary artery (RCA), diagonal (D), intermediate (IM) and circumflex branch (CX).

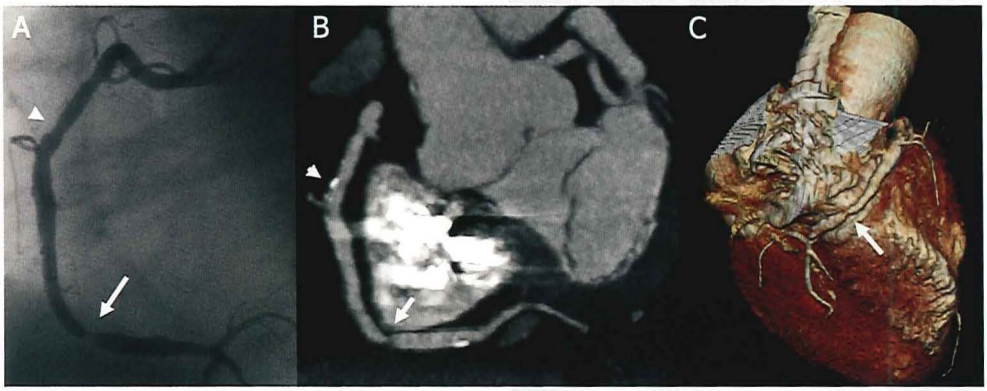

Chapter 6.1, Page 163; Figure 8. Stenosis of the distal right coronary artery. Using thin slab maximum intensity projection (MIP), a stenotic lesion (arrow) is demonstrated in the distal right coronary artery (**A**). Also minor wall irregularities, caused by small calcified lesions (arrow heads), can be observed, and were confirmed by conventional angiography (**B**).

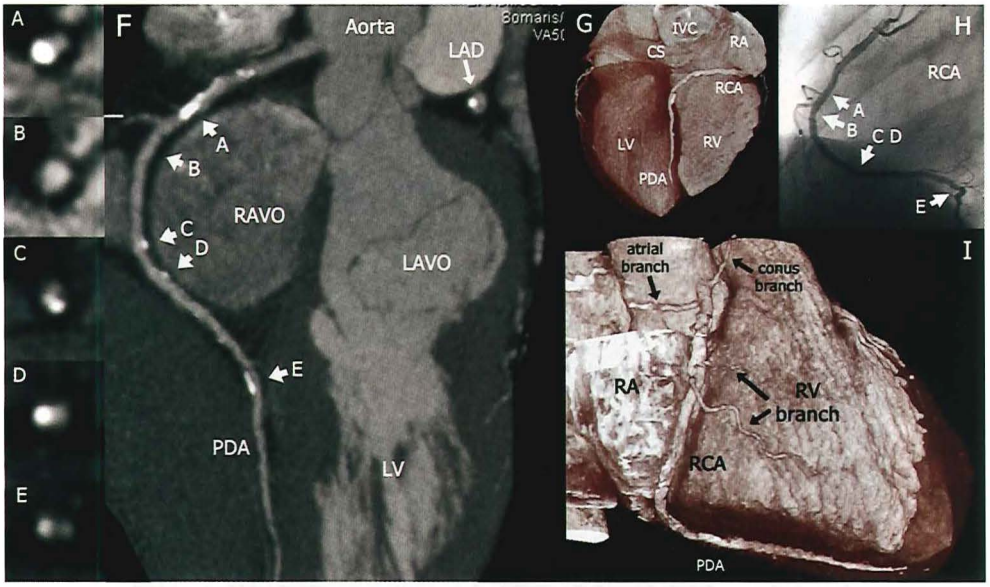

Chapter 6.2, Page 178; Figure 1. H, MSCT and conventional angiogram of an atherosclerotic RCA without significant stenoses. **A** and **F**, Blooming artifacts around the bright calcifications suggest stenosis. Cross-sections **A** through **E** are indicated in panel **F** (curved MSCT reconstruction along the course of the RCA) and H. **G**, Three-dimensional representations from an inferior and **I**, right-oblique angle, show the PDA and side branches. RAVO/LAVO indicates right/left atrioventricular orifices; PDA, posterior descending; LV/RV, right/left ventricles; CS, coronary sinus; RA, right atrium; and IVC, inferior vena cava.

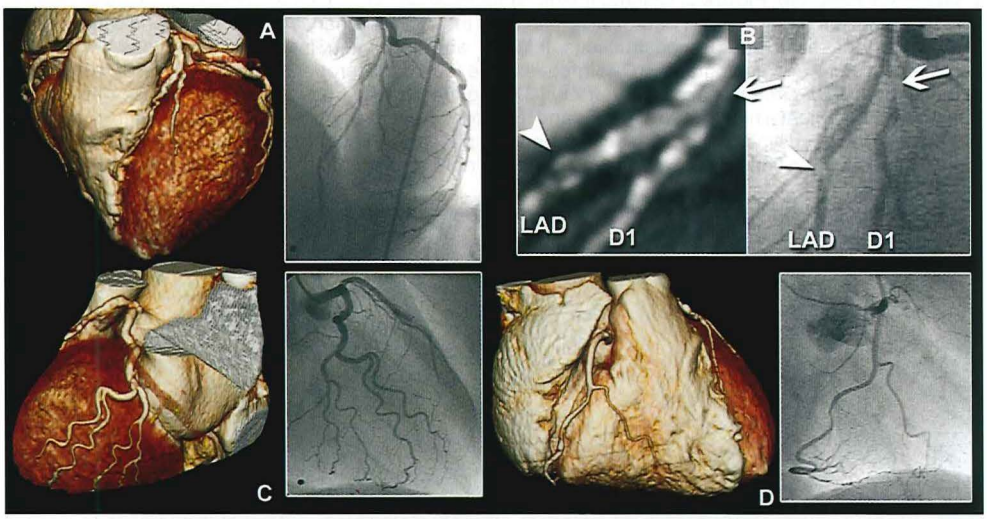

Chapter 6.3, Page 189; Figure 1. Volume-rendered multislice spiral computed tomography images (left) and corresponding conventional angiography images (right) of the left anterior descending (LAD) (**A**), circumflex (**C**), and right coronary artery (**D**) in a 69-year-old woman with stable angina and a positive bicycle test. Significant lesions were found in the proximal part of the LAD coronary artery (arrowhead) and first diagonal (D1) (arrow), which are demonstrated on the inlay (**B**).

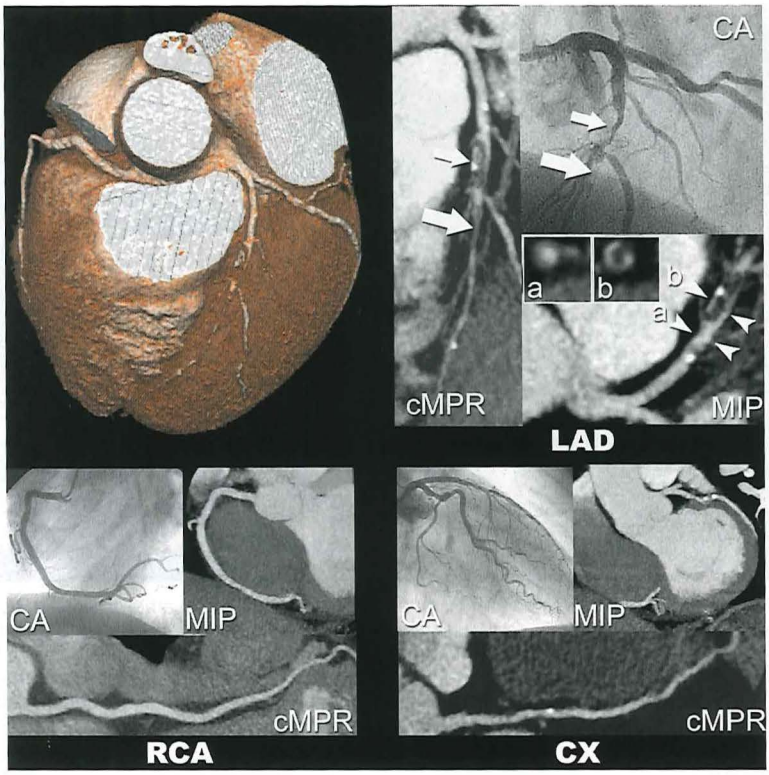

Chapter 6.3, Page 190; Figure 2. Colored image volume rendered multislice spiral computed tomography (MSCT) image providing an overview of the anatomy of the main coronary arteries. Black and white images MSCT (curved multiplanar reconstructions [cMPR] and maximum intensity projections [MIP]) and conventional coronary angiography (**CA**) images of the four main coronary arteries (left main/left anterior descending [**LAD**], circumflex coronary artery [**CX**], right coronary artery [**RCA**]) of a single patient. The small arrows highlight a high-grade stenosis and the large arrows an occlusion located at the midpart of the LAD. The arrowheads indicate cross-sectional images proximal (inlay **a**) and within the occlusion (inlay **b**). Inlay **b** shows calcified (displayed as white) and noncalcified (displayed as black) plaque tissue components.

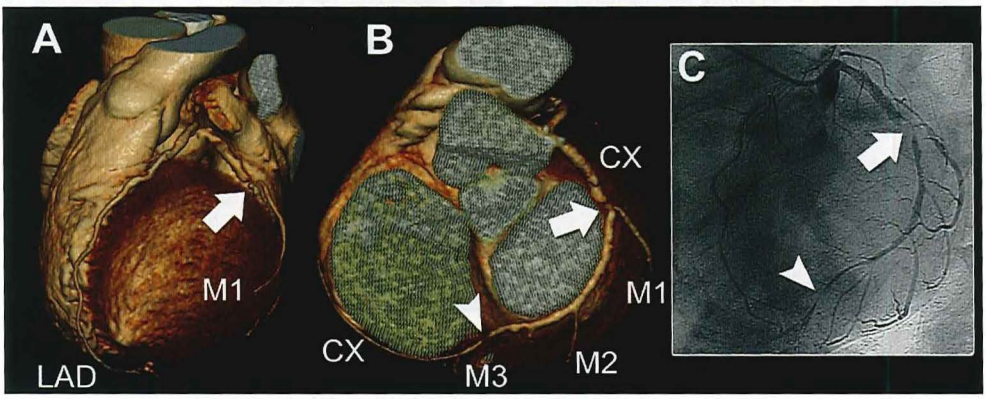

Chapter 6.4, Page 197; Figure 1a. Volume rendered CT images (**A, B**) reveal the presence of 2 significant stenoses (arrow, arrowhead) located at the circumflex coronary artery (CX), which was confirmed on the conventional angiogram (**C**). LAD: left anterior descending coronary artery, M: marginal branch.

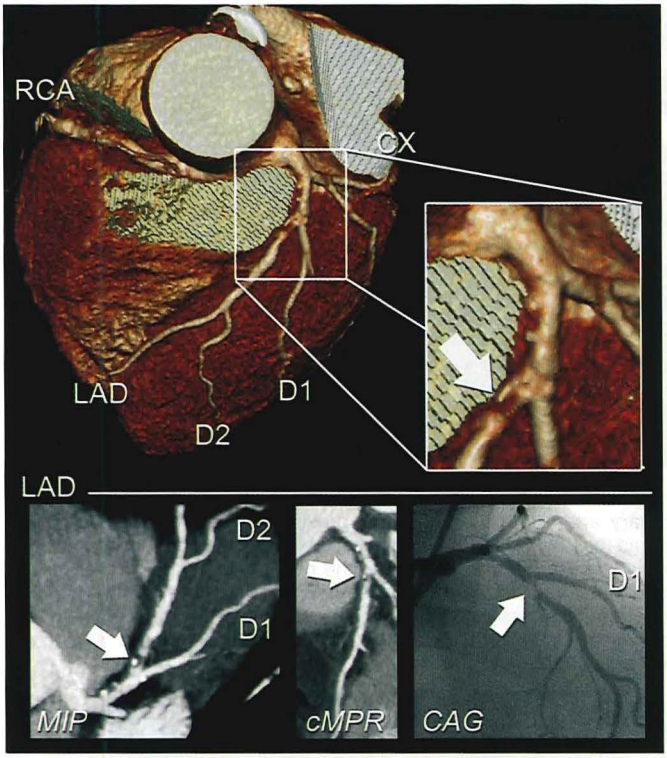

Chapter 6.4, Page 198; Figure 2. Volume rendered (coloured images), maximum intensity projected (**MIP**), and curved multiplanar reconstructed (**cMPR**) CT images demonstrate a significant stenosis (arrow) of the left anterior descending coronary artery (LAD), which was confirmed on the conventional angiogram (**CAG**). CX: circumflex coronary artery, D: diagonal branch, RCA: right coronary artery.

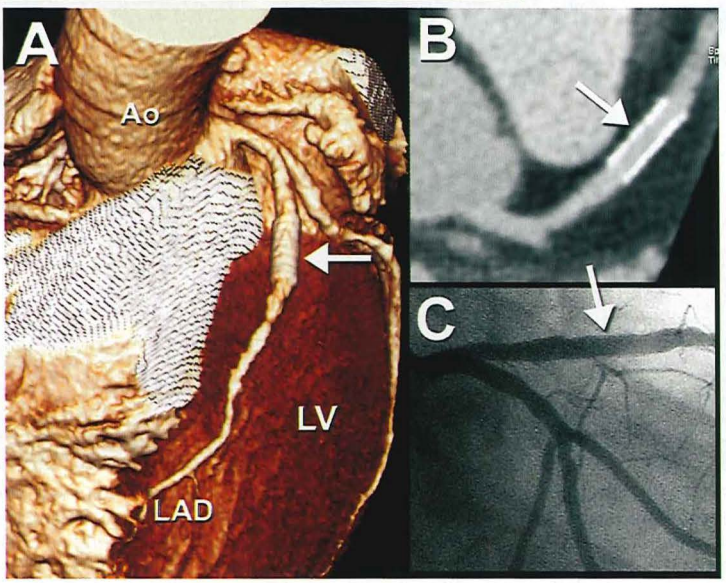

Chapter 7.2, Page 216; Figure 1. Patent stent in LAD. **A:** three-dimensional volume rendering of the heart showing the left coronary artery and a stent in of the proximal LAD (arrow). **B:** a multiplanar reconstructions showing the left main and the LAD with the patent stent (arrow). The contrast enhancement in the lumen of the stent is comparable with the one before and after the stent. **C:** the corresponding diagnostic coronary angiogram with no in-stent restenosis Abbreviations: Ao= ascending aorta; LAD= left anterior descending; LV= left ventricle.

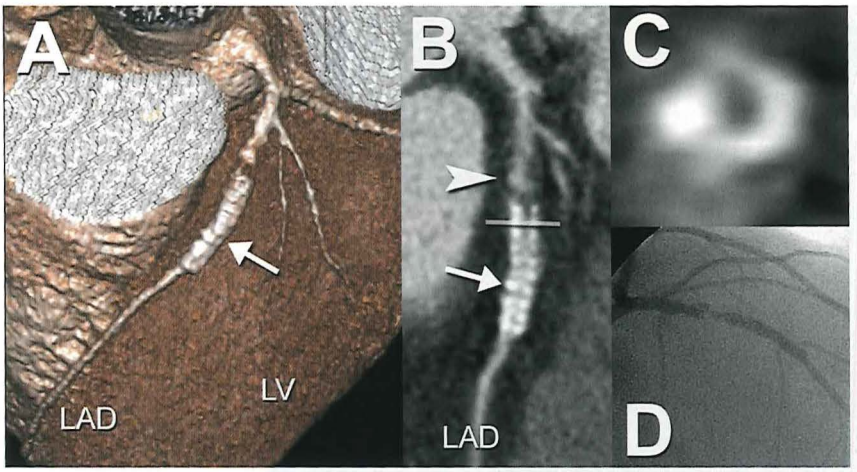

Chapter 7.2, Page 216; Figure 2. In-stent restenosis in a LAD stent. **A:** three-dimensional volume rendering of the heart showing the left coronary artery and a stent in the proximal LAD (arrow). **B:** a curved reconstructions shows the left main and the LAD with the stent (arrow). An obstructive plaque beginning at the proximal edge of the stent (arrowhead) and continuing within the proximal segment of the stent is visualized. A cross section performed at the level of the proximal segment of the stent (**C**) shows the in-stent restenosis appearing as hypoattenuating tissue within the stent. The bright zone represents the remaining lumen and on the right side a stent strut. **D:** the corresponding diagnostic angiogram Abbreviations: LAD= left anterior descending; LV= left ventricle.

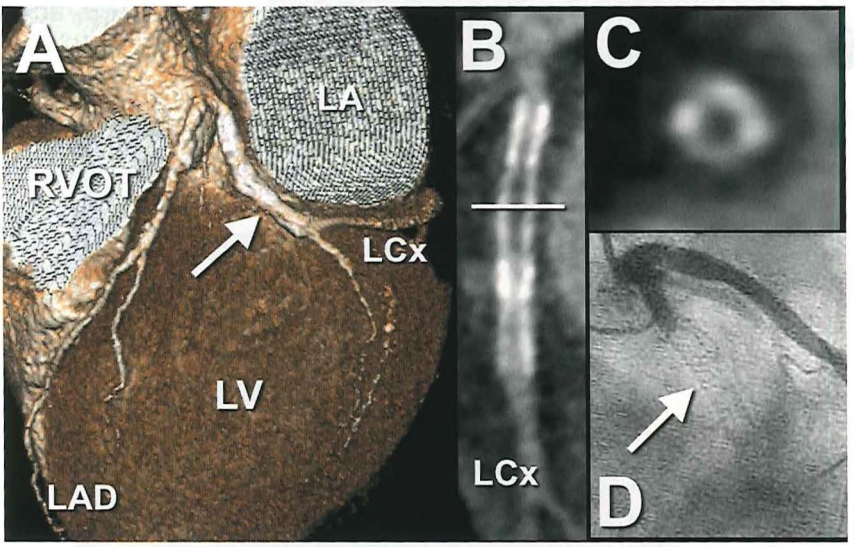

Chapter 7.2, Page 217; Figure 3. Occluded stent in LCx. **A:** a three-dimensional volume rendering of the left coronary artery, showing a stent in the proximal segment of the the LCx (arrow). **B:** a curved multiplanar reconstruction along the lumen of the LCx, shows the in-stent occlusion appearing as a hypoattenuating region, occupying the whole in-stent lumen. An orthogonal view performed at this level (**C**) shows the lack of contrast enhancement (dark zone) within the lumen of the occluded stent. **D:** the corresponding diagnostic angiogram. It should be noticed that with CT coronary imaging the distal segment of LCx appears patent (due to collateral retrograde flow), while at conventional coronary angiography there is only faint distal filling of the occluded vessel. Abbreviations: LAD= left anterior descending; LCx= left circumflex; LV= left ventricle; RVOT= right ventricle outflow tract.

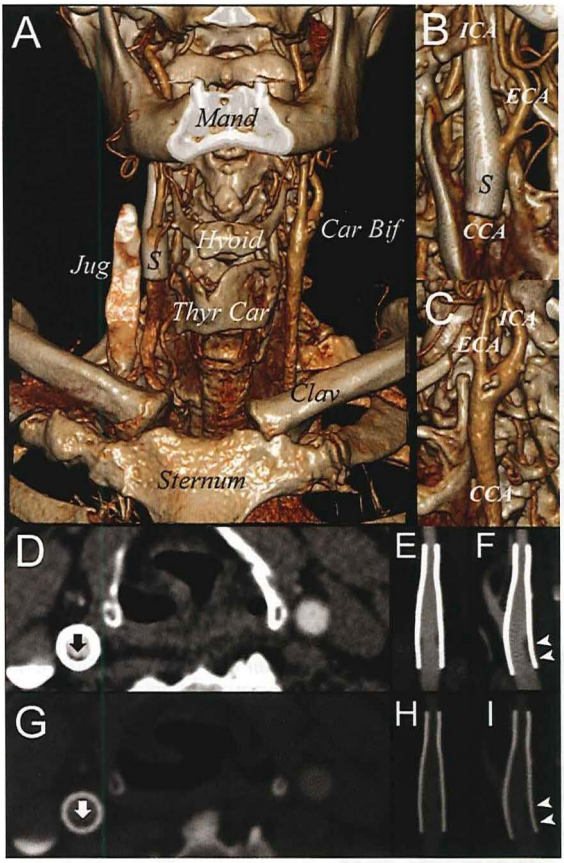

Chapter 7.3, Page 222; Direct 3-dimensional volume rendering (**A, B,** and **C**) shows the anatomy of the arteries of the neck at the level of the carotid bifurcation (Car Bif) (see also Movies IV, V, and VI). Clav indicates clavicle; Hyoid, hyoid bone; Jug, jugular vein; Mand, mandible; and Thyr Car, thyroid cartilage. A magnified view of the right (**B**) and left (**C**) carotid bifurcations permits recognition of the common carotid artery (CCA), the internal and external carotid arteries (ICA and ECA), and the wall stent (S) at the right side. The left carotid bifurcation (**C**) is patent but is slightly dilated at the origin of ICA. A few calcified spots also are present. Note the backflow of iodinated contrast material into the right jugular vein (Jug in A). Multiplanar reformats (**D** through **I**) show the lumen of the stent. One window setting is used for the visualization of soft tissue (**D, E,** and **F**), and another window setting permits the visualization of high-density structures such as stents (**G, H,** and **I**). Intimal hyperplasia can be appreciated in Movie I and in sagittal reformats (arrowheads in **F and I**; Movie II). Because of the spatial orientation of the intimal hyperplasia, the coronal reformats (**E and H**; Movie III) do not allow an optimal visualization.

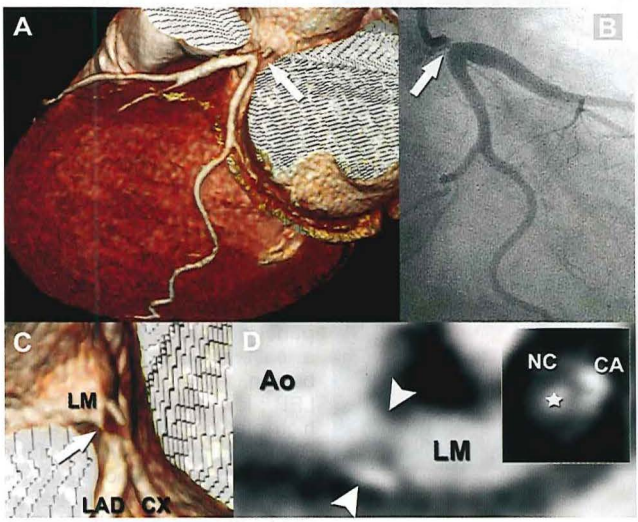

Chapter 7.4, Page 224; Figure 1. Volume Rendered (**A, B**) and Multiplanar Reconstruction (**C**) images show a high-grade stenosis of the left main coronary artery (arrows), afterwards confirmed on conventional angiography (arrow, **D**). A cross-sectional image of the lesion (inlay) shows calcified (CA) and non-calcified (NC) plaque tissue components surrounding the lumen (asterisk).

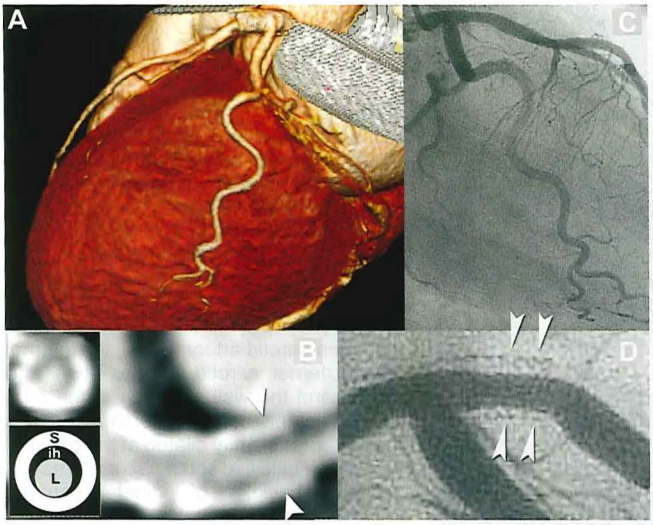

Chapter 7.4, Page 225; Figure 2. Volume Rendered image (**A**) and corresponding conventional angiography image (**D**) after 4 months follow-up. Figure **B** (including inlays) show moderate neo-intimal hyperplasia (ih) presenting as a dark rim surrounding the lumen (L), located at the distal part of the stent (S), afterwards confirmed on conventional angiography (arrowheads, **D**).

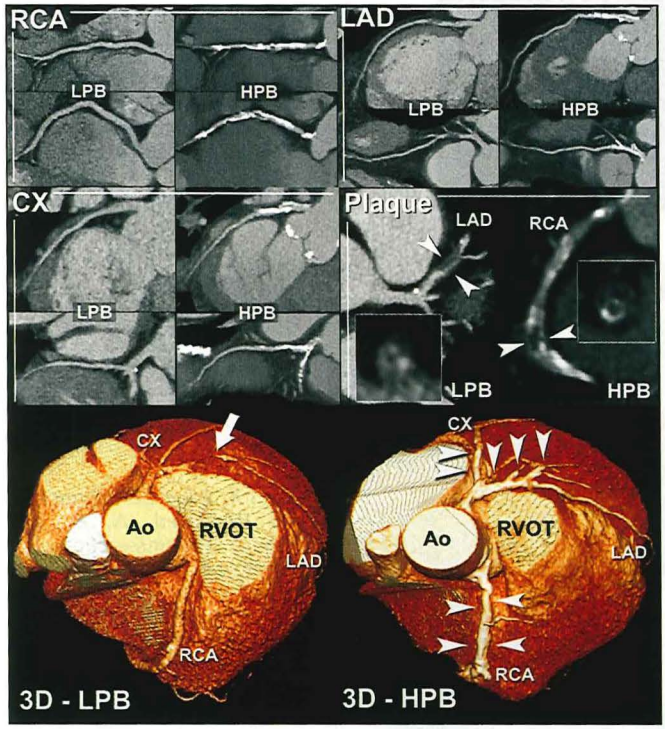

Chapter 8.1, Page 232; Figure 4. Low coronary plaque burden versus high coronary plaque burden. **Upper panels** and left middle panel demonstrate curved multiplanar reconstruction of low versus high plaque burden in RCA, LAD and CX in two orthogonal projections. The **middle right panel** shows multiplanar reconstructions of a large plaque in the proximal LAD (**left**), and a total occlusion of mid RCA. Arrowheads indicates the location of the corresponding cross-sectional images (**small panels**). The 3D images in the **lower panel** are reconstructed using a volume rendering technique. The arrow in the left panel indicates a large plaque of the LAD in a patient with an overall low plaque burden, and the arrowheads in the **right panel** indicate various plaques in a patient with a high plaque burden.
LPB : low plaque burden; HPB: high plaque burden; Ao: aorta; RVOT: right ventricular outflow tract. 3D : 3-dimensional. (A full color version of this illustration can be found in the color section (chapter 12)).